

Università degli Studi di Milano-Bicocca
Facoltà di Scienze Matematiche, Fisiche e Naturali
Dipartimento di Biotecnologie e Bioscienze
Dottorato di ricerca in Biotecnologie Industriali - XXVII ciclo



**LPS - binding proteins:
interaction studies with natural and synthetic
ligands**

Tutor

Prof. Francesco Peri

Stefania Enza Sestito

Matr. 724879

a.a. 2013-2014

Gutta cavat lapidem

Table of contents

Abbreviations.....	4
Abstract	7
1. Introduction	13
1.1. Bacterial endotoxin: the lipopolysaccharide.....	14
1.2. LPS biosynthesis	20
1.2.1. Crossing the periplasmic space.....	24
1.2.2. LptA and LptC.....	30
1.3. Biogenesis of LPS: a new target for antibiotics	33
1.4. Host defences that target lipid A.....	36
1.4.1. LPS and immune system	37
1.4.2. TLR4.....	43
1.4.2.1. LPS-binding protein (LBP)	47
1.4.2.2. CD14	48
1.4.2.3. TLR4 and MD-2.....	51
1.5. Syndromes due to deregulated TLR4 pathway activation	54
1.5.1. Modulation of TLR4 pathway	56
1.5.2. Synthetic TLR4 modulators	59
1.5.3. Natural TLR4 modulators	66
2. Purpose of the work	77
Section I: LptC-LPS binding studies	79
3. Results and discussion	80
3.1. <i>In vitro</i> binding assay setup.....	81

3.1.1. ELISA-type assay with immobilized LptC, and signal amplification by gold nanoparticles (GNP)	81
3.1.2 Co-capture assay on resin with fluorescent ligand.....	83
3.1.3. Co-purification assay.....	87
3.2. Binding studies	88
3.2.1. LptC-LPS interaction studies: kinetic experiments	88
3.2.2. Saturation and competition experiments	90
3.2.3. LptC binding to synthetic ligands.....	93
3.3. Conclusions and future perspectives	98
Section II: Biological characterization of new synthetic and natural small molecule TLR4 modulators.....	101
4. Results and discussion	102
4.1. Synthetic lipid A mimetics.....	103
4.2. Cationic amphiphilic compounds	107
4.2.1. Iaxo monosaccharides dimers	107
4.2.2. Pyrrole-Containing Amphiphiles.....	109
4.2.3. Trehalose- and glucose-derived glycoamphiphiles.....	112
4.2.4. Natural compounds from olive oil.....	122
4.3. Conclusions and future plans.....	127
5. Experimental section	134
5.1. Section I: Biochemistry section	134
5.2. Section II: Biology section	143
6. References	148
Publications	165

Abbreviations

Bi-LPS: biotin-conjugated LPS

BSA: bovine serum albumine

CD14: cluster of differentiation antigen

Cmc: critical micelle concentration

CV: coefficient of variation

DAMPs: danger (or damage) associated molecular patterns

E: eluate

ECD: ectodomain

EVOO: extra virgin olive oil

f-LOS: FITC-conjugated LOS

FITC: fluorescein isothiocyanate

FBS: fetal bovine serum

FT: flow through

GNP: gold nanoparticle

IM: inner membrane

HEK 293: human embryonic kidney 293

Kdo: 3- deoxy-D-*manno*-oct-2-ulosonic acid

Ip: intraperitoneally

LBP: lipid Binding Protein

LOS: lipooligosaccharide

LPS: lipopolysaccharide

Lpt: lipopolysaccharide transport

LRR: leucine-rich repeat domain

OM: outer membrane

MAMP: microbe associated molecular patterns

MD-2: myeloid differentiation 2

MDR: multidrug-resistant

MIC: minimum inhibitory concentration

MTT: thiazolyl blue tetrazolium bromide

NP: nanoparticle

PAMPs: pathogen associated molecular patterns

PDR: pandrug-resistant

PRR: pattern recognition receptor

RLA: relative luciferase activity

SD: standard deviation

SEAP: secreted embryonic alkaline phosphatase

SV: streptavidin

TIR: Toll/Interleukin-1 receptor

TLR: Toll-like receptor

UDP-GlcNAc: UDP-N-acetylglucosamine

VOO: virgin olive oil

W: wash

Abstract

The purpose of this work is the elucidation of some aspects of the interaction between lipopolysaccharide (LPS) binding proteins and their natural ligand or synthetic compounds.

LptC (Lipopolysaccharide transport C) is a bacterial protein belonging to Lpt complex, a molecular machinery composed of 7 essential proteins involved in the transport of LPS to the outer membrane in Gram negative bacteria after its biogenesis. Although many elements of LPS biosynthesis have been clarified, the precise mechanism of transport is still not completely understood. Since LptC can be considered as a model protein of Lpt complex, sharing the same folding of other proteins and being the first one in the periplasm, we have developed and optimized an *in vitro* binding assay to study its interaction with LPS. We have obtained, for the first time, detailed information about the thermodynamic and kinetic parameters of LptC-LPS binding. We have shown that the *in vitro* LptC-LPS binding is irreversible with a K_d of the order of μM . Considering the structural similarities between LptC and the eukaryotic protein CD14, belonging to TLR4 receptor system, the binding between LptC and the synthetic molecule iaxo-102, a known ligand of CD14, has been investigated. It is evident that iaxo-102 shares the same binding site of LPS and that the binding is irreversible with an affinity lower than that LptC-LPS. So, iaxo-102 can be considered as a

lead compound for the development a new generation of antibiotics targeting the biogenesis of LPS.

LPS also binds to other proteins, such as those of innate immunity TLR4, CD14 and MD-2. The LPS recognition by these receptors induces the production of pro-inflammatory cytokines and immunomodulators that trigger the inflammatory and immune responses. These reactions are useful for the organism, but when TLR4 activation is too strong or not well regulated induces sepsis, inflammation and autoimmune syndromes, which still lack a pharmacological treatment. A possible solution to solve this problem consists in the research and development of compounds which modulate this excessive activation. In the second part of thesis work, the biological characterization of some synthetic compounds, with different chemical features, have been reported. All compounds have been screened for their toxicity using MTT assay, and their modulatory activity on TLR4 pathway by using HEK cells stably transfected with TLR4, CD14 and MD-2 genes. The best compounds have been further characterized by *in vitro* assays on HEK cells transfected with the human or murine complex TLR4-MD-2 and *in vivo* studies. Finally, the possible correlation between the known anti-inflammatory properties of some natural compounds, such as the phenolic compounds of olive oil, and TLR4 activity has been investigated. The aim of this study is double: to find a lead compound active on TLR4 pathway, but also to discriminate which chemical features are important to obtain this effect.

In addition, the information obtained could be very useful to guide the rational design of other TLR4 modulators.

Riassunto

Lo scopo di questo lavoro di tesi è elucidare alcuni aspetti dell'interazione tra proteine che legano il lipopolisaccaride (LPS) batterico e il loro ligando naturale o ligandi di sintesi.

LptC (*Lipopolysaccharide transport C*) è una proteina batterica che appartiene al sistema di trasporto Lpt, un sistema di 7 proteine essenziali che trasportano l'LPS sulla membrana esterna dei batteri Gram negativi dopo la sua biosintesi. Sebbene molti elementi della biosintesi dell'LPS siano stati elucidati, il preciso meccanismo di trasporto è ancora poco chiaro. Poiché LptC può essere considerata come proteina modello del sistema Lpt, in quanto presenta lo stesso *folding* delle altre proteine ed è la prima ad essere localizzata nel periplasma, abbiamo sviluppato ed ottimizzato un saggio di *binding in vitro* per studiare la sua interazione con l'LPS. Abbiamo ottenuto, per la prima volta, dettagliate informazioni sui parametri termodinamici e cinetici dell'interazione LptC-LPS. Abbiamo infatti dimostrato che *in vitro* il *binding* LptC-LPS è irreversibile con una K_d dell'ordine del μM . Considerando le analogie strutturali tra LptC e la proteina eucariotica CD14, appartenente al sistema recettoriale del TLR4, in modo analogo è stata studiata l'interazione di LptC con la molecola sintetica iaxo-102, un noto ligando di CD14. È emerso che iaxo-102 condivide lo stesso sito di legame dell'LPS e che l'interazione con la

proteina è irreversibile con un'affinità inferiore a quella calcolata per LptC-LPS. Iaxo-102 può dunque essere considerato un prototipo per lo sviluppo di una nuova generazione di antibiotici che ha come target la biogenesi dell'LPS.

L'LPS è in grado di interagire con molte altre proteine, tra le quali quelle del sistema dell'immunità innata (TLR4, CD14, MD-2). Il riconoscimento dell'LPS da parte di questi recettori induce una forte risposta infiammatoria che termina con la produzione di citochine pro-infiammatorie e fattori immunomodulatori. Questa reazione infiammatoria è utile all'organismo, ma quando si manifesta in modo eccessivamente potente e non ben regolato induce sepsi, processi infiammatori e sindromi autoimmuni per le quali non è ancora disponibile un trattamento farmacologico. Una possibile soluzione al problema consiste nella ricerca e nello sviluppo di composti in grado di modulare questa eccessiva attivazione. Nella seconda parte di questo lavoro, sono riportate le caratterizzazioni biologiche di alcuni composti di sintesi con caratteristiche chimiche differenti. Di tutti i composti è stata valutata la tossicità mediante saggio dell'MTT e l'attività modulatrice del *pathway* del TLR4 utilizzando cellule HEK stabilmente trasfettate con i geni del TLR4, CD14 ed MD-2. Ulteriori caratterizzazioni sono state effettuate sui composti più promettenti, effettuando saggi *in vitro* su cellule HEK trasfettate con il complesso umano o murino TLR4·MD-2 e saggi *in vivo*. Infine, abbiamo investigato la possibile correlazione tra le

note proprietà anti-infiammatorie di alcuni composti naturali, come i composti fenolici presenti nell'olio di oliva, e il *pathway* del TLR4. L'obiettivo di questo lavoro è duplice: individuare un *lead compound* come possibile modulatore del TLR4, ma anche discriminare quali caratteristiche chimiche siano importanti per ottenere questo effetto. Inoltre, le informazioni ottenute potrebbero essere estremamente utili per guidare il *rational design* di altri modulatori del TLR4.

1. Introduction

Bacteria and Archaea account for the largest amount of biomass on earth and are major reservoirs of essential nutrients and energy. They have a simpler internal cell structure than eukaryotic cells and in most cases they lack membrane-enclosed organelles. Bacteria are divided into Gram-negative and Gram-positive bacteria based on the Gram stain, which reflects differences in the cell envelope architecture (Figure 1).

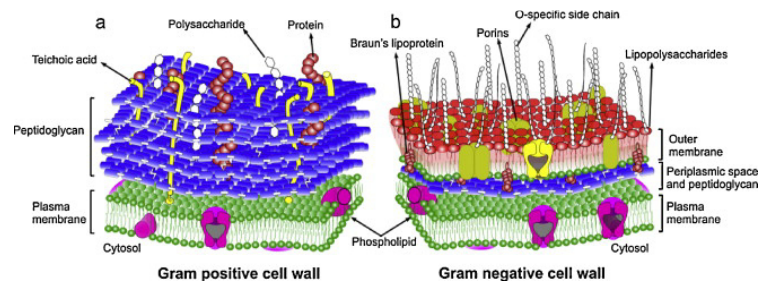


Figure 1. Differences in the cell wall structures of Gram positive and negative bacteria.

Both possess a cytoplasmic membrane made of a phospholipid bilayer, which surrounds the cytosol and provides a physical, semi-permeable barrier regulating the movement of molecules in and out the cell. This

membrane is enclosed by the cell wall peptidoglycan, a rigid layer that confers shape and osmotic strength to the bacterial cell.¹ The peptidoglycan layer is a complex polymer composed of alternating *N*-acetylglucosamine and *N*-acetylmuramic acid with attached tetrapeptide side chains. Gram negative bacteria are further characterized by the presence of a periplasmic space between the cell membrane and the outer membrane.² The outer membrane (OM) is a unique asymmetric phospholipid bilayer; the inner leaflet consists of glycerophospholipids while the external leaflet is rich in lipopolysaccharide (LPS) which covers up to 75% of the cell surface. Embedded in the OM there are also integral membrane proteins like porins, which serve as channels for the passage of small hydrophilic molecules and lipoproteins.

1.1. Bacterial endotoxin: the lipopolysaccharide

Lipopolysaccharide guarantees the viability and survival of Gram negative bacteria, contributing to the correct assembly of the OM. LPS is a heat-stable complex of amphiphilic glycolipid that provides an extraordinary permeability barrier to many different classes of molecules including detergents, antibiotics, and toxic dyes and metals. The barrier properties of the OM depend on its low fluidity, which is due to the highly ordered structure of the LPS monolayer. Owing to their external

location, LPS molecules interact with other biological systems by participating in host-bacterium interactions like adhesion, colonization, virulence and symbiosis.¹

The structure of LPS can be divided in three regions: lipid A, the hydrophobic moiety that anchors LPS to the OM, the oligosaccharide region named core, and the *O*-antigen polysaccharide chain (Figure 2).³

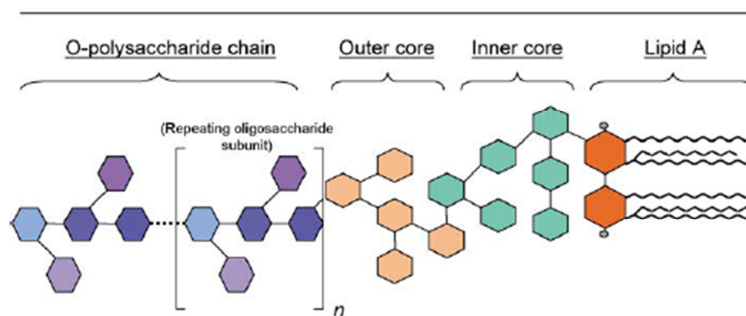


Figure 2. General structure of Gram negative LPS. *O*-chain is highly variable, responsible for serological specificity of LPS variants and represents the primary target for antibody responses against LPS. The outer core is more likely to contain common sugars (hexoses, hexosamines, etc.) while the inner core is highly conserved and contains unusual sugars such as Kdo and heptose. The di-glucosamine backbone of lipid A is very highly conserved and the acyl chain length/substitution pattern is primary determinant for endotoxicity.⁴

The *O*-polysaccharide region is composed by repeating units of one and eight glycosyl residues, which differ among strains by means of the sugars, sequence, chemical linkage, substitution, and ring forms utilized. This leads to an almost limitless diversity of *O*-chain structure and is verified in nature with the observation of hundreds of serotypes for particular Gram negative species. In addition, the number of subunits used to complete the chain varies between 0 and ~50 and a single organism will produce a wide range of these lengths as a result of incomplete synthesis of the chain.⁴

The *O*-polysaccharide is also the outermost part of the LPS molecule expressed on bacteria and is therefore the major antigen targeted by host antibody responses. These responses can be highly *O*-chain specific, and for this reason the *O*-chain is often also referred to as the *O*-antigen. The *O*-polysaccharide region is also recognized by the innate arm of the immune system, playing a role in both the activation and inhibition of complement activation. For many organisms (e.g. *Salmonella*), the *O*-chain is essential for survival in host serum as it prevents penetration of the complement membrane attack complex.^{4,5}

The core region could be divided into two part: the inner and the outer core. The chemical structure of the outer core is variable, whereas the inner core region tends to be quite conserved within a genus or family (Figure 3).

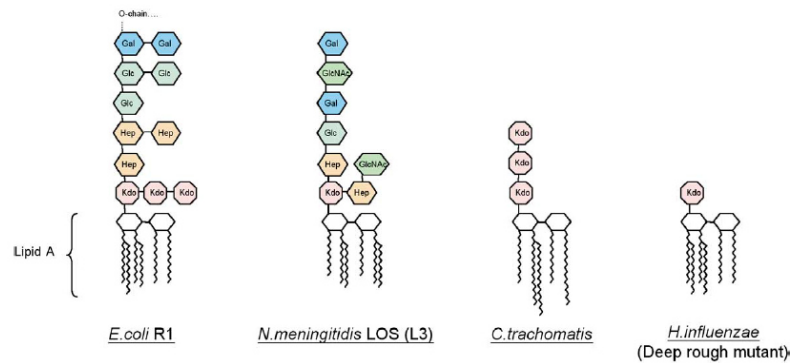


Figure 3. Core structures of selected Gram-negative pathogens. The *E. coli* core shown is that of rough mutant R1; the structure given for *N. meningitidis* relates to the entire LOS of the organism; all isolates of *C. trachomatis* have shown only the Kdo triplet depicted; and the deep rough mutant of *H. influenzae* (I-69 Rd⁻/b⁺) represents the smallest core structure yet seen for any viable Gram-negative bacteria.⁴

The inner core contains at least one residue of 3-deoxy-D-manno-oct-2-ulosonic acid (Kdo) and several heptoses. Kdo is rarely found in other glycans and therefore can be considered as a marker for the presence of LPS.¹ Interestingly, while the O-chain and the majority of the core can be dispensed with in some viable mutants, this Kdo residue is always absolutely required for bacterial viability.

Both inner and outer core sugar residues can be substituted with charged groups like phosphate, pyrophosphate, 2-aminoethylphosphate and 2-aminoethylpyrophosphate. In the inner core, it is thought that

these substituents maintain a close association with the Ca^{2+} and Mg^{2+} ions that are required for membrane structure and function.^{4,6} The abundant anionic groups in the lipid A-core region are tightly associated by electrostatic interactions with divalent cations (Mg^{2+} and Ca^{2+}), which help connecting LPS molecules to each other. This phenomenon contributes to the remarkable stability of the outer membrane and to a significant reduction in membrane permeability, resulting in an efficient protective barrier.

Lipid A is embedded in the outer leaflet of the outer membrane and anchors the LPS molecules through electrostatic and hydrophobic interactions. It is the most conserved portion of the LPS and constitutes the so called endotoxin principle of LPS thus providing the minimal structure responsible for toxicity in vertebrates. In most bacteria lipid A has a β -(1→6)-linked D-glucosamine disaccharide backbone that is phosphorylated at positions 1 and 4'.⁷ This structure is decorated with up to four acyl chains linked by ester or amide bonds. These chains can then in turn be substituted by further fatty acids to provide LPS molecules with up to seven acyl substituents, which vary quite considerably between species in nature, number, length, order and saturation. These can be attached to the lipid A either symmetrically (3+3, e.g. *Neisseria meningitidis*) or asymmetrically (4+2, e.g. *E. coli*).⁴ Despite its general structural conservation, lipid A also has considerable structural microheterogeneity; therefore, it is more appropriate to

consider lipid A as a family of structurally related molecular species with different acylation and phosphorylation patterns rather than as a homogeneous molecule. Variations in structure results from the type of hexosamine present, the degree of phosphorylation, the presence of phosphate substituents, the chain length, number and location of lipid chains. The first structurally elucidated lipid A was from *E. coli*, and consists of 14 carbon length fatty acids (3- hydroxytetradecanoic acid). The hydroxyl groups of the two (R) -3- hydroxyl fatty acid of the distal GlcN-residue (GlcN II) are acylated by non-hydroxylated fatty acids whereas those at the GlcN-residue at the reducing site (GlcN I) are free. Thus the overall acylation pattern is asymmetric (4+2).⁷ Mutants lacking in lipid A and both Kdo show no viability demonstrating that the minimal requirement for bacterial viability is lipid A and at least on Kdo.⁸⁻¹⁰ The detailed structure of LPS varies from one bacterium to another, and this variation could affect the virulence of the bacterium.¹¹ The complete LPS comprising all three regions is termed "smooth" LPS, while LPS lacking the *O*-chain and/or portions of core oligosaccharide the LPS is called "rough" LPS (or lipooligosaccharide - LOS -) (Figure 4).¹²

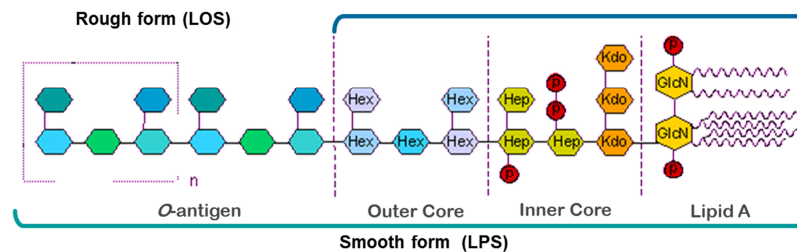


Figure 4. Smooth and rough form of LPS.

1.2. LPS biosynthesis

E. coli is the most favored Gram-negative bacterium to study the LPS biosynthesis. The biosynthesis of LPS is a complex process which requires spatial and temporal coordination of several independent pathways that converge in an ordered assembly line to give the mature molecule.^{7,13} The first stage of the biosynthetic pathway is the synthesis of Kdo₂-lipid A.^{7,14} The pathway is mediated by nine enzymes and takes place in the cytoplasm and on the inner surface of inner membrane. The initial building block of lipid A is UDP-GlcNAc. The first three reactions are catalyzed by soluble enzymes LpxA, LpxC and LpxD, resulting in the addition of two 3-OH fatty acid chains to the 2- and 3-positions of the UDP-GlcNAc to form UDP-diacyl-GlcN.^{15,16} The UDP-diacyl-GlcN is next hydrolyzed by LpxH to form lipid X.^{17,18} LpxB condenses lipid X and its precursor UDP-diacyl-GlcN to form disaccharide-1-P.^{19,20} Both LpxH and

LpxB enzymes catalyzing the reactions are peripheral membrane proteins, while the enzymes that catalyze the followed reactions in the pathway, LpxK, KdtA, LpxL and LpxM, respectively, are integral proteins of the inner membrane. LpxK is a kinase that phosphorylates the 4'-position of the disaccharide-1-P to form lipid IVA.^{21,22} KdtA is a bifunctional enzyme that incorporates two 3-deoxy-D-manno-octulosonic acid (Kdo) residues at the 6'-position of the lipid IVA, using the sugar nucleotide CMP-Kdo as the donor.²³ The resulting Kdo₂-lipid IVA undergoes further reactions, catalyzed by LpxL and LpxM, to form Kdo₂-lipid A (Figure 5). LpxL adds a secondary lauroyl residue and LpxM adds a myristoyl residue to the distal glucosamine unit, respectively.²⁴

The core oligosaccharides are sequentially assembled on lipid A at the cytoplasmic surface of the inner membrane in a process that involves a number of membrane-associated glycosyltransferases, using nucleotide sugars as donors. The biosynthesis of core oligosaccharides is rapid and efficient, suggesting that the glycosyltransferases function as a coordinated complex.

O-antigen, similarly to the core oligosaccharides, is synthesized on the cytoplasmic surface of the inner membrane. Using the sugar nucleotides as donors, the units of *O*-antigen are assembled by glycosyltransferase enzymes on the membrane-bound carrier, undecaprenyl phosphate, which is also used for the synthesis of peptidoglycan and capsular polysaccharides (Figure 5).

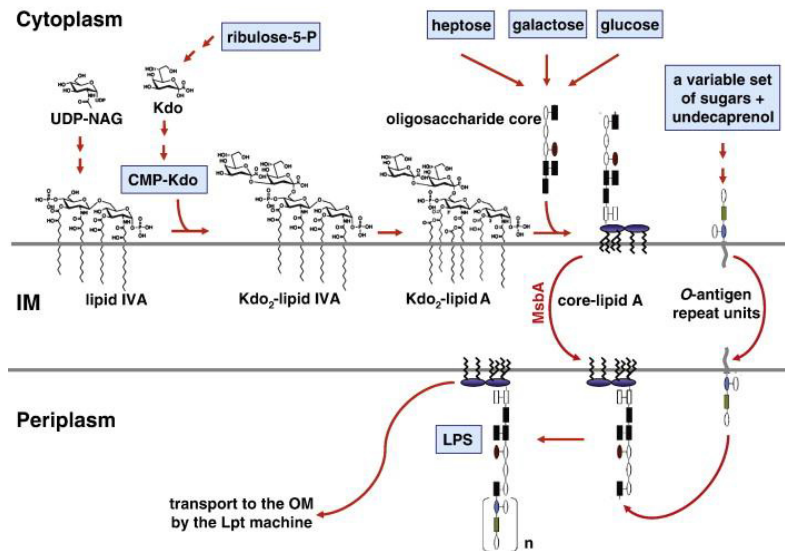


Figure 5. Biosynthetic pathway of LPS in *E. coli*.³

After the biosynthesis, the core-lipid A is anchored to the IM with its hydrophilic moiety exposed to the cytoplasm and is then flipped across the IM by the essential ABC (ATP binding cassette) transporter MsbA, becoming exposed in the periplasm.²⁵⁻²⁷ In *E. coli*, MsbA is a homodimer and each monomer contains six transmembrane helices and a cytosolic ATP-binding domain.²⁸ The basal ATPase activity of purified MsbA reconstituted into liposomes is stimulated by hexa-acylated lipid A, Kdo₂-lipid A, or LPS but not by underacylated lipid A precursors, suggesting that hexa-acylated LPS is the substrate required for the transport.²⁹ MsbA contains 2 substrate-binding sites that communicate with both the nucleotide binding domain and with each other. One is a

high affinity binding site for lipid A and the other side interacts with drugs with comparable affinity. Thus, MsbA may function as both a lipid flippase and a multidrug transporter.³⁰ However, *in vivo* MsbA displays a remarkable selectivity towards the LPS substrates being capable to translocate only hexa-acylated but not penta or tetra-acylated LPS. The transport of the *O*-antigen across the inner membranes is mediated by at least 3 proteins, Wzx, Wzy and Wzz,^{31,32} which might function by recognizing the first sugar phosphate bound to the undecaprenyl-P.³³

An alternative way of transport consists of the ABC transporter-dependent pathway, in which the completion of the *O*-specific polysaccharide occurs at the cytosolic side of the IM and the export of the polymer across IM requires an ABC transport.³⁴ Irrespective of the export and polymerization mode, the assembly of the mature LPS occurs at the periplasmic face of the IM where the lipid A-core and *O*-antigen biosynthetic pathways converge with the ligation of *O*-antigen to the lipid A-core moiety mediated by the WaaL ligase.³⁵ Finally, transport of LPS across the periplasmic space and its insertion and assembly on the outer leaflet of the OM requires a protein complex, the lipopolysaccharide transport (Lpt) machinery, which spans the entire cell envelope.³⁶

1.2.1. Crossing the periplasmic space

The mature LPS molecules must traverse the aqueous periplasmic compartment before being inserted and correctly assembled at the OM,³⁷ but LPS is an amphipatic molecules and so the transport through membranes and in aqueous phases poses several problems. Movement through aqueous phases such as the periplasm would expose the hydrophobic moieties of amphipatic molecules to water molecules, whereas moving across membranes would expose their hydrophilic moieties to the hydrophobic interior of the membranes.³⁸ In 1972, exploiting sucrose density gradient ultracentrifugation to separate IM and OM from *S. enterica*, Osborn et al. demonstrated for the first time that LPS transport from the site of synthesis at the IM to the OM is unidirectional.³⁹ However, it took several decades to unravel the first molecular details of this process. Unlike MsbA, whose role in LPS flipping across the IM has been clearly establish during the last two decades,^{29,40,41} most of the factors involved in LPS transport downstream of MsbA have been identified only in the past 10 years. The *E. coli* Lpt (LPS transport) machinery consists of seven essential proteins (LptABCDEFG) that accomplish LPS transport across the periplasm to its final assembly at the cell surface.^{42-44,46-48} The Lpt complex provides energy for LPS extraction from the IM and mediates its transport across the aqueous periplasm, its insertion and its assembly at the OM,^{3,48}

representing an atypical IM ABC transporter. This complex may be divided in 3 subassemblies: LptBCFG, located at the IM, LptA in the periplasm, and LptDE at the OM (Figure 6).

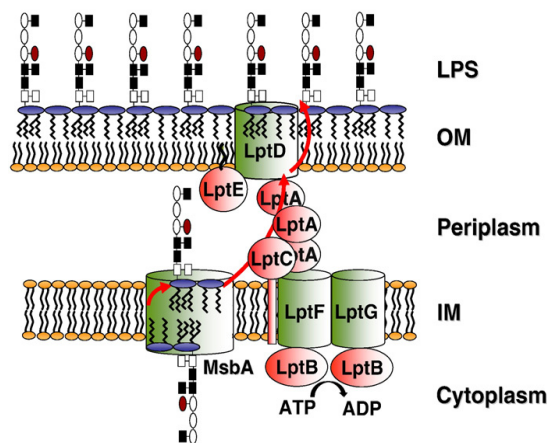


Figure 6. Lpt machinery in *E. coli*.

LptBFG is an IM-associated ABC transporter that harbors an atypical subunit constituted by the bitopic IM protein LptC.⁴³ LptB is a 27-kDa cytoplasmic protein possessing the typical nucleotide-binding fold of this ABC transporters. Earlier, LptB was found associated to an uncharacterized IM high molecular weight protein complex, of approximately 140 kDa, but the other components of the complex were

not identified.⁴⁹ LptF (40.4 kDa) and LptG (39.6 kDa) are the transmembrane subunits of the IM ABC transporter.⁴⁴

LptC is a bitopic protein possessing only one transmembrane domain and cannot fulfil the role of the integral membrane components of typical ABC transporters, which consist of either one IM protein with 12 transmembrane domains or two proteins with 6 transmembrane domains each.⁵⁰

LptA is the periplasmic binding component. LptA is a small protein of 185 amino acids possessing a 23 amino acid signal sequence that is processed in the mature form.⁵¹ LptA presents a novel fold consisting of 16 antiparallel β -strands folded to resemble a semiclosed β -jellyroll; the structure is not completely symmetrical and it opens slightly at the N- and C-termini. In the presence of LPS, LptA associates in a head-to tail fashion forming fibrils containing a hydrophobic groove. According to the hypothesis that LptA physically connect IM and OM, the interior cavity of LptA fibers could accommodate LPS.⁵²

At the OM, the LptD/E complex is required to assemble LPS in the outer leaflet of the OM. LptD is an essential β -barrel protein of 87 kDa whereas LptE (formerly RlpB) is an essential lipoprotein of 21.1 kDa.

LptD possesses a periplasmic N-terminal domain, belonging to the same OstA superfamily as LptA and LptC,³⁸ that is essential for its function.⁴⁵ Initial studies on LptD revealed that this protein exists in a higher molecular weight complex in the OM.⁵³ The interacting protein was

purified by affinity chromatography to a tagged LptD and identified by tandem mass spectrometry as LptE, a previously identified OM lipoprotein of very low abundance.⁵⁴ The essential lipoprotein LptE is functional even without its N-terminal lipid anchor (Figure 7).⁴⁷

Sperandeo et al. showed that upon depletion of LptA, LptB, LptC LptD, and LptE the LPS assembly pathway is blocked in nearly the same fashion, which results in very similar phenotypes and provided a first strong evidence of functional and/or physical interaction between the Lpt proteins.⁴³

Two models have been proposed to explain the LPS transport across the periplasmic space. The first is based on the similarities between Lpt and Lol system: the periplasmic LPS transport may be analogous to the machinery that transports lipoproteins to the OM where the periplasmic carrier LolA escorts lipoproteins across the periplasm and delivers its cargo to its specific OM receptor.⁵⁵ According to this model LptA may function as a soluble periplasmic chaperone that binds LPS, diffuses across the periplasm and delivers it to the LptD/E complex at the OM. The finding that LptA binds LPS *in vitro* is in line with this model.⁴⁴

The second model of LPS transport across the periplasm implicates a membrane bridge that would physically connect the IM and OM allowing for direct efflux of LPS to the cell surface.³⁸ In line with this second model, evidence exists of direct physical interaction between the seven Lpt proteins.⁴⁷ LptA-LptC interaction has been demonstrated *in vitro*:

interestingly Tran et al. also demonstrated that LptA binds LPS with higher affinity than LptC, suggesting that LptC may deliver it to LptA.⁵⁶⁻⁵⁷ A transport model can be proposed as follows: LPS transport starts with LPS extraction from the IM by the LptBFG complex, which transfers the molecule to the periplasmic domain of membrane-bound LptC; LptC then transfers LPS to LptA. LptC may initially use energy provided by the ATP hydrolysis to extract LPS from the IM, after that, LPS unidirectional transit from LptC to LptA can occur by increasing the affinity gradient. By the way, LptC does not affect the kinetic parameter of the ATPase activity of the LptBCFG complex.⁴⁶

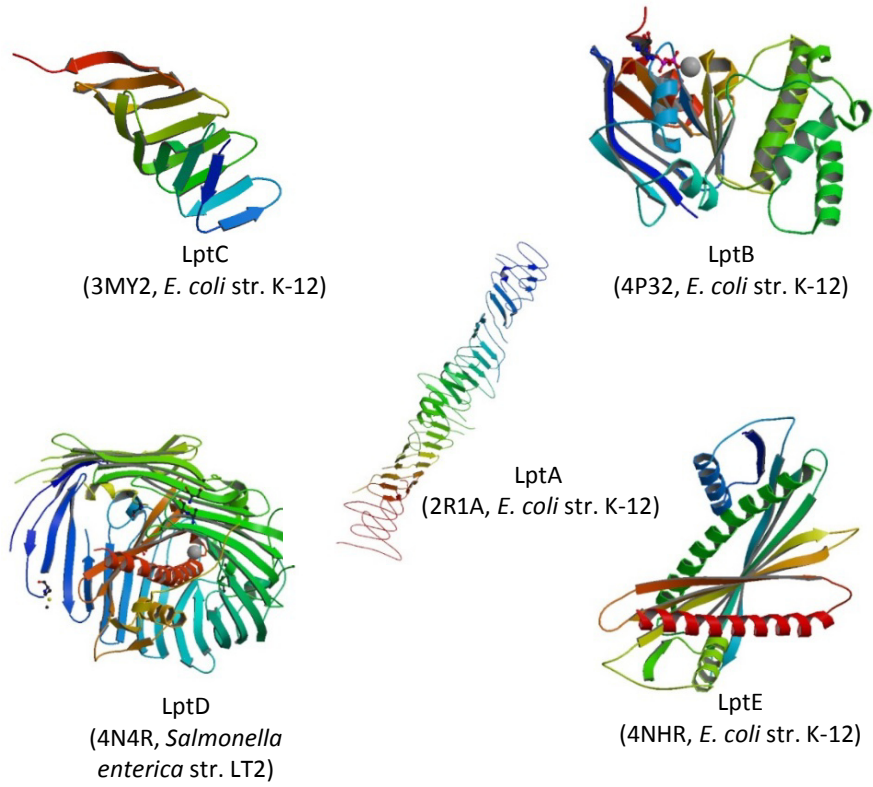


Figure 7. Crystal structures of Lpt proteins with the respective PDB code.

1.2.2. LptA and LptC

LptC is a conserved bitopic inner membrane protein from *E. coli* involved in the export of LPS from its site of synthesis in the cytoplasmic membrane to the outer membrane. LptC forms a complex with the ATP-binding cassette transporter, LptBFG, which is thought to facilitate the extraction of lipopolysaccharide from the inner membrane and release it into a translocation pathway that includes the putative periplasmic chaperone LptA.⁴⁶ Cysteine modification experiments established that the catalytic domain of LptC is oriented toward the periplasm. The X-ray structure of the periplasmic domain (Trp7 - Asp29) of LptC (at resolution of 2.2 Å) has revealed an overall structure consisting of a twisted boat structure with two β -sheets in apposition to each other with an angle of 60° - 85°. The β -sheets contain seven and eight antiparallel β -strands, respectively, which create the binding site with the lipidic portion of the LPS. This structure bears a high degree of resemblance to the crystal structure of LptA although they share limited primary sequence similarities. However, there are some slight differences in the structures (Figure 8). For example, the opening between the two β -sheets is slightly larger in LptC, and the conformations of the C-termini of the two proteins are different. The N-terminus of LptA contains a short α -helix that is sandwiched between the two β -sheets, while the corresponding N-terminus of LptC is disordered. Another notable difference is that loop

2 in LptC is much shorter than its counterpart from LptA; however, loop 7 from LptC is much longer than the comparable loop in LptA.⁵⁷

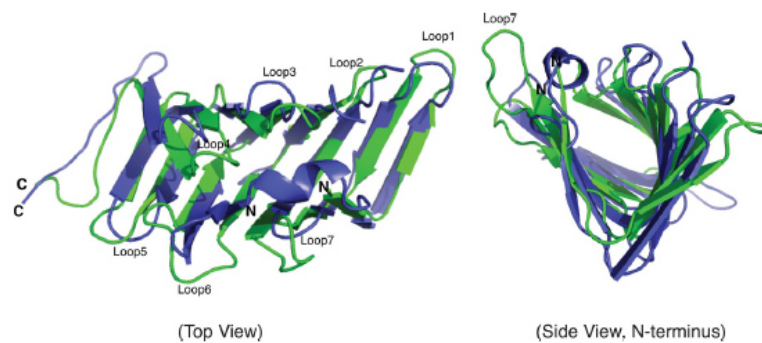


Figure 8. Structural comparison of LptA and His₆-LptC (24 –191). Ribbon diagrams of LptA (blue; 2.15 Å) (Protein Data Bank accession code: 2R19) and His₆ – LptC (24 – 191) (green; 2.2 Å) are superimposed.⁵⁷

Both LptA and LptC possess hydrophobic residues which form a hydrophobic core along the proteins that potentially serve as an LPS-binding site^{7,16} and qualitative *in vitro* assays have shown that both LptA²⁵ and LptC⁷ bind to LPS. *In vitro*, LptA can displace LPS from LptC (but not *vice versa*), consistent with their locations and their proposed placement in a unidirectional export pathway. Co-capture *in vitro*

binding assays, previously used to study LOL transport system,^{51,58} showed that the *O*-antigen is not required for the recognition of LPS in the interaction with LptC, indicating that this interaction occurred with the hydrophobic domain of the ligand that is the Lipid A part. Even if the binding pocket does not seem capable of accommodate all the lipid A of LPS, it's possible that the binding induces a conformational change which create a binding pocket big enough so that the hydrophobic residues could interact with the lipidic portion of the ligand.

Recently, four residues in LptC (Thr47, Phe78, Ala172 and Tyr182) have been found to interact with LPS *in vivo*. The LptC residues directly involved in LPS binding are located almost exclusively inside the β -jellyroll structure, supporting the model of membrane bridge, in which LPS binds inside these proteins and transits through the periplasm bound to the cavity of the conserved β -jellyroll fold (Figure 9).⁵⁹

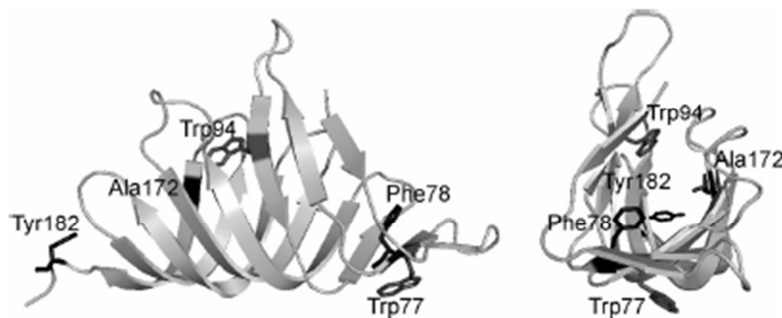


Figure 9. Cartoon representation of the LptC crystal structure (PDB ID: 3MY2). Putative LPS binding residues are labeled.⁶⁰

1.3. Biogenesis of LPS: a new target for antibiotics

In the past 60 years, antibiotics have been critical in the fight against infectious diseases caused by bacteria and other microbes and their use has been a leading cause for the rise of average life expectancy in the Twentieth Century.⁶¹ However, according to WHO the world may be entering a so-called “post antibiotic era”, in which it will be no longer possible to treat the causes of infectious diseases with antibiotics, since many pathogenic bacteria have become resistant to antibiotic drug therapy.⁶² To better understand the magnitude of this phenomenon, it is enough to consider that nowadays about 70% of the pathogenic bacteria that cause infections in hospitals are resistant to at least one of the drugs most commonly used for the treatment.⁶¹ Multidrug-resistant (MDR) and pandrug-resistant (PDR) Gram-negative bacteria represent a serious threat, as these antibiotic resistant pathogens cause infections that are becoming truly untreatable. Strains resistant to some (MDR) or all (PDR) antibiotics commonly used clinically have been isolated in *Acinetobacter baumannii*, *E. coli*, *Klebsiella pneumoniae*, *Pseudomonas aeruginosa* and other pathogenic species.⁶³ Although the resolution of the problem consists in the research for new molecules with antibacterial activity, all antibiotics approved for clinical use between 1960 and 2000, except carbapenems, are synthetic derivatives of scaffolds discovered in the so-called “golden era” (1930-1960) and they

are only partially effective against prevailing resistance mechanisms.^{64,65} Since 1962 only three new classes of antibacterial agents have been approved for clinical use: oxazolidinones⁶⁶ and retapamulin,⁶⁷ both targeting protein synthesis, and daptomycin, a narrow spectrum cyclic lipopeptide disrupting Gram-positive cytoplasmic membranes⁶⁸ (Figure 10).

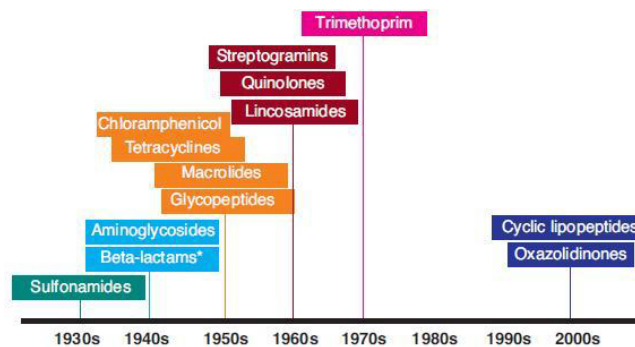


Figure 10. Antibiotics discovered since 1930 to 2000.⁶⁹

So, the increasing and alarming onset and spread of antibiotic resistant strains among pathogenic bacteria together with the unfavorable economics of antibiotic development poses as an urgent need the identification of new antibacterial agents that have a novel mode of action.⁷⁰ Target-driven discovery of novel antibiotics offers the advantage of prior knowledge of the protein/pathway target function

thus potentially expediting the drug discovery process,^{71,72} but a crucial point for the success of this approach is the identification/selection of the appropriate molecular target.

The LPS export to the OM represents an attractive underexploited bacterial pathway, since several features of the Lpt transport proteins suggest that they could be good candidates as antibacterial targets:

- LPS is an essential structure in most Gram-negative bacteria;
- the components of the Lpt machinery are essential;
- the proteins are conserved in many relevant bacterial pathogens;
- the Lpt proteins do not have human counterparts, as LPS is a molecule exclusively present in bacteria.

Despite the Lpt proteins have been only very recently discovered and characterized, two inhibitors of the machinery have already been identified. The first compound targets LptB, the ATPase component of the IM ABC transporter.⁷³ This molecule has been identified by *in vitro* screening with 224 compounds from two commercially available kinase inhibitors libraries composed mostly of ATP-competitive inhibitors and, as expected, it is competitive with respect to ATP with an inhibitor binding constant of 5 μ M; however, it does not display antibacterial activity against a wild type strain of *E. coli* whereas it shows a minimum inhibitory concentration (MIC) against a strain of *E. coli* with a leaky OM. A peptidomimetic antibiotic specifically targeting LptD of *P. aeruginosa* is

the second example of LPS transport inhibitors.⁷⁴ The starting point of this work was the synthesis of libraries of β -hairpin-shaped peptidomimetics based on the membranolytic host defence peptide protegrin I.⁷⁵ Following whole-cell screening, a lead showing low but significant broad-spectrum antibacterial activity was found. This lead was optimized for improved antimicrobial activity through iterative cycles of synthesis and screenings. This effort produced two peptidomimetics POL7001 and POL7080 with potent and selective action only against *P. aeruginosa* (MIC 0.13 and 0.25 $\mu\text{g/ml}$, respectively). Overall, the Lpt machinery could represent a composite cellular target that offers the opportunity not only to inhibit the function of any single protein but also to exploit different aspects of LPS biogenesis, namely the assembly of the complex and its ability to bind LPS.

1.4. Host defences that target lipid A

Considering the intimate contact that humans have with bacteria, the frequency of colonization with pathogenic Gram-negative bacteria is astonishingly low. This is largely attributed to the formidable arsenal of host defences that eliminate invading pathogens by recognizing and responding to highly conserved components of infectious agents, known as Microbe-Associated Molecular Pattern (MAMPs).⁷⁶ Because LPS is an

essential component of the Gram-negative cell surface, it serves as an effective MAMP to trigger the innate immune system.⁷ The host offers a nutrient-rich but perilous environment for a bacterium. For example, the intestinal colonization requires a bacterium to journey through the acidic pH of the stomach and encounter toxic compounds such as bile and antimicrobials during transit,⁷⁷ and the bloodstream is swarming with LPS-binding proteins, antibodies, complement and immune cells primed to detect LPS.⁷⁸⁻⁸¹ Every point of entry for a bacterium is well defended, but as many of the protective mechanisms rely on lipid A detection, the modification of lipid A affords the bacterium an opportunity to evade the immune system and establish an infection.⁸²

1.4.1. LPS and immune system

LPS is a potent elicitor of innate immune responses and plays a key role in the pathogenesis of Gram-negative infections in both plant and animal hosts,⁸³ but also other bacterial products are believed to be responsible for initiating host immunological response leading to inflammation and sometimes unwanted septic shock in mammalian cells.

The immune system has both a less specific and a more specific component. The first one is the innate immune system, which represents the first line of defense against invading microorganisms in vertebrates

and the only line of defense in invertebrates and plants.⁸⁴ Most apparatuses of innate immunity are present before the beginning of infection and constitute a set of disease-resistance mechanisms that are not specific to a particular pathogen but that recognize classes of molecules characteristic of frequently encountered pathogens. Otherwise, the adaptive immune system, which is the more specific component of immunity, is characterized by highly specialized cells that process and eliminate the hosts, affording protection against re-exposure to the same pathogen.

The adaptive system is organized around T and B cells. Since each lymphocyte displays a different kind of unique receptor, the repertoire of antigen receptors is very large and diverse. This recognition diversity increases the probability that an individual lymphocyte will encounter a suitable antigen thereby triggering activation and proliferation of the cells. This process of clonal expansion is absolutely necessary to elicit a correct and efficient immune response. Despite the primary importance of this process, it requires 3 or 5 days to rise an appropriate response, which allows more than enough time for most pathogens to damage the host. The innate immunity compartment fulfills the necessity of a fast response against microbial, fungal or viral infections and directs a correct response of the adaptive compartment against non-self.⁸⁵

Innate immunity recognition relies on a diverse set of germ line encoded receptors, termed pattern recognition receptors (PRR), which recognize

broad classes of molecular structures common to groups of microorganisms, called Pathogen Associated Molecular Patterns (PAMPs),⁸⁶ triggering complex signalling cascades that lead to the release of pro-inflammatory cytokines. PAMPs share some common features:

- they are produced only by microbial pathogens and not by the host;
- structures organized are usually essential for the survival or pathogenicity of invading microorganisms;
- they are usually invariant features shared by entire classes of pathogens.

Bacteria are often recognized by the PRRs through some common components of the cell wall, such as lipid A of lipopolysaccharide, peptidoglycan, lipoteichoic acids and cell wall lipoproteins. There are several distinct classes of PRRs and the best characterized are the Toll Like Receptors (TLRs), non-catalytic receptors that recognize structurally conserved molecules derived from microbes, activating immune cell responses with high sensitivity and selectivity.⁸⁷

TLRs appear to be one of the most widespread and ubiquitous components of the immune system: they are present in vertebrates, as well as in invertebrates and they represent the host defence against infection in plants. It has been estimated that most mammalian species have between ten and fifteen types of TLRs and thirteen TLRs (named

TLR1 to TLR13) have been identified both in humans and mice (Table 1).⁸⁸ TLRs play a critical role in the recognition of PAMPs derived from various microbial pathogens including viruses, bacteria, protozoa, and fungi and in the subsequent initiation of innate immune responses.⁸⁹

Toll-like receptors recognize molecules that are constantly associated and specific for invading pathogens or cell stress. Pathogen-associated molecules that induce a TLR-mediated response are usually critical to pathogen's functions and cannot be eliminated or changed through mutation. From a structural point of view, all TLRs are characterized by two conservative regions: the extracellular leucine-rich repeat (LRR) domain and the TIR (Toll/Interleukin-1 Receptor) domain. The TIR domain is a conserved protein–protein interaction module, which is also found in a number of trans-membrane and cytoplasmic proteins in animals and plants,⁹⁰ involved in the innate immune response. Within the class of Toll-like receptors there are some differences: most of them function as homodimers, but TLR2 forms heterodimers with TLR1 or TLR6, each dimer having a different ligand specificity, and TLR10 seems to form both homodimers and heterodimers with either TLR1 or TLR2. TLRs may also depend on other co-receptors for full ligand sensitivity, such as in the case of TLR4's recognition of LPS, which requires MD-2, CD14 and LPS Binding Protein (LBP).

Receptor	Ligand	Origin of ligand
TLR1	Trypasil lipopeptides Soluble factors	Bacteria, Mycobacteria <i>Neisseria meningitidis</i>
TLR2	Lipoprotein/lipopeptides Peptidoglycan Lipoteichoic acid Lipoarabinomannan Phenol-soluble modulin Glycoinositolphospholipids Glycolipids Porins Atypical lipopolysaccharide Atypical lipopolysaccharide Zymosan Heat-shock protein 70	Various pathogens Gram positive bacteria Gram positive bacteria <i>Mycobacteria</i> <i>Staphylococcus epidermiditis</i> <i>Trypanosoma cruzi</i> <i>Treponema maltophilum</i> <i>Neisseria</i> <i>Leptospira interrogans</i> <i>Porphyromonas gingivalis</i> Fungi Host
TLR3	Double-stranded RNA	Viruses
TLR4	Lipopolysaccharide Taxol Fusion protein Envelope protein Heat-shock protein 60 Heat-shock protein 70 Type III repeat extra domain A of fibronectin Oligosaccharides of hyaluronic acid	Gram negative bacteria Plants Respiratory syncytial virus Mouse mammary - tumor virus <i>Chlamydia pneumonia</i> Host Host Host

	Polysaccharide fragments of heparin sulphate Fibrinogen	Host Host
TLR5	Flagellin	Bacteria
TLR6	Diacyl lipopeptides Lipoteichoic acid Zymosan	<i>Mycoplasma</i> Gram positive bacteria Fungi
TLR7	Imidazoquinolone Loxoribine Bropirimine Single-stranded RNA	Synthetic compounds Synthetic compounds Synthetic compounds Viruses
TLR8	Imidazoquinolone Single-stranded RNA	Synthetic compounds Viruses
TLR9	CpG-containing DNA	Bacteria and viruses
TLR10	N.D.	N.D.
TLR11	N.D.	Urophatogenic bacteria

Table 1. TLRs classification. Not described is noted as N.D.

1.4.2. TLR4

Among TLRs, TLR4 selectively responds to bacterial endotoxin, Gram-negative bacterial lipopolysaccharides and lipooligosaccharides (LOS). In addition, TLR4 recognizes a broad variety of substances from viruses, fungi, and mycoplasma. TLR4 is also activated by endogenous factors, generally known as danger (or damage) associated molecular patterns (DAMPs). Typical DAMPs acting as TLR4 agonists are endogenous substances that are released as a consequence of injury and inflammation. They include β -defensin, high-mobility group protein 1 (HMGB1), heat shock proteins (HSPs), hyaluronic acid, heparin sulfate, substance P, and others.⁸⁹ This receptor is present on a wide variety of cell types, including monocytes, lymphocytes and endothelial cells.⁷ Binding of TLR4·MD-2 to lipid A triggers a signalling cascade that leads to inflammation, cytokine production and the eventual clearance of bacteria through recruitment of effector cells, phagocytosis, cytotoxicity and activation of the complement system.⁸¹ This inflammatory response can be severe, resulting in tissue damage, organ failure and death, especially in cases of sepsis.⁷ Unmodified *E. coli* lipid A, which contains six acyl chains and two phosphate groups, is the strongest known TLR4 ligand, and lipid A modifications can weaken or abolish TLR4 signalling and change the nature of the downstream cytokine profile.⁹¹⁻⁹⁴

The detection of lipid A is achieved by the coordinate and sequential action of four endotoxin binding proteins: LPS binding protein (LBP), the cluster differentiation antigen 14 (CD14), the myeloid differentiation protein (MD-2) and TLR4 itself.⁹⁵ This sequential process starts with the binding of LBP to LPS aggregates, spontaneously released by Gram negative bacteria, and ends with the formations of the activated (TLR4·MD-2·LPS)₂ complex that has a pivotal role in initiating the inflammatory cascade. LBP interacts with endotoxin-rich bacterial membranes or endotoxin aggregates, catalyzing extraction and transfer of LPS monomers to CD14 that in turn transfers LPS monomers to MD-2 and to (TLR4·MD-2·LPS)₂ heterotetramer. Receptor dimerization leads to the recruitment of adapter proteins to the intracellular TIR domain of TLR4, initiating the intracellular signal cascade (Figure 11).

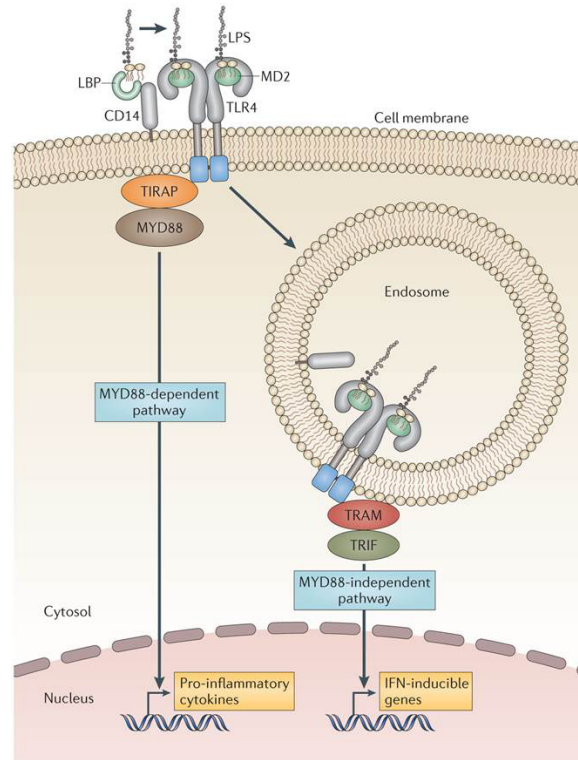


Figure 11. Schematic representation of Toll-like receptor 4 signalling in which the two responses, the MYD88-dependent and TRIF-dependent pathways are illustrated. They can be differentially stimulated on binding of lipid A to the TLR4–MD2 complex. This binding occurs through the association of lipid A with LBP and CD14, and leads to the production of cytokines and clearance of the pathogen. The MYD88-dependent pathway leads to the production of pro-inflammatory cytokines, whereas the less inflammatory TRIF pathway occurs after endocytosis of the TLR4–MD2 receptor and stimulates the expression of interferon-inducible genes that are less inflammatory than those cytokines induced by the MYD88-dependent pathway.⁸²

This complex can then signal through two major pathways, which are named according to their adaptor proteins: myeloid differentiation primary response protein 88 (MYD88) and TIR domain-containing adaptor inducing IFN β (TRIF; also known as TICAM1).⁹⁶ Severe reactions to LPS are attributed to activation of the MYD88 pathway, which induces the production of pro-inflammatory cytokines such as tumor necrosis factor (TNF), interleukin-6 (IL-6) and IL-12.

The less inflammatory TRIF (or MYD88-independent) pathway occurs after endocytosis of the TLR4–MD-2 receptor and is characterized by the production of interferon- β (IFN β) and IFN-inducible proteins such as 10 kDa IFN γ -induced protein (IP10; also known as CXCL10), monocyte chemoattractant protein 1 (MCP1; also known as CCL2), RANTES (also known as CCL5) and granulocyte colony-stimulating factor (G-CSF).⁹⁷ Although it is important for mounting an optimal immune response to pathogens, the TRIF pathway does not lead to severe inflammation. Unmodified LPS from *E. coli* induces signalling through both pathways, but lipid A modifications can cause preferential recruitment of one adaptor protein over the other.⁹⁸ *In vivo*, bacterial lipid A modifications are also known to affect the potency of TLR4 activation.¹²

1.4.2.1. LPS-binding protein (LBP)

Human LBP is a 58-60 kDa serum glycoprotein and is mainly synthesized by hepatocytes.⁹⁹ The tertiary structure of LBP contains two barrel domains arranged in a banana-like shape which are connected by a proline-rich linker. Each domain is composed of an antiparallel β -stranded layer twisted around the long α -helix. In the pocket between the helix and the β -strand, a phospholipid molecule has been co-crystallized in each domain.¹⁰⁰ The tip of the N-terminal domain of LBP contains a cluster of cationic residues, which are essential for the LPS binding and signalling. The phospholipid-binding site of LBP seems like a suitable site for binding of the lipid A moiety. However, the size of the binding pocket is by far too small to accommodate the acyl chains of the typical lipid A. Therefore, the location of the lipid A-binding site on LBP is not quite clear, since the distance between the cationic and hydrophobic site is also too large to allow the interaction of the lipid A molecule with both sites.

C-terminal domain of LBP present a region that promote the interaction with CD14 thus facilitating the transfer of the endotoxin. LPS response is enhanced by the serum LBP that disaggregates LPS micelles with the cooperation of soluble CD14 (sCD14); serum albumin also plays a role in facilitating the extraction of LPS monomers from the aggregates.¹⁰¹

Originally the role of LBP was assumed to be restricted to bind LPS and to transfer it subsequently to membrane-bound CD14. Newer data, however, suggest that the situation is more complex. LBP has a concentration-dependent dual role: low concentrations of LBP enhance the LPS-induced activation, in contrast, the acute phase rise in LBP concentrations inhibits LPS-induced cellular stimulation.¹⁰²

A second function of LBP is to increase the interaction of LPS with soluble CD14 (sCD14) by forming a stable trimolecular complex.¹⁰³ The complex then can be transported to lipoprotein particles or to cells, which can then respond to picomolar concentrations of LPS.

1.4.2.2. CD14

The cluster of differentiation antigen (CD14) has unequivocally been shown to represent an important LPS-binding molecule on monocytes/macrophages (mCD14). It is expressed in myeloid cells and serum (soluble form sCD14) and binds Gram-negative and Gram-positive bacteria as well as endogenous phospholipids.¹⁰² In whole blood, the amount of sCD14 is 100-1000 times higher than that of membrane-bound CD14. sCD14 is a single chain protein containing 10 leucine repeats in its carboxyl-terminal region; unlike the membrane form, which requires LBP, sCD14 can directly bind LPS with a dissociation

constant of 74 nM. Interaction of LPS with CD14 is necessary for specific binding of LPS and activation of human monocytes or murine macrophages. CD14 knock-out mice were found to be resistant to lethal shock induced by either live Gram-negative bacteria or isolated LPS demonstrating the essential role of CD14 in endotoxicity *in vivo*. At low concentrations of LPS, CD14 is required for a cytokine response in macrophages, at high concentrations, however, the responses are independent of CD14. It has been found that the strongest CD14-dependent responses require LPS with a long carbohydrate chain, whereas the CD14-independent response is expressed by LPS with short carbohydrate chain.¹⁰²

The monomeric subunit of CD14 contains 13 strands and 11 of them (from 3 to 13) overlap with conserved leucine-rich repeats (LRRs). The concave surface of the horseshoe-shaped structure consists of a large β -sheet of 11 parallel and 2 antiparallel β -strands. The convex surface contains both helices and loops in no regular pattern, so it is rugged, with several grooves and pockets that are crucial for ligand binding. The main characteristic of its structure is the N-terminal pocket which is hydrophobic except for the perimeter. The main pocket is both wide and deep and contains a smaller sub-pocket at the bottom. This sub-pocket is narrow and deep and formed by hydrophobic residues and connecting loops. Overall, the pocket including the sub-pocket is large enough to accommodate at least part of the lipid chains of LPS. The binding sites for

LPS in CD14 have been intensively studied by mutagenesis and by epitope mapping of antibodies that block LPS binding and 4 regions have been identified within the N-terminal 65 residues.¹⁰⁴⁻¹⁰⁵ Deletion or missense mutations in these regions significantly reduce LPS binding or responsiveness.¹⁰⁶ All of these regions are clustered around the pocket: region 1 is located close to the wall, region 3 is at the bottom of the pocket, regions 2 and 4 are located on the rim of the pocket. Based on structural findings it was proposed that the lipid portion of LPS binds to the N-terminal pocket. It is unlikely that binding of LPS induces a global structural change of CD14, since many residues making up the hydrophobic pocket are in conserved LRR motifs and the overall shape of LRR proteins displays limited variability.

The LPS-binding site of CD14 appears to extend further beyond the N-terminal pocket and includes grooves in the neighboring area. The structural characteristics of the binding site may explain the broad ligand specificity of CD14. Although the hydrophobic bottom and walls of the pocket are rigid, the generous size of the pocket may allow structural variation in the hydrophobic portion of the ligand. Structural diversity in the hydrophilic part of the ligands could be explained by the considerable flexibility of the hydrophilic rim combined with the multiplicity of grooves available for ligand binding. To initiate the signalling, LPS bound to CD14 should be transferred to the TLR4/MD-2 complex on the cell membrane. Several studies have reported that

mutations in the region 1 block LPS binding and others LPS transfer, indicating that this region plays a role in LPS binding and transfer.¹⁰⁷ In addition, all the mutations are located in the same area near the N-terminal pocket, suggesting that the area close to the pocket plays an important role in the transfer of LPS from CD14 to the TLR4/MD-2 complex.

1.4.2.3. TLR4 and MD-2

The primary sequence of TLR4 has the typical features of a class 1 transmembrane receptor, with an extracellular domain (608 residues), a single membrane spanning helix and a globular cytoplasmic domain (187 residues), the TIR. The ectodomain of TLR4 (TLR4-ECD) has 21 LRRs capped by LRR-NT and LRR-CT motifs with a horseshoe-like shape. Three subdomains can be differentiated, N-terminal, central and C-terminal, with different degrees of twist and curvature. The central subdomain contains only one variable residue between the last leucine residue of a preceding LRR motif and the first leucine residue of the next LRR motif, in contrast with the standard two variable residues. The length of these LRR modules also varies between 20 - 30 residues, conferring a smaller radius and greater twist angle to the subdomain. The central subdomains

of human and mouse TLR4 differ most in structure, apparently due to the MD-2 binding to the mTLR4 LRR9 loop.¹⁰⁸

MD-2 is a co-receptor molecule that binds both the extracellular domain of TLR4 and the hydrophobic portion of LPS.¹⁰⁹ MD-2 is a 160- aminoacid glycoprotein with a 16 aminoacids secretion signal at the N-terminal and represents a class of MD-2-related lipid recognition proteins¹¹⁰ that also include mite allergen proteins. MD-2 has a β -cup fold structure composed of two antiparallel β -sheets: one sheet consists of 3 antiparallel β -strands and the other one consists of 6 antiparallel strands. These sheets form a large and deep hydrophobic pocket for ligand binding.^{104,111} LPS binds to this pocket and directly mediates dimerization of the two TLR4–MD-2 complexes (Figure 12 a). The primary contact interface between TLR4 and MD-2 that is formed before LPS binding involves two chemically distinct regions, the A and B patches provided by the N-terminal and the central domains of TLR4, respectively. The main dimerization interface of MD-2 is located on the opposite side of the primary interface and interacts with LRR modules 15 - 17 in the C-terminal domain of TLR4 (Figure 12 a). For dimerization, TLR4 forms hydrophobic and hydrophilic bonds directly with LPS and the surrounding F126 and L87 loops of MD-2. In addition, several secondary interactions contribute to the dimerization: a metal ion found near the 49-phosphate group appears to connect the MD-2–LPS complex to TLR4

either directly, or indirectly through water molecules; TLR4 makes an additional contribution to dimerization by directly contacting TLR4*.⁹¹

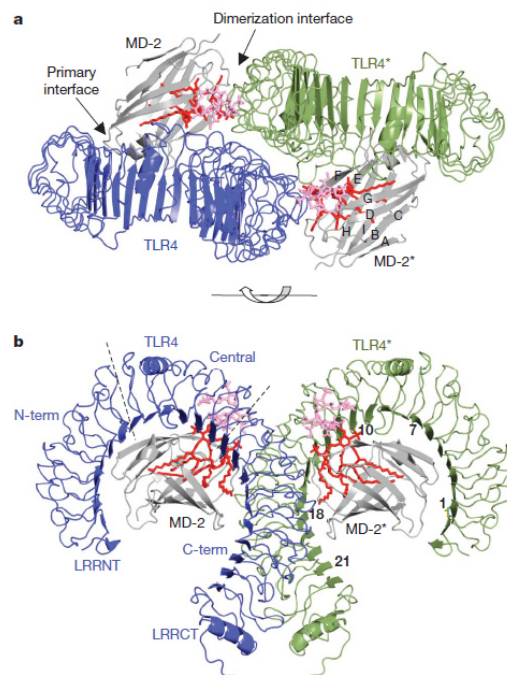


Figure 12. a) Top view of the symmetrical dimer of the TLR4–MD-2–LPS complex. The primary interface between TLR4 and MD-2 is formed before binding LPS and the dimerization interface is induced by binding LPS. **b)** Side view of the complex. The lipid A component of LPS is coloured red, and the inner core carbohydrates of LPS are coloured pink. The module numbers of the LRRs in TLR4 and the names of the β -strands in MD-2 are written in black. TLR4 is divided into N-, central and C-terminal domains. The LRRNT and LRRCT modules cover the amino and carboxy termini of the LRR modules.⁹¹

1.5. Syndromes due to deregulated TLR4 pathway activation

The described activation of TLR4 pathway and the subsequent intracellular signalling in response to bacterial endotoxins are useful processes necessary for optimal host immune responses; however, an excessively potent and deregulated TLR4 activation and signalling cause severe syndromes such as septic shock, associated with a high mortality. Once bacteria are present in the bloodstream (bacteremia), LPS is released from the outer leaflet of the cell wall of Gram negative bacteria. Manifold interactions of LPS with host factors have been described, such as the activation of the complement system, activation of immune cells, and interaction with a variety of serum proteins. The most prominent activity of LPS is its immunostimulatory potency leading to the complex clinical syndrome of Gram-negative sepsis when the initial host response to an infection becomes dysregulated. The clinical manifestation of sepsis is characterized by fever, hypotension, respiratory and renal failure, and intravascular disseminated coagulation. These effects are not the result of LPS toxicity but are rather a consequence of cell activation by LPS and a subsequent dysregulation of the inflammatory host response.¹¹² The pathogenesis of sepsis is very complex and is dependent in part on the individual organism causing the syndrome. Pro-inflammatory cytokines (IL-6 and TNF- α) are released by innate immune system cells in response to recognized factors and bacterial motifs,

which synergize to further stimulate T-cell and B-cell responses, often with tissue-damaging consequences. Platelet activating factor, leukotrienes, and prostaglandins are released, along with other bioactive metabolites of the arachidonic pathway, priming additional granulocytes to release toxic oxidative radicals. Septic shock eventually ensues, leading to outcomes of multiple organ failure and poor prognosis.²

Treatment is most likely to be effective if it is begun early in the infection, but diagnosis of septic shock in its early stages is not straightforward, because the early symptoms of shock (fever, hypotension, and tachycardia) are nonspecific. Also, the transition from the early stages to multiple-organ failure can occur with frightening rapidity. Even if bacteria are the microorganisms most frequently implicated in septic shock, many different species of Gram-positive and Gram-negative bacteria can cause shock and no single antibiotic is effective against all of these bacterial pathogens.

In the last years, also other syndromes have been related to the deregulation of TLR4, including asthma, cardiovascular disorder, diabetes, obesity, metabolic syndrome, autoimmune disorders, neuroinflammatory disorders, neuropathic pain, CNS disorders such as amyotrophic lateral sclerosis and Alzheimer disease, psychiatric diseases, skin inflammations (dermatitis), psoriasis, and some tumors. Considering that the majority of these pathologies, including septic shock, still lack specific pharmacological treatment, it's clear the increasing interest to

found new molecules able to inhibit TLR4 activation, acting as antagonists.⁸⁹ By the contrast, molecules that activate TLR4 pathway (agonists) can be employed as vaccine adjuvants.^{98,113}

1.5.1. Modulation of TLR4 pathway

A number of natural and synthetic immunomodulators targeting TLR4 have been identified. They can inhibit (antagonists) or activate (agonists) the TLR4 pathway at different levels, by binding and sequestering LPS, antagonizing LBP and CD14/LPS interactions, and targeting of MD-2, TLR4-MD-2, or TLR4.¹¹⁴

One of the most successful approaches for down-regulation of TLR4 signalling involves application of compounds which compete with endotoxic LPS in binding to the same site on MD-2 and, thereby, inhibit the induction of the signal transduction pathway by impairing LPS-initiated receptor dimerization. To date, several lipid A variants that specifically block the LPS-binding site on human (h) MD-2 have been identified, such as lipid IVa (a biosynthetic precursor of *E. coli* lipid A) and a nonpathogenic lipid A from *R. sphaeroides*, which served as structural basis for the synthetic antisepsis drug candidate Eritoran (E5564). Ground-breaking X-ray structural analyses of variably acylated lipid A bound to MD-2/TLR4 complexes revealed strikingly different modes of

binding of agonistic and antagonistic ligands. All four acyl chains of the tetraacylated antagonists Eritoran and lipid IVa were fully inserted into the hydrophobic binding pocket of hMD-2. The binding of the ligand did not induce dimerization of hMD-2/TLR4–Lipid A complexes, therefore, the intracellular signalling cascade was not initiated (Figure 13 B). In contrast, the orientation of endotoxic hexaacylated *E. coli* lipid A within the binding pocket of MD-2 was turned by 180°. Only five long-chain acyl residues were intercalated in the interior of the binding cavity, whereas the sixth acyl chain was exposed onto the surface of MD-2, constituting, together with the patch of hydrophobic amino acids (Phe126 loop), the core hydrophobic interface for the interaction with the second TLR4*/MD-2*–LPS complex (Figure 13 D). Hydrophobic contacts of the exposed acyl chain of lipid A with the second TLR4*, along with intermolecular ionic interactions of the lipid A phosphates, triggered the formation of an active homodimeric signalling ligand–receptor complex. Remarkably, tetraacylated lipid IVa acts as antagonist on human but as an agonist on mouse TLR4 presenting one lipid chain on the surface of mMD-2, which reveals striking similarity to the crystal structure of hexaacylated lipid A–hMD-2/TLR4 (Figure 13 C, D).

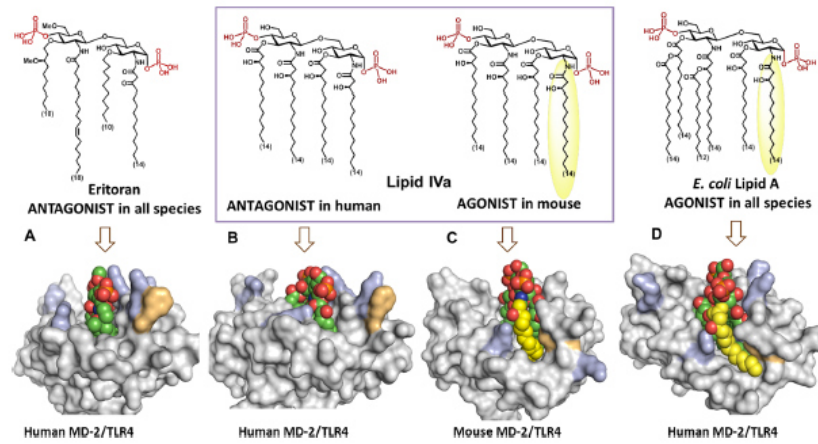


Figure 13. Side view of PDB co-crystal structures of (A) hybrid TLR4/hMD-2 with bound antagonist Eritoran (TLR4 is not shown); (B) hMD-2 with bound antagonist lipid IVa; (C) mTLR4/MD-2 with bound agonist lipid IVa; (D) hTLR4/MD-2 with bound *E.coli* Re-LPS (for clarity only lipid A portion is shown). Orientation of the ligand is inverted by 180° for parts C and D. Arg and Lys involved in ionic interactions with 1- and 4'-phosphates of lipid A at the rim of the binding pocket of MD-2 are depicted in blue; Phe126 is in orange. Phe 126 points outside in antagonist co-crystal structures (A, B) and is located inward in agonist structures (C, D) wherein Phe 126 establishes hydrophobic contacts to the exposed lipid chain (in yellow).

This species-specific activity of lipid IVa is attributed, among other factors, to the dissimilarities in the shape of the hydrophobic binding pocket of h- and mMD-2 and to the variations in the electrostatic potentials at the rim of the binding cavity of MD-2 and at the dimerization interface. However, particular structural features of the

ligand, such as lipid IVa, which could be responsible for the species-specific TLR4 activation have not yet been assessed. Despite a huge volume of accumulated data on the activity of both isolated and synthetic lipid A derivatives, there is no universal correlation between the chemical structure of lipid A and its function in TLR4/MD-2 complex, which would allow the prediction of biological activity of a particular lipid A variant. Subtle differences in the length and distribution pattern of acyl chains, changes in the volume and the overall shape of the hydrophobic portion of lipid A, as well as the phosphorylation status of the diglucosamine backbone are known to profoundly affect the biological activity of lipid A.¹¹⁵

1.5.2. Synthetic TLR4 modulators

The chemical modification of the lipid A structure is a well-established approach to obtain TLR4 active molecules. Modifications of fatty acid acyl chains of lipid A, namely, the removal of two or more fatty acid chains, give the so-called underacylated lipid A variants containing less than six acyl chains.⁸⁹ E5531 (Figure 14) is a first generation lipid A analogue, derived from the lipid A structure from the endotoxin of *Rhodobacter capsulatus*. It blocks LPS *in vitro* without any endotoxin-like activity. E5531 protects mice from lethal doses of LPS and viable *E. coli*

infections in combination with antibiotics. It also blocks the endotoxin response in human healthy volunteers exposed to intravenous LPS. Some issues on E5531, such as decreased activity over time in human blood due to the interaction with plasma lipoproteins, led to the search for second generation LPS antagonist.¹¹⁶

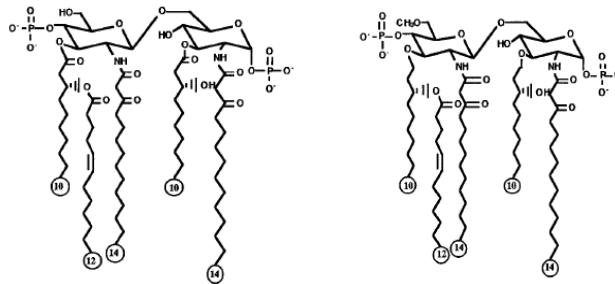


Figure 14. *R. capsulatus* lipid A (left) and its synthetic derivative E5531 (right).

Like E5531, E5564 (Eritoran, Figure 15) is a stable synthetic molecule derived from the nonpathogenic *Rhodobacter sphaeroides*, developed by Eisai (Tokyo, Japan). E5564 is a TLR4 pure antagonist that potently inhibits endotoxin-mediated activation of immune cells *in vitro* and in animal models. The crystal structure of the TLR4·MD-2 complex with bound Eritoran was recently described and suggests that Eritoran directly binds to the hydrophobic pocket of MD-2, competitively inhibits

LPS from binding to MD-2 and prevents the dimerization of TLR4, as well as TLR4 signalling.¹¹⁴ Consequently, Eritoran blocks the *in vitro* production of cytokines in human whole blood and induces a downregulation of intracellular generation of pro-inflammatory cytokines. In addition, Eritoran could also modulate other noninfectious disease processes, using TLR4 pathway, such as myocardial ischemia-reperfusion syndrome.^{116,117}

Lipid A dephosphorylation or replacement of the reducing-end sugar with an amino acid allowed not toxic TLR4 stimulants to be obtained with agonist action. Synthetic low toxicity TLR4 agonists monophosphoryl lipid A (MPLA) and aminoalkylglucosaminide 4-phosphates (AGPs) (Figure 15) are in use as vaccine adjuvants and in cancer immunotherapy.^{98,118} Other TLR4 agonists and antagonists were obtained by lipid A structure simplification, including monosaccharides (GLA and ONO compounds)^{86,119} (Figure 15) and mimetics with a linear backbone (ER112022). These compounds are amphiphilic molecules with a polar (charged) head linked to a variable number of lipophilic chains. The amphiphilic character results in the formation of micelles in an aqueous environment above their critical micellar concentration (cmc) that is normally very low (nanomolar range). As a consequence, aggregated forms of synthetic lipid A mimetic and of natural lipid A and LPS should predominate in the concentration range relevant for biological responses and for biochemical characterization *in vitro*.

Accordingly, variables in the aggregation state and in the 3D form of endotoxin or synthetic molecule aggregates may directly influence the kinetics and potency of TLR4 activation and signalling.

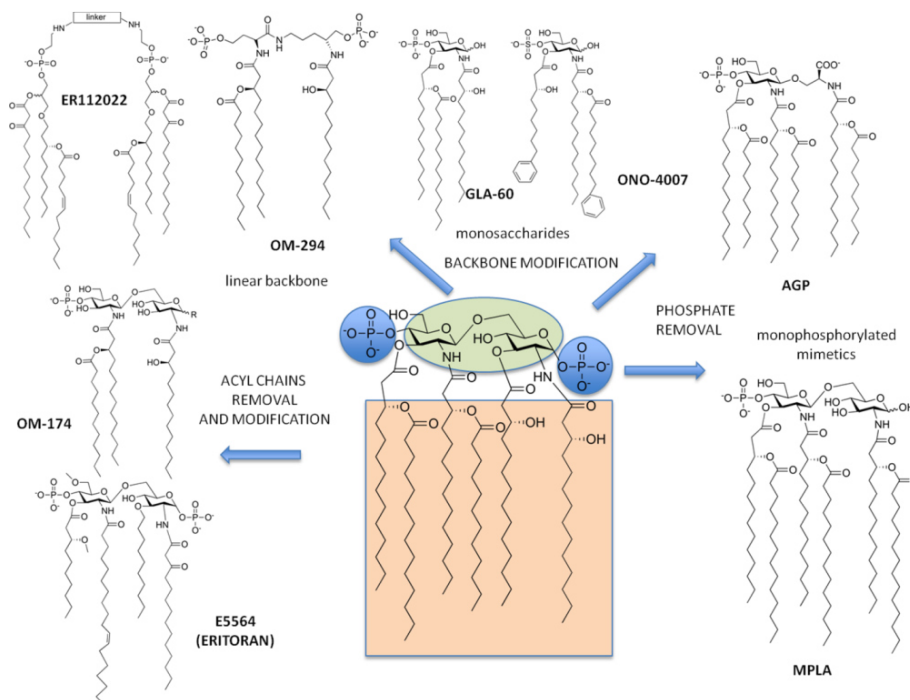


Figure 15. TLR4 agonists and antagonists obtained by chemical elaboration of *E. coli* lipid A structure.⁸⁹

Differences in lipid A/LPS molecular structure may therefore influence the kinetics and potency of TLR4 activation by affecting the 3D structure of aggregates of these molecules to which LBP, albumin, and CD14 must first interact to yield the monomeric endotoxin–protein (CD14, albumin) complexes that provide endotoxin monomer to MD-2 and MD-2·TLR4. Moreover, aggregates structure influences the geometry of monomeric endotoxin·MD-2·TLR4 complexes that determine TLR4 agonist or antagonist function. Another important consequence of the amphiphilic character of these molecules is their low water solubility which sometimes complicates their handling *in vitro* and *in vivo*, and it is associated with poor distribution properties.

While the described synthetic and natural variants of lipid A are anionic amphiphiles, also cationic amphiphiles, such as polyamines, are active in modulating the TLR4 signaling, by acting as “LPS sequestrant” forming stable aggregates with LPS molecules or interacting directly with LBP or CD14.¹²⁰ Different series of monosaccharidic glycolipids were found to activate or inhibit LPS-TLR4 signalling. Positively charged glycolipids with two C14 alkyl chains and a protonatable amine group on position C-6 of a methyl- α -D-glucopyranoside (iauxo 101 and iauxo 102, Figure 16) and aromatic compound iauxo 103 (Figure 16) inhibited TLR4 signalling *in vitro* and suppressed some TLR4-related pathologies such as acute sepsis and neuropathic pain in mice.¹²¹ Experiments with purified receptors and NMR binding studies showed that iauxo compounds bind CD14 with

higher affinity than MD-2.¹²² Despite the striking structural difference with negatively charged lipid A, cationic iaxo compounds are active as TLR4 antagonists.

Synthetic serine-based analogues of α -galactosylceramide, in particular compounds 729 (CCL-34, Figure 16), stimulated TLR4-dependent TNF- α production, while the natural α -galactosylceramide turned out to be inactive. Some variants of this molecule have been recently synthesized to unravel the relationship between their chemical structures and immunostimulating properties. While the anomeric α -configuration is essential to the biological activity, the galactose moiety can be replaced by other monosaccharides (α -fucose, α - or β -glucose, α -galacturonic acid) retaining the TLR4-stimulating activity, as assessed by experiments on HEK cells stably transfected with TLR4, MD-2, and CD14 receptors.

An alternative strategy to target TLR4 is to design low molecular weight inhibitors with a chemical structure totally different from lipid A, as in the case of compound TAK 242 (ethyl-(6R)-[N-(2-chloro-4-fluorophenyl) sulfamoyl] cyclohex-1-ene-1-carboxylate) (Takeda pharmaceuticals)¹²³ (Figure 16). TAK 242 is a small compound developed to inhibit inflammatory mediators production. It initially was demonstrated to decrease NO and various cytokines production in LPS stimulated mouse macrophages, as well as in a mice endotoxin model. A further study demonstrated its ability to inhibit intracellular signalling, with decreased MAP kinases phosphorylation and $\text{I}\kappa\text{B}$ degradation, without any

interference with LPS binding to TLR4. Since the effects of ligands to other TLR were not affected, this effect was specific for TLR4. Takashima et al. only recently demonstrated that TAK 242 to inhibit TLR4 signalling by direct binding to a specific amino acid (Cys747) in the TLR4-intracellular domain, thus forming a covalent adduct with TLR4.^{116,124}

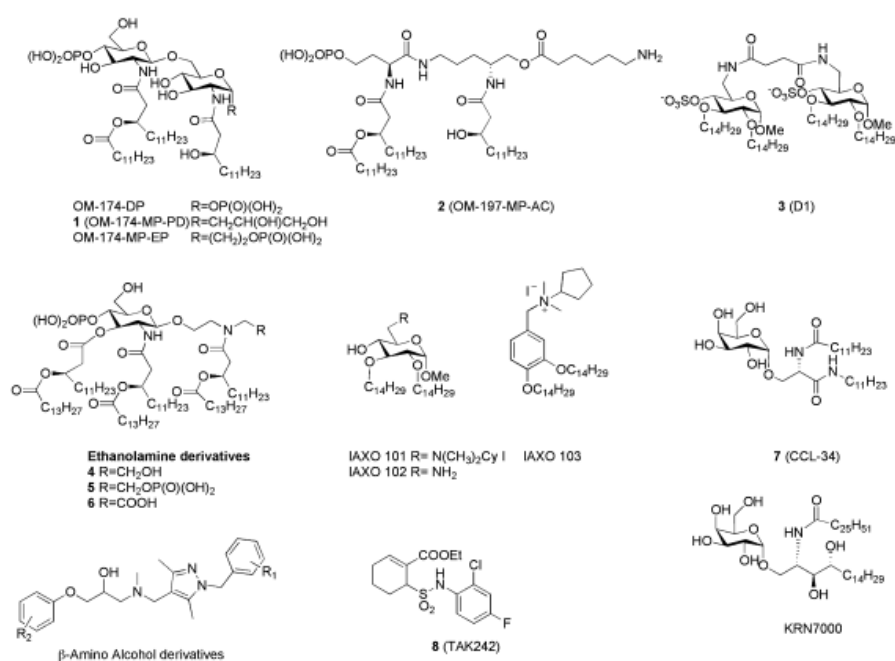


Figure 16. Recently developed synthetic TLR4 modulators (agonists and antagonists).⁸⁹

1.5.3. Natural TLR4 modulators

For thousands of years, natural products derived from plants, animals and microorganisms have been used as treatments for human diseases such as cancer, cardiovascular and inflammatory disease. Natural products with anti-inflammatory activity have long been used as a folk remedy for inflammatory conditions such as fevers, pain, migraine and arthritis. Recently, plant extracts and many herbs, used in traditional Chinese medicine and Ayurvedic medicine have been identified as potential modulators of TLR4. These include green tea, *Glycyrrhiza uralensis*, *Magnolia officinalis*, ginger (*Zingiber officinalis*), *Salvia miltiorrhiza* (red sage), and curcumin. Most of them are polyphenolic and aromatic compounds and their main mechanism of action is based on the formation of covalent bonds, which induces the disruption of TLR4·MD-2 heterodimer; indeed, compounds like isoliquiritigenin,⁹¹ 6-shogaol, caffeic acid phenethyl ester (CAPE) and cinnamaldehyde are able to form covalent adducts with solvent-exposed MD-2 and/or TLR4 cysteines.⁸⁹

Curcumin (**10** in Figure 17), a low molecular weight polyphenol, is derived from the rhizomes of the plant turmeric (*Curcuma longa*), which is endemic to peninsular India. Turmeric has been used to relieve pain and inflammation. Extensive scientific research including preclinical and clinical studies revealed that curcumin has anti-inflammatory action,

which is mainly due to the inhibition of arachidonic acid metabolism, cyclooxygenase (COX), lipoxygenase (LOX), cytokines interleukin (IL), TNF and NF- κ B. It has been shown that curcumin inhibits not only the κ B kinase (IKK) β in the MyD88 signalling pathway but also the MyD88-independent pathway upstream of Toll/IL-1R domain-containing adaptor-inducing IFN- β (TRIF). Gradisar et al. demonstrated that curcumin competes with LPS for the same MD-2 binding pocket without the formation of a covalent linkage with Cys133 exposed on the inner surface of the MD-2 hydrophobic pocket.¹²⁵

Sulforaphane (1-isothiocyanato-4-(methylsulfinyl)-butane, compound **11** in Figure 17) is an organosulfur compound obtained from cruciferous vegetables such as broccoli or cabbages. Several studies documented that the well-established anti-inflammatory activity of sulforaphane depends on suppression of TLR4 signalling.¹²⁶ It attenuates LPS-induced nitric oxide synthase (iNOS), cyclooxygenase-2 (COX-2), and tumor necrosis factor- α (TNF- α) production in macrophage cell lines and inhibits NF κ B translocation and I κ B α degradation in LPS-stimulated endothelial cells and suppress LPS-induced expression of inflammatory genes. Recently, it has been observed that sulforaphane preferentially forms adducts with Cys133 in the hydrophobic pocket of MD-2, blocking the interaction with LPS and lipid IVa.⁸⁹

Parthenolide is the major sesquiterpene lactone found in Mexican India medicinal plants and in feverfew (*Tanacetum parthenium*). It has shown

many antitumor effects against human acute myeloid leukemia, acute and chronic lymphocytic leukemia, and such solid tumors as breast and pancreatic cancer. Parthenolide has a strong anti-inflammatory effect *in vivo* and has long been used as a folk remedy for fevers, migraine and arthritis. Parthenolide exerts its anti-inflammatory effect by several mechanisms: it inhibits the expression of genes involved in inflammation such as nitric oxide (NO) synthase, intracellular adhesion molecule-1, and pro-inflammatory cytokines, TNF- α , IL-1, IL-4, IL-8 and IL-12. Park et al. have demonstrated that parthenolide inhibits TRIF-dependent signalling pathway of TLRs, showing that this compound inhibits NF- κ B and interferon regulatory factor 3 activation induced by LPS, and the LPS-induced phosphorylation of interferon regulatory factor 3 as well as interferon-inducible genes such as interferon inducible protein-10.¹²⁷

Green tea polyphenolic fraction possesses anti-inflammatory and chemopreventive effects and contains several active compounds which are catechin, (-)-epicatechin, (-)-epigallocatechin, (-)-epicatechin 3-gallate and (-)-epigallocatechin 3-gallate (EGCG). Among these, EGCG (**15** in Figure 17) is known to possess the most potent antioxidative and chemopreventive properties, and it has been demonstrated not to prevent LPS-induced dimerization of TLR4 but to inhibit the TLR4 signal downstream, blocking both MyD88- and TRIF-dependent signal pathways by targeting IKK β and TBK1 kinases, respectively.¹²⁸

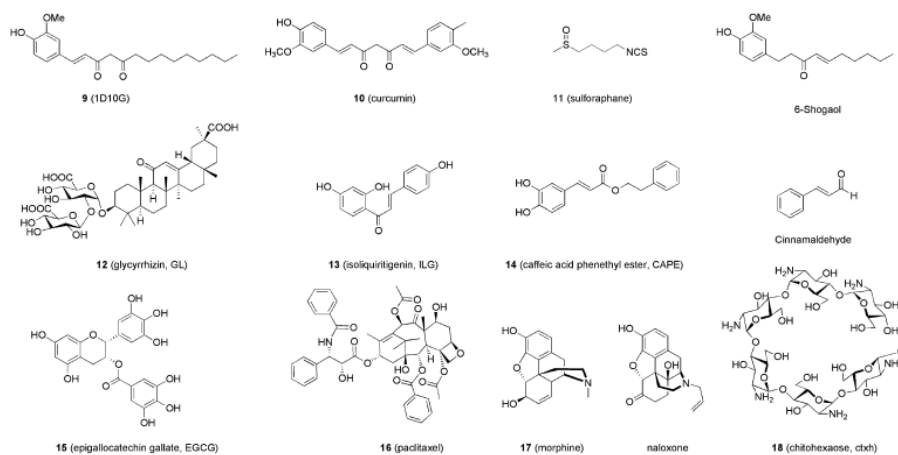


Figure 17. Some recently studied TLR4-active compounds from natural sources.⁸⁹

In the last years, it has been highlighted that dietary patterns such as the traditional Mediterranean diet of countries that surround the Mediterranean Sea may confer protection from certain chronic diseases related to oxidative stress, inflammation and the immune system. The traditional Mediterranean diet is characterized by a large amounts of foods naturally derived and in comparison with other healthy diets, Mediterranean diet has a high content of total fat as its most distinctive feature. This is due to the usual high intake of olive oil, from olive tree (*Olea europaea*). Virgin olive oil (VOO) is composed by a glycerol fraction and a non-glycerol or unsaponifiable fraction.

The main component of the olive oil is monounsaturated oleic acid and the others major fatty acids present are the polyunsaturated linoleic acid and the saturated palmitic acid. In addition, extra virgin olive oil (EVOO) is rich in phenolic compounds, whereas other vegetable oils do not contain them. Traditionally, the beneficial effects of VOO have been attributed to its high content in oleic acid as it protects lipoproteins and cellular membranes, from oxidative damage. In addition to oleic acid, evidences have accumulated on the favourable properties of minor though highly bioactive components of VOOs, particularly the phenolic compounds, which have shown a broad spectrum of antioxidant, free radical scavenger and anti-inflammatory effects commonly associated with the origin of the main chronic diseases. There are at least thirty-six structurally distinct olive oil phenolics that have been identified¹²⁹ (Table 2).

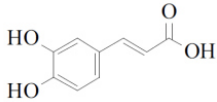
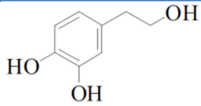
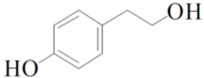
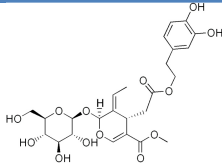
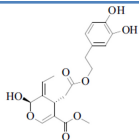
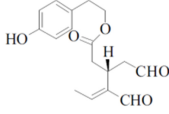
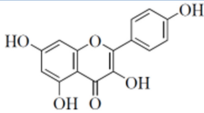
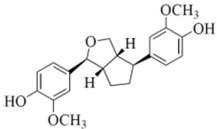
Group	Name of compound	Structure
Cinnamic acid derivatives	Caffeic acid	
Phenolic alcohols	Hydroxytyrosol/ 2-(3,4-Dihydroxyphenyl) ethanol/ 3,4-DHPEA	
	Tyrosol p-Hydroxyphenyl ethanol/ 4-Hydroxyphenylethanol/ p-HPEA	
Secoiridoids	Oleuropein	
	Oleuropein aglycone/3,4-DHPEA-EA	
	Oleocanthal /p-HPEA-EDA	
Flavonoids	Kaempferol	
Lignans	(+)- Pinoresinol	

Table 2. Chemical structures of the main phenols present in virgin olive oil.

Thus, they can be grouped according to their similar chemical structure in the following groups:

- Phenolic acids: which have the basic chemical structure of C₆–C₁ for benzoic acids and C₆–C₃ for cinnamic acids. These compounds can be divided into three subgroups: i) benzoic acid derivatives, ii) cinnamic acid derivatives, and iii) other phenolic acids and derivatives.
- Phenolic alcohols: which have a hydroxyl group attached to an aromatic hydrocarbon group (hydroxytyrosol, tyrosol, vanillic acid, caffeic acid, syringic acid, ocoumaric, protocatechuic, p-hydroxybenzoic). Hydroxytyrosol is the most potent phenolic antioxidant of olive oil and olive mill waste water which biological activities have stimulated research on its potential role in cardiovascular protection.
- Secoiridoids: which is characterized by the presence of either elenolic acid or elenolic acid derivatives in their molecular structure (oleuropein glucoside and the aglycone form of oleuropein, oleocanthal and ligstroside).¹³⁰
- Hydroxy-isocromans: 3,4-dihydro- 1Hbenzo[c]pyran derivatives mainly naturally occurring in nature as part of a complex fused ring system.¹³¹⁻¹³³
- Flavonoids: which contain two benzene rings joined by a linear three carbon chain. They can be further divided into flavones and flavanols (e.g. apigenine, luteoline).

- Lignans: the exact structure of this type of phenolic is not well understood but is based on aromatic aldehydes condensation (pinoresinol (P), 1-acetoxypinoresinol, hydroxypinoresinol).¹²⁹

In vitro and *in vivo* studies have shown that olive oil phenols exhibited anti-inflammatory properties. NF-κB is recognized as a target of several anti-inflammatory agents, and its inhibition down-regulates the expression of various inflammation mediators, including TNF.¹³⁴ The most important phenolic compounds active as anti-inflammatory agents were found to be oleuropein,¹³⁵ hydroxytyrosol¹³⁶ and oleocanthal.^{137,138} A large number of *in vitro* studies support the anti-inflammatory actions of olive oil polyphenols. The explanation of these actions may be due to the ability of polyphenols to inhibit the pro-inflammatory activity of ROS-generating enzymes including cyclooxygenase-2 (COX-2) and inducible nitric oxide synthase (iNOS) and to modulate different intracellular signalling pathways from NF-κB to mitogen-activated protein kinases (MAPKs) through perturbation of redox-sensible networks in immune cells (Figure 18).

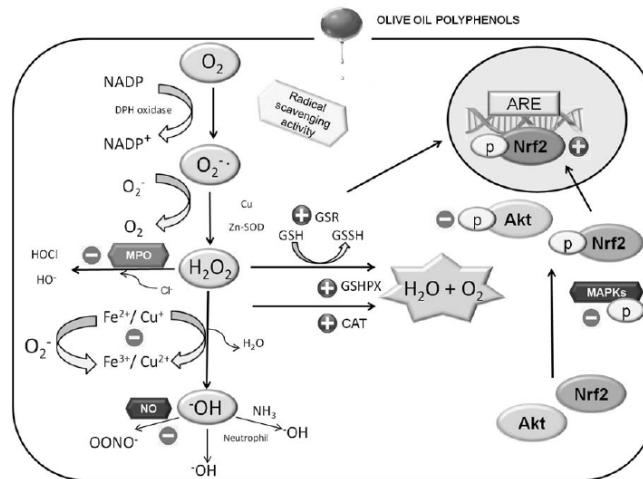


Figure 18. Anti-inflammatory pathways of olive oil polyphenols.¹²⁹

Maiuri et al. showed that hydroxytyrosol blocked the NF- κ B activation, but also the signal transducer and activator of transcription-1 α (STAT-1 α) and interferon regulatory factor-1 (IRF-1), suggesting that the polyphenol might represent a non-toxic agent for the control of pro-inflammatory genes.¹³⁶ EVOO phenolic extract and oleuropein-aglycone prevents the stimulation of MMP-9 expression in TNF- α - treated THP-1 cells, as demonstrated by Dell'Agli et al.¹³⁹ Oleuropein-aglycone was active at concentrations found in the extract (μ M range), although other compounds probably could contribute to the biological activity. They also found that the effect of the extract and individual compounds on MMP-9 was also due to impaired NF- κ B signalling, providing further evidence on the mechanisms by which EVOO reduces the inflammatory

associated disorders.¹³⁹ In 1993, oleocanthal, a new phenolic compound, present in the secoridoid fraction of VOO, was identified and chemically described as 2-(4-hydroxyphenyl)ethyl (3S,4E)-4-formyl-3-(2-oxorthyl)hex-4-enoate by Montedoro et al.¹⁴⁰ They found that this compound displayed non-steroidal anti-inflammatory activity similar to the non-steroidal anti-inflammatory drug ibuprofen. However, oleocanthal was more potent than ibuprofen at equimolar concentrations inhibiting the COX-1 and COX-2 expression.¹³⁸ Subsequent studies have shown that oleocanthal and some derivatives exhibit various modes of action in reducing inflammatory-related diseases, including neurodegenerative diseases, specific cancer and degenerative joint diseases, since they proved to be able to down-regulate iNOS protein expression in LPS-challenged chondrocytes, resulting in a reduction of nitrite production.¹³⁷

Also some flavonoids and lignans from olive oil (apigenin, luteolin and pinoresinol) have been associated with anti-inflammatory activity.^{141,142} In particular, the ability of several flavonoids to modulate the production of pro-inflammatory molecules from LPS-stimulated macrophages was compared and their mechanism of action was investigated. Pre-treatment of RAW 264.7 cells with luteolin and luteolin-7-glucoside inhibited both the LPS-stimulated TNF- α and IL-6 release and luteolin was the most potent in inhibiting cytokine production with IC₅₀ values of less than 1 μ M for TNF- α release.¹⁴²

The efficacy of olive oil phenolic compounds in *in vivo* inflammatory models has been also reported largely. Oleuropein-aglycone has anti-inflammatory activities in mice subjected to collagen-induced arthritis, improving histological status in the joint and paw, the degree of oxidative and nitrosative damage and plasma levels of the proinflammatory cytokines.¹²⁹ Martínez-Domínguez et al. have examined the effect of a VOO diet enriched with polyphenols (15% EVOO + 600 ppm phenols) in acute and chronic inflammation models in rats, describing important protective effects of this diet in both models of inflammation and improved the disease associated.¹⁴³ Finally, current epidemiological and experimental studies support a beneficial role of dietary polyphenols in several gastrointestinal diseases, including inflammatory intestinal bowel disease.¹⁴⁴

2. Purpose of the work

The lipopolysaccharide's (LPS) world appears very huge and complex, due to the large number of proteins with which it interacts. This work proposes to elucidate the binding of LPS with the bacterial protein LptC, belonging to Lpt machinery, and with TLR4, MD-2 and CD14, that form the receptor system of the innate immunity.

For the first purpose, we have developed an *in vitro* binding assay based on the co-purification of LptC and its ligand properly labeled. This assay has allowed us to determine for the first time the thermodynamic and kinetic parameters of this interaction. Since LPS biogenesis represents an interesting target to develop new antibiotics against Gram negative bacteria, the assay has also been used to study the binding between LptC and some small molecules, previously designed as TLR4 antagonists.

The second part of this thesis work consists in a detailed study of the modulation of TLR4 pathway by small molecules. In particular, the biological effects of different classes of synthetic compounds will be described in order to find a possible lead compound as TLR4 antagonist but also to understand the chemical features useful for the rational design of others. Finally, considering that a great number of natural compounds, in particular olive oil phenolics, have anti-inflammatory

properties, their possible correlation with TLR4 has been investigated, by evaluating the anti-inflammatory effects of the olive oil phenolic extracts and some isolated phenolic constituents on LPS-induced TLR4 pathway activation.

Section I

LptC-LPS binding studies

3. Results and discussion

An innovative biochemical approach to understand the molecular details of LPS transport across the periplasmic space consists in its dissection in single steps. Towards this aim, we needed to set up a sensitive and reliable method to reproduce *in vitro* the binding between LPS and Lpt proteins. Radiolabeled LPS is generally used for LPS binding studies, because radioactivity allows high sensibility, that is detection of labeled ligands at very low concentrations (nM to pM). However, radioactive ligands are relatively expensive, problematic to dispose of, and the short half-lives of some isotopes can be inconvenient. We tried to find alternatives to radioactive assay, turning to a colorimetric or fluorescent one. In particular, biotin (Bi) or fluorescein isothiocyanate (FITC)-conjugated LOS have been used for two different binding assays. In both assays a truncated version of LptC (lacking the first 23 amino acids of the transmembrane helix) fused to a N-terminal His₆-tag (sH-LptC) has been used as the model protein of Lpt complex. Several reasons have driven this choice: LptC shares the same folding of the other Lpt proteins, is the first located in the periplasm and is easier to purify, not being a membrane protein.

In this section, will be illustrated the setup of an *in vitro* binding assay, which has allowed to characterize the binding between sH-LptC and its natural ligand or synthetic compounds.

3.1. *In vitro* binding assay setup

3.1.1. ELISA-type assay with immobilized LptC, and signal amplification by gold nanoparticles (GNP)

The main problem of the replacement of radioactivity by other techniques consists in the decrease of sensitivity. We envisaged to solve this problem through the amplification of the ligand signal by using nanoparticles. Nanoparticles can be functionalized on their surface by several copies of the same molecule or by different molecules, covalently linked or non-covalently adsorbed. We envisaged the use of a method was similar to ELISA assay, but without the use of antibodies, based on the use of gold nanoparticles (GNPs) coated with several molecules of streptavidin (SV) and of horseradish peroxidase (HRP), that were synthesized in collaboration with Prof. Arben Merkoçi (Institut Català de Nanotecnologia, Barcelona, Spain).

sH-LptC, previously immobilized on Ni-NTA plates through His₆-tag, was incubated with biotin-LPS (Bi-LPS). Bi-LPS interacted with surface-immobilized LptC, and subsequently the complex was recognized by the

streptavidin present on GNPs. The detection occurred by the addition of the substrate of HRP also conjugated to GNPs. The multivalent presentation of SV and HRP on GNP should have ensured, in our project, an amplification of the signal, thus increasing the sensitivity in the detection of the formed LptC-LPS complexes.

The immobilization of LptC on Ni-NTA plates was checked by ELISA assay by using an antibody against LptC protein. The immobilized LptC-Bi-LPS complexes were then detected by adding GNP decorated with SV and HRP in solution, and a dose dependent LptC-LPS binding has been obtained (Figure 19, left).

To validate the method, competition assays have been performed by using a fixed amount of Bi-LPS (2 $\mu\text{g}/\text{ml}$) and increasing concentrations of unlabeled LPS (2-4 $\mu\text{g}/\text{ml}$) (Figure 19, right).

It's clear from the figure that unlabeled LPS is not able to displace Bi-LPS. The poor reproducibility of the competition assay, revealed that this method is not reliable to be used in quantitative characterizations of LptC-LPS binding.

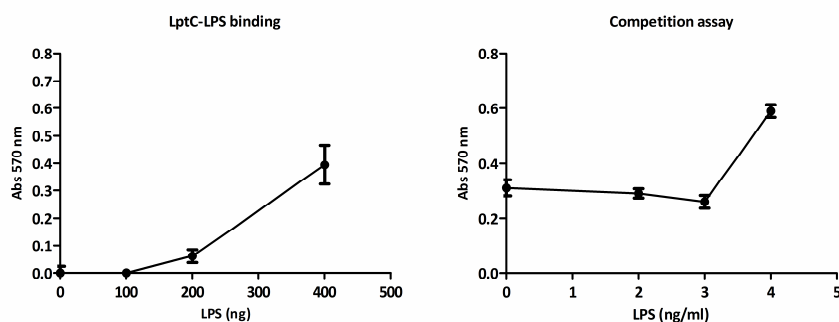


Figure 19. LptC-LPS binding: different amounts of Bi-LPS bind immobilized LptC in a dose dependent manner. **Competition assay:** effects of increasing concentrations of unlabeled LPS on LptC-Bi-LPS complex.

The results represent the average with SD of three independent experiments.

3.1.2 Co-capture assay on resin with fluorescent ligand

LPS-LptC binding has been extensively studied by Tran et al. through the co-capture assay, by which the authors demonstrated the capability of LptC to bind LPS.⁵⁷ Considering that fluorescence is another widespread method for binding studies, we projected to set up a co-capture assay properly modified to be applied to the use of a fluorescent rough type LPS (LOS).

The main issue with the use of commercial fluorescent LOS labeled by fluorescein (f-LOS) is the low level of fluorescence incorporation, and the

risk of altering LOS activity and binding properties by introducing the fluorescent moiety.

In this work a rough type LPS from *E. coli* MG1655 (LOS) has been used, unmodified or labeled by reacting it with fluorescein isothiocyanate (FITC), thus obtaining f-LOS. The purity and the chemical identity of f-LOS produced in our laboratory were assessed by NMR and SDS-PAGE analysis. The labeling ratio was determined to be 1:1 (LPS/FITC), higher than for commercial FITC-LPS from Sigma–Aldrich (~50:1 LPS/FITC). High levels of fluorescein incorporation are essential to obtain reliable signals in binding experiments.⁶⁰

The co-capture assay was based on the pre-incubation of sH- LptC with its natural ligand and the consequent capture of the LptC-LPS complex on Ni-NTA resin. The resin unbound complexes were removed (flow through - FT -), the resin bound complexes washed 3 times (wash fractions - W -) and then eluted (eluted fractions - E -). To verify the efficiency of the assay, the fluorescence of each collected fraction (FT, W and E) related to the total fluorescence has been considered. This evaluation has been performed for the samples with or without sH-LptC in order to consider the specific and nonspecific binding (Figure 20).

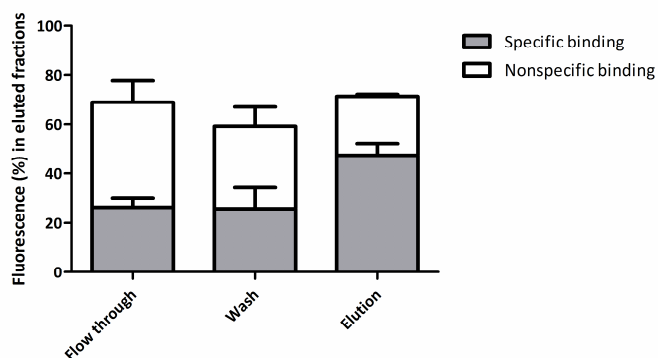


Figure 20. Fluorescence (%) present in the different fractions in samples containing sH-LptC (specific binding) and without sH-LptC (nonspecific binding).

We observed that the fluorescence detected in the eluates representing the specific interaction was 47.87%, about two-fold higher than the other collected fractions (FT = 26.73 ± 3.79% and W = 25.91 ± 8.58%). However, this percentage was strongly affected by nonspecific binding (24%) (Figure 20). Considering that the specific binding was affected by nonspecific interaction for about 50%, we hypothesized that some sites on the resin were available and responsible of nonspecific interaction with the ligand. In order to solve this problem, we saturated resin free binding sites by adding bovine serum albumin (BSA) to the buffer to wash the resin (before the capture of sH-LptC-LPS complex) (Figure 21, bar 1) or to the buffer to perform the wash steps (W) before the elution

(Figure 21, bar 2). As control, a co-capture assay without the addition of BSA to the buffers was included (Figure 21, bar No BSA).

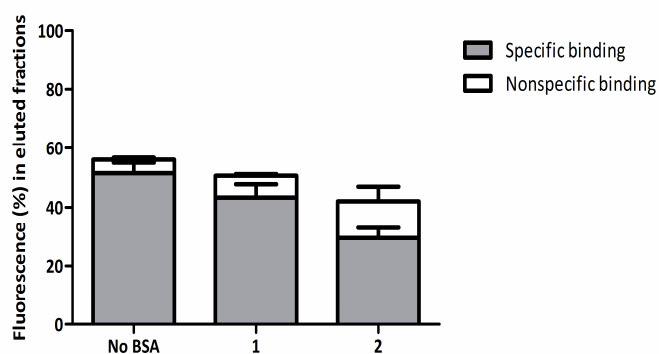


Figure 21. Effects on the specific and nonspecific binding of the addition of BSA in the buffer used to wash the resin (1) or immobilized LptC-LOS complex (2). The results represent the fluorescence (%) detected in the eluted fractions.

The addition of BSA 5% in both steps induced a decrease of the specific interaction and an increase of the nonspecific one, as evident considering the control (no BSA). Since the nonspecific binding appeared too high to perform binding characterization, this assay has been replaced by the co-purification assay.

3.1.3. Co-purification assay

In order to decrease the background due to the nonspecific interaction of f-LOS to the resin, a step of the co-capture assay has been reverted originating a co-purification assay, in which LptC-LOS binding occurred after the pre-immobilization of the protein on the resin. As for the co-capture assay, all the different fractions have been collected to well compare how the nonspecific binding (without LptC) affected the specific one (with LptC).

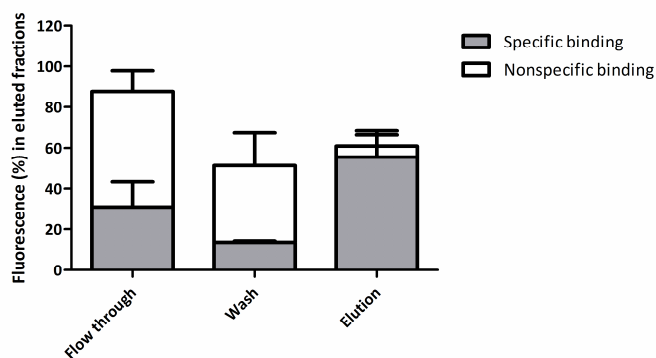


Figure 22. Fluorescence (%) present in the different fractions in samples containing LptC (specific binding) and without LptC (not specific binding).

In this way, both the fluorescence detected in the eluted fractions containing LptC and in the flow through fractions in absence of protein

increased, indicating a good decrease of the nonspecific binding that appeared 10% of the specific one. Whereas applying this protocol nonspecific interaction has been reduced by 80%, the co-purification assay has been used to quantify LptC-LOS binding *in vitro*. In particular, three types of binding experiments have been performed: kinetic, saturation and competition experiments.

3.2. Binding studies

3.2.1. LptC-LPS interaction studies: kinetic experiments

Kinetic experiments, where the binding of one or more concentrations of labeled ligand is measured at an incrementing series of time points, allow to estimate association (k_{on}) and dissociation (k_{off}) rate constants. In our studies, a fixed amount of f-LOS has been incubated with immobilized LptC for various periods and co-purification assays have been performed each 15 minutes (Figure 23). After 150 minutes, the dissociation kinetics have been performed by adding an excess of unlabeled LPS and sampling the eluates till 150 minutes (Figure 24). Nonspecific binding was calculated in different experiments to be less than 15% of the amount of absorbed f-LOS in the presence of the protein.

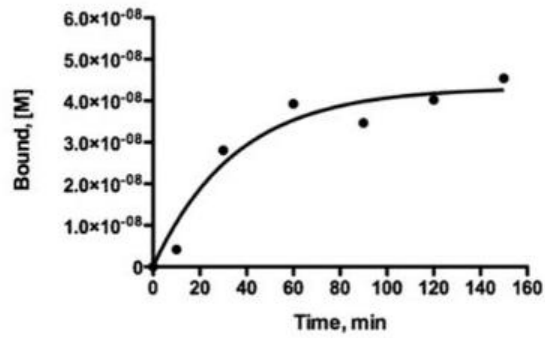


Figure 23. Association time-courses of f-LOS binding to immobilized LptC. The curve represents the fit to the appropriate equation (see Materials and methods) and is derived from analysis of three independent experiments, each in triplicate.

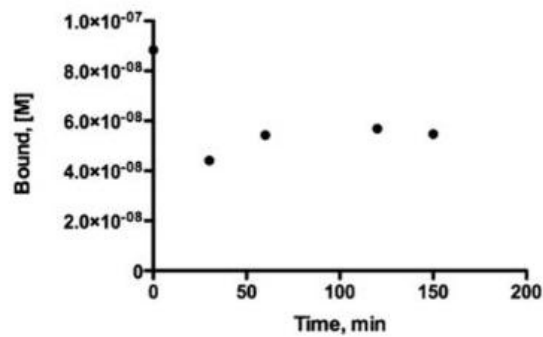


Figure 24. Dissociation time-courses of f-LOS binding to immobilized LptC. The curve represents the fit to the appropriate equation (see the Materials and methods) and is derived from analysis of three independent experiments, each in triplicate.

f-LOS specifically binds to LptC with a one-phase association rate constant ($k = 0.028 \text{ min}^{-1} \pm 29\%$ coefficient of variation (CV)), reaching maximum saturation with a half-time of 24.4 minutes. To note, f-LOS binding proved to be mostly irreversible, as dissociation time-course experiments with unlabeled LPS failed to displace the bound ligand (Figure 24). Consequently, it was not possible to calculate the true equilibrium constant, thus we report values for “apparent” K_d .

3.2.2. Saturation and competition experiments

In order to calculate the affinity of LPS for its transporter, equilibrium binding experiments have been performed by saturating LptC with increasing f-LOS concentrations (0.1 - 50 μM) (black square in Figure 25). These experiments have revealed that the affinity K_a was $1.4 \times 10^4 \text{ L/mol} \pm 27\%$ CV, corresponding to an apparent K_d of 71.4 μM . Although f-LOS - LptC binding was essentially irreversible, it has been possible to perform competition experiments, as long as the competing ligands are added simultaneously to the reaction mixture containing the binding target (white circles in Figure 25). Similar affinities for unlabeled LOS ($\text{IC}_{50} = 62.3 \mu\text{M} \pm 49\%$ CV; apparent $K_i = 35 \mu\text{M}$) and for f-LOS have been found, thus indicating that they interact with LptC and that the presence of the fluorescent moiety does not affect LPS binding properties. Therefore,

simultaneous analysis of saturation and competition curves allowed us to calculate the affinity of LOS for its transporter LptC as $K_a = 1.91 \times 10^4$ L/mol \pm 21 %CV corresponding to a $K_d = 52.4 \mu\text{M}$.

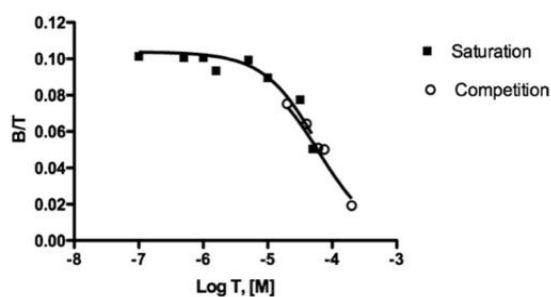


Figure 25. Saturation (0.1 - 50 μM f-LPS) and competition (10 μM f-LOS (tracer) competing with different concentrations of unlabeled LPS) curves of f-LPS binding to resin absorbed LptC under pseudo-equilibrium conditions. Binding is expressed as the concentration ratio of bound to total ligand (B/T), versus the logarithm of total unlabeled ligand concentration (log T).

LptC is an essential protein and the irreversible binding with its natural ligand appeared weird. So, in order to confirm these results, a different method, based on the quenching of LptC intrinsic fluorescence due to the presence of tryptophan residues, has been applied. LptC has two tryptophan residues: Trp94 buried in the hydrophobic cavity of the

protein and Trp77 exposed to the solvent at the edge of the β -jellyroll. Tryptophan fluorescence emission decreased progressively upon incubation with increasing f-LOS concentrations (Figure 25 A, insert), thus indicating that f-LOS is an efficient quencher of sH-LptC fluorescence. The upward curve at high f-LOS concentrations in Stern–Volmer plot (Figure 25 A) indicated that two distinct quenching mechanisms occurred: de-excitation of the fluorophore by random collisions with f-LPS molecules (dynamic quenching), due to Trp77, and formation of a LptC–f-LOS nonfluorescent complex (static quenching), ascribable to Trp94. K_d has been estimated of 28.8 μM , similar to that obtained by the co-purification method ($K_d = 71.4 \mu\text{M}$).

To evaluate the nature of the binding, Trp quenching has been monitored by keeping the ligand concentration constant and diluting the protein. The fluorescence values were normalized for protein concentration (as a function of the protein dilution factor), and compared to the expected values for reversible binding, by using the above-estimated K_d and K_{dyn} values (Figure 25 B). The experimental data deviate drastically from the theoretical trend (reversible binding); rather, they are consistent with simple progressive dilution of a fixed amount of fluorophore (this would be expected to yield a horizontal line in the plot), confirming that LptC–f-LOS binding is not reversible.

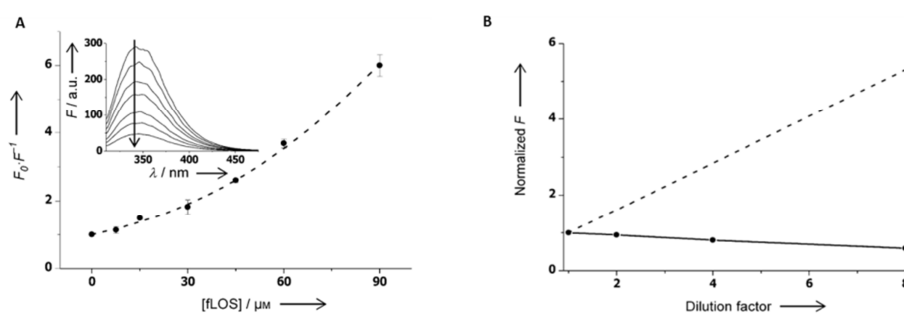


Figure 25. A) LptC fluorescence quenching by f-LOS. Relative fluorescence is plotted against total f-LOS concentration. The dashed line was obtained fitting data to Equation (6) (see materials and methods). Inset: fluorescence spectra (the arrow indicates the direction of spectral changes with increasing f-LOS concentration). **B)** Normalized fluorescence upon dilution of LptC–f-LOS complex. The dashed line indicates the expected trend for reversible binding with $K_d = 28.8 \mu M$.

3.2.3. LptC binding to synthetic ligands

laxo compounds (namely 101 and 102) (Figure 26) are glycolipids and benzylammonium lipids designed in our laboratory to act as TLR4 antagonists. They have been shown to potently modulate the CD14 and TLR4 pathway *in vitro* and *in vivo* and are efficient in rodent models of inflammatory diseases, neuropathic pain and LPS induced septic shock.¹⁴⁹ Structure-activity studies showed that the pharmacophore of laxo compounds is composed by the glucopyranosidic ring core, a

protonated (positively charged) nitrogen on C-6 position and two C14 linear aliphatic chains.^{122,150} As CD14 and LptC share the same ligand and the binding occur we explored the possibility that these molecules can be used as scaffolds to generate compounds able to bind and interfere with LptC activity. To test this idea, the compound iaxo-102 has been conjugated with fluorescein at the C-6 primary amine (compound **1**, chemical structure not shown). This conjugation should preserve the interaction with CD14, and consequently with LptC, because the interaction is due to the hydrophobic linear ether chains of iaxo-102, as previously shown by NMR analyses.

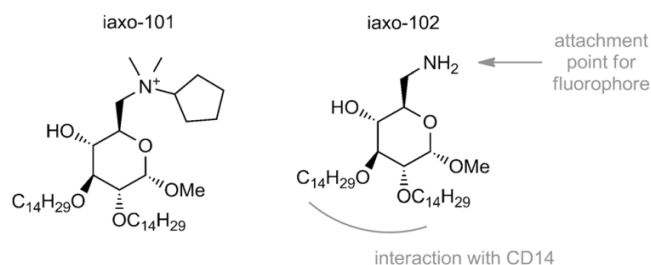


Figure 26. Chemical structure of iaxo 101 and iaxo 102. The site of interaction with CD14 and the attachment point for fluorescein are labeled in grey.

The LptC-compound **1** binding has been characterized by performing the same assays that have been used for LptC-LPS binding. Association and dissociation time-courses experiments (Figure 27 A and B) revealed that compound **1** rather rapidly and specifically bound to LptC, again with a one-phase association rate constant ($k = 0.058 \text{ min}^{-1} \pm 40 \text{ \%CV}$), and reached maximum saturation with a half-time of 12 min. Also in this case, binding of **1** proved to be essentially irreversible (Figure 29 B), because the unlabeled analogue was not able to displace compound **1**. The saturation (Figure 27 C, black square) and homologous competition (Figure 27 C, white circle) experiments have revealed affinities similar for iaxo-102 and **1** thus allowing pooling of the data and simultaneous analysis of saturation and competition curves. In particular, the affinity of iaxo-102 (K_a) was $4.52 \times 10^3 \text{ M}^{-1} \pm 36 \text{ \%CV}$ (apparent $K_d = 221 \text{ }\mu\text{M}$), statistically different ($p < 0.01$) but still in the range of affinity for LPS. To assess the specificity of iaxo-102 for LptC, heterologous competition experiments have been performed by incubating $50 \text{ }\mu\text{M}$ **1** (tracer) and increasing concentrations of unlabeled LPS. LPS was able to compete for the site occupied by **1** (Figure 27 D), with an affinity not significantly different from that calculated when using f-LOS as a tracer ($K_a = 1.15 \times 10^4 \text{ M}^{-1} \pm 31 \text{ \%CV}$, apparent $K_i = 87.2 \text{ }\mu\text{M}$).

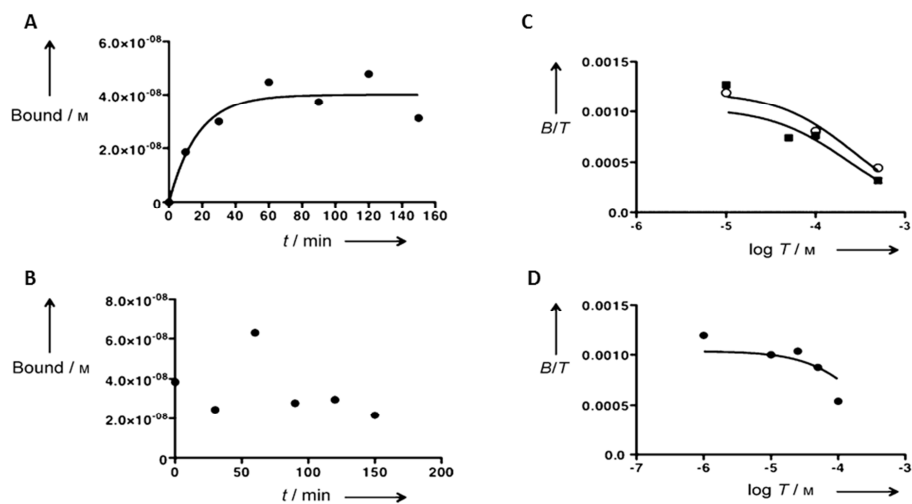


Figure 27. A, B) Association and dissociation time-courses of **1** binding to LptC immobilized on Ni-NTA resin. For association kinetics, 50 μ M **1** was incubated with LptC for up to 150 min. Dissociation was induced by perturbing the equilibrium with addition of 500 μ M corresponding unlabeled ligand. **C)** Saturation (10 - 500 μ M **1**) (black square) and competition (50 μ M **1** as tracer competing with increasing concentrations of iaxo-102) (white circle) curves of **1** binding to resin absorbed LptC under pseudo-equilibrium conditions. **D)** Binding curves for 50 μ M **1** competing with increasing concentrations of LPS. Binding is expressed as the concentration ratio of bound to total ligand (B/T) against the logarithm of total unlabeled ligand concentration (log T).

Finally, considering that iaxo-102 and its fluorescent analogue (**1**) bound specifically LptC, their capability to inhibit the growth of some bacterial strains (*E. coli* strains MG1655 and two permeable mutants – AS19 and $\Delta TolC$) has been evaluated by the micro-broth dilution method (Table 3). However, these compounds have not shown antibiotic effects.

Microorganism	MIC		
	iaxo-102	Compound 1	Tetracycline
<i>E. coli</i> MG1655	>1 mM	>1 mM	<2 μ M
<i>E. coli</i> AS19	>1 mM	>1 mM	<1 μ M
<i>E. coli</i> $\Delta TolC$	>1 mM	>1 mM	<1 μ M

Table 3. MICs of iaxo-102, compound **1** and tetracycline against different strains of *E. coli*.

3.3. Conclusions and future perspectives

The development of the co-purification assay based on the use of fluorescent probes (f-LOS or compound **1**) has allowed us to calculate and publish, for the first time, the thermodynamic and kinetic parameters of LPS–LptC interaction.

Kinetic experiments and binding assays based on the co-purification of LptC-fLOS complex and on LptC Trp quenching have revealed that LPS binds LptC in a not reversible way. This unexpected result could be explained considering the lack of energy in both methods. Indeed, LptC function *in vivo* requires energy from the LptBFG ABC transporter, and a round of ATP hydrolysis is necessary to extract LPS from the IM. A second round of ATP hydrolysis is then required *in vivo* for LPS delivery from LptC to LptA. Previous works demonstrated that *in vitro* transfer of LPS from LptC to LptA (but not vice versa) occurs in the absence of ATP, demonstrating different affinities for LPS by the two proteins and confirming the unidirectionality of the transport.⁵⁷

The hypothesis that a gradient of affinities is the basis of LPS transport is also supported by considering that MsbA, a member of the ATP-binding cassette (ABC) superfamily of transporters which operates upstream of LptC, shows an affinity for LPS of 2 - 6 μM .¹⁵¹ According our data, LptC-LPS binding is characterized by an apparent K_d (52.4 μM) of the same order of magnitude as K_d for the MsbA - LPS interaction. These similar K_d

values are consistent with a model of LPS shuttling from MsbA to LptC; irreversible binding between LptC and LPS (observed in this study) reflects the peculiar nature of LPS transport across the periplasm. LPS needs to be properly transferred through the Lpt chain and not released into the aqueous periplasm.

The dissection into single steps of LPS binding and release through the Lpt machinery provides important information on the molecular mechanisms underlying LPS transport. Moreover, the ability to block LPS transport to the cell surface by small molecules represents an appealing strategy for a new generation of antibiotics against multidrug-resistant Gram-negative bacteria. With this purpose, the capability of iaxo 102 and its fluorescent analogue **1** to interact with LptC has been tested. These are small molecules, previously designed and synthesized by our group as antagonists of TLR4 pathway, are able to bind the LPS binding protein CD14. We found that these compounds are also able to interact with LptC with fourfold lower affinity than LPS (apparent $K_d = 221 \mu\text{M}$), sharing the same binding site, as demonstrated through the competition experiments. As noted for LPS, binding by **1** is mostly irreversible, thus suggesting a common mechanism of interaction with LptC. Although the lack of antibacterial activity *in vitro*, iaxo-102 and its fluorescent analogue could represent a scaffold for new antibiotics targeting the LPS transport mechanism. However, the rational optimization of their molecular structures with the aim of improving bioavailability, cell

penetration, and LptC affinity, is strongly required. With this purpose, a high-throughput assay will be development and Saturation-Transfer Difference (STD) NMR analyses will be performed to study in more detail the binding between LptC and other compounds.

Section II

Biological characterization of new synthetic and natural small molecule TLR4 modulators

4. Results and discussion

In this section, the biological effects of new synthetic compounds on LPS-triggered TLR4 activation and signaling will be presented. The TLR4 activity of molecules has been assessed in HEK-Blue-4™ cells (Invivogen), which are HEK 293 cells stably transfected with human TLR4, MD-2 and CD14 genes. In addition, HEK-blue cells stably express an optimized alkaline phosphatase gene engineered to be secreted (SEAP), placed under the control of an IL-12 p40 minimal promoter fused to five NF-κB and AP-1-binding sites. Stimulation with a TLR4 agonist activates NF-κB and AP-1 which induce the production of SEAP. Levels of SEAP can be easily determined by adding the chromogenic SEAP substrate *p*-nitrophenyl phosphate (pNPP), which is hydrolyzed to the yellow compound 4-nitrophenolate detectable by reading the absorbance (405 nm). As a negative control, a HEK 293 cell line (InvivoGen) transfected with the same plasmids as HEK-Blue™ but without TLR4, MD-2 and CD14 genes was used.

4.1. Synthetic lipid A mimetics

The biological activity of the natural bacterial endotoxins (lipid A, LPS and LOS) and of the synthetic variants of lipid A is determined by the geometry of the interaction with the hydrophobic binding pocket of MD-2. A proved strategy to design new TLR4 antagonists consists in the simplification of lipid A structure, for instance taking as template the structure of lipid X (Figure 28), a biosynthetic precursor of lipid A, whose structure corresponds to the reducing GlcN monosaccharide of *E. coli* lipid A and that is still active as TLR4 antagonist.

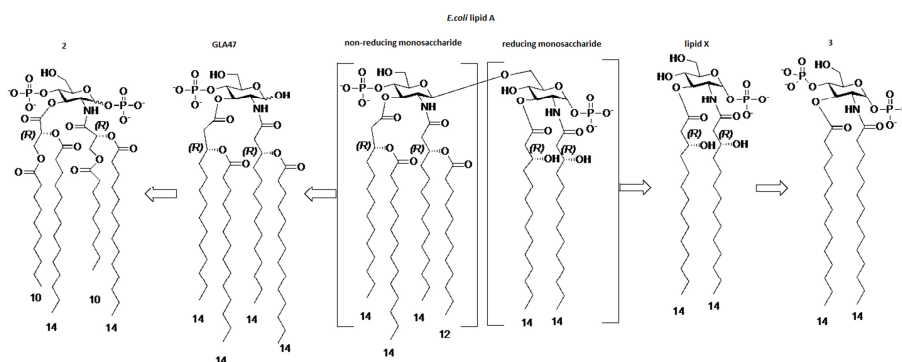


Figure 28. Structure simplification of lipid A into monosaccharides. From *E. coli* lipid A, (in the middle, 4 + 2 fatty acid chains) to reducing unit mimetics lipid X and synthetic monosaccharide **3** (right, 2 fatty acid chains) and to non-reducing unit mimetics GLA47 (Gifu University, Japan) and compound **2** (left, 2 branched fatty acid chains, 4 chains in total).

Compound **3** (Figure 28) has been synthesized by the group of Prof. Jacquelyn Gervay Hague (University of California, Davis) and studied from a biological point of view by our group. Compound **3** corresponds to the non-reducing monosaccharide moiety of lipid A, with two branched fatty acid chains, 4 fatty acid chains in total. The novelties in the chemical structure of **3** compared to GLA47, a monosaccharide lipid A analogue previously synthesized at the Gifu University (Japan), are the introduction of anomeric phosphate in the α configuration and the presence of fatty acid chains mimetics based on diacylated (*R*)-glyceric acid scaffold. The myristic acid chain (C_{14}) attached to the glyceric acid secondary hydroxyl mimics the lipid A secondary C_{14} or C_{12} fatty acid chain, while the decanoic acid chain attached to the primary hydroxyl, together with the four-atom glyceric acid moiety, mimics the length of the lipid A primary C_{14} fatty acid chains. Previous works have demonstrated that similar structures are able to bind MD-2 interfering with TLR4 pathway activation.¹⁵³

The ability of **3** to interfere with LPS-triggered TLR4 activation was first investigated in HEK-Blue TLR4 cells (Figure 29). When supplied alone, compound **3** was unable to stimulate TLR4-dependent SEAP, thus showing no agonist activity on human TLR4. In presence of LPS (Figure 29), only 20% decrease has been obtained after the administration of sub-micromolar concentrations of compound **3**. A switch in the

biological behavior has been observed at concentrations higher than 1 μM , since compound **3** has strongly enhanced the TLR4 activation.

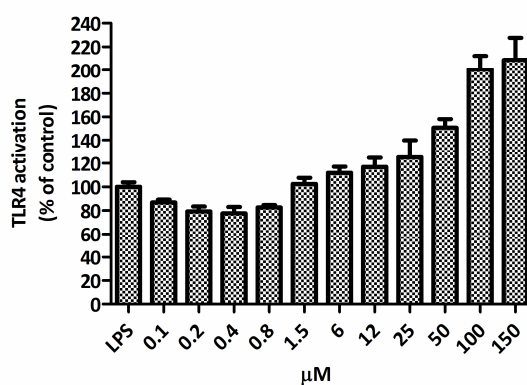


Figure 29. Activity of compound **3** in HEK-Blue TLR4 cells stimulated by LPS (*E. coli* O55:B5, 50 ng mL^{-1}). LPS was administered 30 min after treatment with increasing concentrations of compound **3**. A dose-dependent antagonism is observed. Image realized with GraphPad Prism.

The loss of biological activity could be explained in terms of formation of aggregates, considering that compound **3**, similarly to natural lipid A and other synthetic lipid A mimetics, is an anionic amphiphile that easily forms aggregates in aqueous environment. Its aggregation properties have been investigated by using an established technique based on the polarity-induced change in the fluorescence spectra of pyrene when

incorporated in micelles formed by synthetic compounds. The critical micelle concentrations (cmc) of **3** in distilled water has been calculated to be 7.4 μM similar to that of *E. coli* LPS (1.3 - 1.6 μM). The activity/aggregation data suggest that the biological activity of this type of lipid A mimetic based on a monosaccharide core is related to the molecular recognition of mono-dispersed molecules in solution by MD-2 and CD14 receptors, though the hypothesis that the quality of TLR4 response is influenced by supramolecular aggregate structures¹⁰² is still not completely demonstrated.

4.2. Cationic amphiphilic compounds

4.2.1. Iaxo monosaccharides dimers

Iaxo compounds are a family of cationic amphiphiles synthesized in our laboratory, active in inhibiting LPS-stimulated TLR4-dependent cytokine production in cells and *in vivo* by binding CD14 through the acyl chains.^{122,154} Since docking studies with iaxo-102-MD-2 interaction model suggest that the MD-2 binding cavity is large enough to accommodate four fatty acid chains, dimers of iaxo-102, formed by two α -D-glucopyranose units connected through a C4 linker attached to C-6 nitrogen, have been designed and synthesized by our group (compounds **4** and **5**, Figure 30).

The ability of compounds **4** and **5** to interfere with TLR4 pathway is reported in Figure 31 A.

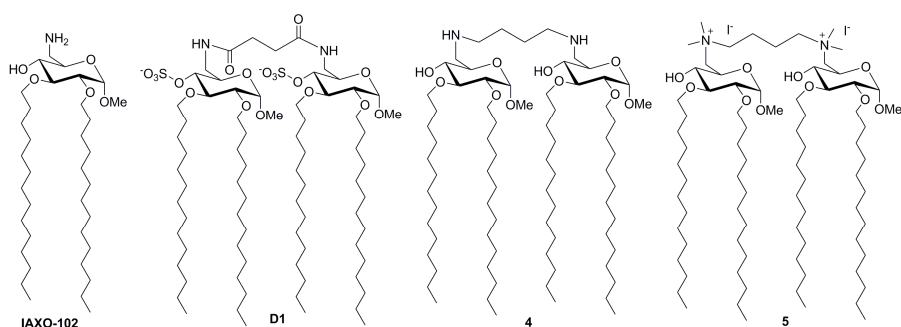


Figure 30. Chemical structures of iaxo-102, compounds **D1**, **4** and **5**.

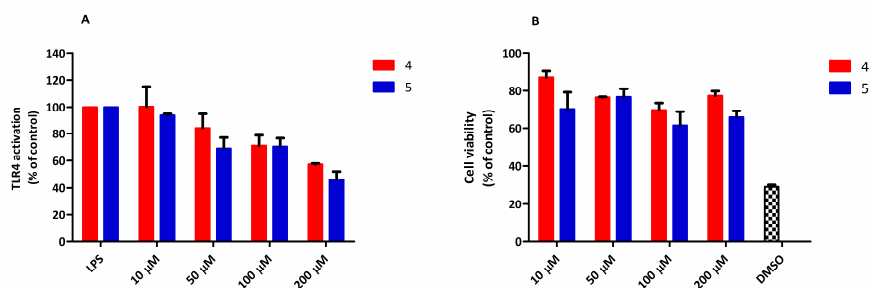


Figure 31. Activity (A) and toxicity (B) of compound 4 (red bars) and 5 (blue bars) in HEK Blue cells.

Both compounds have shown a moderate dose dependent antagonistic activity on LPS-stimulated TLR4 signalling with an IC_{50} of 240 and 173 μ M, respectively. When supplied alone, compounds 4 and 5 were unable to stimulate TLR4-dependent SEAP production (data not shown), indicating the lack of any agonist activity on human TLR4. The toxicity of both compounds is low in the concentration range used for biological characterization, as assessed by MTT test (Figure 31 B). The highest concentrations of compound 4 and 5 induce a death rate of 20% and 30%, respectively.

4.2.2. Pyrrole - containing amphiphiles

The pyrrole-containing amphiphiles (**6-9**, figure 32) are long-chain analogues of compounds extensively studied as antifungal activity.¹⁵⁵ They have been synthesized in the laboratory of Prof. Roelens and Dr. Francesconi (University of Firenze) as potential TLR4 modulators by combining important structural elements previously employed in the design of TLR4-active molecules. Indeed, these compounds consist of a polar head, featuring a variable number of secondary amines (protonatable at physiological pH) linked to pyrroles, installed on an aromatic ring bearing one to three lipid chains. Noteworthy is the compound **9**, in which two out of the three alkyl chains of the scaffold have been removed and a hydrophilic polyoxyethylene fragment (tetraethylene glycol, TEG) has been inserted between the polar head of compound **8** and the alkyl chain, in order to ascertain how the lipophilic/hydrophilic properties of these molecules would affect their biological activity.

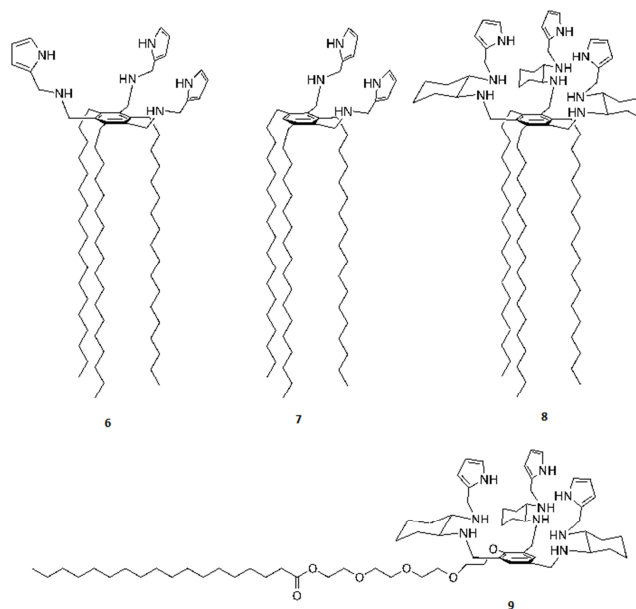


Figure 32. Structures of cationic amphiphiles **6-9**.

These compounds have been tested as modulators (agonists or antagonists) in HEK Blue cells. All compounds were inactive as agonists, and did not activate TLR4 when administered alone to cells. In presence of LPS, only compound **9** has inhibited LPS-stimulated TLR4 activation in a dose-dependent way with an IC_{50} of about 15 μ M (Figure 33 A), but, unfortunately, a high toxicity has been correlated to this activity as evident considering the MTT assay (Figure 33 B).

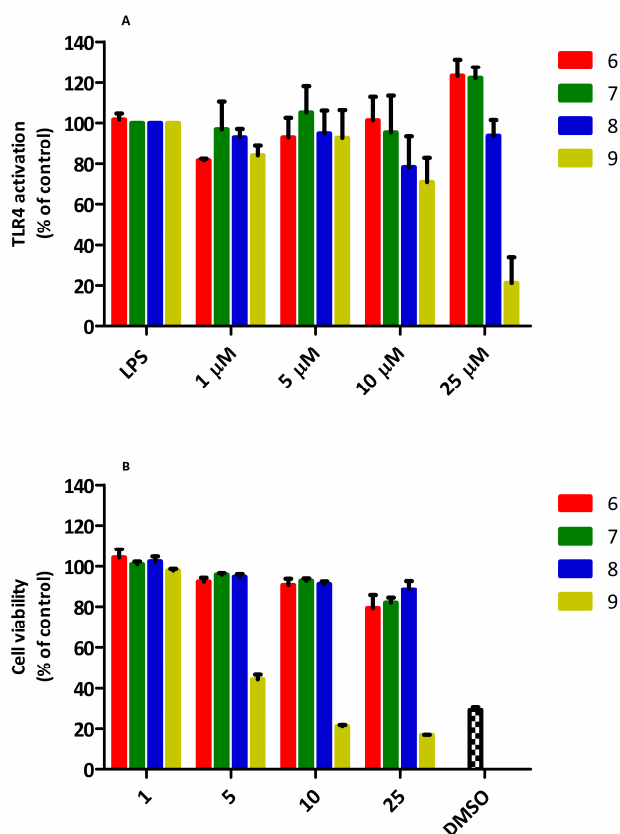


Figure 33. A) TLR4 activity of increasing concentrations of compounds **6-9** in HEK Blue TLR4 cells stimulated with *E. coli* O55:B5 LPS. The results are normalized to activation by LPS alone and expressed as the mean of percentage \pm SD of 3 independent experiments. **B)** Viability assay (MTT) in HEK Blue cells. The results are normalized on the positive control (cells treated with PBS) and expressed as the mean of percentage \pm SD of 3 independent experiments.

4.2.3. Trehalose- and glucose-derived glycoamphiphiles

Cationic amino glycolipids derived from methyl α -D-glucopyranoside (**10–20**, figure 34) and from α,α' -trehalose have been designed and synthesized by Dr. Julio Rodriguez Lavado of the group of Prof. García Fernández and Prof. Carmen Ortiz-Mellet (University and CSIC, Sevilla, Spain). Structural modifications have been projected by varying the number, the nature, and the length of the lipid chains and the number and disposition of amino groups in order to evaluate how these structural elements influence the TLR4 activity.

First, the capability of these compounds to modulate LPS-induced TLR4 activation has been screened on HEK Blue cells and IC_{50} values have been reported in Table 4.

Only 4 compounds (**14**, **18**, **19** and **20**) have shown a potent activity in inhibiting the TLR4 activation with IC_{50} ranging to 0.6 and 5 μ M with low associated toxicity (Figure 35). In particular, some toxic effects were found but at concentrations higher than IC_{50} values, inducing to exclude the possible correlation activity/toxicity.

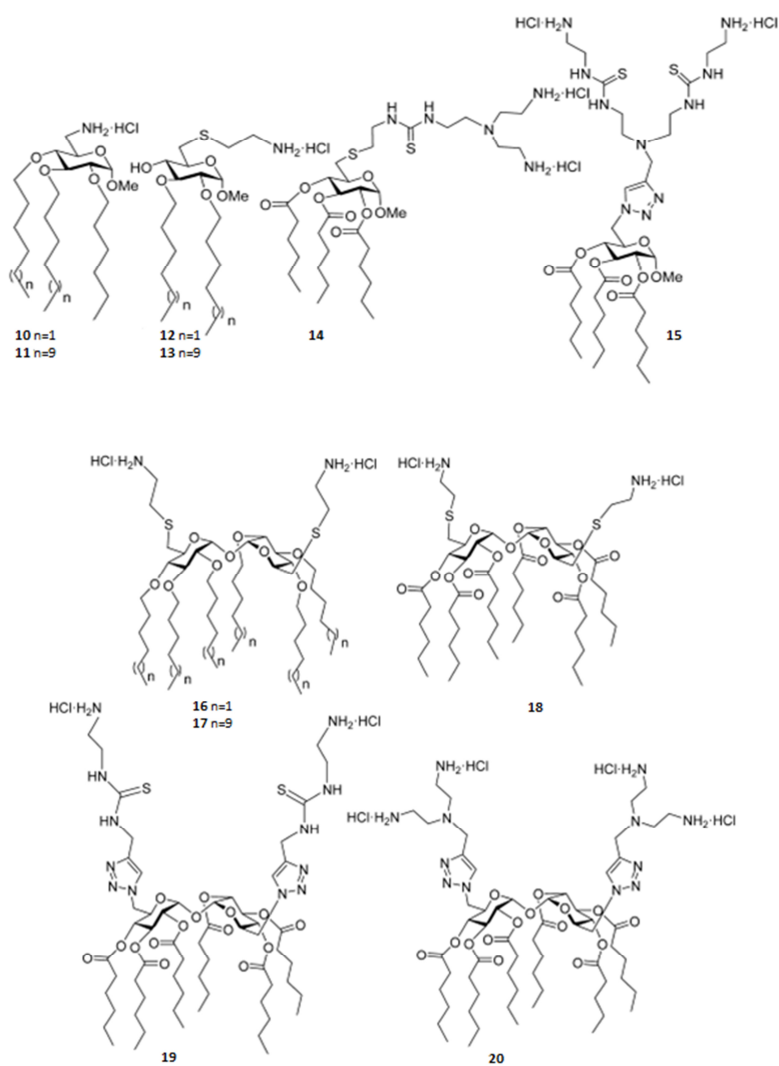


Figure 34. Structures of glucose derived amphiphiles (**10 - 15**), with 2 or 3 lipid chains and 1 or 2 positive charges, and trehalose - derived compounds (**16 – 20**), with 6 lipid chains and 2 or 6 positive charges. Trehalose - derived are dimeric homologous of the glucose derivatives.

Glucose - derived		Trehalose - derived	
Compound	IC ₅₀ (μM)	Compound	IC ₅₀ (μM)
10	>25	16	>25
11	>25	17	>25
12	>25	18	1.3 ± 0.1
13	>25	19	5.0 ± 1
14	3.7 ± 0.4	20	0.6 ± 0.05
15	>25		

Table 4. IC₅₀ values of compounds **10-20** in HEK Blue cells. The values have been calculated by non-linear regression analysis using GraphPad Prism.

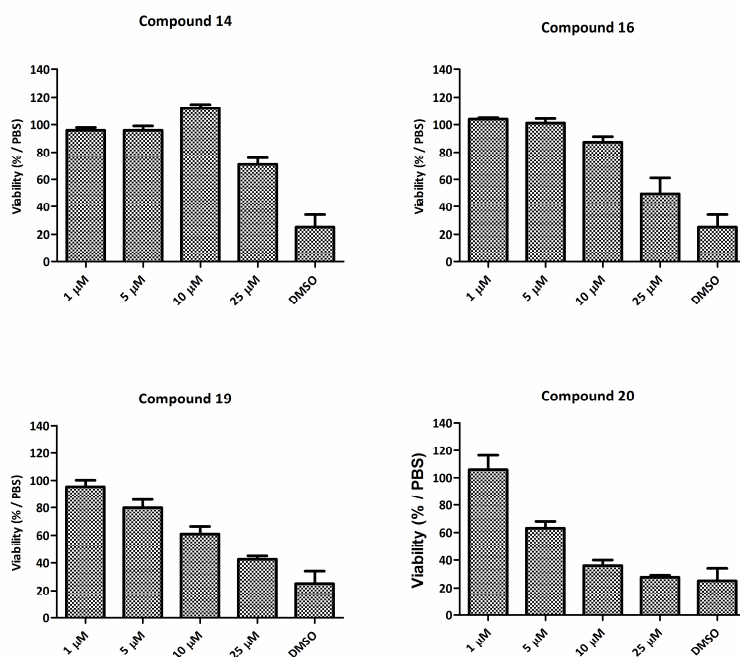


Figure 35. MTT assay of compounds **14**, **16**, **19** and **20**.

Further biological characterizations have been performed in collaboration with Prof. Roman Jerala and Dr. Alja Oblak (Chemistry Institute, Ljubljana, Slovenia). In particular, the most active compounds were further examined for their capacity to stimulate or to inhibit LPS-induced TLR4 activation and signalling in HEK 293 cells transfected with human or murine TLR4 and MD-2 and a dual luciferase reporter gene

(Figure 36). In the absence of LPS, none of the cationic glycolipids have shown agonist activity in cells transfected with hMD-2·hTLR4 or mMD-2·mTLR4. Conversely, all compounds have inhibited human and murine MD-2·TLR4 activation in a concentration-dependent way with similar potencies in both complexes (Table 5) and those found in HEK Blue cells: triacylated monosaccharide **14** and hexacylated disaccharide **16** were less active ($IC_{50} = 3.3 - 3.9$ and $0.8 - 1.4 \mu\text{M}$, respectively) than disaccharides **19** and **20** ($IC_{50} = 0.6$ and $0.2 \mu\text{M}$, respectively).

Compound	IC_{50} (μM)		
	hMD-2/hTLR4	mMD-2/mTLR4	HEK Blue
14	3.9 ± 1.5	3.3 ± 1.2	3.7 ± 0.4
18	1.4 ± 0.3	0.8 ± 0.2	1.3 ± 0.1
19	0.6 ± 0.02	0.6 ± 0.03	5.0 ± 1.0
20	0.2 ± 0.02	0.2 ± 0.03	0.6 ± 0.05

Table 5. IC_{50} values of compounds **14**, **18**, **19** and **20** in HEK 293 cells transfected with human or murine MD-2/TLR4 complex compared to those calculated in HEK Blue cells.

Section II: Biological characterization of new small molecule TLR4 modulators

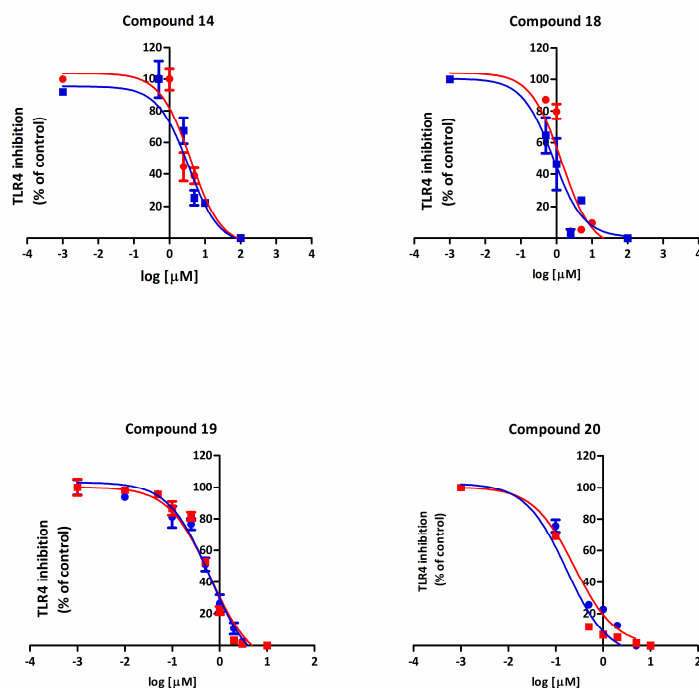


Figure 36. Dose-dependent inhibition of LPS-stimulated TLR4 activation by synthetic glycolipids. HEK 293 cells transfected with human MD-2·TLR4 (red line) or murine MD-2/TLR4 (blue line) were treated with increasing concentrations of compounds and stimulated with LPS (5 nM). Normalized data are representative of three independent experiments.

The effects of these compounds on the production of TNF- α and IL-6 have been evaluated in bone marrow-derived murine macrophages (BMDM), by performing ELISA assays (Figure 37). The treatment with compound **20** has induced a decrease of both inflammatory cytokines

when used at concentrations higher than 1 μ M. On the contrary, the levels of TNF- α and IL-6 have remained unchanged after the treatment with compound **14** or have increased by using compound **18**.

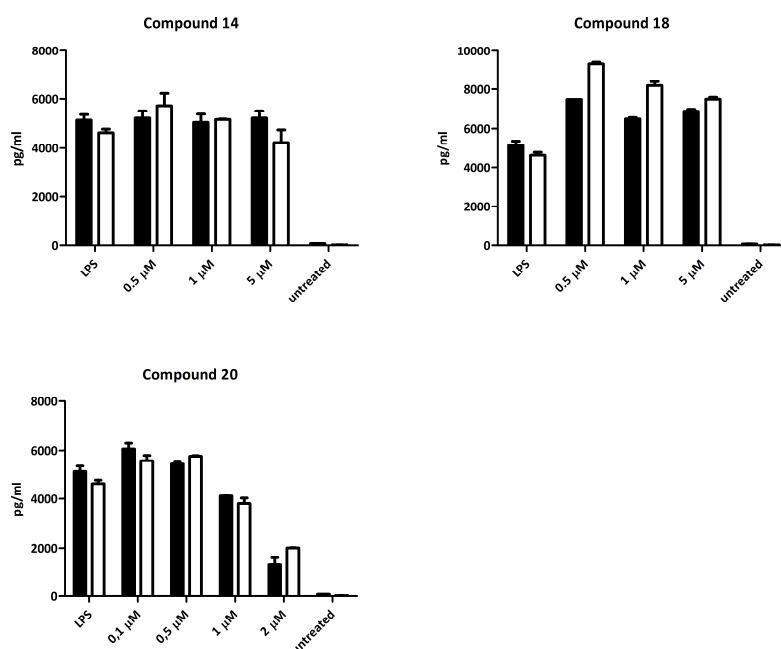


Figure 37. BMDM have been treated with increasing concentrations of compounds **14**, **18** and **20** in RPMI + FBS 10% and then stimulated with LPS. The production of TNF- α (black bars) and IL-6 (white bars) has been quantified through ELISA assay performed after overnight incubation. Cytokines productions in cells not treated with LPS are reported as negative controls.

In order to clarify whether aggregated species or single molecules are the active species, the critical micelle concentration (cmc) have been calculated (Table 6). In all cases, the cmc values of active compounds are higher than the corresponding IC₅₀ values as TLR4 antagonists, suggesting that the biologically active species are prevalently single molecules in solution.

Compound	cmc (μM)
14	59.7 ± 7.4
18	97.7 ± 10.0
19	10.9 ± 2.1
20	350.5 ± 70.5

Table 6. Critical Micelle Concentrations (cmc) in aqueous environment of compounds **14**, **18**, **19** and **20** estimated via pyrene fluorescence measurements.

The strong *in vitro* antagonist activities have been also evaluated *in vivo* in C57/ BL6 mice (Figure 38). All four compounds potently inhibited the LPS-induced immune with an order of potency similar to that found in *in*

vitro experiments: the strongest inhibition was exhibited by compound **20**, which totally abolished LPS-induced immune activation.

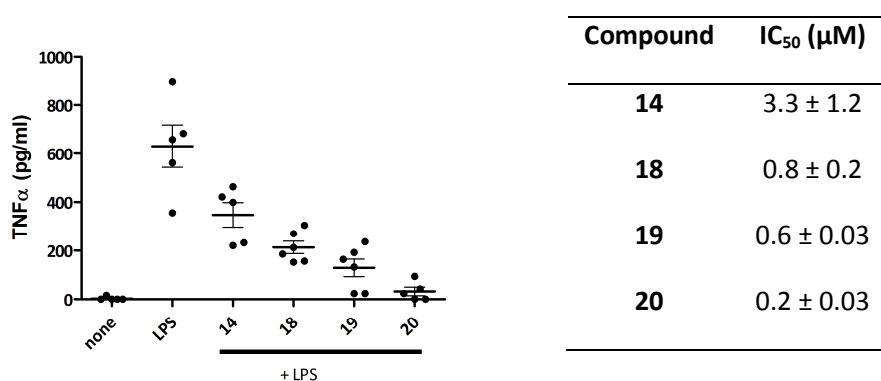


Figure 38. *In vivo* activity of cationic amphiphiles. C57/Bl6 mice were injected ip with the indicated compounds (2×10^{-7} mol/mouse), followed 1 h later by ip injection of LPS (1×10^{-9} mol/mouse). Three hours later, sera were collected and TNF- α concentration was determined by ELISA assay.

As it is known that agonist or antagonist action of TLR4 ligands can be potentiate by mimicking the 3D-structure of LPS aggregates by immobilizing them on nanoparticles, gold nanoparticles have been coated with the most active compound **20** (DTT-Au-NP-20) and tested in HEK cells transfected with human or murine MD2/TLR4 complex. DTT-Au-NP-20 have maintained the biological inhibitory activity already at

very low concentrations (Figure 39 A,B) on both MD-2·TLR4 receptor complexes.

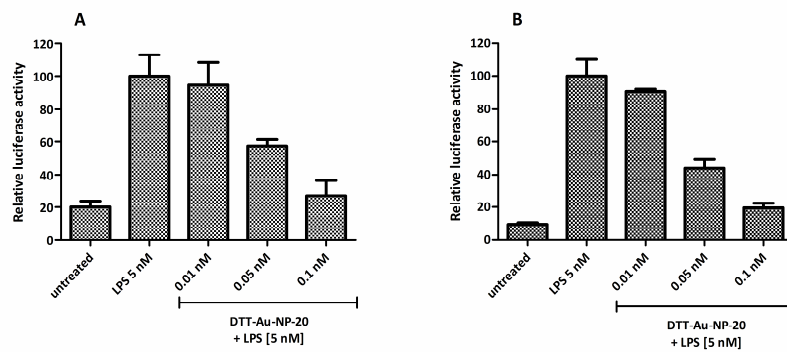


Figure 39. Dose-dependent TLR4 antagonism in HEK 293 cells treated with DTT-Au-NP-20. HEK 293 cells were transfected with NF- κ B-dependent luciferase and constitutive Renilla luciferase reporter plasmids as well as with (A) human or (B) murine MD-2 and TLR4 plasmids. The indicated amount of the DTT-Au-NP-20 was added to the cells, followed 1 h later by stimulation with LPS. Luciferase activity was measured 16 h later.

4.2.4. Natural compounds from olive oil

The antioxidant and anti-inflammatory activity of extra virgin olive oil (EVOO), caused mainly by phenolic compounds, has been demonstrated in many studies over recent. Despite the large number of studies, these anti-inflammatory effects have never been related to TLR4 activation, until now. To test this possible correlation, we have performed preliminary assays by screening the *in vitro* TLR4 antagonist activity of total phenolic contents extracted from Taggiasco, Tuscan and Sagra EVOO (Figure 40 A). The total phenols have been extracted and quantified through the gallic acid equivalence method.

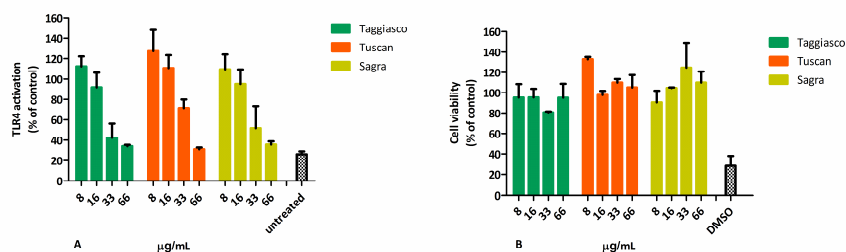


Figure 40. Activity (A) and toxicity (B) of total phenolic extracts derived from different EVOOs.

All samples have decreased the LPS-induced TLR4 activation in a strong dose dependent way, inducing a total inhibition when used at the higher

concentration. These activities have not been associated to toxicity as revealed by MTT assay (Figure 40 B). Since these data have supported our hypothesis about the correlation between the anti-inflammatory effects of the phenols from olive oil and TLR4, a second screening has been performed by using the main single components of olive oil, commercially available (Figure 41).

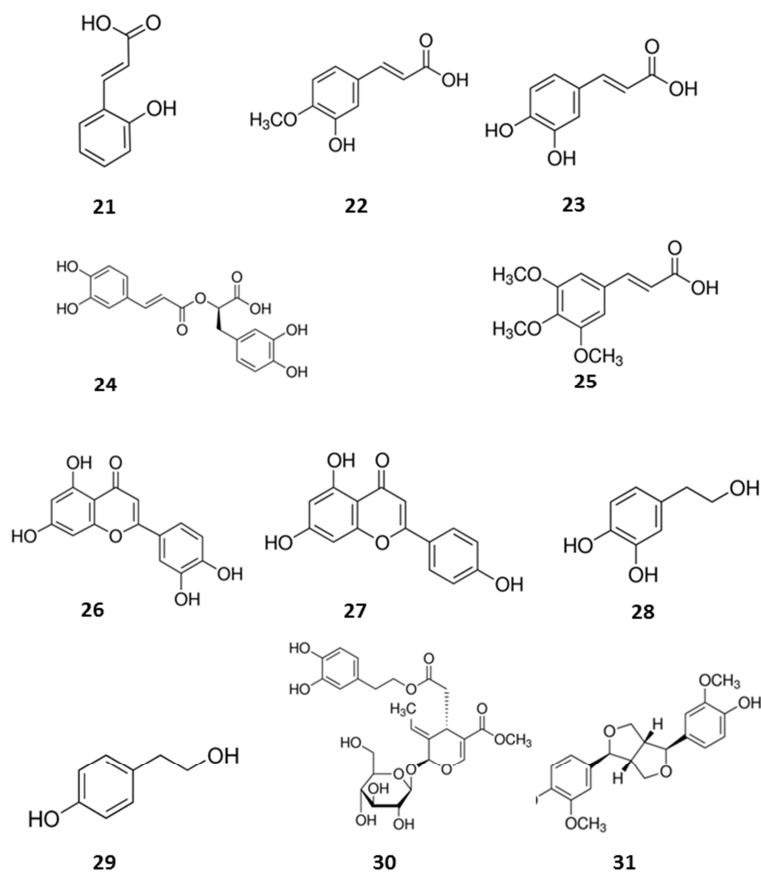


Figure 41. Chemical structures of olive oil phenolics: dihydroxycinnamic acid (**21**), 4-hydroxy-3-methoxycinnamic acid (**22**), caffeic acid (**23**), rosmarinic acid (**24**), trimethoxycinnamic acid (**25**), luteolin (**26**), apigenin (**27**), hydroxytyrosol (**28**), tyrosol (**29**), oleuropein (**30**), pinorosinol (**31**).

All acid compounds were not active in inhibit the TLR4 pathway (Figure 42 A). In addition, despite several studies reported the pharmacological activities, including anti-inflammatory action, of the main phenolic compounds, hydroxytyrosol and oleuropein, this effect cannot be related to the inhibition of TLR4 (Figure 42 B). The only compounds which have shown a good inhibition of LPS-induced TLR4 activation were apigenin and luteolin (Figure 43) with IC_{50} values of 15.7 and 14.3 μ M, respectively.

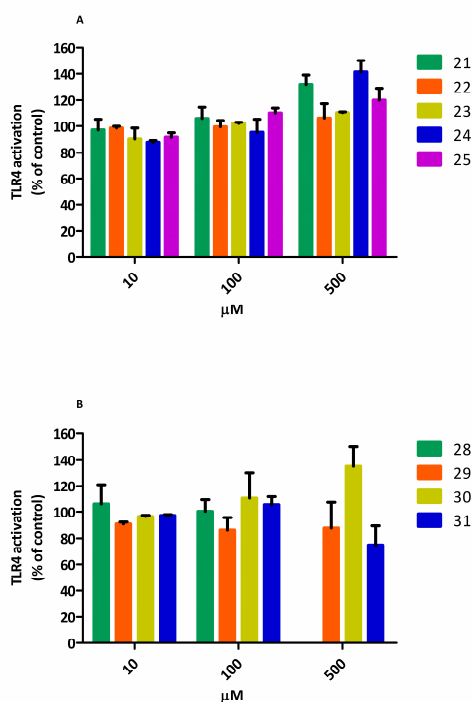


Figure 42. Activity on TLR4 of known acids and polyphenols present in EVOO.

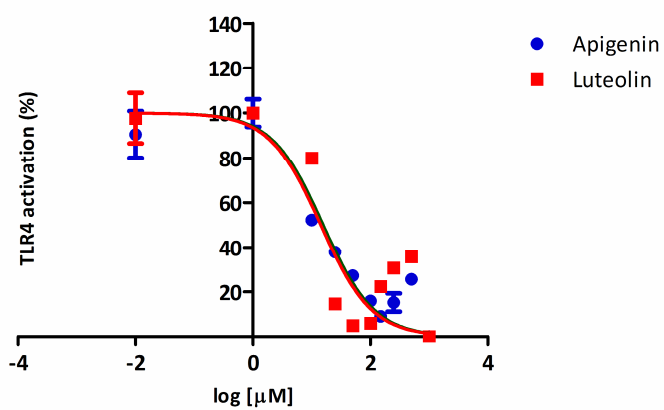


Figure 43. TLR4 activity of apigenin and luteolin in HEK Blue cells. Normalized data are representative of three independent experiments. The IC₅₀ values have been calculated by non-linear regression analysis using GraphPad Prism.

4.3. Conclusions and future plans

The recent knowledge of the crystallographic structures of the human and murine activated complex (LPS·MD-62·TLR4)₂ has allowed the rational design of TLR4 modulators (e.g. Eritoran) based on modifications of the chemical structure of the lipid A. The rational design of TLR4 modulators could take into account both factors which influence the biological activity of the bacterial endotoxins and the synthetic variants of lipid A: the geometry of the interaction of lipid A with the hydrophobic binding pocket of MD-2 and the tridimensional structure of the aggregates. Unfortunately, a reliable prediction of the SAR is not so simple and the chemical synthesis of lipid A mimetics is more complex. A proved strategy to design new TLR4 modulators consists in the simplification of lipid A structure, starting from the lipid X (Figure 28), a biosynthetic precursor of lipid A, whose structure corresponds to the reducing GlcN monosaccharide of *E. coli* lipid A. According to this strategy several compounds have been synthesized: for example, **GLA47** (Gifu University, Japan),¹⁵⁶ which mimics the non-reducing lipid A glucosamine, and compound **2** (synthesized by our group), a lipid X analogue lacking the C-3 hydroxyls of fatty acid acyl chains, with two C₁₄ fatty acid chains with an additional phosphate on sugar C-4 (Figure 28). Both compounds have shown to be good *in vitro* and *in vivo* TLR4 antagonists. As a continuation of this work we have studied compound

3, corresponding to the non-reducing monosaccharide moiety of lipid A with 4 fatty acid chains, synthesized in the University of California. Unlike other lipid A mimetics, compound **3** presents a double activity on TLR4, showing a weak antagonism at low concentrations (till 1 μM) and an enhancement of the TLR4 activation at higher concentrations. This dual behavior could be due to the amphiphilic character of molecule **3** which results in the formation of micelles in aqueous environment, since the switch in the activity almost coincides with the cmc value (7 μM). The possibility that the TLR4 activity of LPS and lipid A is related to the formation of aggregates in aqueous solution and that the intensity and quality of TLR4 response is influenced by supramolecular aggregate structures¹⁰² is still controversial. However, the activity/aggregation data relative to compound **3** strongly suggest that the antagonistic activity of this type of lipid A mimetics based on a monosaccharide core is related to the molecular recognition of mono-dispersed molecules in solution by MD-2 and CD14 receptors.

Despite the negative charges on phosphate are important for the interaction of lipid A and its synthetic analogues with the CD14 and MD-2 receptors, it has been recently found that also cationic lipids with positively charged headgroups are active in modulating TLR4 activity as agonists or antagonists. However, in this case the rules for the rational design of TLR4 modulators are still lacking. In the last years, our group has developed several TLR4 antagonists based on positively charged

amphiphiles, constituted by a carbohydrate^{122,150,157} or aromatic¹⁴⁹ core, a polar head possessing a positively charged ammonium ion, and two lipid chains. In particular, iaxo compounds are active in inhibiting LPS-stimulated TLR4-dependent cytokine production in cells and *in vivo* by binding CD14 through the acyl chains.^{122,154} Docking studies with iaxo-102-MD-2 interaction model have suggested that the MD-2 binding cavity is large enough to accommodate extra chains. This prediction has been confirmed by the TLR4 antagonist activity of molecule **D1** (Figure 30), with a structure composed of two glucoside units, as iaxo-102, connected by a linker both units bearing on C-4 an anionic sulfate group.¹⁵⁸ The TLR4 antagonist activity and binding properties of **D1** have suggested that 4 acyl chains could be optimal for MD-2 binding. In order to more investigate this hypothesis, the TLR4 antagonistic activity of dimers of iaxo-102 (compounds **4** and **5**, Figure 30) have been evaluated. Unexpectedly, these molecules have shown to be less potent (240 and 173 μM , respectively) than the corresponding monomer iaxo-102 ($\text{IC}_{50} = 5.5 \mu\text{M}$). This low TLR4 activity could be due to the fact that very few residual molecules that interact with CD14 and MD-2 receptors, since pyrene fluorescence measurements have revealed that the critical micelle concentrations (cmc) for compounds **4** and **5** are 18 and 30 μM , respectively, indicating that they have been used as aggregates in the concentration range used for the biological assays (10 to 200 μM).

The self-assembling capabilities and the ability of cationic amphiphiles to interact with CD14 as liposomes or micellar aggregates seem to have a strong impact on their TLR4 modulatory activity, but very little is still known on the molecular aspects underlying the mechanisms at play, mainly because structural data of cationic compounds bound to MD-2 or CD14 receptors are still lacking. With the aim of clarify this aspect, a series of homologous cationic amphiphiles, amino glycolipids derived from methyl α -D-glucopyranoside (**10** - **15**) and from α,α' -trehalose (**16** - **20**, Figure 34), has been developed by the group of Prof. Garcia Fernandez (University of Sevilla) and biologically characterized by us in collaboration with Prof. Roman Jerala (Chemistry Institute, Ljubljana). Two characteristics make glucose-derived cationic glycolipids particularly appealing to reach this purpose: the secondary hydroxyls of the glucopyranose ring are well suited anchoring points to link lipophilic chains in a similar orientation as the fatty acid acyl chains in lipid A; then, the incorporation of protonatable headgroups at the primary position imparts facial amphiphilicity to the molecule, a biomimetic feature that is associated with improved cell membrane crossing abilities and proneness to form supramolecular complexes with complementary biomolecules by either electrostatic or hydrophobic interactions. Among all compounds of this group, glucose-based compound **14** and trehalose-based compounds **18-20** were active in inhibiting the LPS- triggered TLR4 activation and signalling in HEK Blue cells, with IC₅₀ values ranging from

about 0.6 to 5 μ M and very low cell toxicity. The activities of these compounds have been further evaluated in HEK 293 cells transfected with human or murine TLR4 and MD-2 and a dual luciferase reporter gene, founding IC₅₀ values very similar to those calculated in HEK Blue cells. Of note, both human and murine pathway have been inhibited by all compounds with very similar potency, similarly to the very efficient TLR4 antagonist Eritoran and differently from the natural TLR4 antagonist lipid IVa that has species-specific activity (antagonist on human and agonist on mice MD-2-TLR4). When used *in vivo*, these compounds have maintained the order of potency found in *in vitro* experiments. In addition, the maintained biological activity, without apparent increase in cytotoxicity, of nanoparticles coated with compound **20**, represents the proof-of-concept of the possibility of developing nanoparticulate systems based on cationic glycolipids as modulators of TLR4 signalling pathway.

The biological evaluation of active compounds compared to inactive, structurally related monosaccharides (compounds **10–13** and **15**) and disaccharides (compounds **16** and **17**), suggests some general structure–activity relationships in this type of compounds. First, the presence of acyl lipophilic chains at the hydrophobic domain seems to be a primary requisite because all compounds with ether bonds are inactive; then, considering the higher *in vitro* and *in vivo* activity of compound **20**, the trehalose scaffold seems to favors the biological

activity, probably by providing a well-ordered facial amphiphilic character. Moreover, the experimentally determined cmc values for cationic glycolipids **14** and **18–20** are one order of magnitude higher than the corresponding IC_{50} as TLR4 antagonists, suggesting that they are active as single monomers in solution. This very likely means that specific molecular interaction with CD14 and MD-2 receptors regulate the TLR4 activity of these compounds.

Another class of synthetic cationic compounds (**6–9**) has been presented in this work. These molecules, synthesized in the laboratory of Prof. Roelens and Dr. Francesconi (University of Firenze), are constituted by a polar protanatable head, featuring aminopyrrolic arms, linked to an aromatic scaffold endowed with lipid chains. Only compound **9**, in which three diaminopyrrolic arms are linked to an aromatic scaffold possessing a mixed hydrophilic/hydrophobic chain, inhibited in a dose-dependent manner the LPS-stimulated TLR4 activation in HEK-Blue cells but, unfortunately, this strong activity was associated to an high toxicity (Figure 33).

It will be important in the future to define more precisely the molecular determinants of the interaction with CD14 and MD-2 receptors to allow a structure-based rational design of cationic TLR4 modulators. NMR studies and binding assays with purified receptors, wild type and mutants, appear suitable to reach this aim.

Finally, we have explored the possibility to modulate TLR4 pathway by using natural compounds such as polyphenols from olive oil. Even if a great number of studies have reported the anti-inflammatory activity of some olive oil phenolics, this activity has not been directly correlated to the activity of TLR4 receptor system. Considering this background, total phenol contents extracted from different kind of olive oil have been screened for their agonist or antagonist activity on TLR4 pathway. Interestingly, it has been found that the whole phenolic extracts inhibit TLR4 signalling pathway, in a dose dependent way. As expected, different potency of inhibition have been found related to the origin of olive oil, since it is known that the phenolic compound content of the oil depends on the place of cultivation, the climate, the variety, and the olives' level of maturation at the time of harvesting. To deeply understand which constituents plays the major rule for this effect, some constituents of olive oil phenolic fraction have been screened alone as antagonists and apigenin and luteolin have been found to be very active ($IC_{50} = 15.7$ and $14.3 \mu M$, respectively) in inhibiting the inflammatory responses due to LPS-induced TLR4 activation. Considering these promising results, other natural compounds will be screened and chemical modifications of the active molecules will be done in order to improve water stability and resistance to enzyme hydrolysis and to obtain a new generation of synthetic TLR4 modulators.

5. Experimental section

5.1. Section I: Biochemistry section

Purification of sH-LptC. *E. coli* M15[pREP4] (Qiagen) harboring plasmid pQEsH-lptC,[10] which expresses N-terminal His₆-tagged. LptC lacking the first 23 residues (sH-LptC), was grown at 30 °C in LD medium containing kanamycin (25 µg/mL) and ampicillin (100 µg mL⁻¹) for 16 h. The culture was diluted (1:100) in fresh LD medium and grown to mid-logarithmic phase (OD₆₀₀=0.6). Expression of sH-LptC was induced by addition of isopropyl-b-d-thiogalactopyranoside (IPTG; 0.5 mM; Sigma–Aldrich) and further incubated for 16–18 h at 20 °C. Cells were then harvested by centrifugation (5000g, 20 min). The cell pellet was resuspended in buffer A (NaH₂PO₄ (50 mM, pH 8.0), NaCl (300 mM), imidazole (10 mM), glycerol (10 %)), followed by incubation for 30 min at 4 °C with shaking in the presence of lysozyme (0.2 mg/mL), DNase I (100 µg/mL), MgCl₂ (10 mM), and phenylmethylsulfonyl fluoride (PMSF, 1 mM; Sigma–Aldrich). Cells were disrupted by a single pass through a One Shot model French press (Constant Systems, Daventry, UK) at 25000 psi. Unbroken cells and cell debris were removed by centrifugation (39000 g, 30 min, 4 °C). The soluble protein was purified from the supernatant on

Ni-NTA agarose columns (Qiagen). The column was washed with 10 column volumes of 4% buffer B (NaH₂PO₄ (50 mM, pH 8.0) NaCl (300 mM), imidazole (500 mM), glycerol (10 %)) with buffer A. The protein was eluted by using a stepwise gradient of buffer B (10, 20, 50, 70, and 100%) with buffer A. At each step, one column volume was passed through the column. Elution fractions were monitored by 12.5% polyacrylamide SDS-PAGE. The pooled fractions containing purified protein (> 90%) were dialyzed twice against 100 volumes of buffer C (NaH₂PO₄ (50 mM, pH 8.0), NaCl (150 mM)) in cellulose tubing (12 000 Da cut-off; Thermo Scientific), and finally concentrated in a Vivaspin 15R column (10000 molecular weight cut-off; Sartorius, Göttingen, Germany). Protein concentration was determined by a Coomassie (Bradford) assay kit (Thermo Scientific), with bovine serum albumin as the standard.

LPS. Rough LPS (lipooligosaccharide or LOS) has been extracted from *E. coli* MG1655 by applying PCP procedure (phenol, chloroform, petroleum ether).¹⁴⁵ Purified LOS has labeled with fluorescein isothiocyanate (FITC) applying the protocol described by Troelstra with some modifications.¹⁴⁶ The thiobarbituric assay (Kdo assay) showed a LOS:FITC ratio equal to 1:1. Both LOS have been dissolved in water and store at -20 °C.

LPS biotinylation. Rough LPS from *E.coli* F583 (1 mg) (Sigma Aldrich) has been dissolved in PBS (0.5 mL) in presence of trimethylamine (20 μ l), EDTA (58 μ g) and carbodiimide (2 mg). Then, an excess of EZ-link®Amine-PEO₃-Biotin (7.5 mg) (Thermo Scientific) dissolved in PBS (0.5 mL) have been added and the mixture has been incubated for 2 h at room temperature. The unbound PEO₃-biotin has been removed by ultracentrifugation in a Vivaspin 15R column (3000 molecular weight cut-off; Sartorius, Göttingen, Germany). The product has been lyophilized and maintained at -20 °C. Biotinylation of LPS was confirmed by using 4-Hydroxyazobenzene-2-carboxylic acid (HABA)-avidin reagent (Sigma-Aldrich).

ELISA-type assay with immobilized LptC, and signal amplification by gold nanoparticles (GNP). sH-LptC (200 ng/well) has been immobilized on Ni-NTA plate through His tag (o.n. 4 °C). The unbound protein has been removed and the wells have been washed 4 times with PBS + 0.05% Tween 20 (PBST). Different amounts (0, 1, 2 and 4 μ g mL⁻¹) of biotin-conjugated LPS (Bi-LPS) from *E. coli* (100 μ L/well) have been added in each well and incubated for 3 h at room temperature under shaking condition. The wells have been washed 3 times as described before and gold nanoparticles (GNP) coated with streptavidin (SV) and horseradish peroxidase (HRP) have been added (GNP = 2.5×10^{-4} M; SV = 100 μ g mL⁻¹). After 45 min, the wells have been washed 4 times with PBST and 100

μL /well of TMB have been added. Plates have been incubated for 30 min in the dark, then H_2SO_4 0.5 M (100 μL /well) has been added and the plate reading has been assessed by using a spectrophotometer ($\lambda = 450$ nm). For competition assays, increasing concentrations of unlabeled LPS (0 – 4 $\mu\text{g mL}^{-1}$) have been used to compete with Bi-LPS (2 $\mu\text{g mL}^{-1}$) for the binding with immobilized LptC.

Co-capture binding assay. FITC labeled LOS (f-LOS) 9 μM and sH-LptC 50 μM have been incubated at room temperature in the dark on a rotary shaking for 90 min. Then, sH-LptC-f-LOS complex has been captured on HisLink™ resin (Promega, Madison, WI, USA), previously washed 4 times with buffer C (2 h, on a rotary shaking, at room temperature, in the dark). After incubation, the unbound fraction (flow through, FT) has been removed by decanting the resin, the resin has been washed 3 times with buffer C and the wash fractions (W) have been collected. The protein–LPS complex was eluted in four steps, each with buffer C (1 mL) containing imidazole (500 mM), and each fraction has been collected (E). Nonspecific binding was determined as the binding of the same concentration of f-LOS to Ni-NTA resin in the absence of adsorbed sH-LptC. Each fraction (100 μL) was placed in a Costar white flat-bottomed microtiter plate (Corning, NY), and fluorescence was measured in a Cary Eclipse spectrophotometer ($\lambda_{\text{ex}} = 490$ nm, $\lambda_{\text{em}} = 510$ nm, slit = 5 nm;

Varian). The fluorescence present in each collected fraction has been reported to the total fluorescence and expressed as percentage.

Co-purification binding assay: saturation experiments. Purified sH-LptC (50 μM) was incubated in buffer C (1 mL) with HisLink protein purification resin (100 μL ; Promega) for 90 min on a rotary shaker at room temperature, to allow absorption of protein to the resin. Unbound protein was removed by decanting the resin-bound sH-LptC and eliminating the supernatant. Resin-bound sH-LptC was incubated in buffer C (1 mL) at room temperature in the dark on a rotary shaking in the presence of different concentrations of f-LOS (0.1 - 50 μM) or **1** (10 - 500 μM) for a further 90 min to allow binding of ligand to the resin-bound sH-LptC. The supernatant (flow through, FT) was discarded, and the resin was washed three times with buffer C. The protein-LPS complex was eluted in four steps, each with buffer C (1 mL) containing imidazole (500 mM). Nonspecific binding was determined as the binding of the same concentration of f-LOS to Ni-NTA resin in the absence of absorbed sH-LptC. Each fraction (100 μL) was placed in a Costar white flat-bottomed microtiter plate (Corning, NY), and fluorescence was measured in a Cary Eclipse spectrophotometer ($\lambda_{\text{ex}} = 490 \text{ nm}$, $\lambda_{\text{em}} = 510 \text{ nm}$, slit = 5 nm; Varian). The concentration of tracer present in each sample was determined by interpolation with a standard curve (f-LOS or **1**) and corrected by subtraction of the nonspecific-binding value. The

amount of sH-LptC bound to the resin and eluted with imidazole was evaluated for the pooled elution fractions with a Coomassie (Bradford) assay kit (Thermo Scientific), with bovine serum albumin as the standard.

Co-purification binding assay: association and dissociation time courses. For the association experiments, labeled ligand f-LOS (500 μ M) or **1** (50 μ M) has been added at room temperature, in the dark, to sH-LptC (50 μ M) adsorbed to the resin in buffer C (1 mL); the mixture was incubated with shaking for different times (10 - 150 min). For each time, the supernatant was removed and samples were washed and eluted as described above. Dissociation kinetics experiments were performed with the same tracer concentrations, and incubation with immobilized sH-LptC for 150 min (volume of reaction = 800 μ L). Then, LOS (50 μ M) or iaxo-102 (500 μ M) in buffer C (1 mL) were added for different times (10 - 150 min). For each time, the sample was treated as above.

Co-purification binding assay: competition experiments. Competition experiments were performed for sH-LptC binding to f-LOS or **1**. For f-LOS, resin-bound sH-LptC (50 μ M) was incubated (90 min) with a mixture of f-LOS (10 μ M) and different concentrations of unlabeled LOS (20, 40, 60 and 75 μ M) in buffer C. After wash and elution steps, the concentration of f-LOS bound to sH-LptC was quantified as described above. For **1**, resin-bound sH-LptC (50 μ M) was incubated with **1** (50 μ M) in buffer C

(800 μL) for 90 min. Homologous and heterologous competition experiments were performed by adding iaxo-102 (200 μL , 100 or 500 μM) or LOS (200 μL , 10 - 100 μM) and incubated for a further 90 min. Wash and elution steps were performed; concentrations of tracer bound to resin were determined as described above.

Data and statistical analysis. Data from fluorescent ligand binding assays were evaluated by a nonlinear, least-squares curve-fitting procedure in Prism (version 4, GraphPad Software, La Jolla, CA). Association and dissociation time courses were analyzed by one-phase association and one-phase dissociation exponential decay curves, respectively. Equilibrium binding data were analyzed in Prism by using the n-ligand m-binding site model in the Ligand¹⁴⁷ and DESIGN¹⁴⁸ computer programs. Parameter errors are expressed as percentage CV and were calculated by simultaneous analysis of at least three independent experiments performed in duplicate or triplicate. Parameter comparisons were performed based on the F-test for extra sum of square principle. All curves are computer generated.

LptC intrinsic fluorescence quenching. Samples containing sH-LptC (40.7 μM) and f-LOS (0 - 90 μM) were prepared in sodium phosphate (50 mM, pH 8) with NaCl (50 mM), incubated (22 °C, 90 min) with agitation (300 rpm), then transferred into a quartz cuvette (1 cm path length).

Fluorescence emission spectra (310 - 475 nm) were recorded at 22 °C with an Eclipse spectrofluorimeter (Varian; excitation 295 nm, excitation/emission slits 5 nm). To test binding reversibility, aliquots of the 45 μM f-LOS sample were diluted (up to 1:8) at fixed f-LOS concentration, and incubated for a further 120 min before fluorescence measurements.

Data analysis for quenching experiments. In the presence of dynamic quenching, the fraction of fluorescence intensities in the absence (F_0) and presence (F) of the quencher (f-LOS) is given by the ratio of the decay rate in the presence ($\gamma+k_q[\text{fLOS}]$) and absence (γ) of the quencher (Equation (1)):

$$\frac{F_0}{F} = \frac{\gamma + k_q[\text{fLOS}]}{\gamma} = 1 + K_{\text{dyn}}[\text{fLOS}] \quad (1)$$

When static quenching also occurs due to binding, Equation (1) applies only for fluorophores that are not involved in a complex. The contribution of this fraction can be expressed by Equation (2):

$$\frac{F_0}{F} = \frac{[\text{LptC}]_{\text{tot}}}{[\text{LptC}]} (1 + K_{\text{dyn}}[\text{fLOS}]) \quad (2)$$

The equations that define the dissociation constant (K_d) and the conservation of total protein and ligand are as follows [Eqs (3), (4), and (5)]:

$$K_d = \frac{[\text{LptC}][\text{fLOS}]}{[\text{complex}]} \quad (3)$$

$$[\text{complex}] = [\text{LptC}]_{\text{tot}} - [\text{LptC}] \quad (4)$$

$$[\text{fLOS}] = [\text{fLOS}]_{\text{tot}} - [\text{complex}] = [\text{fLOS}]_{\text{tot}} - [\text{LptC}]_{\text{tot}} + [\text{LptC}] \quad (5)$$

Combining Equations (1)–(5) it is possible to express F_0/F as a function of total protein and total ligand concentrations, K_{dyn} and K [Eq. (6)]:

$$\frac{F_0}{F} = \frac{[\text{LptC}]_{\text{tot}} \left(2 + K_{\text{dyn}} \left([\text{fLOS}]_{\text{tot}} - [\text{LptC}]_{\text{tot}} - K_d + \sqrt{([\text{LptC}]_{\text{tot}} - [\text{fLOS}]_{\text{tot}} - K_d)^2 + 4K_d[\text{LptC}]_{\text{tot}}} \right) \right)}{[\text{LptC}]_{\text{tot}} - [\text{fLOS}]_{\text{tot}} - K_d + \sqrt{([\text{LptC}]_{\text{tot}} - [\text{fLOS}]_{\text{tot}} - K_d)^2 + 4K_d[\text{LptC}]_{\text{tot}}} \quad (6)$$

The K_d value was determined by a nonlinear, least-squares curve-fitting procedure of fluorescence data by Equation (6), by using the K_{dyn} value obtained from free tryptophan experiments.

Minimum Inhibitory Concentration (MIC). Appropriate concentrations of iaxo-102, compound **1** and tetracycline (dissolved in DMSO:ethanol 1:1) were added to a 96-well plate containing 1:1,000 dilutions of the appropriate overnight cultures (*E. coli* MG1655, *E. coli* AS19 e *E. coli* ΔTolC). Serial dilutions (1:2) of the antibiotics were performed across the plate and the cells were grown overnight at 37 °C. Growth was determined by measuring the OD (630 nm), by using a spectrophotometer (LT 4000 Labtech).

5.2. Section II: Biology section

HEK-Blue™ cell culture. HEK-Blue™-4 cells were purchased from InvivoGen and cultured according to manufacturer's instructions. Briefly, cells were cultured in DMEM high glucose medium supplemented with 10% fetal bovine serum (FBS), 2 mM glutamine, 100 U/mL penicillin, 100 µg/ml streptomycin, 1x Normocin™ (Invivogen). HEK-Blue™-4 cells were maintained with the addition of 1x HEK-Blue™ Selection (Invivogen).

HEK-Blue™ cells assay. HEK-Blue-TLR4 cells (InvivoGen) were cultured as described before. Cells were detached by the use of a cell scraper, and the cell concentration was estimated by using Trypan Blue (Sigma-Aldrich). The cells were diluted in DMEM high glucose medium supplemented as described before and seeded in multiwall plate at a density of 2×10^4 cells/well in 200 µL. After overnight incubation (37 °C, 5% CO₂, 95% humidity), supernatant was removed and cell monolayers were washed with warm PBS without Ca²⁺ and Mg²⁺ and treated with increasing concentrations of compounds dissolved in DMSO–ethanol (1:1). After 30 min, the cells were stimulated with 10 nM LPS from *E. coli* O55:B5 (Sigma- Aldrich) and incubated overnight at 37 °C, 5% CO₂ and 95% humidity. As a control, the cells were treated with or without LPS (10 nM) alone. Then the supernatants were collected, and 50 µL of each sample was added to 100 µL PBS, pH 8, 0.84 mM

paranitrophenylphosphate (pNPP) for a final concentration of 0.8 mM pNPP. Plates were incubated for 2 - 4 h in the dark at rt, and then the plate reading was assessed by using a spectrophotometer at 405 nm (LT 4000, Labtech). The results were normalized with positive control (LPS alone) and expressed as the mean of percentage \pm SD of at least three independent experiments. The IC₅₀ values have been calculated by non-linear regression analysis using GraphPad Prism.

NF- κ B-Luciferase Reporter Assay. Expression plasmid for mouse MD-2 was a gift from Dr. Y. Nagai (University of Tokyo, Japan). Expression plasmid for mouse TLR4 was purchased from InvivoGen (CA, USA). Expression plasmids containing sequences of human TLR4 and MD-2 as well as the pELAM-1 firefly luciferase plasmid were a gift from Dr. C. Kirschning (Technical University of Munich, Germany). The Renilla luciferase phRL-TK plasmid was purchased from Promega (WI, USA). The human embryonic kidney (HEK) 293 cells were provided by Dr. J. Chow (Eisai Research Institute, Andover, MA, USA). HEK 293 cells were grown in DMEM supplemented with 10% fetal bovine serum (FBS). Cells were seeded in 96-well Costar plates (Corning, NY, USA) at 1.6×10^4 cells/well and incubated overnight in a humidified atmosphere (5% CO₂) at 37 °C. The next day, when cells were 40–60% confluent, they were cotransfected with human or murine MD-2 (10 ng), NF- κ B-dependent luciferase (70 ng), and constitutive Renilla (15 ng) reporter plasmids and

human or murine TLR4 plasmid (1 ng) using PEI (7.5 molar polyethylenimine pH 7.5, PolySciences) transfection reagent. Cells were stimulated 4 h after transfection with the synthetic compounds, previously dissolved in 100% DMSO to provide 4 mM stock solutions, and further working dilutions were prepared immediately before stimulation with cell medium (DMEM supplemented with 10% FBS). Then 1 h later with LPS (5 nM) that was extensively vortexed immediately prior to stimulation. Cells were lysed after 16 h of stimulation in 1× reporter assay lysis buffer (Promega, USA) and analyzed for reporter gene activities using a dual-luciferase reporter assay system. Relative luciferase activity (RLA) was calculated by normalizing each sample's firefly luciferase activity for constitutive Renilla activity measured within the same sample. When plotting the data, the value of the wild type MD-2·TLR4 sample stimulated with LPS was normalized to 100 and other values were adjusted accordingly.

MTT Cell Viability Assay. HEK-Blue-TLR4 cells were seeded in 100 µL of DMEM without Phenol Red at a density of 2×10^4 cells per well. After overnight incubation, 10 µL of compounds were added and the plates were incubated overnight at 37 °C, 5% CO₂, 95% humidity. DMSO and PBS were included as control. Then 10 µL of MTT solution (5 mg/mL in PBS) were added to each well. After 3 h incubation (37 °C, 5% CO₂, 95% humidity), HCl 0.1 N in 2-propanol was added (100 µL/well) to dissolve

formazan crystals. Formazan concentration in the wells was determined by measuring the absorbance at 570 nm (LT 4000, Labtech). The results were normalized with untreated control (PBS) and expressed as the mean of percentage \pm SD of three independent experiments.

ELISA assay. Murine IL-6 and TNF- α concentrations were determined in the supernatants of BMDM. The cells were treated with increasing concentrations (0 - 5 μ M) of compound **14**, **18** and **20** for 1 h and then stimulated with LPS (5 nM). After 16 hours, the supernatants were harvested and the amount of human IL-6 and TNF- α was determined using ReadySetGo ELISA kit (e-Bioscience).

***In Vivo* Endotoxin Inhibition.** C57BL/6J mice (11 - 13 weeks old) were randomly assigned into groups and injected intraperitoneally with vehicle control (5% DMSO in PBS) (groups none and LPS only) or the inhibitory compound (2×10^{-7} mol compound/mouse, all in 5% DMSO solution). One hour later, the mice were injected intraperitoneally with vehicle control (PBS) (group none) or with LPS from *E. coli* 055:B5 (1×10^{-9} mol/mouse \approx 10 μ g LPS/mouse). Three hours later, the blood was collected. Serum was tested with the mouse TNF- α ELISA kit ("ReadySetGo", eBioscience) to determine the levels of mouse TNF- α . The experiment was performed according to the manufacturer's instructions.

Determination of cmc via Pyrene Fluorescence Measurements. To assess the amphiphilicity, the critical micelle concentrations (cmc) of all compounds have been determined using an established fluorescence technique based on pyrene.¹⁵² This extremely hydrophobic dye is preferentially incorporated in the interior of micelles. The onset of micelle formation can be observed in a shift of the fluorescence excitation spectra of the samples at an emission wavelength of 372 nm. In the concentration range of aqueous micellar solutions, a shift of the excitation band in the 335 nm region toward higher wavelengths confirms the incorporation of pyrene in the hydrophobic interior of micelles. The ratio of the fluorescence intensities at 339 and 335 nm was used to quantify the shift of the broad excitation band. The critical micelle concentrations were determined from the crossover point in the low concentration range. Fluorescence spectra were recorded with an F-2500 Hitachi spectrofluorophotometer and conventional 1 cm quartz cuvettes at 37 ± 0.1 °C, using 2.5 mm excitation and emission slits.

6. References

1. Silipo, A.; Molinaro, A. Lipid A structure. In *Bacterial lipopolysaccharides. Structure, chemical, synthesis, biogenesis and interaction with host cells*. Knirel, Y. A.; Valvano., M. A., Eds. Springer, **2011**.
2. Actor, J. K. Basic bacteriology. *Immunology and microbiology*. Elsevier's integrated review, II edition, **2007**.
3. Sperandio, P.; Dehò, G.; Polissi, A. The lipopolysaccharide transport system of Gram negative bacteria. *Biochimica et Biophysica Acta*, **2009**, 1791, 594-602.
4. Erridge, C.; Bennett-Guerrero, E.; Poxton, I. R. Structure and function of lipopolysaccharides. *Microbes and Infection*, **2002**, 4, 837–851.
5. Joiner, K. A.; Grossman, N.; Schmetz, M.; Leive, L. C3 binds preferentially to long-chain lipopolysaccharide during alternative pathway activation by *Salmonella Montevideo*. *Journal of Immunology*, **1986**, 136, 710-715.
6. Rietschel, E.T.; Kirikae, T.; Schade, F.U.; Mamat, U.; Schmidt, G.; Loppnow, H.; Ulmer, A.J.; Zähringer, U.; Seydel, U.; Di Padova, F.; Schreier, M.; Brade, H. Bacterial endotoxin: molecular relationships of structure to activity and function. *FASEB Journal*, **1994**, 8, 217–225.
7. Raetz, C. R.; Whitfield, C. Lipopolysaccharide endotoxins. *Annual Review of Biochemistry*, **2002**, 71, 635-700.
8. Bhattacharya, I.; Gautam, H.; Das, H. R. Characterization of LPS mutants of peanut specific Bradyrhizobium (GN17). *Glycoconjugate journal*, **2002**, 19, 395-402.
9. Evrard, B.; Balestrino, D.; Dosgilbert, A.; Bouya-Gachancard, J. L.; Charbonnel, N.; Forestier, C.; Tridon, A. Roles of capsule and lipopolysaccharide O-antigen in interactions of human monocyte-derived dendritic cells and *Klebsiella pneumoniae*. *Infection and Immunity*, **2010**, 78, 210-219.

10. Rioux, S. B.; C. Dubreuil, J.D.; Jacques, M. Isolation and characterization of LPS mutants of *Actinobacillus pleuropneumoniae* serotype 1. *Current Microbiology*, **1997**, *35*, 139-144.
11. Wilkinson, S. G. Bacterial lipopolysaccharides-themes and variations. *Progress in Lipid Research*, **1996**, *35*, 283-343.
12. Raetz, C. R.; Reynolds, C. M.; Trent, M. S.; Bishop, R. E. Lipid A modification systems in gram-negative bacteria. *Annual Review of Biochemistry*, **2007**, *76*, 295-329.
13. Valvano, M. A. Export of O specific lipopolysaccharide. *Frontiers in Bioscience*, **2003**, *8*, s452-471.
14. Doerrler, W. T. Lipid trafficking to the outer membrane of Gram-negative bacteria. *Molecular Microbiology*, **2006**, *60*, 542-552.
15. Williams, A. H.; Raetz, C. R. Structural basis for the acyl chain selectivity and mechanism of UDP-N-acetylglucosamine acyltransferase. *Proc Natl Acad Sci U S A*, **2007**, *104*, 13543-13550.
16. Buetow, L.; Smith, T. K.; Dawson, A.; Fyffe, S.; Hunter, W. N. Structure and reactivity of LpxD, the N-acyltransferase of lipid A biosynthesis. *Proc Natl Acad Sci U S A* **2007**, *104*, 4321-4326.
17. Babinski, K. J.; Kanjilal, S. J.; Raetz, C. R. Accumulation of the lipid A precursor UDP-2,3-diacetylglucosamine in an *Escherichia coli* mutant lacking the lpxH gene. *Journal of Biological Chemistry*, **2002**, *277*, 25947-56.
18. Babinski, K. J.; Ribeiro, A. A.; Raetz, C. R. The *Escherichia coli* gene encoding the UDP-2,3-diacetylglucosamine pyrophosphatase of lipid A biosynthesis. *Journal of Biological Chemistry*, **2002**, *277*, 25937-46.
19. Crowell, D. N.; Anderson, M. S.; Raetz, C. R. Molecular cloning of the genes for lipid A disaccharide synthase and UDP-N-acetylglucosamine acyltransferase in *Escherichia coli*. *Journal of Bacteriology*, **1986**, *168*, 152-159.
20. Crowell, D. N.; Reznikoff, W. S.; Raetz, C. R. Nucleotide sequence of the *Escherichia coli* gene for lipid A disaccharide synthase. *Journal of Bacteriology*, **1987**, *169*, 5727-5734.

21. Garrett, T. A.; Kadrmaz, J. L.; Raetz, C. R. Identification of the gene encoding the *Escherichia coli* lipid A 40-kinase. Facile phosphorylation of endotoxin analogs with recombinant LpxK. *Journal of Biological Chemistry*, **1997**, *272*, 21855–21864.
22. Garrett, T. A.; Que, N. L.; Raetz, C. R. Accumulation of a lipid A precursor lacking the 40-phosphate following inactivation of the *Escherichia coli* lpxK gene. *Journal of Biological Chemistry*, **1998**, *273*, 12457–12465.
23. Brozek, K. A.; Hosaka, K.; Robertson, A. D.; Raetz, C. R. Biosynthesis of lipopolysaccharide in *Escherichia coli*. Cytoplasmic enzymes that attach 3- deoxy-D-manno-octulosonic acid to lipid A. *Journal of Biological Chemistry*, **1989**, *264*, 6956–6966.
24. Brozek, K. A.; Raetz, C. R. Biosynthesis of lipid A in *Escherichia coli*. Acyl carrier protein-dependent incorporation of laurate and myristate. *Journal of Biological Chemistry*, **1990**, *265*, 15410–15417.
25. Polissi, A.; Georgopoulos, C. Mutational analysis and properties of the msbA gene of *Escherichia coli*, coding for an essential ABC family transporter. *Molecular Microbiology*, **1996**, *20*, 1221-1233.
26. Zhou, Z.; White, K. A.; Polissi, A.; Georgopoulos, C.; Raetz, C. R. Function of *Escherichia coli* MsbA, an essential ABC family transporter, in lipid A and phospholipid biosynthesis. *Journal of Biological Chemistry*, **1998**, *273*, 12466-12475.
27. Davidson, A. L.; Dassa, E.; Orelle, C.; Chen, J. Structure, function, and evolution of bacterial ATP-binding cassette systems. *Microbiology and Molecular Biology Review*, **2008**, *72*, 317-364.
28. Ward, A.; Reyes, C. L.; Yu, J.; Roth, C. B.; Chang, G. Flexibility in the ABC transporter MsbA: Alternating access with a twist. *Proc Natl Acad Sci U S A*, **2007**, *104*, 19005-10.
29. Doerrler, W. T.; Reedy, M. C.; Raetz, C. R. An *Escherichia coli* mutant defective in lipid export. *Journal of Biological Chemistry*, **2001**, *276*, 11461-11464.

30. Siarheyeva, A.; Sharom, F. J. The ABC transporter MsbA interacts with lipid A and amphipathic drugs at different sites. *Biochemical Journal*, **2009**, *419*, 317-328.
31. Alaimo, C.; Catrein, I.; Morf, L.; Marolda, C. L.; Callewaert, N.; Valvano, M. A.; Feldman, M. F.; Aebi, M. Two distinct but interchangeable mechanisms for flipping of lipid-linked oligosaccharides. *EMBO Journal*, **2006**, *25*, 967-976
32. Liu, D.; Cole, R. A.; Reeves, P. R. An O-antigen processing function for Wzx (RfbX): a promising candidate for O-unit flippase. *Journal of Bacteriology*, **1996**, *178*, 2102–2107.
33. Marolda, C. L.; Vicarioli, J.; Valvano, M. A. Wzx proteins involved in biosynthesis of O antigen function in association with the first sugar of the O-specific lipopolysaccharide subunit. *Microbiology*, **2004**, *150*, 4095-4105.
34. Zhang, L.; al-Hendy, A.; Toivanen, P.; Skurnik, M. Genetic organization and sequence of the rfb gene cluster of *Yersinia enterocolitica* serotype O:3: similarities to the dTDP-L-rhamnose biosynthesis pathway of *Salmonella* and to the bacterial polysaccharide transport systems. *Molecular Microbiology*, **1993**, *9*, 309-321.
35. Reeves, P. R.; Hobbs, M.; Valvano, M. A.; Skurnik, M.; Whitfield, C.; Coplin, D.; Kido, N.; Klena, J.; Maskell, D.; Raetz, C. R.; Rick, P. D. Bacterial polysaccharide synthesis and gene nomenclature. *Trends in Microbiology*, **1996**, *4*, 495-503.
36. Wang, X.; Quinn, P. J. Lipopolysaccharide: Biosynthetic pathway and structure modification. *Progress in Lipid Research*, **2010**, *49*, 97-107.
37. Oliver, D. B., Periplasm. In *E. coli and Salmonella: cellular and molecular biology*, Neidhardt, F. C., Ed. American Society for Microbiology Press: WASHINGTON, DC, **1996**; 88-103.
38. Bos, M. P.; Robert, V.; Tommassen, J. Biogenesis of the gram-negative bacterial outer membrane. *Annual Review of Microbiology*, **2007**, *61*, 191-214.
39. Osborn, M. J.; Gander, J. E.; Parisi, E. Mechanism of Assembly of the Outer Membrane of *Salmonella typhimurium*. Isolation and

- characterization of cytoplasmic and outer membrane. *The Journal of Biological Chemistry*, **1972**, *247*, 3973-3986.
40. Doerrler, W. T.; Raetz, C. R. ATPase activity of the MsbA lipid flippase of *Escherichia coli*. *Journal of Biological Chemistry*, **2002**, *277*, 36697-36705.
 41. Doerrler, W. T.; Gibbons, H. S.; Raetz, C. R. MsbA-dependent translocation of lipids across the inner membrane of *Escherichia coli*. *Journal of Biological Chemistry*, **2004**, *279*, 45102-45109.
 42. Sperandio, P.; Cescutti, R.; Villa, R.; Di Benedetto, C.; Candia, D.; Dehò, G.; Polissi, A. Characterization of lptA and lptB, two essential genes implicated in lipopolysaccharide transport to the outer membrane of *Escherichia coli*. *Journal of Bacteriology*, **2007**, *189*, 244-253.
 43. Sperandio, P.; Lau, F. K.; Carpentieri, A.; De Castro, C.; Molinaro, A.; Dehò, G.; Silhavy, T. J.; Polissi, A. Functional analysis of the protein machinery required for transport of lipopolysaccharide to the outer membrane of *Escherichia coli*. *Journal of Bacteriology*, **2008**, *190*, 4460-4469.
 44. Ruiz, N.; Gronenberg, L. S.; Kahne, D.; Silhavy, T. J. Identification of two inner-membrane proteins required for the transport of lipopolysaccharide to the outer membrane of *Escherichia coli*. *Proc Natl Acad Sci U S A*, **2008**, *105*, 5537-5542.
 45. Chng, S. S.; Ruiz, N.; Chimalakonda, G.; Silhavy, T. J.; Kahne, D. Characterization of the two-protein complex in *Escherichia coli* responsible for lipopolysaccharide assembly at the outer membrane. *Proc Natl Acad Sci U S A*, **2010**, *107*, 5363-5368.
 46. Narita, S.; Tokuda, H. Biochemical characterization of an ABC transporter LptBFGC complex required for the outer membrane sorting of lipopolysaccharides. *FEBS Letters*, **2009**, *583*, 2160-2164.
 47. Chng, S. S.; Gronenberg, L. S.; Kahne, D. Proteins required for lipopolysaccharide assembly in *Escherichia coli* form a transenvelope complex. *Biochemistry*, **2010**, *49*, 4565-4567.

48. Ruiz, N.; Kahne, D.; Silhavy, T. J. Transport of lipopolysaccharide across the cell envelope: the long road of discovery. *Nature Review Microbiology*, **2009**, *7*, 677-683.
49. Stenberg, F.; Chovanec, P.; Maslen, S. L.; Robinson, C. V.; Ilag, L. L.; von Heijne, G.; Daley, D. O. Protein complexes of the *Escherichia coli* cell envelope. *Journal of Biological Chemistry*, **2005**, *280*, 34409-34419.
50. Linton, K. J.; Higgins, C. F. Structure and function of ABC transporters: the ATP switch provides flexible control. *Pflugers Arch*, **2007**, *453*, 555-567.
51. Tran, A. X.; Trent, M. S.; Whitfield, C. The LptA protein of *Escherichia coli* is a periplasmic lipid A-binding protein involved in the lipopolysaccharide export pathway. *Journal of Biological Chemistry*, **2008**, *283*, 20342-20349.
52. Suits, M. D.; Sperandio, P.; Dehò, G.; Polissi, A.; Jia, Z. Novel structure of the conserved gram-negative lipopolysaccharide transport protein A and mutagenesis analysis. *Journal of Molecular Biology*, **2008**, *380*, 476-488.
53. Braun, M.; Silhavy, T. J. Imp/OstA is required for cell envelope biogenesis in *Escherichia coli*. *Molecular Microbiology*, **2002**, *45*, 1289-1302.
54. Wu, T.; McCandlish, A. C.; Gronenberg, L. S.; Chng, S. S.; Silhavy, T. J.; Kahne, D., Identification of a protein complex that assembles lipopolysaccharide in the outer membrane of *Escherichia coli*. *Proc Natl Acad Sci U S A*, **2006**, *103*, 11754-11759.
55. Tokuda, H., Biogenesis of outer membranes in Gram-negative bacteria. *Bioscience Biotechnology Biochemistry*, **2009**, *73*, 465-473.
56. Bowyer, A.; Baardsnes, J.; Ajamian, E.; Zhang, L.; Cygler, M., Characterization of interactions between LPS transport proteins of the Lpt system. *Biochemical and Biophysical Research Communication,s* **2011**, *404*, 1093-1098.
57. Tran, A. X.; Dong, C.; Whitfield, C. Structure and functional analysis of LptC, a conserved membrane protein involved in the lipopolysaccharide

- export pathway in Escherichia coli. *Journal of Biological Chemistry*, **2010**, *285*, 33529-33539.
58. Taniguchi, N.; Tokuda, H. Molecular events involved in a single cycle of ligand transfer from an ATP binding cassette transporter, LolCDE, to a molecular chaperone, LolA. *Journal of Biological Chemistry*, **2008**, *283*, 8538-8544.
59. Okuda, S.; Freinkman, E.; Kahne, D. Cytoplasmic ATP hydrolysis powers transport of lipopolysaccharide across the periplasm in *E. coli*. *Science*, **2012**, *33*, 1214-1217.
60. Sestito, S. E.; Sperandio, P.; Santambrogio, C.; Ciaramelli, C.; Calabrese, V.; Rovati, G. E.; Zambelloni, L.; Grandori, R.; Polissi, A.; Peri, F. Functional characterization of *E. coli* LptC: interaction with LPS and a synthetic ligand. *Chembiochem*, **2014**, *15*, 734-742.
61. Todar, K. Bacterial resistance to antibiotics. In *Textbook of Bacteriology.net*
62. Kerwat, K.; Kerwat, M.; Graf, J.; Wulf, H. Resistance to antibiotics and multiresistant pathogens. *Anesthesiol Intensivmed Notfallmed Schmerzther*, **2010**, *45*, 242-243.
63. Falagas, M. E.; Bliziotis, I. A.; Kasiakou, S. K.; Samonis, G.; Athanassopoulou, P.; Michalopoulos, A. Outcome of infections due to pandrug-resistant (PDR) Gram-negative bacteria. *BMC Infectious Diseases*, **2005**, *5*, 24.
64. Donadio, S.; Maffioli, S.; Monciardini, P.; Sosio, M.; Jabes, D. Sources of novel antibiotics--aside the common roads. *Applied Microbiology and Biotechnology*, **2010**, *88*, 1261-1267.
65. Walsh, C. Where will new antibiotics come from? *Nature Review Microbiology*, **2003**, *1*, 65-70.
66. Patel, U.; Yan, Y. P.; Hobbs, F. W.; Kaczmarczyk, J.; Slee, A. M.; Pompliano, D. L.; Kurilla, M. G.; Bobkova, E. V. Oxazolidinones mechanism of action: inhibition of the first peptide bond formation. *Journal of Biological Chemistry*, **2001**, *276*, 37199-37205.
67. Yan, K.; Madden, L.; Choudhry, A. E.; Voigt, C. S.; Copeland, R. A.; Gontarek, R. R. Biochemical characterization of the interactions of the

- novel pleuromutilin derivative retapamulin with bacterial ribosomes. *Antimicrobial Agents and Chemotherapy*, **2006**, *50*, 3875-3881.
68. Jung, D.; Rozek, A.; Okon, M.; Hancock, R. E. Structural transitions as determinants of the action of the calcium-dependent antibiotic daptomycin. *Chemistry Biology*, **2004**, *11*, 949-957.
69. Singh, M. P.; Greenstein, M. Antibiotic selection pressure and resistance in *Streptococcus pneumoniae* and *Streptococcus pyogenes*. Antibacterial leads from microbial natural products discovery. *Current Opinion in Drug Discovery and Development*, **2000**, *3*, 167-176.
70. Fischbach, M. A.; Walsh, C. T. Antibiotics for emerging pathogens. *Science*, **2009**, *325*, 1089-1093.
71. Weber, A.; Casini, A.; Heine, A.; Kuhn, D.; Supuran, C. T.; Scozzafava, A.; Klebe, G. Unexpected nanomolar inhibition of carbonic anhydrase by COX-2-selective celecoxib: new pharmacological opportunities due to related binding site recognition. *Journal of Medicinal Chemistry*, **2004**, *47*, 550-557.
72. Kinnings, S. L.; Liu, N.; Buchmeier, N.; Tonge, P. J.; Xie, L.; Bourne, P. E. Drug Discovery Using Chemical Systems Biology: Repositioning the Safe Medicine Comtan to Treat Multi-Drug and Extensively Drug Resistant Tuberculosis. *PLoS Computational Biology*, **2009**, *5*, e1000423.
73. Gronenberg, L. S.; Kahne, D. Development of an activity assay for discovery of inhibitors of lipopolysaccharide transport. *JACS*, **2010**, *132*, 2518-2519.
74. Srinivas, N.; Jetter, P.; Ueberbacher, B. J.; Werneburg, M.; Zerbe, K.; Steinmann, J.; Van der Meijden, B.; Bernardini, F.; Lederer, A.; Dias, R. L.; Misson, P. E.; Henze, H.; Zumbunn, J.; Gombert, F. O.; Obrecht, D.; Hunziker, P.; Schauer, S.; Ziegler, U.; Käch, A.; Eberl, L.; Riedel, K.; DeMarco, S. J.; Robinson, J. A. Peptidomimetic antibiotics target outer-membrane biogenesis in *Pseudomonas aeruginosa*. *Science*, **2010**, *327*, 1010-1013.
75. Kokryakov, V. N.; Harwig, S. S.; Panyutich, E. A.; Shevchenko, A. A.; Aleshina, G. M.; Shamova, O. V.; Korneva, H. A.; Lehrer, R. I. Protegrins:

- leukocyte antimicrobial peptides that combine features of corticostatic defensins and tachyplesins. *FEBS Letters*, **1993**, *327*, 231-236.
76. Ausubel, F. M. Are innate immune signaling pathways in plants and animals conserved? *Nature Immunology*, **2005**, *6*, 973-979.
77. Gallo, R. L.; Hooper, L. V. Epithelial antimicrobial defence of the skin and intestine. *Nature Reviews Immunology*, **2012**, *12*, 503-516.
78. Giangrande, C.; Colarusso, L.; Lanzetta, R.; Molinaro, A.; Pucci, P.; Amoresano, A. Innate immunity probed by lipopolysaccharides affinity strategy and proteomics. *Analytical and Bioanalytical Chemistry*, **2013**, *405*, 775-784.
79. Tan, L. A.; Yang, A. C.; Kishore, U.; Sim, R. B. Interactions of complement proteins C1q and factor H with lipid A and *Escherichia coli*: further evidence that factor H regulates the classical complement pathway. *Protein Cell*, **2011**, *2*, 320-332.
80. Lewis, L. A.; Shafer, W. M.; Dutta Ray, T.; Ram, S.; Rice, P. A. Phosphoethanolamine residues on the lipid A moiety of *Neisseria gonorrhoeae* lipooligosaccharide modulate binding of complement inhibitors and resistance to complement killing. *Infection and Immunity*, **2013**, *81*, 33-42.
81. Krauel, K.; Weber, C.; Brandt, S.; Zähringer, U.; Mamat, U.; Greinacher, A.; Hammerschmidt, S. Platelet factor 4 binding to lipid A of Gram-negative bacteria exposes PF4/heparin-like epitopes. *Blood*, **2012**, *120*, 3345-3352.
82. Needham, B. D.; Trent, M. S., Fortifying the barrier: the impact of lipid A remodelling on bacterial pathogenesis. *Nature Reviews Microbiology*, **2013**, *11*, 467-481.
83. Takeuchi, O.; Akira, S. Pattern recognition receptors and inflammation. *Cell*, **2010**, *140*, 805-820.
84. Akira, S.; Uematsu, S.; Takeuchi, O. Pathogen recognition and innate immunity. *Cell*, **2006**, *124*, 783-801.
85. Beutler, B. Toll-like receptors and their place in immunology. Where does the immune response to infection begin? *Nature Reviews Microbiology*, **2004**, *4*, 498.

86. Peri, F.; Piazza, M. Therapeutic targeting of innate immunity with Toll-like receptor 4 (TLR4) antagonists. *Biotechnology Advance*, **2012**, *30*, 251-260.
87. Imler, J. L. H., J.A. Toll receptors in innate immunity. *Trends in Cell Biology*, **2001**, *11*, 304-311.
88. Beutler, B. Toll-like receptors: how they work and what they do. *Current Opinion in Hematology*, **2002**, *9*, 2-10.
89. Peri, F.; Calabrese, V. Toll-like receptor 4 (TLR4) modulation by synthetic and natural compounds: an update. *Journal of Medicinal Chemistry*, **2014**, *57*, 3612-3622.
90. Medzhitov, R. Toll-like receptors and innate immunity. *Nature Reviews Microbiology*, **2001**, *1*, 135-145.
91. Park, S. J.; Youn, H. S. Suppression of homodimerization of toll-like receptor 4 by isoliquiritigenin. *Phytochemistry*, **2010**, *71*, 1736-1740.
92. Kong, Q.; Six, D. A.; Liu, Q.; Gu, L.; Roland, K. L.; Raetz, C. R.; Curtiss, R. Palmitoylation state impacts induction of innate and acquired immunity by the *Salmonella enterica* serovar typhimurium msbB mutant. *Infection and Immunity*, **2011**, *79*, 5027-5038.
93. Hajjar, A. M.; Ernst, R. K.; Tsai, J. H.; Wilson, C. B.; Miller, S. I., Human Toll-like receptor 4 recognizes host-specific LPS modifications. *Nature Immunology*, **2002**, *3*, 354-359.
94. Kong, Q.; Six, D. A.; Liu, Q.; Gu, L.; Wang, S.; Alamuri, P.; Raetz, C. R.; Curtiss, R. Phosphate groups of lipid A are essential for *Salmonella enterica* serovar Typhimurium virulence and affect innate and adaptive immunity. *Infectious and Immunology*, **2012**, *80*, 3215-3224.
95. Miyake, K. Innate recognition of lipopolysaccharide by Toll-like receptor 4-MD-2. *Trends in Microbiology*, **2004**, *12*, 186-192.
96. Casella, C. R.; Mitchell, T. C. Putting endotoxin to work for us: monophosphoryl lipid A as a safe and effective vaccine adjuvant. *Cellular and Molecular Life Science*, **2008**, *65*, 3231-3240.
97. Yamamoto, M.; Akira, S. Lipid A receptor TLR4-mediated signaling pathways. *Advance in Experimental Medicine and Biology*, **2010**, *667*, 59-68.

98. Mata-Haro, V.; Cekic, C.; Martin, M.; Chilton, P. M.; Casella, C. R.; Mitchell, T. C. The vaccine adjuvant monophosphoryl lipid A as a TRIF-biased agonist of TLR4. *Science*, **2007**, *316*, 1628-1632.
99. Schumann, R. R. Function of lipopolysaccharide (LPS)-binding protein (LBP) and CD14, the receptor for LPS/LBP complexes: a short review. *Research in immunology*, **1992**, *143*, 11-15.
100. Beamer, L. J.; Carroll, S. F.; Eisenberg, D. Crystal Structure of Human BPI and Two Bound Phospholipids at 2.4 Angstrom Resolution. *Science*, **1997**, *276*, 1861-1864.
101. Gioannini, T. L.; Zhang, D.; Teghanemt, A.; Weiss, J. P. An essential role for albumin in the interaction of endotoxin with lipopolysaccharide-binding protein and sCD14 and resultant cell activation. *Journal of Biological Chemistry*, **2002**, *277*, 47818-47825.
102. Gutschmann, T.; Schromm, A. B.; Brandenburg, K. The physicochemistry of endotoxins in relation to bioactivity. *International Journal of Medical Microbiology*, **2007**, *297*, 341-352.
103. Thomas, C. J.; Kapoor, M.; Sharma, S.; Bausinger, H.; Zyilanb, U.; Lipskerb, D.; Hanaub, D.; Surolia, A. Evidence of a trimolecular complex involving LPS, LPS binding protein and soluble CD14 as an effector of LPS response. *FEBS Letters* **2002**, *531*, 184-188.
104. Kim, J. I.; Lee, C. J.; Jin, M. S.; Lee, C. H.; Paik, S. G.; Lee, H.; Lee, J. O. Crystal structure of CD14 and its implications for lipopolysaccharide signaling. *Journal of Biological Chemistry*, **2005**, *280*, 11347-11351.
105. Muroi, M.; Ohnishi, T.; Tanamoto, K. Regions of the mouse CD14 molecule required for toll-like receptor 2- and 4-mediated activation of NF-kappa B. *Journal of Biological Chemistry*, **2002**, *277*, 42372-42379.
106. Wright, S.; Ramos, R.; Tobias, P.; Ulevitch, R. CD14, a receptor for complexes of lipopolysaccharide (LPS) and LPS binding protein. *Science*, **1990**, *249*, 1431-1433.
107. Triantafilou, M.; Triantafilou, K.; Fernandez, N. Rough and smooth forms of fluorescein-labelled bacterial endotoxin exhibit CD14/LBP dependent and independent binding that is influenced by endotoxin

- concentration. *European Journal of Biochemistry*, **2000**, *267*, 2218–2226.
108. Botos, I.; Segal, D. M.; Davies, D. R. The structural biology of Toll-like receptors. *Structure*, **2011**, *19*, 447-459.
109. Visintin, A.; Iliev, D. B.; Monks, B. G.; Halmen, K. A.; Golenbock, D. T. MD-2. *Immunobiology*, **2006**, *211*, 437-447.
110. Gruber, A.; Mancek, M.; Wagner, H.; Kirschning, C. J.; Jerala, R. Structural model of MD-2 and functional role of its basic amino acid clusters involved in cellular lipopolysaccharide recognition. *Journal of Biological Chemistry*, **2004**, *279*, 28475-28482.
111. Ohto, U.; Fukase, K.; Miyake, K.; Satow, Y. Crystal structures of human MD-2 and its complex with antiendotoxic lipid IVa. *Science*, **2007**, *316*, 1632-1634.
112. Mueller, M.; Lindner, B.; Kusumoto, S.; Fukase, K.; Schromm, A. B.; Seydel, U. Aggregates are the biologically active units of endotoxin. *Journal of Biological Chemistry*, **2004**, *279*, 26307-26313.
113. Kanzler, H.; Barrat, F. J.; Hessel, E. M.; Coffman, R. L. Therapeutic targeting of innate immunity with Toll-like receptor agonists and antagonists. *Nature Medicine*, **2007**, *13*, 552-559.
114. Awasthi, S. Toll-like receptor-4 modulation for cancer immunotherapy. *Frontiers in Immunology*, **2014**, *5*, 328.
115. Artner, D.; Oblak, A.; Ittig, S.; Garate, J. A.; Horvat, S.; Arrieumerlou, C.; Hofinger, A.; Oostenbrink, C.; Jerala, R.; Kosma, P.; Zamyatina, A. Conformationally constrained lipid A mimetics for exploration of structural basis of TLR4/MD-2 activation by lipopolysaccharide. *ACS Chemical Biology*, **2013**, *8*, 2423-2432.
116. Wittebole, X.; Castanares-Zapatero, D.; Laterre, P. F. Toll-like receptor 4 modulation as a strategy to treat sepsis. *Mediators of Inflammation*, **2010**, *2010*, 1-8.
117. Hawkins, L. D.; Christ, W. J.; Rossignol, D. P. Inhibition of endotoxin response by synthetic TLR4 antagonists. *Current Topics in Medicinal Chemistry*, **2004**, *4*, 1147-1171.

118. Bowen, W. S.; Minns, L. A.; Johnson, D. A.; Mitchell, T. C.; Hutton, M. M.; Evans, J. T. Selective TRIF-dependent signaling by a synthetic toll-like receptor 4 agonist. *Science Signaling*, **2012**, 5, 13–20.
119. Wang, X.; Smith, C.; Yin, H. Targeting Toll-like receptors with small molecule agents. *Chemical Society Reviews*, **2013**, 42, 4859–4866.
120. Lonez, C.; Vandenbranden, M.; Ruyschaert, J.M. Cationic lipids activate intracellular signaling pathways. *Advanced Drug Delivery Reviews*, **2012**, 64, 1749–1758.
121. Bettoni, I.; Comelli, F.; Rossini, C.; Granucci, F.; Giagnoni, G.; Peri, F.; Costa, B. Glial TLR4 receptor as new target to treat neuropathic pain: efficacy of a new receptor antagonist in a model of peripheral nerve injury in mice. *Glia*, 2008, 56, 1312-1319.
122. Piazza, M.; Yu, L.; Teghanemt, A.; Gioannini, T.; Weiss, J.; Peri, F. Evidence of a specific interaction between new synthetic antisepsis agents and CD14. *Biochemistry* **2009**, 48, 12337-12344.
123. Yamada, M.; Ichikawa, T.; li, M.; Sunamoto, M.; Itoh, K. Tamura, N.; Kitazaki T. Discovery of novel and potent small-molecule inhibitors of NO and cytokine production as antisepsis agents: synthesis and biological activity of alkyl 6-(N-substituted sulfamoyl)cyclohex-1-ene-1-carboxylate. *Journal of Medicinal Chemistry*, 2005, 48; 7457-7467.
124. Takashima, K.; Matsunaga, N.; Yoshimatsu, M.; Hazeki, K.; Kaisho, T.; Uekata, M.; Hazeki, O.; Akira, S.; Iizawa, Y.; li, M. Analysis of binding site for the novel small.molecule TLR4 signal trasduction inhibitor TAK-242 and its the therapeutic effect on mouse sepsi model. *British Journal of Pharmacology*, **2009**, 157, 1250-1260.
125. Gradisar, H.; Keber, M. M.; Pristovsek, P.; Jerala, R. MD-2 as the target of curcumin in the inhibition of response to LPS. *Journal of Leukocyte Biology*, **2007**, 82, 968-974.
126. Koo, J. E.; Park, Z. Y.; Kim, N. D.; Lee, J. Y. Sulforaphane inhibits the engagement of LPS with TLR4/MD-2 complex by preferential binding to Cys133 in MD-2. *Biochemical and Biophysical Research Communications*,. **2013**, 434, 600–605.

127. Park, S. J.; Shin, H. J.; Youn, H. S. Parthenolide inhibits TRIF-dependent signaling pathway of Toll-like receptors in RAW264.7 macrophages. *Molecular Cells*, **2011**, *31*, 261-265.
128. Youn, H. S.; Lee, J. Y.; Saitoh, S. I.; Miyake, K.; Kang, K. W.; Choi, Y. J.; Hwang, D. H. Suppression of MyD88- and TRIF-dependent signaling pathways of Toll-like receptor by (-)-epigallocatechin-3-gallate, a polyphenol component of green tea. *Biochemical Pharmacology*. **2006**, *72*, 850–859.
129. Cárdeno, A.; Sánchez-Hidalgo, M.; Alarcón-de-la-Lastra, C., An Up-date of Olive Oil Phenols in Inflammation and Cancer: Molecular Mechanisms and Clinical Implications. *Current Medicinal Chemistry*, **2013**, *20*, 4758-4776.
130. Lavelli, V.; Bondesan, L. Secoiridoids, tocopherols, and antioxidant activity of monovarietal extra virgin olive oils extracted from destoned fruits. *Journal of Agricultural and Food Chemistry*, **2005**, *53*, 1102-1107.
131. Carrasco-Pancorbo, A.; Cerretani, L.; Bendini, A.; Segura-Carretero, A.; Gallina-Toschi, T.; Fernandez-Gutierrez, A. Analytical determination of polyphenols in olive oils. *Journal of Separation Science*, **2005**, *28*, 837-858.
132. Gallina-Toschi, T.; Cerretani, L.; Bendini, A.; Bonoli-Carbognin, M.; Lercker, G. Oxidative stability and phenolic content of virgin olive oil: an analytical approach by traditional and high resolution techniques. *Journal of Separation Science*, **2005**, *28*, 859-870.
133. Owen, R. W.; Giacosa, A.; Hull, W. E.; Haubner, R.; Würtele, G.; Spiegelhalder, B.; Bartsch, H. Olive-oil consumption and health: the possible role of antioxidants. *The Lancet Oncology*, **2000**, *1*, 107-112.
134. Sangiovanni, E.; Colombo, E.; Fumagalli, M.; Abbiati, F.; Caruso, D.; Dell'Agli, M. Inhibition of NF- κ B activity by minor polar components of extra-virgin olive oil at gastric level. *Phytotherapy Research*, **2012**, *26*, 1569-1571.
135. Visioli, F.; Poli, A.; Gall, C., Antioxidant and other biological activities of phenols from olives and olive oil. *Medicinal Research Review* **2002**, *22*, 65-75.

136. Maiuri, M. C.; De Stefano, D.; Di Meglio, P.; Irace, C.; Savarese, M.; Sacchi, R.; Cinelli, M. P.; Carnuccio, R. Hydroxytyrosol, a phenolic compound from virgin olive oil, prevents macrophage activation. *Naunyn-Schmiedeberg's Archives of Pharmacology*, **2005**, *371*, 457-465.
137. Iacono, A.; Gómez, R.; Sperry, J.; Conde, J.; Bianco, G.; Meli, R.; Gómez-Reino, J. J.; Smith, A. B.; Gualillo, O. Effect of oleocanthal and its derivatives on inflammatory response induced by lipopolysaccharide in a murine chondrocyte cell line. *Arthritis and Rheumatology*, **2010**, *62*, 1675-1682.
138. Beauchamp, G. K.; Keast, R. S.; Morel, D.; Lin, J.; Pika, J.; Han, Q.; Lee, C. H.; Smith, A. B.; Breslin, P. A. Phytochemistry: ibuprofen-like activity in extra-virgin olive oil. *Nature*, **2005**, *437*, 45-46.
139. Dell'Agli, M.; Fagnani, R.; Galli, G. V.; Maschi, O.; Gilardi, F.; Bellosta, S.; Crestani, M.; Bosisio, E.; De Fabiani, E.; Caruso, D. Olive oil phenols modulate the expression of metalloproteinase 9 in THP-1 cells by acting on nuclear factor-kappaB signaling. *J Agric Food Chem* **2010**, *58* (4), 2246-52.
140. Montedoro, G.; Servili, M., Simple and hydrolyzable compounds in virgin olive oil. Spectroscopic characterizations of the secoiridoid derivatives. *Journal of Agricultural and Food Chemistry*, **1993**, *41*, 2228-2234.
141. Xagorari, A.; Roussos, C.; Papapetropoulos, A. Inhibition of LPS-stimulated pathways in macrophages by the flavonoid luteolin. *British Journal of Pharmacology*, **2002**, *136*, 1058-1064.
142. Xagorari, A.; Papapetropoulos, A.; Mauromatis, A.; Economou, M.; Fotsis, T.; Roussos, C., Luteolin inhibits an endotoxin-stimulated phosphorylation cascade and proinflammatory cytokine production in macrophages. *Journal of Pharmacology and Experimental Therapeutics*, **2001**, *296*, 181-187.
143. Martínez-Domínguez, E.; de la Puerta, R.; Ruiz-Gutiérrez, V. Protective effects upon experimental inflammation models of a polyphenol-supplemented virgin olive oil diet. *Inflammation Research*, **2001**, *50*, 102-106.

144. Frontela, C.; Canali, R.; Virgili, F. Use of dietary phenols to modulate inflammatory bowel response. *Journal of Gastroenterology and Hepatology*, **2010**, *33*, 307-312.
145. Galanos, C.; Luderitz, O.; Westphal, O. A new method for the extraction of R lipopolysaccharides. *European journal of biochemistry*, **1969**, *9*, 245-249.
146. Troelstra, A.; Antal-Szalmas, P.; de Graaf-Miltenburg, L. A.; Weersink, A. J.; Verhoef, J.; Van Kessel, K. P.; Van Strijp, J. A. Saturable CD14-Dependent Binding of Fluorescein-Labeled Lipopolysaccharide to Human Monocytes. *Infection and immunity*, **1997**, *65*, 2272-2277.
147. Munson, P. J.; Rodbard, D. LIGAND: A versatile computerized approach for characterization of ligand-binding systems. *Analytical Biochemistry*, **1980**, *107*, 220–239.
148. Rovati, G. E.; Rodbard, D.; Munson, P. J. DESIGN: computerized optimization of experimental design for estimating K_d and B_{max} in ligand binding experiments. I. Homologous and heterologous binding to one or two classes of sites. *Analytical Biochemistry*, **1988**, *174*, 636-649.
149. Piazza, M.; Calabrese, V.; Baruffa, C.; Gioannini, T.; Weiss, J.; Peri, F. The cationic amphiphile 3,4-bis(tetradecyloxy)benzylamine inhibits LPS signaling by competing with endotoxin for CD14 binding. *Biochemical Pharmacology*, **2010**, *80*, 2050-2056.
150. Peri, F.; Granucci, F.; Costa, B.; Zanoni, I.; Marinzi, C.; Nicotra, F. Inhibition of lipid A stimulated activation of human dendritic cells and macrophages by amino and hydroxylamino monosaccharides. *Angew Chem Int Ed Engl* **2007**, *46*, 3308-3312.
151. Eckford, P. D.; Sharom, F. J., Functional characterization of *Escherichia coli* MsbA: interaction with nucleotides and substrates. *Journal of Biological Chemistry*, **2008**, *283*, 12840-12850.
152. Hofmann, A. M.; Wurm, F.; Frey, H. Rapid Access to Polyfunctional Lipids with Complex Architecture via Oxyanionic Ring-Opening Polymerization. *Macromolecules*, **2011**, *44*, 4648–4657.

153. Park, B. S.; Song, D. H.; Kim, H. M.; Choi, B. S.; Lee, H.; Lee, J. O. The structural basis of lipopolysaccharide recognition by the TLR4-MD-2 complex. *Nature*, **2009**, *458*, 1191-1195.
154. Gutschmann, T.; Schromm, A.; Brandenburg, K. The physicochemistry of endotoxins in relation to bioactivity. *International Journal of Medical Microbiology*, **2007**, *297*, 341-352.
155. Piazza, M.; Rossini, C.; Della Fiorentina, S.; Pozzi, C.; Comelli, F.; Bettoni, I.; Fusi, P.; Costa, B.; Peri, F. Glycolipids and benzylammonium lipids as novel antiseptics agents: synthesis and biological characterization. *Journal of Medicinal Chemistry*, **2009**, *52*, 1209-1213.
156. Nativi, C.; Francesconi, O.; Gabrielli, G.; De Simone, I.; Turchetti, B.; Mello, T.; Di Cesare Mannelli, L.; Ghelardini, C.; Buzzini, P.; Roelens, S. Aminopyrrolic synthetic receptors for monosaccharides: a class of carbohydrate-binding agents endowed with antibiotic activity versus pathogenic yeasts. *Chemistry*, **2012**, *18*, 5064-5072.
157. Funatogawa, K.; Matsuura, M.; Nakano, M.; Kiso, M.; Hasegawa, A. Relationship of structure and biological activity of monosaccharide lipid A analogues to induction of nitric oxide production by murine macrophage RAW264.7 cells. *Infection and Immunity*, **1998**, *66*, 5792-5798.
158. Rodriguez Lavado, J.; Sestito, S. E.; Cighetti, R.; Aguilar Moncayo, E. M.; Oblak, A.; Lainšček, D.; Jiménez Blanco, J. L.; García Fernández, J. M.; Ortiz Mellet, C.; Jerala, R.; Calabrese, V.; Peri, F., Trehalose- and Glucose-Derived Glycoamphiphiles: Small-Molecule and Nanoparticle Toll-Like Receptor 4 (TLR4) Modulators. *Journal of Medicinal Chemistry*, **2014**, *57*, 9105-9123.
159. Piazza, M.; Calabrese, V.; Damore, G.; Cighetti, R.; Giannini, T.; Weiss, J.; Peri, F. A synthetic lipid A mimetic modulates human TLR4 activity. *ChemMedChem*, **2012**, *7*, 213-217.

Publications

- Functional characterization of *E. coli* LptC: interaction with LPS and a synthetic ligand (*ChemBioChem*, 2014, 15, 734 – 742)
- Trehalose- and glucose-derived glycoamphiphiles: small-molecule and nanoparticle toll-like receptor 4 (TLR4) modulators (*J. Med. Chem.*, 2014, 57, 9105–9123)
- Modulation of CD14 and TLR4·MD-2 activities by a synthetic lipid a mimetic (*ChemBioChem*, 2014, 15, 250 – 258)
- Clicked and long spaced galactosyl- and lactosylcalix[4]arenes: new multivalent galectin-3 ligands (*Beilstein J. Org. Chem.*, 2014, 10, 1672–1680)

Functional Characterization of *E. coli* LptC: Interaction with LPS and a Synthetic Ligand

Stefania E. Sestito,^[a] Paola Sperandeo,^[a] Carlo Santambrogio,^[a] Carlotta Ciaramelli,^[a] Valentina Calabrese,^[a] G. Enrico Rovati,^[b] Luca Zambelloni,^[a] Rita Grandori,^[a] Alessandra Polissi,^{*[a]} and Francesco Peri^{†*[a]}

Lipopolysaccharide (LPS), the main cell-surface molecular constituent of Gram-negative bacteria, is synthesized in the inner membrane (IM) and transported to the outer membrane (OM) by the Lpt (lipopolysaccharide transport) machinery. Neosynthesized LPS is first flipped by MsbA across the IM, then transported to the OM by seven Lpt proteins located in the IM (LptBCFG), in the periplasm (LptA), and in the OM (LptDE). A functional OM is essential to bacterial viability and requires correct placement of LPS in the outer leaflet. Therefore, LPS biogenesis represents an ideal target for the development of novel antibiotics against Gram-negative bacteria. Although the structures of Lpt proteins have been elucidated, little is known about the mechanism of LPS transport, and few data are available on Lpt–LPS binding. We report here the first determination of the thermodynamic and kinetic parameters of the interaction between LptC and a fluorescent lipo-oligosaccharide (fLOS) in vitro. The apparent dissociation constant (K_d) of the

fLOS–LptC interaction was evaluated by two independent methods. The first was based on fLOS capture by resin-immobilized LptC; the second used quenching of LptC intrinsic fluorescence by fLOS in solution. The K_d values by the two methods (71.4 and 28.8 μM , respectively) are very similar, and are of the same order of magnitude as that of the affinity of LOS for the upstream transporter, MsbA. Interestingly, both methods showed that fLOS binding to LptC is mostly irreversible, thus reflecting the fact that LPS can be released from LptC only when energy is supplied by ATP or in the presence of a higher-affinity LptA protein. A fluorescent glycolipid was synthesized: this also interacted irreversibly with LptC, but with lower affinity (apparent $K_d = 221 \mu\text{M}$). This compound binds LptC at the LPS binding site and is a prototype for the development of new antibiotics targeting LPS transport in Gram-negative bacteria.

Introduction

Gram-negative bacteria are typically surrounded by two membranes, an inner membrane (IM) and an outer (OM) membrane, separated by an aqueous compartment, the periplasm, which contains a thin layer of peptidoglycan.^[1] The OM is an asymmetric lipid bilayer with lipopolysaccharide (LPS), a complex glycolipid in the outer leaflet, and phospholipids in the inner leaflet.^[2] The tightly packed, amphipathic LPS molecules in the outer leaflet prevent the entry of both large polar molecules and small hydrophobic molecules into the cell, thus protecting the bacterium from toxic chemicals and antibiotics.^[1] The OM is essential for bacterial cell viability and represents the first

site of interaction with the host. The functionality of OM requires proper assembly of this structure and correct placement of LPS in the outer leaflet. Therefore LPS biogenesis represents an ideal target for development of novel chemicals with antibiotic action against Gram-negative bacteria.

Smooth LPS is formed of lipid A, the core oligosaccharide, and a long polysaccharide chain known as O-antigen^[2] (Figure 1A); rough LPS (or lipo-oligosaccharide, LOS) lacks the O-antigen. Lipid A, the most conserved portion of LPS is the pathogen-associated molecular pattern (PAMP) component that is sensed by the combined action of Toll-like receptor 4 (TLR4), MD-2, and CD14 co-receptors of the host innate immune system.^[3] Although the steps along the LPS biosynthetic pathway have been clarified, the precise mechanism of transport and assembly at the cell surface are still poorly understood. The lipid A core moiety is synthesized in the cytoplasm, and its translocation across the IM is performed by the essential ABC transporter MsbA.^[4] The final step of LPS biosynthesis takes place at the periplasmic face of the IM, where the lipid A core moiety is ligated to O-antigen.^[2] Export of complete LPS to the cell surface is mediated by the lipopolysaccharide transport (Lpt) machinery, which is composed of seven essential proteins (LptABCDEFG),^[5,6] located in the IM (LptBCFG), in the periplasm (LptA), and in the OM (LptDE; Fig-

[a] S. E. Sestito, Dr. P. Sperandeo, Dr. C. Santambrogio, C. Ciaramelli, Dr. V. Calabrese, L. Zambelloni, Prof. R. Grandori, Prof. A. Polissi, Prof. F. Peri
Department of Biotechnology and Biosciences
University of Milano-Bicocca
Piazza della Scienza 2, 20126 Milano (Italy)
E-mail: alessandra.polissi@unimib.it
francesco.peri@unimib.it

[b] Prof. G. E. Rovati
Laboratory of Molecular Pharmacology
Department of Pharmacological and Biomolecular Sciences
Università di Milano
Via Balzaretti 6, 20124 Milano (Italy)

Supporting information for this article is available on the WWW under <http://dx.doi.org/10.1002/cbic.201300805>.

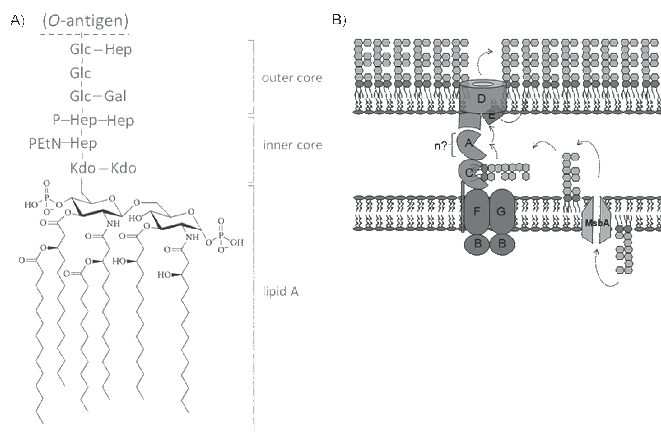


Figure 1. LPS structure and transport in *E. coli*. A) Molecular structure of *E. coli* K12 LPS. B) LPS transport from IM to OM. MsbA flips LPS across the IM, and seven Lpt proteins transport it to the cell surface.

ure 1 B). All seven proteins interact and form a transenvelope complex.^[7] The IM ABC transporter LptBFG^[8] interacts with the bitopic IM protein LptC.^[9] Then, homologous domains mediate the interactions between the C-terminal region of LptC and the N-terminal region of LptA, and between the C terminus of LptA and the N-terminal periplasmic region of LptD.^[6,10] The oligomeric structure formed by LptC, LptA, and LptD constitutes the protein bridge that connects the IM and OM.^[7] Although the overall architecture of the transenvelope bridge has been defined,^[6] the mechanism of LPS transport across the periplasm to the outer leaflet of the OM is not yet understood.

Qualitative *in vitro* assays have shown that both LptA^[11] and LptC^[12] bind to LPS. The crystal structures of LptA^[13] and the periplasmic domain of LptC^[12] revealed that the two proteins present a very similar β -jellyroll fold, although they do not share significant sequence similarity. Both LptA and LptC possess hydrophobic residues; these form a hydrophobic core along the proteins that potentially serve as an LPS-binding site.^[12,13] Interestingly, LptA can displace LPS from LptC *in vitro* (but not vice versa), consistent with their location in the protein bridge and the (unidirectional) LPS export pathway.^[12] However, despite the increasing information obtained on LptC–LPS and LptA–LPS interactions, no quantitative measurements of binding have been performed. Very recently the mechanism of transport of the LPS molecule has been dissected both *in vivo* and *in vitro*, by crosslinking the LPS ligand to the different components of the Lpt machinery.^[14] Specifically, four residues in LptC and five in LptA were found to interact with LPS *in vivo*.^[14] LptC residues directly involved in LPS binding are Thr47, Phe78, Ala172, and Tyr182 (Figure 2), located almost exclusively inside the β -jellyroll structure, thus suggesting that LPS binds inside these proteins and transits through the periplasm bound to the cavity of the conserved β -jellyroll fold.^[14]

Based on these results, it was proposed that LPS transport starts with LPS extraction from the IM by the LptBFG complex, which transfers the molecule to the periplasmic domain of membrane-bound LptC; LptC then transfers LPS to LptA. At least two energy-dependent steps are involved in LPS transport: extraction from the IM to the periplasmic domain of membrane-bound LptC, and transfer of LPS from LptC to LptA.^[14] The *in vitro* reconstitution of LPS transport allowed dissection of LPS transport mechanism into discrete steps from IM to LptC and from LptC to LptA. These are representative of LPS transfer by the Lpt proteins *in vivo*.^[14]

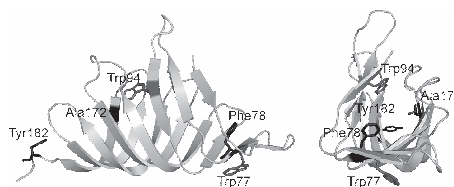


Figure 2. Cartoon representation of the LptC crystal structure (PDB ID: 3MY2).^[12] Putative LPS binding residues^[13] are labeled.

We report here the first determination of thermodynamic and kinetic parameters of the *in vitro* interaction between a heterologously expressed, truncated version of LptC and fluorescently conjugated LOS (fLOS), by two independent methods. Such studies represent a necessary step to understanding the LPS transport mechanism by Lpt proteins. We also describe the rational design, synthesis, and binding properties of a synthetic fluorescent ligand that competes with LPS for LptC binding.

Results and Discussion

Preparation of fluorescent lipo-oligosaccharide (fLOS) and sH-LptC

Radiolabeled LPS is generally used for LPS binding studies. We replaced radioactivity with the safer fluorescence labeling. The main issues with fluorescent LPS are 1) low sensitivity with commercial fluorescein isothiocyanate (FITC)-LPS because of the low level of fluorescence incorporation, and 2) the risk of altering LPS activity and binding properties by introducing the fluorescent moiety. The LPS in this work was Ra-LPS (a rough

type LPS from *Escherichia coli* MG1655); this was extracted from cells by the phenol/chloroform/petroleum ether (PCP) method,^[15] then labeled with FITC by a procedure modified from Troelstra et al.^[16] The purity and the chemical identity of fLOS were assessed by NMR and SDS-PAGE analysis. The labeling ratio was determined to be 1:1 (LOS/FITC), higher than for commercial FITC-LPS from Sigma-Aldrich (~50:1 LPS/FITC). High levels of fluorescein incorporation are essential to obtain reliable signals in binding experiments.

LptC is a bitopic protein, composed of a single transmembrane (TM) helix (Trp7–Asp29) near the N terminus and a large periplasmic domain that is able to bind LPS in vitro.^[12] We used a truncated version of LptC (lacking the first 23 amino acids of the transmembrane helix) fused to a N-terminal His₆ tag (sH-LptC)^[10] as a model to characterize the binding of LPS to the periplasmic C-terminal domain of LptC. Deletion of the LptC TM region yields a stable, soluble, functional protein.^[9,10] sH-LptC was purified to near homogeneity by nickel-nitrilotriacetic acid (Ni-NTA) affinity chromatography, and the overall protein structure (secondary and tertiary) was verified by circular dichroism analysis (data not shown).

fLOS binding to resin-immobilized sH-LptC

Our first objective was to develop a sensitive and reliable test for detecting and quantifying LPS binding to LptC in vitro. We first investigated the time-dependence of LptC–LPS association. sH-LptC was immobilized on Ni-NTA resin, then fLOS (500 nm) was added and incubated for various periods (10–150 min). The resin was then washed, the LptC–fLOS complex was eluted from resin with imidazole, and fluorescence emission was quantified in the eluate. Nonspecific binding (binding of the same concentration of fLOS to Ni-NTA resin in the absence of absorbed sH-LptC) was calculated in different experiments to be less than 15% of the amount of absorbed fLOS in the presence of the protein. It is clear that LPS specifically binds to LptC with a one-phase association rate constant ($k = 0.028 \text{ min}^{-1} \pm 29\% \text{ CV}$; Figure 3A); it reached maximum saturation with a half-time of 24.4 min.

Interestingly, fLOS binding proved to be mostly irreversible, and the addition of increasing concentrations of unlabeled LPS did not result in displacement of fLOS from the protein (Figure 3B). Consequently, it was not possible to calculate the true equilibrium constant, thus we report values for “apparent” K_d . An incubation time of 90 min was used for all subsequent equilibrium binding experiments.

Saturation curves of fLOS binding to resin-immobilized sH-LptC, and competition by unlabeled LPS

In order to calculate the affinity of LPS for its transporter, sH-LptC was immobilized on Ni-NTA resin, and equilibrium binding experiments were performed with fLOS as the ligand. We first carried out a series of saturation experiments (90 min incubation) with sH-LptC protein and increasing fLOS concentrations (0.1–50 μM). The quantity of fLOS captured by resin-bound sH-LptC was determined by the method described

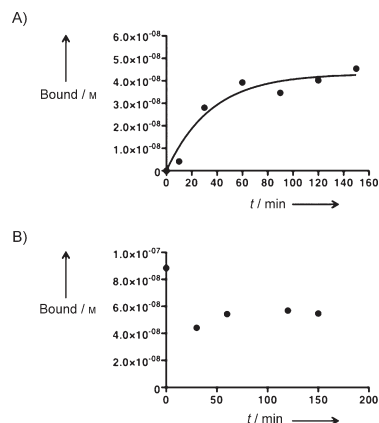


Figure 3. Association and dissociation time-courses of fLOS binding to sH-LptC immobilized on Ni-NTA resin. A) For association kinetics, 500 nm fLOS was incubated with 50 nm sH-LptC at room temperature. B) Dissociation was induced by perturbing the equilibrium with addition of 50 μM unlabeled LOS. The curve represents the fit to the appropriate equation (see the Experimental Section), and is derived from analysis of three independent experiments, each in triplicate.

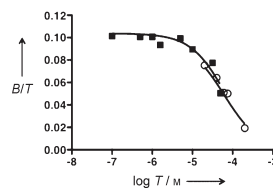


Figure 4. Saturation (■) and competition (○) curves of fLOS binding to resin-immobilized sH-LptC under pseudo-equilibrium conditions. Saturation (0.1–50 μM fLOS) and competition (10 μM fLOS (tracer) competing with different concentrations of unlabeled LPS) experiments were performed at room temperature, with 90 min incubation. Binding is expressed as the concentration ratio of bound to total ligand (B/T), versus the logarithm of total unlabeled ligand concentration ($\log T$). Curves represent the fit to the appropriate equation (see the Experimental Section) and are derived from analysis of three independent experiments, each in triplicate.

above. Nonspecific binding of fLOS to the resin was always determined in the absence of absorbed sH-LptC. In these experiments (Figure 4) the calculated affinity K_d was $1.4 \times 10^4 \text{ M}^{-1} \pm 27\% \text{ CV}$, corresponding to an apparent K_d of 71.4 μM . To assess whether fLOS has the same affinity as unlabeled LPS, we also plotted competition curves with increasing amounts of unlabeled LOS as a competitor at a fixed concentration of fLOS (Figure 4). Despite the fact that binding of fLOS to sH-LptC is essentially irreversible, it is possible to perform competition experiments, as long as the competing ligands are added simultaneously to the reaction mixture containing the binding target. The obtained competition curve follows the simple “mass-action law” under “pseudo-equilibrium” conditions.

These experiments revealed similar affinities for unlabeled LOS ($IC_{50}=62.3 \mu\text{M} \pm 49\% \text{ CV}$; apparent $K_i=35 \mu\text{M}$) and for fLOS, thus confirming that the presence of the fluorescent moiety does not affect LOS binding properties, so allowing pooling of data to calculate binding parameters.¹⁷ Therefore, simultaneous analysis of saturation and competition curves allowed us to calculate the affinity of LOS for its transporter sH-LptC as $K_d=1.91 \times 10^4 \text{ M}^{-1} \pm 21\% \text{ CV}$ (apparent $K_d=52.4 \mu\text{M}$).

sH-LptC-fLOS binding in solution by tryptophan fluorescence quenching

sH-LptC-fLOS affinity was also estimated in solution, in order to rule out any bias arising from resin capture. Binding was monitored as quenching of LptC intrinsic fluorescence. LptC has two tryptophan residues: Trp94 buried in the hydrophobic cavity of the protein and Trp77 exposed to the solvent at the edge of the β -jellyroll (Figure 2). Tryptophan fluorescence emission reduced progressively upon incubation with increasing fLOS concentration (Figure 5A, insert), thus indicating that fLOS is an efficient quencher of sH-LptC fluorescence. The Stern–Volmer plot of the data (Figure 5A) reveals an upward curve at high fLOS concentrations, consistent with two distinct quenching mechanisms: de-excitation of the fluorophore by

random collisions with fLOS molecules (dynamic quenching) and formation of a sH-LptC-fLOS nonfluorescent complex (static quenching). Based on their position in the sH-LptC structure, we ascribe dynamic and static quenching to Trp77 and Trp94, respectively. The constant for dynamic quenching (K_{dyn}) was estimated from titration of free tryptophan by fLOS (see Figure S1 in the Supporting Information); the influence of the protein structure on the quenching of the exposed Trp77 side chain was neglected. The resulting K_{dyn} value ($14.7 \times 10^3 \text{ M}^{-1}$) was then employed to calculate the apparent dissociation constant of the sH-LptC-fLOS complex by the combined equation for static and dynamic quenching. The obtained value ($K_d=28.8 \mu\text{M}$) is similar to that obtained by the capture method ($K_d=71.4 \mu\text{M}$).

In order to test the reversibility of binding, samples containing $40.7 \mu\text{M}$ sH-LptC and $45 \mu\text{M}$ fLOS were treated as above to allow complex formation. Aliquots were mixed to solutions of $45 \mu\text{M}$ fLOS, in order to dilute the protein while keeping the ligand concentration constant; the mixtures were incubated for a further 120 min before fluorescence measurement. The fluorescence values were normalized for protein concentration (as a function of the protein dilution factor), and compared to the expected values for reversible binding, by using the above-estimated K_d and K_{dyn} values (Figure 5B). The experimental data deviate drastically from the theoretical trend (reversible binding); rather, they are consistent with simple progressive dilution of a fixed amount of fluorophore (this would be expected to yield a horizontal line in the plot). This result confirms that sH-LptC-fLOS binding is irreversible, at least on the timescales tested here.

Design and synthesis of an artificial LptC ligand

Our group recently developed small molecules that interact with the LPS-binding protein CD14 with high affinity and specificity (compounds iaxo-101 and iaxo-102, Scheme 1), thereby inhibiting TLR4 activation and signaling in cells¹⁸ and in

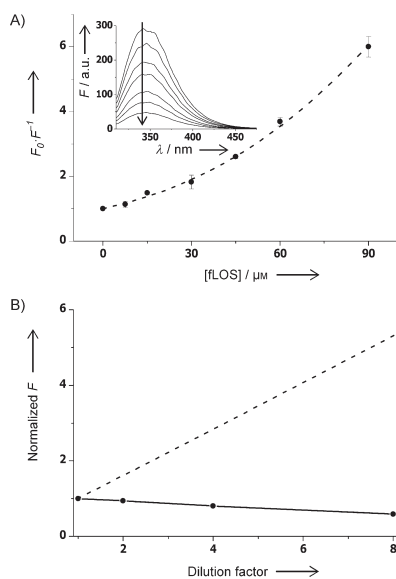
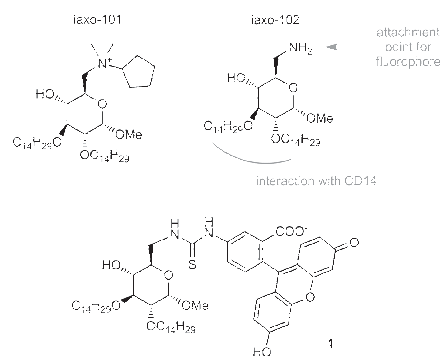


Figure 5. LptC fluorescence quenching by fLOS. A) Relative fluorescence is plotted against total fLOS concentration. The dashed line was obtained fitting data to Equation (6). Inset: fluorescence spectra (the arrow indicates the direction of spectral changes with increasing fLOS concentration). B) Normalized fluorescence upon dilution of LptC-fLOS complex. The dashed line indicates the expected trend for reversible binding with $K_d=28.8 \mu\text{M}$.



Scheme 1. Rational design of 1. The C-6 amine group of iaxo-102 was conjugated to FITC by a thiourea linker.

mice.^[19] Structure–activity studies showed that the pharmacophore is composed of a cyclic sugar core, a protonated (positively charged) nitrogen on C-6, and two C₁₄ linear aliphatic ether chains. Like CD14,^[20] LptA and LptC proteins have been demonstrated to bind LPS within the interior of the hydrophobic cavities formed by their β -sheets.^[14] We thus reasoned that new Lpt ligands could be designed, based on the high-affinity CD14 ligand iaxo-102^[19] (Scheme 1). NMR data showed that the hydrophobic linear ether chains of iaxo-102 directly interact with the CD14 binding site,^[21] thus suggesting that conjugation of a fluorophore at the C-6 primary amine should preserve the interaction with CD14 (Scheme 1). In compound 1, iaxo-102 is chemically linked to fluorescein by a three-atom thiourea linker.

Binding of fluorescent probe 1 to sH-LptC and association kinetics

The *in vitro* binding of 1 to sH-LptC was investigated by using the resin-capture procedure described above. Nonspecific binding was also determined as above, by quantitating fLOS adsorbed on the resin in the absence of the protein, and found to be less than 30% of the signal in the presence of adsorbed protein. Association time course of fluorescent probe 1 binding to sH-LptC was performed by incubating 50 μM of 1 at room temperature for different times (10–150 min).

Compound 1 rather rapidly and specifically bound to LptC, again with a one-phase association rate constant ($k = 0.058 \text{ min}^{-1} \pm 40\% \text{ CV}$), and reached maximum saturation with a half-time of 12 min (Figure 6A). As observed with LPS, binding of 1 proved to be essentially irreversible (Figure 6B).

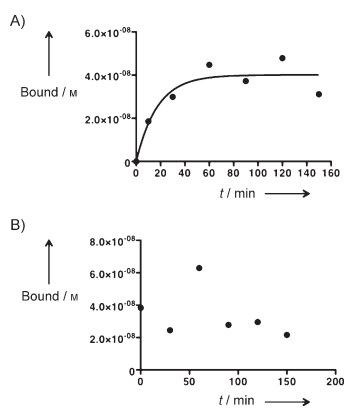


Figure 6. Association and dissociation time-courses of 1 binding to sH-LptC immobilized on Ni-NTA resin. A) For association kinetics, 50 μM 1 was incubated with sH-LptC at room temperature for up to 150 min. B) Dissociation was induced by perturbing the equilibrium with addition of 500 μM corresponding unlabeled ligand. Curves represent the fit to the appropriate equation (see the Experimental Section) and are derived from analysis of three independent experiments, each in triplicate.

Saturation experiment for compound 1 binding to sH-LptC, and competition curves with unlabeled precursors iaxo-102 or LOS

In order to calculate affinity of iaxo-102 for sH-LptC, a series of binding experiments were performed with 1 as the tracer. The amount of 1 captured by resin-bound sH-LptC was determined by the method described above for kinetics experiments. For each concentration of 1, nonspecific binding was determined as binding to Ni-NTA resin in the absence of adsorbed sH-LptC.

Saturation experiments were performed by incubation for 90 min with increasing concentrations of 1 (10–500 μM ; Figure 7A, saturation curve); heterologous competition experi-

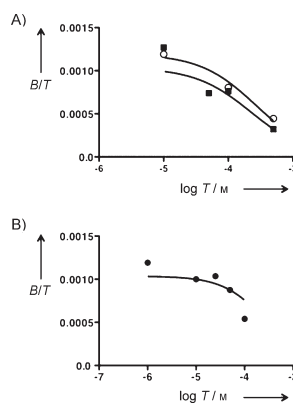


Figure 7. Saturation (■) and competition (○) curves of 1 binding to resin-adsorbed sH-LptC under pseudo-equilibrium conditions. A) Saturation (10–500 μM 1) and competition (50 μM 1 (tracer) competing with increasing concentrations of iaxo-102) binding experiments were performed at room temperature for 90 min. B) Binding curves for 50 μM 1 competing with increasing concentrations of LPS (●). Binding is expressed as the concentration ratio of bound to total ligand (B/T) against the logarithm of total unlabeled ligand concentration ($\log T$). Curves represent the fit to the appropriate equation (see the Experimental Section) and are derived from analysis of three independent experiments, each in triplicate.

ments were performed by incubating 50 μM 1 with increasing concentrations of iaxo-102 (Figure 7B, competition curve). These experiments revealed affinities similar for iaxo-102 and 1, thus allowing pooling of the data and simultaneous analysis of saturation and competition curves (as performed above for fLOS and unlabeled LOS). Computer-assisted analysis yields affinity $K_d = 4.52 \times 10^3 \text{ M}^{-1} \pm 36\% \text{ CV}$ (apparent $K_d = 221 \text{ }\mu\text{M}$) for iaxo-102; this is statistically different ($p < 0.01$), but still in the range of affinity for LOS.

Finally, we performed heterologous competition experiments with 50 μM 1 (tracer) and increasing concentrations of LOS. LOS was indeed able to compete for the site occupied by 1 (Figure 7B), with a calculated affinity, as expected, not signifi-

cantly different from that calculated when using fLOS as a tracer ($K_d = 1.15 \times 10^4 \text{ M}^{-1} \pm 31\% \text{ CV}$, apparent $K_d = 87.2 \text{ } \mu\text{M}$).

The antibacterial activities of iaxo-102 and **1** were evaluated *in vivo* by the micro-broth dilution method^[22] against wild-type *E. coli* strains MG1655^[23] and AS19 (permeable mutant).^[24] No antibacterial activity was observed against either strain (up to 1 mM; data not shown).

Conclusions

The development of fluorescent LOS (fLOS) with high levels of fluorescein incorporation allowed us to calculate, for the first time, the thermodynamic parameters of LOS–LptC interaction. Experiments based on resin-captured sH-LptC–fLOS complex yielded reliable association/dissociation and saturation/competition curves. In saturation and competition experiments (Figure 4), fLOS and unlabeled LOS precursor showed similar affinities towards LptC (apparent calculated dissociation constant $K_d = 71.4$ and $52.4 \text{ } \mu\text{M}$, respectively). The very similar affinity values found for fLOS and LOS suggest that fLOS interacts with LptC similarly to unlabeled LOS. The introduction of the fluorescent moiety did not significantly alter the binding properties or biological activity of LOS; this demonstrates that fLOS can be used as a tracer in quantitative analysis. In kinetic experiments, we observed that binding of LOS to LptC is mostly irreversible, as dissociation time-course experiments with unlabeled LOS failed to displace the bound ligand. Binding experiments in solution based on LptC tryptophan quenching corroborated the results obtained by the resin-capture method, thus giving an apparent dissociation constant of the same order of magnitude ($K_d = 28.8 \text{ } \mu\text{M}$) and confirming the apparent irreversibility of fLOS binding.

In vitro transfer of LPS from LptC to LptA—but not vice versa—occurs in the absence of ATP, possibly implying different affinities for LPS by the two proteins, and consistent with a unidirectional export pathway.^[12] LptC function *in vivo* requires energy from the LptBFG ABC transporter, and a round of ATP hydrolysis is necessary to extract LPS from the IM. A second round of ATP hydrolysis is then required *in vivo* for LPS delivery from LptC to LptA.^[14] Our data indicate that LPS bound to LptC cannot be released in the absence of either energy or the higher-affinity LptA protein. Indeed, it has been recently shown that release of LPS into the periplasm (caused by defective transport) triggers the extracytoplasmic stress response.^[25] Overall these data are consistent with the idea that binding and release of LPS by the Lpt proteins is tightly controlled, to avoid LPS mistargeting and its release into the periplasm.

The Lpt machinery operates downstream of MsbA-mediated flipping of LPS across the IM, so LptC could be the first protein of the machinery to interact in the periplasm with newly translocated LPS. MsbA is a member of the ATP-binding cassette (ABC) superfamily of transporters; it alternates between inward-facing and outward-facing conformations, thereby presenting the substrate-binding pocket to the cytoplasmic and periplasmic faces of the IM, respectively. These conformational changes are guided by binding to and hydrolysis of ATP.^[26] The

MsbA interaction with lipid A and Ra- and deep rough LPS (Re LPS) has been studied by ligand-induced quenching of MsbA intrinsic tryptophan fluorescence.^[27] Interestingly, lipid A and the Ra- and Re-LPS variants quenched MsbA Trp fluorescence, with K_d between 2 and $6 \text{ } \mu\text{M}$.^[27] We calculated here an apparent K_d of $52.4 \text{ } \mu\text{M}$ for the LPS–LptC interaction, typical for the affinity of a transporter, and of the same order of magnitude as K_d for the MsbA–LPS interaction. The similar K_d values for LPS–MsbA and LPS–LptC interactions are consistent with a model of LPS shuttling from MsbA to LptC; irreversible binding between LptC and LPS (observed in this study) reflects the peculiar nature of LPS transport across the periplasm. LPS needs to be properly transferred through the Lpt chain and not released into the aqueous periplasm.

In this study, new compounds were identified to interact with LptC at the LPS-binding site. Two compounds, iaxo-102 and its fluorescent analogue **1**, were identified as good candidates to compete with LOS for binding to LptC. We have previously shown that iaxo compounds interact with the LPS-binding protein CD14, with high affinity and specificity, thereby leading to TLR4 signaling inhibition in cells and in mice.^[18,19] As CD14 and LptC share the same ligand, we explored the possibility that compounds interfering with CD14 activity (e.g., iaxo) can be used as scaffolds to generate compounds able to bind to, and interfere with, LptC activity. Compared to LPS, **1** displayed faster association kinetics to LptC, but with fourfold lower affinity for the protein (apparent $K_d = 221 \text{ } \mu\text{M}$). As in the case of LPS, the presence of the fluorophore did not profoundly affect LptC binding affinity, as iaxo-102 presented an apparent K_d of $129 \text{ } \mu\text{M}$.

Interestingly, **1** and LPS appear to bind to the LptC protein at the same site, as demonstrated in competition experiments. As noted for LPS, binding by **1** is mostly irreversible, thus suggesting a common mechanism of interaction with LptC.

The dissection into single steps of LPS binding and release through the Lpt machinery provides important information on the molecular mechanisms underlying LPS transport. Moreover, the ability to block LPS transport to the cell surface by small molecules suggests an appealing strategy for a new generation of antibiotics targeting multiresistant Gram-negative bacteria. Rational optimization of the molecular structures of these compounds (with the aim of improving bioavailability, cell penetration, and LptC affinity) could afford the first generation of Gram-negative bacteria-specific antibiotics targeting the LPS transport mechanism.

Experimental Section

LOS extraction and labeling with fluorescein: For rough LPS (LOS, Ra-LPS) extraction, *E. coli* strain MG1655 (laboratory collection)^[23] was grown at $37 \text{ } ^\circ\text{C}$ in LD medium (tryptone (1%), yeast extract (0.5%), NaCl (0.5%))^[28] for 16 h. This culture was diluted 1:100 in fresh medium and grown to mid-logarithmic phase ($\text{OD}_{600} = 0.6$). Cells were then harvested by centrifugation (5000 g, 20 min), washed in $\text{Na}_2\text{H}_2\text{P}_2\text{O}_7$ (50 mM, pH 8.0), and stored at $-20 \text{ } ^\circ\text{C}$ before extraction. LOS was selectively extracted from dry cells by the PCP method.^[15] Briefly, a solution of phenol (90%)/chloroform/light petroleum (2:5:8, v/v/v) was prepared; to this was added solid

phenol until the solution went clear. Dry cells (9.73 g) were suspended in PCP solution (2.5%, (w/v)), stirred for 30 min, and extracted three times. Then, the light solvents were removed under vacuum, and LOS was precipitated from the remaining phenol solution by adding water. The solid was centrifuged, collected, suspended in water and dialysed (cut-off 1000 Da) against distilled water for three days. Finally, it was lyophilized, and 85 mg of pure LOS was recovered (yield: 0.9% (W_{LOS}/W_{cells})). The sample obtained from this procedure was screened by ^1H NMR spectroscopy and discontinuous SDS-PAGE for contaminants.^[29] The gel was prepared with a 15% separating gel (lower gel) and a 5% stacking gel (upper gel). The gel was silver stained for lipopolysaccharide,^[30] this has a sensitivity limit of 1 μg for S-type LPS and 10 μg for of R-type LPS.

LOS conjugation to FITC: LOS obtained from *E. coli* MG1655 (see above) was labeled with fluorescein by the following procedure. FITC was conjugated to LOS by using an optimized protocol of a published procedure.^[16] LOS (20 mg) was treated with triethylamine (0.5%, 10 mL) and sonicated on ice for 15 min, then EDTA (100 mM, 1 mL) was added, followed by HCl (1 M) addition to pH 5. FITC (100 mg) in borate buffer (0.25 M, pH 10.5, 4 mL) was added, and the mixture was sonicated for 5 min. After addition of sodium deoxycholate (1.6%, 5 mL), the solution was stirred at 37 °C for 30 h. The reaction mixture was centrifuged (10000g, 30 min) to eliminate aggregates, and the supernatant was dialysed (cut-off 1000 Da) against NaCl (137 mM). The sample was concentrated and purified with Sephadex G-25 in a PD-10 desalting column (GE Healthcare), and eluted in water. Fractions containing fLOS were collected and lyophilized (16 mg). To evaluate labeling efficiency, the ratio between LOS and FITC concentrations in the sample was calculated. The concentration of FITC was determined spectrophotometrically ($\epsilon_{492\text{ nm}} = 85000\text{ M}^{-1}\text{ cm}^{-1}$); the concentration of LOS was determined by a thiobarbiturate assay,^[31] which evaluates the level of KDO (2-keto-3-deoxyoctulosonic acid), a marker sugar for LPS. In these measurements, a sample of commercial LPS-FITC (Sigma-Aldrich) was used as the reference. A LOS/FITC labeling ratio of 1.02:1 was calculated for the sample; the reference showed a ratio of about 50:1 (LPS/FITC).

Purification of sH-LptC: *E. coli* M15[pREP4] (Qiagen) harboring plasmid pQES-H-lptC,^[10] which expresses N-terminal His₆-tagged LptC lacking the first 23 residues (sH-LptC), was grown at 30 °C in LD medium^[28] containing kanamycin (25 $\mu\text{g mL}^{-1}$) and ampicillin (100 $\mu\text{g mL}^{-1}$) for 16 h. The culture was diluted (1:100) in fresh LD medium and grown to mid-logarithmic phase ($\text{OD}_{600} = 0.6$). Expression of sH-LptC was induced by addition of isopropyl- β -D-thiogalactopyranoside (IPTG; 0.5 mM; Sigma-Aldrich) and further incubated for 16–18 h at 20 °C. Cells were then harvested by centrifugation (5000g, 20 min). The cell pellet was resuspended in buffer A (NaH_2PO_4 (50 mM, pH 8.0), NaCl (300 mM), imidazole (10 mM), glycerol (10%)), followed by incubation for 30 min at 4 °C with shaking in the presence of lysozyme (0.2 mg mL^{-1}), DNase I (100 $\mu\text{g mL}^{-1}$), MgCl_2 (10 mM), and phenylmethylsulfonyl fluoride (PMSF, 1 mM; Sigma-Aldrich). Cells were disrupted by a single pass through a One Shot model French press (Constant Systems, Daventry, UK) at 25000 psi. Unbroken cells and cell debris were removed by centrifugation (39000g, 30 min, 4 °C). The soluble protein was purified from the supernatant on Ni-NTA agarose columns (Qiagen). The column was washed with 10 column volumes of 4% buffer B (NaH_2PO_4 (50 mM, pH 8.0) NaCl (300 mM), imidazole (500 mM), glycerol (10%)) with buffer A. The protein was eluted by using a stepwise gradient of buffer B (10, 20, 50, 70, and 100%) with buffer A. At each step, one column volume was passed through the

column. Elution fractions were monitored by 12.5% polyacrylamide SDS-PAGE. The pooled fractions containing purified protein (> 90%) were dialysed twice against 100 volumes of buffer C (NaH_2PO_4 (50 mM, pH 8.0), NaCl (150 mM)) in cellulose tubing (12000 Da cut-off; Thermo Scientific), and finally concentrated in a Vivaspin 15R column (10000 molecular weight cut-off; Sartorius, Göttingen, Germany). Protein concentration was determined by a Coomassie (Bradford) assay kit (Thermo Scientific), with bovine serum albumin as the standard.

Ligand binding studies by the resin-capture method

Saturation experiments: The in vitro LPS binding assay was based on a previous protocol with modifications.^[12] Briefly, purified sH-LptC (50 μM) was incubated in buffer C (1 mL) with HisLink protein purification resin (100 μL ; Promega) for 90 min on a rotary shaker at room temperature, to allow absorption of protein to the resin. Unbound protein was removed by decanting the resin-bound sH-LptC and eliminating the supernatant. Resin-bound sH-LptC was incubated in buffer C (1 mL) at room temperature in the dark on a rotary shaking in the presence of different concentrations of fLOS (0.1–50 μM) or 1 (10–500 μM) for a further 90 min to allow binding of ligand to the resin-bound sH-LptC. The supernatant (unbound ligand) was discarded, and the resin was washed three times with buffer C. The protein-LPS complex was eluted in four steps, each with buffer C (1 mL) containing imidazole (500 mM). Nonspecific binding was determined as the binding of the same concentration of fLOS to Ni-NTA resin in the absence of absorbed sH-LptC. Each fraction (100 μL) was placed in a Costar white flat-bottomed microtiter plate (Corning, NY), and fluorescence was measured in a Cary Eclipse spectrophotometer ($\lambda_{\text{exc}} = 490\text{ nm}$, $\lambda_{\text{em}} = 510\text{ nm}$, slit = 5 nm; Varian). The concentration of tracer present in each sample was determined by interpolation with a standard curve (fLOS or 1) and corrected by subtraction of the nonspecific-binding value. The amount of sH-LptC bound to the resin and eluted with imidazole was evaluated for the pooled elution fractions with a Coomassie (Bradford) assay kit (Thermo Scientific), with bovine serum albumin as the standard.

Association and dissociation time courses: For the association experiments, labeled ligand (fLOS (500 nM) or 1 (50 μM)) was added at room temperature, in the dark, to sH-LptC (50 μM) adsorbed to the resin in buffer C (1 mL); the mixture was incubated with shaking for different times (10–150 min). For each time, the supernatant was removed and samples were washed and eluted as described above. Dissociation kinetics experiments were performed with the same tracer concentrations, and incubation with immobilized sH-LptC for 150 min (volume of reaction = 800 μL). Then, LOS (50 μM) and iaxo-102 (500 μM) in buffer C (1 mL) were added for different times (10–150 min). For each time, the sample was treated as above.

Competition experiments: Competition experiments were performed for sH-LptC binding to fLOS and 1. For fLOS, resin-bound sH-LptC (50 μM) was incubated (90 min) with a mixture of fLOS (10 μM) and different concentrations of unlabeled LOS (20, 40, 60 and 75 μM) in buffer C. After wash and elution steps, the concentration of fLOS bound to sH-LptC was quantified as described above. For 1, resin-bound sH-LptC (50 μM) was incubated with 1 (50 μM) in buffer C (800 μL) for 90 min. Homologous and heterologous competition experiments were performed by adding iaxo-102 (200 μL , 100 or 500 μM) or LOS (200 μL , 10–100 μM) and incubated for a further 90 min. Wash and elution steps were performed; concentrations of tracer bound to resin were determined as described above.

Data and statistical analysis: Data from fluorescent ligand binding assays were evaluated by a nonlinear, least-squares curve-fitting procedure in Prism (version 4, GraphPad Software, La Jolla, CA). Association and dissociation time courses were analyzed by one-phase association and one-phase dissociation exponential decay curves, respectively. Equilibrium binding data were analyzed in Prism by using the n -ligand m -binding site model in the Ligand³² and DESIGN³³ computer programs. Parameter errors are expressed as percentage CV and were calculated by simultaneous analysis of at least three independent experiments performed in duplicate or triplicate. Parameter comparisons were performed based on the F-test for extra sum of square principle. All curves are computer generated.

LptC intrinsic fluorescence quenching: Samples containing sH-LptC (40.7 μ M) and fLOS (0–90 μ M) were prepared in sodium phosphate (50 mM, pH 8) with NaCl (50 mM), incubated (22 °C, 90 min) with agitation (300 rpm), then transferred into a quartz cuvette (1 cm path length). Fluorescence emission spectra (310–475 nm) were recorded at 22 °C with an Eclipse spectrofluorimeter (Varian; excitation 295 nm, excitation/emission slits 5 nm). To test binding reversibility, aliquots of the 45 μ M fLOS sample were diluted (up to 1:8) at fixed fLOS concentration, and incubated for a further 120 min before fluorescence measurements.

Data analysis for quenching experiments: In the presence of dynamic quenching, the fraction of fluorescence intensities in the absence (F_0) and presence (F) of the quencher (fLOS) is given by the ratio of the decay rate in the presence ($\gamma + k_q[\text{fLOS}]$) and absence (γ) of the quencher (Equation (1)):

$$\frac{F_0}{F} = \frac{\gamma + k_q[\text{fLOS}]}{\gamma} = 1 + K_{\text{dyn}}[\text{fLOS}] \quad (1)$$

When static quenching also occurs due to binding, Equation (1) applies only for fluorophores that are not involved in a complex. The contribution of this fraction can be expressed by Equation (2):

$$\frac{F_0}{F} = \frac{[\text{LptC}]_{\text{tot}}}{[\text{LptC}]} (1 + K_{\text{dyn}}[\text{fLOS}]) \quad (2)$$

The equations that define the dissociation constant (K_d) and the conservation of total protein and ligand are as follows [Eqs (3), (4), and (5)]:

$$K_d = \frac{[\text{LptC}][\text{fLOS}]}{[\text{complex}]} \quad (3)$$

$$[\text{complex}] = [\text{LptC}]_{\text{tot}} - [\text{LptC}] \quad (4)$$

$$[\text{fLOS}] = [\text{fLOS}]_{\text{tot}} - [\text{complex}] = [\text{fLOS}]_{\text{tot}} - [\text{LptC}]_{\text{tot}} + [\text{LptC}] \quad (5)$$

Combining Equations (1)–(5) it is possible to express F_0/F as a function of total protein and total ligand concentrations, K_{dyn} and K [Eq. (6)]

$$\frac{F_0}{F} = \frac{[\text{LptC}]_{\text{tot}} \left(2 + K_{\text{dyn}} \left([\text{fLOS}]_{\text{tot}} - [\text{LptC}]_{\text{tot}} - K_d + \sqrt{([\text{LptC}]_{\text{tot}} - [\text{fLOS}]_{\text{tot}} - K_d)^2 + 4K_d[\text{LptC}]_{\text{tot}}} \right) \right)}{[\text{LptC}]_{\text{tot}} - [\text{fLOS}]_{\text{tot}} - K_d + \sqrt{([\text{LptC}]_{\text{tot}} - [\text{fLOS}]_{\text{tot}} - K_d)^2 + 4K_d[\text{LptC}]_{\text{tot}}} \quad (6)$$

The K_d value was determined by a nonlinear, least-squares curve-fitting procedure of fluorescence data by Equation (6), by using the

K_{dyn} value obtained from free tryptophan experiments (see the Supporting Information).

Acknowledgements

F.P. thanks the COST Action BM 1003 "Microbial cell surface determinants of virulence as targets for new therapeutics for Cystic Fibrosis"; the COST Action CM1102 "Multivalent Glycosystems for Nanoscience–MultiGlycoNano"; the Italian Ministry of University and Research (MIUR), PRIN 2010-11, project: "Italian network for the development of multivalent nanosystems". A.P. thanks the Fondazione Cariplo (Grant no. 2010-0653), Regione Lombardia "Cooperazione scientifica e tecnologica internazionale" (Grant 16876 SAL-18), MIUR-Regione Lombardia (ID 30190679), and Fondazione Banca del Monte di Lombardia.

Keywords: antibiotics · ligand design · LPS · LptC · medicinal chemistry

- [1] H. Nikaido, *Microbiol. Mol. Biol. Rev.* **2003**, *67*, 593–656.
- [2] C. R. H. Raetz, C. Whitfield, *Annu. Rev. Biochem.* **2002**, *71*, 635–700.
- [3] S. Akira, S. Uematsu, O. Takeuchi, *Cell* **2006**, *124*, 783–801.
- [4] A. Polissi, C. Georgopoulos, *Mol. Microbiol.* **1996**, *20*, 1221–1233.
- [5] a) P. Sperandio, R. Cescutti, R. Villa, C. Di Benedetto, D. Candia, G. Dehò, A. Polissi, *J. Bacteriol.* **2007**, *189*, 244–253; b) P. Sperandio, F. K. Lau, A. Carpentieri, C. De Castro, A. Molinaro, G. Dehò, T. J. Silhavy, A. Polissi, *J. Bacteriol.* **2008**, *190*, 4460–4469; c) N. Ruiz, L. S. Gronenberg, D. Kahne, T. J. Silhavy, *Proc. Natl. Acad. Sci. USA* **2008**, *105*, 5537–5542; d) S.-S. Chng, N. Ruiz, G. Chimalakonda, T. J. Silhavy, D. Kahne, *Proc. Natl. Acad. Sci. USA* **2010**, *107*, 5363–5368.
- [6] a) E. Freinkman, S. Okuda, N. Ruiz, D. Kahne, *Biochemistry* **2012**, *51*, 4800–4806; b) C. Santambrogio, P. Sperandio, R. Villa, F. Sobott, A. Polissi, R. Grandori, *J. Am. Soc. Mass Spectrom.* **2013**, *24*, 1593–1602.
- [7] S.-S. Chng, L. S. Gronenberg, D. Kahne, *Biochemistry* **2010**, *49*, 4565–4567.
- [8] S. Narita, H. Tokuda, *FEBS Lett.* **2009**, *583*, 2160–2164.
- [9] R. Villa, A. M. Martorana, S. Okuda, L. J. Gourlay, M. Nardini, P. Sperandio, G. Dehò, M. Bolognesi, D. Kahne, A. Polissi, *J. Bacteriol.* **2013**, *195*, 1100–1108.
- [10] P. Sperandio, R. Villa, A. M. Martorana, M. Samalikova, R. Grandori, G. Dehò, A. Polissi, *J. Bacteriol.* **2011**, *193*, 1042–1053.
- [11] A. X. Tran, M. S. Trent, C. Whitfield, *J. Biol. Chem.* **2008**, *283*, 20342–20349.
- [12] A. X. Tran, C. Dong, C. Whitfield, *J. Biol. Chem.* **2010**, *285*, 33529–33539.
- [13] M. D. L. Suits, P. Sperandio, G. Dehò, A. Polissi, Z. Jia, *J. Mol. Biol.* **2008**, *380*, 476–488.
- [14] S. Okuda, E. Freinkman, D. Kahne, *Science* **2012**, *338*, 1214–1217.
- [15] C. Galanos, O. Lüderitz, O. Westphal, *Eur. J. Biochem.* **1969**, *9*, 245–249.
- [16] A. Troelstra, P. Antal-Szalmas, L. A. de Graaf-Miltenburg, A. J. Weersink, J. Verhoef, K. P. Van Kessel, J. A. Van Strijp, *Infect. Immun.* **1997**, *65*, 2272–2277.
- [17] G. E. Rovati, *Trends Pharmacol. Sci.* **1998**, *19*, 365–369.
- [18] a) F. Peri, F. Granucci, B. Costa, I. Zanoni, C. Marini, F. Nicotra, *Angew. Chem. Int. Ed.* **2007**, *46*, 3308–3312; *Angew. Chem.* **2007**, *119*, 3372–3376; b) M. Piazza, V. Calabrese, C. Baruffa, T. Gioannini, J. Weiss, F. Peri, *Biochem. Pharmacol.* **2010**, *80*, 2050–2056.
- [19] a) I. Bettoni, F. Comelli, C. Rossini, F. Granucci, G. Giagnoni, F. Peri, B. Costa, *Glia* **2008**, *56*, 1312–1319; b) M. Piazza, C. Rossini, S. Della Fiorentina, C. Pozzi, F. Comelli, I. Bettoni, P. Fusi, B. Costa, F. Peri, *J. Med. Chem.* **2009**, *52*, 1209–1213.

- [20] a) J.-I. Kim, C. J. Lee, M. S. Jin, C.-H. Lee, S.-G. Paik, H. Lee, J.-O. Lee, *J. Biol. Chem.* **2005**, *280*, 11347–11351; b) S. L. Kelley, T. Lukk, S. K. Nair, R. I. Tapping, *J. Immunol.* **2013**, *190*, 1304–1311.
- [21] M. Piazza, L. Yu, A. Teghanemt, T. Gioannini, J. Weiss, F. Peri, *Biochemistry* **2009**, *48*, 12337–12344.
- [22] I. Wiegand, K. Hilpert, R. E. Hancock, *Nat. Protoc.* **2008**, *3*, 163–175.
- [23] F. R. Blattner, G. Plunkett III, C. A. Bloch, N. T. Perna, V. Burland, M. Riley, J. Collado-Vides, J. D. Glasner, C. K. Rode, G. F. Mayhew, J. Gregor, N. W. Davis, H. A. Kirkpatrick, M. A. Goeden, D. J. Rose, B. Mau, Y. Shao, *Science* **1997**, *277*, 1453–1462.
- [24] M. Sekiguchi, S. Iida, *Proc. Natl. Acad. Sci. USA* **1967**, *58*, 2315–2320.
- [25] S. Lima, M. S. Guo, R. Chaba, C. A. Gross, R. T. Sauer, *Science* **2013**, *340*, 837–841.
- [26] D. A. P. Gutmann, A. Ward, I. L. Urbatsch, G. Chang, H. W. van Veen, *Trends Biochem. Sci.* **2010**, *35*, 36–42.
- [27] P. D. W. Eckford, F. J. Sharom, *J. Biol. Chem.* **2008**, *283*, 12840–12850.
- [28] P. Sabbattini, F. Forti, D. Ghisotti, G. Dehò, *J. Bacteriol.* **1995**, *177*, 1425–1434.
- [29] U. K. Laemmli, *Nature* **1970**, *227*, 680–685.
- [30] R. Kittelberger, F. Hilbink, *J. Biochem. Biophys. Methods* **1993**, *26*, 81–86.
- [31] H. Brade, C. Galanos, *Anal. Biochem.* **1983**, *132*, 158–159.
- [32] P. J. Munson, D. Rodbard, *Anal. Biochem.* **1980**, *107*, 220–239.
- [33] G. E. Rovati, D. Rodbard, P. J. Munson, *Anal. Biochem.* **1988**, *174*, 636–649.

Received: December 20, 2013
Published online on February 13, 2014

Trehalose- and Glucose-Derived Glycoamphiphiles: Small-Molecule and Nanoparticle Toll-Like Receptor 4 (TLR4) Modulators

Julio Rodríguez Lavado,[†] Stefania E. Sestito,[‡] Roberto Cighetti,[‡] Eva M. Aguilar Moncayo,[†] Alja Oblak,[§] Duško Lainšček,[§] José Luis Jiménez Blanco,[†] José Manuel García Fernández,^{||} Carmen Ortiz Mellet,[†] Roman Jerala,[§] Valentina Calabrese,[‡] and Francesco Peri^{*,‡}

[†]Department of Organic Chemistry, Faculty of Chemistry, University of Sevilla, E-41012 Sevilla, Spain

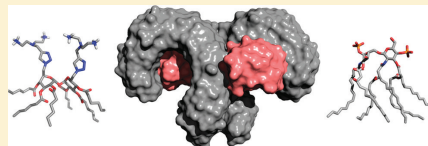
[‡]Department of Biotechnology and Biosciences, University of Milano Bicocca, Piazza della Scienza, 2, 20126 Milano, Italy

[§]Department of Biotechnology, National Institute of Chemistry and EN-FIST Center of Excellence, Hajdrihova 19 SI-1001 Ljubljana, Slovenia

^{||}Instituto de Investigaciones Químicas (IIQ), CSIC—University of Sevilla, E-41092 Sevilla, Spain

Supporting Information

ABSTRACT: An increasing number of pathologies have been linked to Toll-like receptor 4 (TLR4) activation and signaling, therefore new hit and lead compounds targeting this receptor activation process are urgently needed. We report on the synthesis and biological properties of glycolipids based on glucose and trehalose scaffolds which potently inhibit TLR4 activation and signaling in vitro and in vivo. Structure–activity relationship studies on these compounds indicate that the presence of fatty ester chains in the molecule is a primary prerequisite for biological activity and point to facial amphiphilicity as a preferred architecture for TLR4 antagonism. The cationic glycolipids here presented can be considered as new lead compounds for the development of drugs targeting TLR4 activation and signaling in infectious, inflammatory, and autoimmune diseases. Interestingly, the biological activity of the best drug candidate was retained after adsorption at the surface of colloidal gold nanoparticles, broadening the options for clinical development.



INTRODUCTION

Toll-like receptors (TLRs) play a critical role in the recognition of conserved pathogen-associated molecular patterns (PAMPs) derived from various microbial pathogens, including viruses, bacteria, protozoa, and fungi, and in the subsequent initiation of innate immune response.¹ Among TLRs, TLR4 selectively responds to bacterial endotoxin (E), composed of bacterial lipopolysaccharides (LPS) or part of it (lipooligosaccharides, LOS, lipid A).^{2,3} LPS is the main chemical component of the Gram negative bacteria outer membrane, and the lipid A, a negatively charged phosphorylated lipopolysaccharide represents the LPS moiety that is responsible for TLR4 activation through specific molecular recognition processes (Figure 1).

TLR4 is also activated by endogenous molecules, generally known as danger-associated molecular patterns (DAMPs).⁴ Typical DAMPs acting as TLR4 agonists are released as a consequence of injury and inflammation. Most of the reported DAMPs are proteins, which are very different from lipid A, and the molecular details of DAMP interaction with the TLR4 receptor system are still unknown, although in some cases endotoxin contamination seems to be responsible for TLR4 activity of DAMPs. Chemical entities that block TLR4 activation by bacterial endotoxin (LPS), thus acting as antagonists, are hit compounds for developing drugs active

against acute sepsis and septic shock derived from excessive and deregulated TLR4 activation and signaling.⁵ On the other hand, the inhibition of TLR4 stimulation by DAMPs could be used to contrast a wide range of inflammatory and autoimmune disorders associated with the release of inflammatory cytokines. In this context, TLR4 is an emerging molecular target related to an impressively broad spectrum of modern day disorders including autoimmune disorders, chronic inflammations, allergies, asthma, atherosclerosis, aortic aneurysm, CNS diseases such as neuropathic pain, amyotrophic lateral sclerosis (ALS), Alzheimer's disease (AD), and some types of cancer.⁶ As the majority of these pathologies still lack specific pharmacological treatment, small molecules active in inhibiting TLR4 activation have attracted increasing interest in a wide range of possible clinical settings.⁷

The molecular mechanism by which endotoxin activate TLR4 is a complex process⁸ and depends on LPS binding protein (LBP)⁹-catalyzed extraction and transfer of individual LPS molecules from aggregated LPS to the CD14 (cluster of differentiation 14) receptor¹⁰ and then from CD14 to myeloid differentiation protein 2 (MD-2).^{11,12} This process is followed

August 1, 2014

Published: September 30, 2014



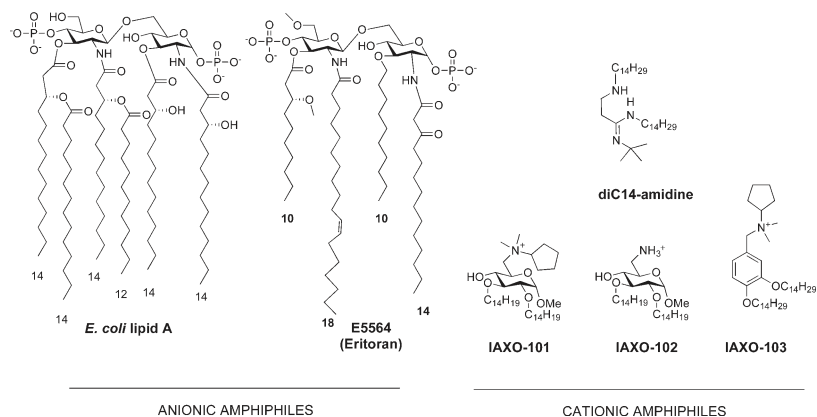


Figure 1. Anionic and cationic TLR4 modulators. From the left: lipid A from *Escherichia coli*, the natural TLR4 agonist, synthetic anionic (the antagonist Eritoran), and cationic amphiphiles (diC14-amidine, IAXO compounds).

by engagement and dimerization of TLR4, thus forming the cell surface complex (LPS-MD-2-TLR4),¹³ which initiates the intracellular signaling by recruiting specific adaptor proteins and activating downstream signaling pathways.

Several natural and synthetic small molecules are known to modulate TLR4 activation and subsequent intracellular signaling acting as agonists (activators) or antagonists (inhibitors).⁶ The majority of these molecules are lipid A variants and synthetic lipid A mimetics that reproduce the structural motif of the anionic disaccharide. Monophosphoryl lipid A (MPL) and some aminoalkyl glucosaminide phosphates (AGPs) are agonists in use as vaccine adjuvants,¹⁴ while underacylated variants such as natural lipid IVa¹⁵ and synthetic Eritoran¹⁶ are antagonists (Figure 1). In general, lipid A variants are anionic lipids, bearing one or two negatively charged phosphate groups and a hydrophobic domain (lipid chains). Although counter-intuitive, several cationic lipids made of positively charged headgroups (usually tertiary or quaternary ammonium salts or polyamines) and a hydrophobic domain (alkyl chains or steroids) have been found to be active in modulating TLR4 activity,¹⁷ acting either as agonists or antagonists of TLR4. Thus, some positively charged liposomes formed by cationic amphiphiles induce the expression of pro-inflammatory mediators. For instance, diC14-amidine (Figure 1) liposomes trigger the secretion of a cytokine pattern reminiscent of the TLR4-dependent LPS secretion pattern by activating both MyD88/NF- κ B/JNK and TRAM/TRIF pathways.¹⁸ Other cationic lipids activate cytokine production through NF- κ B-independent, TRIF-dependent pathways, which requires the presence of CD14.^{19,20} Structural changes make cationic lipids switch from agonism to antagonism, as in the case of dioleoyl trimethylammonium propane (DOTAP), that inhibits TLR4 signal by competing with LPS for interaction with LBP and/or CD14.²⁰ Complexes of the commercial cationic lipid formulation lipofectamine with LPS reduce its TLR4 activity. Interestingly LPS complexed with lipofectamine colocalizes with CD14 at the cell surface and inside cells but does not colocalizes with TLR4-MD-2 complex, suggesting that the

mechanism of inhibition may result from the uncoupling of CD14 from TLR4-MD-2.²¹

Specific binding of amino glycolipids and aromatic ammonium salts to CD14 (compounds IAXO-101, -102, -103, Figure 1), was recently shown by our group.^{22,23} These compounds are active in inhibiting LPS-stimulated TLR4-dependent cytokine production in cells and in animals.²⁴

Evaluation of transfer of LOS from the monomeric soluble form of CD14 (sCD14) to His₆-tagged CD14 or MD-2 by cocapture to a metal chelating resin clearly showed that the cationic lipids derived from D-glucose or benzylamine inhibit the transfer of LOS from sCD14 to CD14-His₆, but not the transfer of LOS from sCD14 to MD-2.²² Finally, saturation transfer difference (STD) NMR data demonstrated direct binding of the cationic lipids to CD14, mainly through alkyl chains.²² Altogether, these data suggest that the lipid tails of cationic amphiphiles interact with the hydrophobic binding site of CD14²⁵ and compete with LPS or LOS chains. The carbohydrate scaffold in amino glycolipids probably acts by preventing random conformations and providing a favorable orientation of the lipid chains that is reminiscent of that found in lipid A. Most interestingly, through the interplay of regioselective functionalization methodologies and conformational bias, the installation of differentiated cationic and hydrophobic domains in carbohydrate platforms can be made compatible with molecular diversity-oriented strategies and structure-activity relationship (SAR) studies. As a proof of concept, we have now prepared a series of new cationic glycoamphiphiles using the monosaccharide methyl α -D-glucopyranoside and the disaccharide α,α' -trehalose as the sugar cores. Systematic modification of the cationic heads and the lipophilic tails and evaluation of their capacity to interfere with TLR4 activation and signaling in vitro and in vivo allowed the identification of a drug lead that has been further incorporated in gold nanoparticles to test the effect of multivalent presentation on its biological activity.

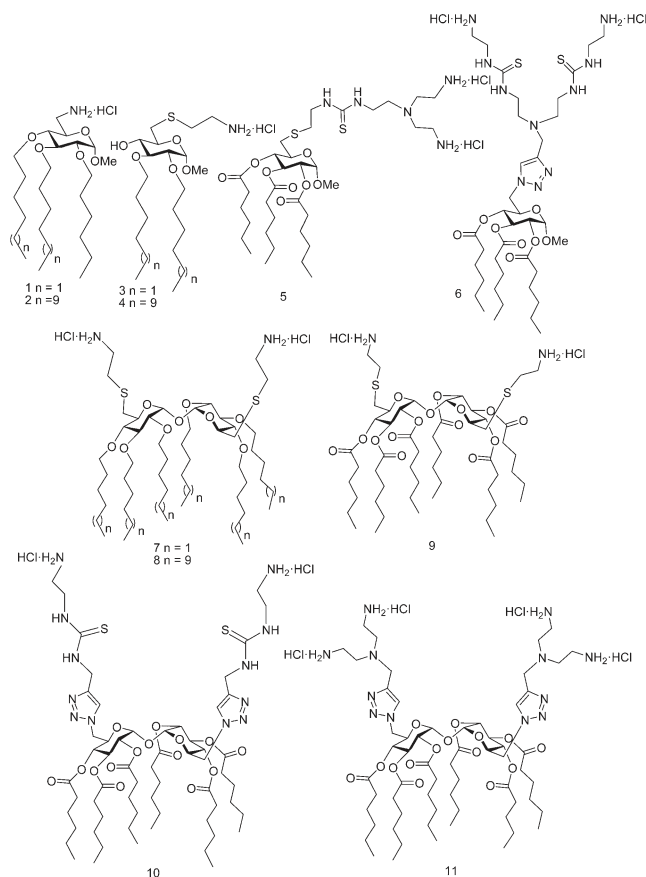


Figure 2. Synthetic monosaccharide and disaccharide protonatable amphiphiles derived, respectively, from D-glucose (1–6) and α, α' -trehalose (7–11).

RESULTS AND DISCUSSION

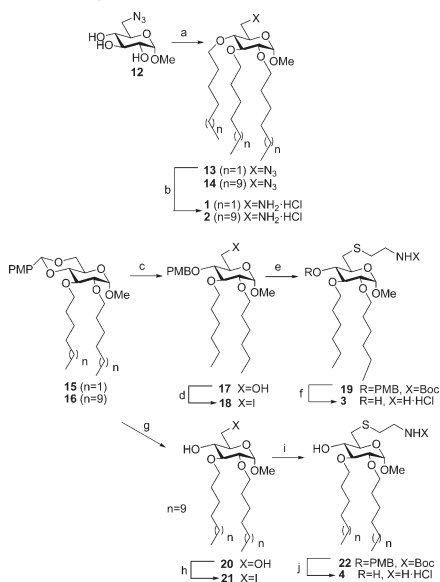
Ligand-Based Rational Design. It is known that the self-assembling capabilities and the ability of cationic amphiphiles to interact with CD14 as liposomes or micellar aggregates have a strong impact on their TLR4 modulatory activity.¹⁷ Yet, very little is still known on the molecular aspects underlying the mechanisms at play, mainly because structural data of cationic compounds bound to MD-2 or CD14 receptors are still lacking. Conducting SAR studies on series of homologous cationic amphiphiles and relating the biological activity to the aggregation properties is expected to provide new insights in this matter. Glucose-derived cationic glycolipids are particularly appealing for this purpose. First, the secondary hydroxyls of the glucopyranose ring are well suited anchoring points to link lipophilic chains in a similar orientation as the fatty acid acyl

chains in lipid A. Second, the incorporation of protonatable headgroups at the primary position imparts facial amphiphilicity to the molecule, a biomimetic feature that is associated with improved cell membrane crossing abilities and proneness to form supramolecular complexes with complementary biomolecules by either electrostatic or hydrophobic interactions.²⁶ On these grounds, we have now synthesized amino glycolipids derived from methyl α -D-glucopyranoside (1–6) and from α, α' -trehalose (7–11, Figure 2). The latter can be formally considered as dimeric homologues of the glucose amphiphiles. We keep in mind that the confluence of two exoanomeric effects at the 1–1 interglycosidic linkage in α, α' -trehalose strongly limits rotation about the glycosidic bonds,²⁷ preserving a rigid conformation that warrants facial anisotropy after differential functionalization at the primary and secondary

positions, even in highly constrained constructs.²⁸ Both the methyl α -D-glucopyranoside and the α,α' -trehalose scaffolds have previously demonstrated their efficiency in the design of TLR4 modulators with anionic amphiphilic structures.^{29,30} Structural modifications have been projected by varying the number, the nature, and the length of the lipid chains and the number and disposition of amino groups in order to evaluate how these structural elements influence the TLR4 activity.

Synthesis of Glucose-Derived Cationic Glycolipids. The syntheses of the tri-*O*-alkylated 6-amino-6-deoxyglucoside derivatives **1** and **2** (Scheme 1) were successfully accomplished

Scheme 1. Syntheses of Monosaccharides 1–4^a



^aReagents and conditions: (a) 1-bromohexane, NaH, DMF, overnight, 48% or 1-bromotetradecane, NaH, DMF, 55 °C, 52%; (b) H₂, Pd/C, MeOH, 2 h, 87% or PPh₃, THF, then, NH₄OH, 50 °C, overnight, 82%; (c) 1M LiAlH₄ in THF, AlCl₃, DCM, Et₂O, 83%; (d) I₂, PPh₃, imidazole, toluene, 94%; (e) HS(CH₂)₂NHBoc, Cs₂CO₃, DMF, 60 °C, 99%; (f) 1:1 TFA-DCM, 80%; (g) AlCl₃, DCM, Et₂O, 87%; (h) I₂, PPh₃, imidazole, toluene, 91%; (i) HS(CH₂)₂NHBoc, Cs₂CO₃, DMF, 60 °C, 95%; (j) 1:1 TFA-CH₂Cl₂, quant.

by reaction of the known methyl 6-azido-6-deoxy- α -D-glucopyranoside **12**³¹ with hexyl or tetradecyl bromide and sodium hydride (**13** and **14**), followed by reduction of the azido group by either catalytic hydrogenation or Staudinger reaction with triphenylphosphine and hydrolysis of the corresponding phosphazene intermediate.³² The target ether-type amino glycolipids **1** and **2** were isolated as the corresponding hydrochloride salts.

The 2,3-di-*O*-hexyl and -*O*-tetradecyl glucose derivatives **3** and **4** were synthesized from the corresponding 4,6-*O*-(*p*-methoxybenzylidene) protected precursor **15** and **16**,³³

respectively, which at their turn were obtained by standard alkylation of methyl 4,6-*O*-(*p*-methoxybenzylidene)- α -D-glucopyranoside.³⁴ The regioselective opening of the acetal ring of **15** using lithium aluminum hydride (LiAlH₄) gave the 4-*O*-*p*-methoxybenzyl (PMB) ether **17**. Compound **16** on this side was completely deprotected on C-4 and C-6 positions using aluminum trichloride, affording compound **20**. Iodination of the C-6 hydroxyl groups of **17** and **20** using Garegg's conditions³⁵ afforded compounds **18** and **21**, which were subjected to cesium carbonate-promoted nucleophilic displacement with *t*-butoxycarbonyl (Boc)-protected cysteamine (**20** and **22**) and final Boc removal in acidic conditions to give compounds **3** and **4**.

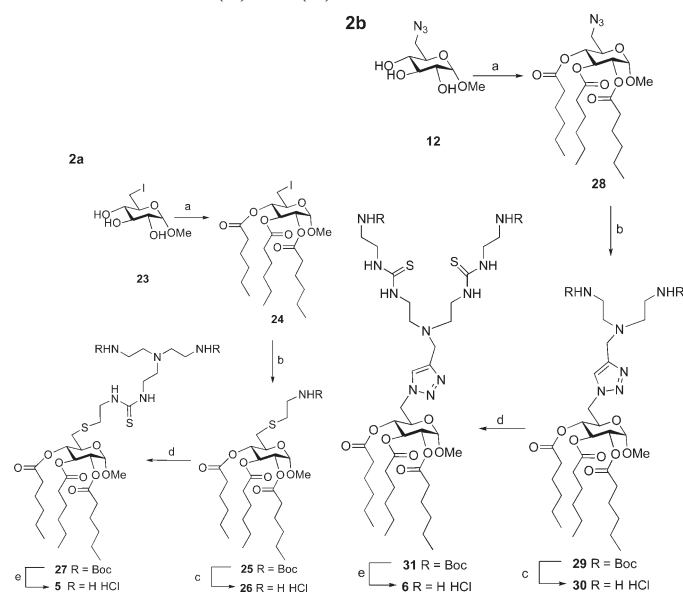
The synthetic routes to obtain compounds **5** and **6**, having a tertiary and two primary amino groups in the cationic head (Scheme 2), are based on the thiourea-forming and the copper(I)-catalyzed azide-alkyne cycloaddition (CuAAC) reactions, two "click"-type ligation strategies already proven very efficient to generate polycationic clusters.³⁶ The preparation of **5** started by hexanoylation of methyl 6-deoxy-6-iodo- α -D-glucopyranoside **23**³⁵ (**24**; Scheme 2, 2a), followed by nucleophilic displacement of the iodine by Boc-protected cysteamine (**25**) and carbamate hydrolysis, afforded the cysteaminylic derivative **26** in 92% overall yield. Condensation of **26** with 2-[*N,N*-bis(2-(*N*-*tert*-butoxycarbonylamino)ethylamino)ethyl isothiocyanate³⁷ and final acid-promoted Boc deprotection provided **5**, which was isolated as the dihydrochloride salt.

The cationic amphiphile **6** was obtained in good yield from azide **12** by following a divergent synthetic strategy in which the hydrophobic and cationic domains are sequentially installed onto the glucopyranoside scaffold. Acylation of **12** with hexanoic anhydride and *N,N*-dimethylaminopyridine (DMAP) in DMF afforded triester **28** (Scheme 2, 2a) that was reacted with 3-bis[2-(*tert*-butoxycarbonylamino)ethyl]-propargylamine³⁸ in the presence of silica-based particles incorporating bis(pyridyl)amine (BPA) Cu(I) chelating agent³⁹ to give the triazol adduct **29** in 78% yield. The use of the solid-supported catalyst has proven advantageous even in multi-CuAAC ligation strategies, highly simplifying the purification step to a simple filtration process.⁴⁰ Acid hydrolysis of the Boc protecting groups in **29** provided the corresponding triamine **30**, which was next reacted with 2-(*N*-*tert*-butoxycarbonylamino)ethyl isothiocyanate³¹ to give bis-(thiourea) **31**. Final hydrolysis of the Boc protecting groups led to the target compound **6**.

Syntheses of Trehalose-Derived Cationic Glycolipids.

The strategies implemented for the preparation of the α,α' -trehalose amino glycolipids **7–11** parallel those above commented for the corresponding ether- (1–4) or ester-type (5–7) methyl α -D-glucopyranoside counterparts. Thus, compounds **7** and **8** were obtained in good overall yield in an efficient five-step synthesis starting from 6,6'-di-*O*-trityl- α,α' -trehalose **32**⁴² after alkylation of the six secondary hydroxyl groups (**33** and **34**), trityl cleavage with *p*-toluenesulfonic acid in DCM-MeOH (**35** and **36**), Garegg's iodination of the primary hydroxyls (**37** and **38**), nucleophilic displacement of the iodines with Boc-protected cysteamine (**39** and **40**), and hydrolysis of the carbamate groups (Scheme 3). The hexanoylated analogue **9** was similarly obtained from 6,6'-dideoxy-6,6'-diiodo- α,α' -trehalose **41**⁴³ by esterification of the secondary hydroxyls (**42**), incorporation of the Boc-protected

Scheme 2. Syntheses of Monosaccharides 5 (2a) and 6 (2b)^a



^aReagents and conditions (2a): (a) hexanoic anhydride, DMAP, DMF, Ar, rt, 4 h, 55%; (b) *tert*-butyl *N*-(2-mercaptoethyl)carbamate, Cs₂CO₃, DMF, Ar, overnight, 85%; (c) 1:1 TFA-DCM, quant; (d) 2-[*N,N*-bis(2-(*N*-*tert*-butoxycarbonyl)ethylamino)ethyl]isothiocyanate, Et₃N, DCM, Ar, overnight, 50%; (e) 1:1 TFA-DCM, rt, 1 h, quant. Reagents and conditions (2b): (a) hexanoic anhydride, DMAP, DMF, Ar, 4 h, 55%; (b) 3-bis[2-(*tert*-butoxycarbonylamino)ethyl]propargylamine, Si-BPA-Cu⁺, 9:1 H₂O/^tBuOH, 85 °C, 36 h, 78%; (c) 1:1 TFA/H₂O, rt, 1 h, quant; (d) 2-(*N*-*tert*-butoxycarbonyl)ethyl isothiocyanate, Et₃N, DCM, overnight, 52%; (e) 1:1 TFA/H₂O, rt, 1 h, quant.

cysteamine substituents at the primary positions (43), and final deprotection (Scheme 4).

The cationic trehalose amphiphiles **10** and **11** were prepared starting from the common diazide precursor **44**, readily accessed by nucleophilic displacement of the iodine in **42** with sodium azide by CuAAC ligation using the silica-supported Si-BPA-Cu⁺ catalyst. Thus, sequential reaction of **44** with *N*-Boc-propargylamine (**45**), carbamate hydrolysis (**46**), thiourea-coupling with Boc-protected 2-aminoethyl isothiocyanate (**47**), and final Boc removal yielded the diaminoethylthioureido adduct **10**. Alternatively, the CuAAC coupling of **44** with 3-bis[2-(*tert*-butoxycarbonylamino)ethyl]propargylamine (**48**) followed by carbamate hydrolysis afforded compound **11** (Scheme 5).

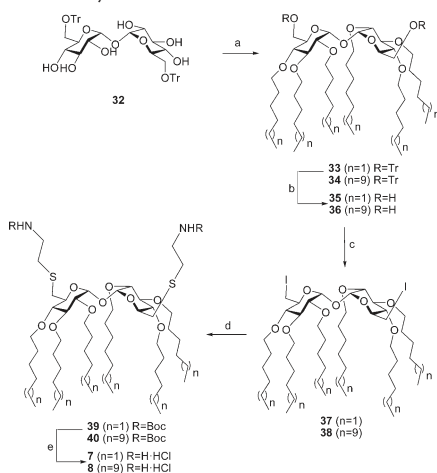
TLR4 Modulation in HEK-Blue Cells. Cationic amphiphiles **1–11** were first screened for their capacity to interfere with TLR4 activation and signaling on HEK-Blue cells. HEK-Blue cells are stably transfected with TLR4, MD-2, and CD14 genes. In addition, these cells stably express an optimized alkaline phosphatase gene engineered to be secreted (sAP), placed under the control of a promoter inducible by several transcription factors such as NF- κ B and AP-1.²⁹ This reporter gene allows monitoring the activation of TLR4 signal pathway by endotoxin. Compounds **5** and **9–11** were inactive in stimulating TLR4 signal when provided alone while inhibited in a dose-dependent way the LPS-stimulated TLR4 signal (Table

1). Compounds **1–4** and **6–8** resulted as being inactive or with very low activity both as agonists and antagonists.

The lack of significant activity of all compounds bearing C₆ or C₁₄ ether-linked lipophilic chains, namely compounds **1–4** and **7–8**, strongly suggests that the presence of ester-type linkages at the hydrophobic domain is a primary structural requirement to elicit LPS-antagonist behavior in cationic glycolipids. From the acylated sublibrary, all compounds are active with the exception of compound **6**, meaning that the cationic head also has an impact on the TLR4 antagonist activity. Among these, the trehalose-based disaccharides **9–11**, bearing more compact cationic headgroups, showed higher potency as TLR4 antagonists than monosaccharide **5**. The observed trend points to a positive relationship between well-ordered facial amphiphilicity and TLR4 antagonist activity of cationic glycolipids. In agreement with this, disaccharide **11**, with six hexanoyl chains and six protonable amino groups oriented toward opposite faces in a rather compact arrangement (Figure 3), proved to be the most active TLR4 antagonist. Compounds **5**, **9**, **10**, and **11** were further tested for their toxicity by a standard MTT viability test, and all resulted in being nontoxic or with very low toxicity in the concentration range used to test their activity (Supporting Information).

Activity on HEK293 Cells Transfected with Human and Murine MD-2-TLR4. Biologically active cationic glyco-

Scheme 3. Syntheses of Trehalose Derivatives 7 and 8^a



^aReagents and conditions: (a) hexyl bromide, NaH, DMF, overnight, 92% or 1-bromotetradecane, NaH, DMF, 50 °C, 77%; (b) *p*-toluenesulfonic acid, 1:1 DCM–MeOH, rt, 4 h, 48% for 35 and 47% for 36; (c) I₂, PPh₃, imidazole, toluene, 70 °C, 3 h, 94% for 37 and 96% for 38; (d) HS(CH₂)₂NHBoc, Cs₂CO₃, DMF, 60 °C, overnight, 85% for 39 and 99% for 40; (e) 1:1 TFA/DCM, rt, 15 min, quant for 7, 98% for 8.

lipids 5, 9, 10, and 11 were further examined for their capacity to stimulate or to inhibit LPS-induced TLR4 activation and signaling in HEK293 cells transfected with human or murine TLR4 and MD-2 and a dual luciferase reporter gene (Figure 4).

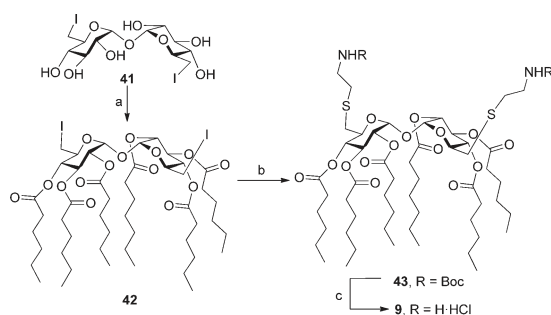
In the absence of LPS, none of the cationic glycolipids stimulate TLR4 signaling (no agonist activity) in cells transfected with hMD-2-hTLR4 or mMD-2-mTLR4. Conversely, in the presence of LPS, all compounds were able to inhibit human and murine MD-2-TLR4 activation in a

concentration-dependent manner. The antagonist potency (IC₅₀ values, Table 1) of 5, 9, 10, and 11 was similar in cells transfected with human and mouse receptors and also very similar to the activity found in HEK-Blue cells (Table 1). In cells transfected with hMD-2-hTLR4 or mMD-2-mTLR4, triacylated monosaccharide 5 and hexacylated disaccharide 9 were less active (IC₅₀ = 3.3–3.9 and 0.8–1.4 μM, respectively) than disaccharides 10 and 11 (IC₅₀ = 0.6 and 0.2 μM, respectively). The high potency of trehalose-derived glycolipids 9 and 11 in inhibiting both mouse and human MD-2-TLR4 signals is reminiscent of the activity of synthetic Eritoran that has potent TLR4 antagonist activity in all species.^{16,44} In contrast, natural lipid IVa is agonist on murine and antagonist on human TLR4.⁴⁵

Experiments on Murine Macrophages. The activity of compounds 5, 9, and 11 on LPS-induced TLR4 signaling in bone marrow-derived murine macrophages (BMDM) was subsequently tested. Compounds 5 and 9 showed very low/no activity in activating TLR4 or in inhibiting LPS-stimulated TLR4 signal (Supporting Information), while compound 11 (Figure 5) gave a concentration-dependent inhibition of IL-6 and TNF-α production at concentrations of 1 and 2 μM (Figure 5), while at 0.1 and 0.5 μM, concentrations had no effect or a slightly potentiating effect.

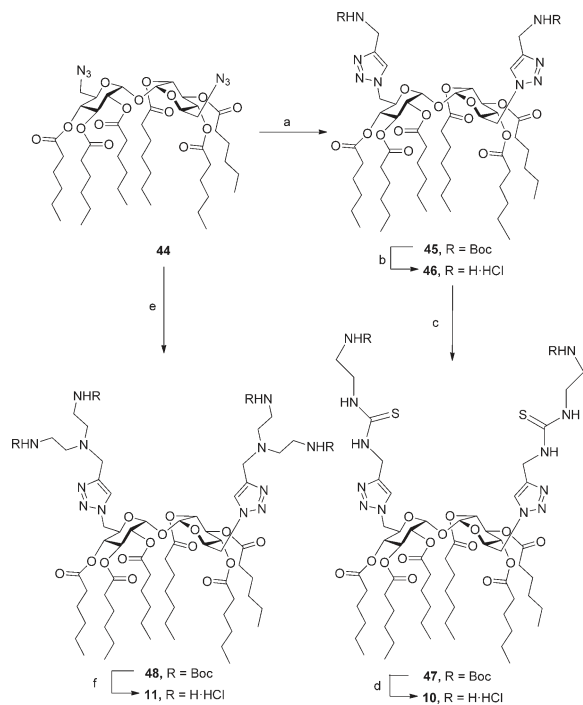
Aggregation Properties of Cationic Glycolipids. Cationic lipids can spontaneously assemble into liposomal structures. Some cationic liposomes induce the expression of pro-apoptotic and pro-inflammatory mediators through the activation of cellular pathways.¹⁷ However, it is still controversial if the initiation of inflammatory and apoptotic response is due to specific interaction with receptors at the cell surface or to the internalization of liposomes into cells through endocytosis and endocytosis-like mechanisms followed by interaction of charged compounds with downstream effectors. In the particular case of cationic lipids modulating TLR4 activity, there is no information available on whether aggregated species or single molecules are the active species. To have an insight in this question, we have determined the critical micelle concentrations (CMC) of cationic glycolipids 5, 9, 10, and 11 using an established technique based on the polarity-induced change in the fluorescence spectra of pyrene when incorporated in micelles formed by synthetic compounds (Table 2).⁴⁶ In all

Scheme 4. Synthesis of Trehalose Derivative 9^a



^aReagents and conditions: (a) HS(CH₂)₂NHBoc, Cs₂CO₃, DMF, 60 °C, 24 h, 58%; (b) 1:1 TFA/DCM, rt, 15 min, quant.

Scheme 5. Syntheses of Trehalose Derivatives 10 and 11^a



^aReagents and conditions: (a) *N*-*tert*-butoxycarbonylpropylamine, Si-BPA-Cu⁺, 9:1 H₂O/^tBuOH, 24 °C, 36 h, quant; (b) 1:1 TFA/H₂O, rt, 1 h, 97%; (c) *tert*-butyl-*N*-(2-isothiocanoethyl)carbamate, Et₃N, DCM, overnight, 67%; (d) 1:1 TFA/H₂O, rt, 1 h, quant; (e) 3-bis[2-(*tert*-butoxycarbonylamino)ethyl]propylamine, Si-BPA-Cu⁺, 9:1 H₂O/^tBuOH, reflux, 36 h, 91%; (f) 1:1 TFA/H₂O, rt, 1 h, quant.

Table 1. TLR4 Antagonist Activity of Cationic Glycolipids 5 and 9–11 on HEK-Blue Cells, HEK293 hMD-2/hTLR4, and HEK293 mMD-2-mTLR4 Stimulated with *E. coli* O55:B5 LPS (10 nM)

compd	IC ₅₀ (μM)		
	HEK-Blue	HEK293 hMD-2/hTLR4	HEK293 mMD-2-mTLR4
5	3.7 ± 0.4	3.9 ± 1.5	3.3 ± 1.2
9	1.3 ± 0.1	1.4 ± 0.3	0.8 ± 0.2
10	5.0 ± 1.0	0.6 ± 0.02	0.6 ± 0.03
11	0.6 ± 0.05	0.2 ± 0.02	0.2 ± 0.03

cases, the CMC values of active compounds are higher than the corresponding IC₅₀ values as TLR4 antagonists, suggesting that the biologically active species are prevalently single molecules in solution.

Synthesis and Biological Activity of Gold Nanoparticles Coated with Glycolipid 11. LPS is an amphiphilic molecule, and it is mainly present in the form of micellar aggregates in a concentration range that is relevant for its biological activity. It has been recently proposed that the multiple presentation of LPS or other TLR4 ligands on nanoparticles could be a way to potentiate the agonist or antagonist action of chemicals by mimicking the 3D-structure

of LPS aggregates.^{47,48} Moreover, the possibility of *in vitro* and/or *in vivo* delivery based on NP is considered advantageous for clinical development, as it can maximize the effectiveness of drugs, minimize the invasiveness and toxic side effects, and speed up the clinical development program. To test the suitability of this approach in the case of cationic glycolipids, the preparation and biological evaluation of gold nanoparticles coated with the most active compound 11 has been undertaken. Colloidal gold nanoparticles were synthesized by a variation of the Brust–Schiffrin method⁴⁹ and coated by surface adsorption with the α,α'-trehalose derivative 11. The resulting cationic glycolipid-modified nanoparticles (11-NP)

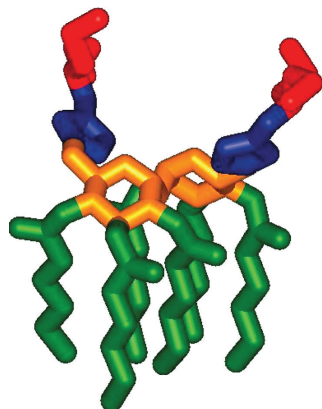


Figure 3. 3D molecular model of compound 11 (cationic headgroups in red, triazol linkers in blue, α,α' -trehalose scaffold in orange, hexanoyl chains in green) evidencing its compact facial amphiphilic character. Hydrogens have been omitted for the sake of clarity.

kept a small size with low polydispersity. Most interestingly, they retained the biological activity without apparent increase in cytotoxicity. These results represent a proof-of-concept of the possibility of developing nanoparticulate systems based on cationic glycolipids as modulators of TLR4 signaling pathway,

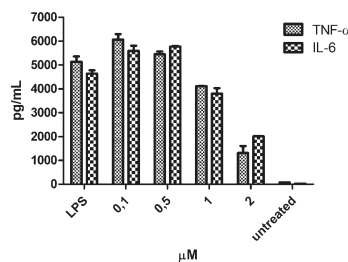


Figure 5. BMDM were treated with increasing concentrations (0–2 μM) of compound 11 in RPMI + FBS 10% in the presence of LPS, administered 1 h after the treatment with synthetic compound. The ELISA assay, performed after overnight incubation, revealed a dose dependent decrease of LPS-induced IL-6 and TNF- α production. Cytokines productions in cells not treated with LPS are reported as negative controls.

Table 2. Critical Micelle Concentrations (CMC) in Aqueous Environment of TLR4 Antagonists

compd	CMC (μM)
5	59.7 \pm 7.4
9	97.7 \pm 10.0
10	10.9 \pm 2.1
11	350.5 \pm 70.5

an approach previously demonstrated only for LPS itself.⁴⁷ On the basis of these data, the prepared 11-NP nanoparticles were

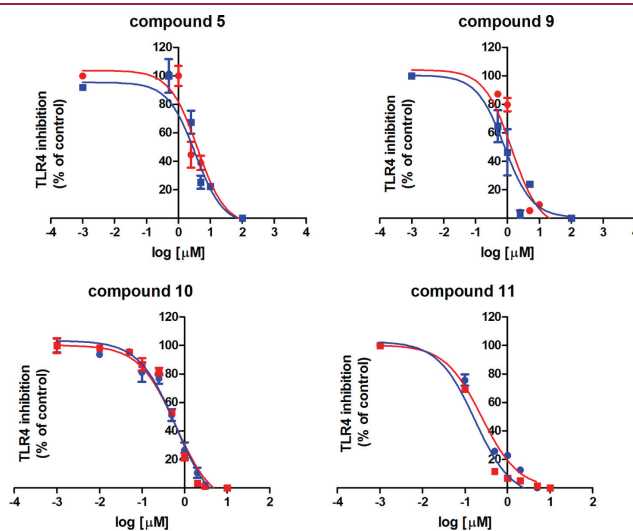


Figure 4. Dose-dependent inhibition of LPS-stimulated TLR4 activation by synthetic glycolipids. HEK293 cells transfected with human MD-2/TLR4 (red line) or murine MD-2/TLR4 (blue line) were treated with increasing concentrations of compounds and stimulated with LPS (5 nM). Normalized data are representative of three independent experiments.

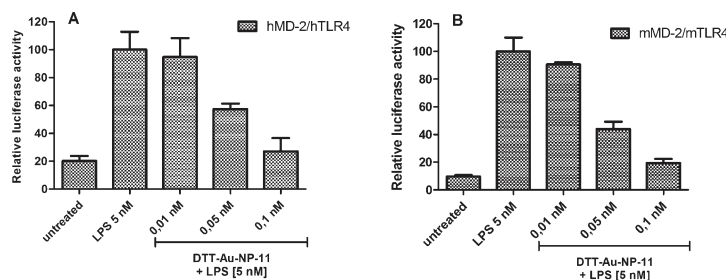


Figure 6. Dose-dependent TLR4 antagonism in HEK293 cells treated with DTT-Au-NP-11. HEK293 cells were transfected with NF- κ B-dependent luciferase and constitutive Renilla luciferase reporter plasmids as well as with (A) human or (B) murine MD-2 and TLR4 plasmids. The indicated amount of the DTT-Au-NP-11 was added to the cells, followed 1 h later by stimulation with LPS. Luciferase activity was measured 16 h later.

engaged in an *in vivo* assay. The inhibitory activity of the nanoparticles coated with glycolipid 11 was tested on HEK293 cells. They exhibited strong LPS inhibitory activity already at very low concentrations (Figure 6A,B) on the human as well as the murine MD-2-TLR4 receptor complex.

In Vivo Activity. Because the synthesized compounds exhibited strong inhibition of the LPS-induced MD-2-TLR4 activation *in vitro*, we next wished to determine their inhibitory potential *in vivo*. All four selected candidates (5, 9, 10, and 11) potently inhibited the LPS-induced immune activation in C57/Bl6 mice (Figure 7). The strongest inhibition was exhibited by

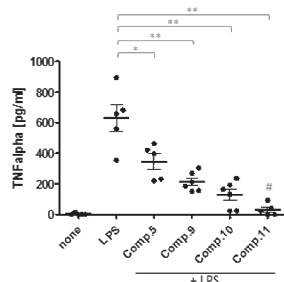


Figure 7. *In vivo* activity of cationic amphiphiles. C57/Bl6 mice were injected ip with the indicated compounds (2×10^{-7} mol/mouse), followed 1 h later by ip injection of LPS (1×10^{-9} mol/mouse). Three hours later, sera were collected and TNF- α concentration was determined by ELISA (data shown with mean and standard error, $N = 5-6$) two-tailed *t* test (* $p < 0.1$; ** $p < 0.01$ —compared to \gg LPS \ll) (# not significant—compared to \gg none \ll).

compound 11, which totally abolished LPS-induced immune activation. Results in Figure 7 show that compounds 5, 9, 10, and 11 are strong MD-2-TLR4 inhibitors not only *in vitro* but also *in vivo*.

CONCLUSIONS AND PERSPECTIVES

New cationic amphiphiles 1–11 based on monosaccharide and disaccharide glycolipid scaffolds have been designed, synthesized, and their capacity to modulate TLR4 activation and signaling evaluated. Glucose-based compound 5 and trehalose-

based compounds 9–11 were active in inhibiting the LPS-triggered TLR4 activation and signaling in HEK cells, with IC_{50} values ranging from about 5 to 0.2μ M. The cell toxicity of these molecules is low, and the potency of TLR4 antagonism is in the same order of magnitude of the best synthetic TLR4 antagonists so far tested by us²⁹ and other groups.³⁰ The active molecules inhibited the TLR4 signal in HEK cells transfected with human and murine MD-2-TLR4 complexes with very similar potency, similarly to the very efficient TLR4 antagonist Eritoran and differently from the natural TLR4 antagonist lipid IVa that has species-specific activity (antagonist on human and agonist on mice MD-2-TLR4). Compounds 5, 9, 10, and 11 significantly inhibited LPS-triggered IL-6 production in mice, with compound 11 showing the most evident effect. Because these compounds are active *in vitro* and *in vivo* and show low toxicity, they represent good leads for the development of drugs targeting TLR4 signaling.

The biological evaluation of active compounds compared to inactive, structurally related monosaccharides (compounds 1–4 and 6) and disaccharides (compounds 7 and 8) suggests some general structure–activity relationships in this type of compounds: (i) the presence of acyl lipophilic chains at the hydrophobic domain seems to be a primary requisite because all compounds with ether bonds are inactive, and (ii) the higher *in vitro* and *in vivo* activity of compound 11 suggests that the trehalose scaffold favors the biological activity, probably by providing a well-ordered facial amphiphilic character. Compound 11 adsorbed on gold nanoparticles (11-NP) is still active as TLR4 antagonist in cells, but the high toxicity of these functionalized nanoparticles could prevent their use *in vivo* as carriers for TLR4 antagonists.

Finally, the experimentally determined CMC values for cationic glycolipids 5 and 9–11 are 1 order of magnitude higher than the corresponding IC_{50} as TLR4 antagonists, suggesting that they are active as single monomers in solution. This very likely means that specific molecular interaction with CD14 and MD-2 receptors regulate the TLR4 activity of these compounds. It will be important in the future to define more precisely the molecular determinants of the interaction with CD14 and MD-2 receptors to allow a structure-based rational design of cationic TLR4 modulators.

EXPERIMENTAL SECTION

General Synthetic Methods. Optical rotations were measured at 20 ± 2 °C in 1 dm tubes on a Jasco P-2000 polarimeter. Ultraviolet–

visible (UV) spectra were recorded in 1 cm tubes on a Jasco V-630 spectrophotometer. Infrared (IR) spectra were recorded on a Jasco ATR MIRacle spectrophotometer. ^1H (and ^{13}C NMR) spectra were recorded at 300 (75.5) and 500 (125.7) MHz with Bruker 300 AMX, 500 AMX, and 500 DRX. 1D TOCSY, 2D COSY, HMQC, and HSQC experiments were used to assist on NMR assignments. Thin-layer chromatography (TLC) was carried out on aluminum sheets coated with Silica Gel 60 F₂₅₄ Merck with visualization by UV light and by charring with 10% H₂SO₄. With preparative purposes, column chromatography was carried out on Silica Gel 60 F₂₅₄ Merck. ESI mass spectra were recorded in the positive mode on a Bruker Daltonics esquire6000 ion-trap mass spectrometer. Typically, samples were dissolved in appropriate volumes of deionized water to give samples concentration of 50 mg/L. Aliquots were mixed with 25:25:1 deionized water–methanol–trifluoroacetic acid, generally in a ratio of 1:1:0, to give a total volume of 200 μL . Samples were introduced by direct infusion, using a Cole–Parmer syringe at a flow rate of 2 $\mu\text{L}/\text{min}$. Ions were scanned between 300 and 3000 Da with a scan speed of 13000 Da/s at unit resolution using resonance ejection at the multiple resonance of one-third of the radio frequency ($\Omega = 781.25$ kHz). Calibration of the mass spectrometer was performed using ES tuning mix (Hewlett-Packard). Recorded data were processed using Bruker Daltonics Esquire 5.0 software (Bruker). Elemental analyses were carried out at the Instituto de Investigaciones Químicas (Sevilla, Spain) using an elemental analyzer Leco CHNS-932 or Leco TruSpec CHN.

Methyl 6-azido-6-deoxy- α -D-glucopyranoside,²⁸ methyl 4,6-O-(4-methoxybenzylidene)- α -D-glucopyranoside,³⁴ methyl 6-deoxy-6-iodo- α -D-glucopyranoside,³⁵ 2-[N,N-bis(2-(N-tert-butoxyaminocarbonyl)ethylamino)ethyl isothiocyanate],³⁷ 6,6'-dideoxy-6,6'-diiodo- α,α' -trehalose 41,⁴³ 6,6'-di-O-trityl- α,α' -trehalose 32,⁴² N-(2-isothiocyanatoethyl) tert-butylcarbamate,⁴¹ and 3-bis[2-tert-butoxycarbonylamino)ethyl]propylamine³⁸ were obtained according to described procedures. Purity of all final compounds was confirmed to be $\geq 95\%$ by ^1H NMR and combustion microanalysis.

Methyl 6-Azido-6-deoxy-2,3,4-tri-O-hexyl- α -D-glucopyranoside (13). To a solution of methyl 6-azido-6-deoxy- α -D-glucopyranoside (0.40 m, 1.82 mmol) in dry DMF (9 mL), NaH (0.65 g, 16.42 mmol) was added, under Ar atmosphere, at 0 °C. Then 1-bromohexane (2.3 mL, 16.42 mmol) was added dropwise, and the reaction mixture was stirred overnight at rt. The solvent was evaporated and the residue diluted in DCM (10 mL) and washed with H₂O (2 \times 10 mL). The organic layer was dried (MgSO₄), concentrated, and purified by column chromatography (1:30 EtOAc–cyclohexane). Yield 48% (0.50 m, 1.06 mmol); $R_f = 0.34$ (1:18 EtOAc–cyclohexane); $[\alpha]_D^{20} = +90.0$ (c 1.0, DCM). IR: $\nu_{\text{max}} = 2099, 1094$ cm⁻¹. ^1H NMR (300 MHz, CDCl₃): $\delta = 4.74$ (d, 1 H, $J_{1,2} = 3.5$ Hz, H-1), 3.79, 3.64, 3.58 (m, 6 H, OCH₂), 3.67 (m, 1 H, H-5), 3.64–3.24 (m, 2 H, H-3, H-6a), 3.39 (s, 3 H, OCH₃), 3.35 (m, 1 H, H-6b), 3.23 (dd, 1 H, $J_{2,3} = 9.6$ Hz, H-2), 3.12 (t, 1 H, $J_{3,4} = J_{4,5} = 9.3$ Hz, H-4), 1.55 (m, 6 H, CH₂), 1.27 (m, 18 H, CH₂), 0.86 (m, 9 H, CH₃). ^{13}C NMR (75.5 MHz, CDCl₃): $\delta = 98.0$ (C-1), 81.3 (C-3), 80.7 (C-2), 78.8 (C-4), 73.7, 73.6, 71.8 (OCH₂), 70.2 (C-5), 55.2 (OCH₃), 51.5 (C-6), 31.7–22.6 (CH₂), 14.3 (CH₃). ESI MS: $m/z = 965.8$ [2 M + Na]⁺, 494.6 [M + Na]⁺. Anal. Calcd for C₂₅H₄₉N₃O₅: C, 63.66; H, 10.47; N, 8.91. Found: C, 63.72; H, 10.97; N, 8.33.

Methyl 6-Amino-6-deoxy-2,3,4-tri-O-hexyl- α -D-glucopyranoside Hydrochloride (1). To a solution of 13 (0.15 g, 0.32 mmol) in degassed MeOH (12 mL), Pd/C (10%, 0.06 g) was added and the mixture was stirred under H₂ atmosphere (1 bar) at rt until complete consumption of the starting compound. The catalyst was filtered off, the solution concentrated, and the resulting residue purified by column chromatography (1:9 EtOAc–cyclohexane \rightarrow 45:5:3 EtOAc–EtOH–H₂O) and freeze-dried from 0.1 N HCl solution. Yield 87% (0.12 g, 0.26 mmol); $[\alpha]_D^{20} = +83.0$ (c 1.0, DCM). ^1H NMR (300 MHz, CD₃OD): $\delta = 4.82$ (d, 1 H, $J_{1,2} = 3.4$ Hz, H-1), 3.81, 3.64, 3.56 (m, 6 H, OCH₂), 3.65 (m, 1 H, H-5), 3.53 (t, 1 H, $J_{2,3} = J_{3,4} = 9.3$ Hz, H-3), 3.41 (s, 3 H, OCH₃), 3.25 (dd, 1 H, H-2), 3.11 (dd, 1 H, $J_{6a,6b} = 13.1$ Hz, $J_{5,6a} = 2.7$ Hz, H-6a), 3.01 (t, 1 H, $J_{4,5} = 9.3$ Hz, H-4), 2.84 (dd, 1 H, $J_{5,6b} = 8.5$ Hz, H-6b), 1.56 (m, 6 H, CH₂), 1.33 (m, 18 H, CH₂),

0.91 (m, 9 H, CH₃). ^{13}C NMR (75.5 MHz, CD₃OD): $\delta = 99.1$ (C-1), 82.6 (C-3), 81.8 (C-2), 81.1 (C-4), 74.5, 74.3, 72.2 (OCH₂), 70.7 (C-5), 55.8 (OCH₃), 42.9 (C-6), 33.0–24.2 (CH₂), 14.4 (CH₃). ESIMS: $m/z = 891.7$ [2 M + H]⁺, 446.5 [M + H]⁺. Anal. Calcd for C₂₅H₅₁N₃O₅·HCl: C, 62.28; H, 10.87; N, 2.91. Found: C, 62.33; H, 10.69; N, 2.70.

Methyl 6-Azido-6-deoxy-2,3,4-tri-O-tetradecyl- α -D-glucopyranoside (14). To a solution of methyl 6-azido-6-deoxy- α -D-glucopyranoside (0.28 g, 1.30 mmol) in dry DMF (4 mL), NaH (0.55 mg, 13.60 mmol) was added, under Ar atmosphere, at 0 °C. Then 1-bromotetradecane (4.1 mL, 13.60 mmol) was added dropwise, and the reaction mixture was stirred overnight at 55 °C. The solvent was evaporated and the residue diluted in DCM (10 mL) and washed with H₂O (2 \times 10 mL). The organic layer was dried (MgSO₄), concentrated, and purified by column chromatography (cyclohexane \rightarrow 1:40 EtOAc–cyclohexane). Yield 42% (0.45 g, 0.26 mmol); $R_f = 0.25$ (1:15 EtOAc–cyclohexane); $[\alpha]_D^{20} = +52.1$ (c 1.0, DCM). IR: $\nu_{\text{max}} = 2100, 1096$ cm⁻¹. ^1H NMR (300 MHz, CDCl₃): $\delta = 4.76$ (d, 1 H, $J_{1,2} = 3.4$ Hz, H-1), 3.79, 3.64, 3.58 (m, 6 H, OCH₂), 3.69 (m, 1 H, H-5), 3.66–3.44 (m, 2 H, H-3, H-6a), 3.39 (s, 3 H, OCH₃), 3.37 (dd, 1 H, $J_{6a,6b} = 13.3$ Hz, $J_{5,6b} = 5.5$ Hz, H-6b), 3.25 (dd, 1 H, $J_{2,3} = 9.4$ Hz, H-2), 3.13 (t, 1 H, $J_{3,4} = J_{4,5} = 9.4$ Hz, H-4), 1.57 (m, 6 H, CH₂), 1.27 (m, 66 H, CH₂), 0.86 (m, 9 H, CH₃). ^{13}C NMR (75.5 MHz, CDCl₃): $\delta = 98.0$ (C-1), 81.3 (C-3), 80.7 (C-2), 78.8 (C-4), 73.7, 73.6, 71.8 (OCH₂), 70.2 (C-5), 55.2 (OCH₃), 51.5 (C-6), 31.9–22.7 (CH₂), 14.1 (CH₃). ESI MS: $m/z = 830.8$ [M + Na]⁺. Anal. Calcd for C₄₀H₇₉N₃O₅: C, 72.81; H, 12.10; N, 5.20. Found: C, 72.89; H, 11.87; N, 4.88.

Methyl 6-Amino-6-deoxy-2,3,4-tri-O-tetradecyl- α -D-glucopyranoside Hydrochloride (2). To a solution of 14 (0.15 g, 0.19 mmol) in THF (16.4 mL), TPP (0.10 g, 0.39 mmol) was added and the mixture was stirred at rt for 15 min. Then NH₄OH (1.6 mL) was added, the solution was stirred overnight at 50 °C, and then concentrated. The resulting residue was purified by column chromatography (EtOAc \rightarrow 9:1 DCM–MeOH) and freeze-dried from 10:1 H₂O–HCl 0.1 N solution. Yield 82% (0.13 mg, 0.16 mmol); $[\alpha]_D^{20} = +43.2$ (c 1.0, DCM). IR: $\nu_{\text{max}} = 1092$ cm⁻¹. ^1H NMR (300 MHz, CDCl₃): $\delta = 4.79$ (d, 1 H, $J_{1,2} = 3.4$ Hz, H-1), 3.78, 3.60, 3.55 (m, 7 H, OCH₂, H-3), 3.73 (m, 1 H, H-5), 3.46 (s, 3 H, OCH₃), 3.27 (m, 1 H, H-6a), 3.22 (dd, 1 H, $J_{1,2} = 9.5$ Hz, H-2), 2.95 (m, 2 H, H-4, H-6b), 1.55 (m, 6 H, CH₂), 1.25 (m, 66 H, CH₂), 0.87 (t, 9 H, $J_{\text{H,H}} = 6.6$ Hz, CH₃). ^{13}C NMR (75.5 MHz, CD₃OD): $\delta = 98.0$ (C-1), 81.0 (C-3), 80.4 (C-2), 79.9 (C-4), 77.2 (C-5), 73.7, 73.5, 71.8 (OCH₂), 67.1 (C-6), 55.9 (OCH₃), 31.9–22.7 (CH₂), 14.0 (CH₃). ESI MS: $m/z = 783.0$ [M + H]⁺. Anal. Calcd for C₄₀H₇₉N₃O₅·HCl: C, 71.88; H, 12.31; N, 1.71. Found: C, 71.64; H, 12.26; N, 1.49.

Methyl 4,6-O-(4-Methoxybenzylidene)-2,3-di-O-hexyl- α -D-glucopyranoside (15). To a solution of methyl 4,6-O-(4-methoxybenzylidene)- α -D-glucopyranoside (0.80 g, 2.57 mmol) in DMF (8 mL), NaH (0.62 g, 15.42 mmol) was added. Then, 1-bromohexane (1.8 mL, 12.85 mmol) was added dropwise, and the resulting mixture was stirred at 60 °C overnight. After cooling to rt, the reaction was quenched with MeOH (2 mL) and the solution was stirred for 20 min. Solvents were then evaporated, and the residue was diluted with EtOAc (50 mL) and citric acid (satd aq soln, 40 mL). The layers were separated, and the organic phase was washed with H₂O (3 \times 40 mL), dried (MgSO₄), evaporated, and purified by column chromatography (1:9 EtOAc–cyclohexane). Yield 57% (0.71 g, 0.15 mmol); $R_f = 0.44$ (1:9 EtOAc–cyclohexane); $[\alpha]_D^{20} = +37.2$ (c 1.0, DCM). ^1H NMR (300 MHz, CDCl₃): $\delta = 7.39, 6.87$ (2 d, 4 H, A₂X₂, aromatics), 5.49 (s, 1 H, PhCH), 4.78 (d, 1 H, $J_{1,2} = 3.8$ Hz, H-1), 4.25 (dd, 1 H, $J_{6a,6b} = 9.6$ Hz, $J_{5,6a} = 4.5$ Hz, H-6a), 3.80 (s, 3 H, PhOCH₃), 3.76 (m, 1 H, H-5), 3.72 (t, 1 H, $J_{2,3} = J_{3,4} = 9.2$ Hz, H-3), 3.72–3.57 (m, 5 H, H-6b, OCH₂), 3.47 (t, 1 H, $J_{4,5} = 9.2$ Hz, H-4), 3.42 (s, 3 H, OCH₃), 3.34 (dd, 1 H, H-2), 1.66–1.49 (m, 4 H, CH₂), 1.41–1.18 (m, 12 H, CH₂), 0.88, 0.84 (2 t, 6 H, $J_{\text{H,H}} = 6.5$ Hz, CH₃). ^{13}C NMR (75.5 MHz, CDCl₃): $\delta = 159.9$ –113.5 (Ph), 101.2 (PhCH), 99.1 (C-1), 81.9 (C-4), 80.4 (C-2), 78.2 (C-3), 73.4, 72.2 (OCH₂), 69.0 (C-6), 62.4 (C-5), 55.6 (OCH₃), 31.7–22.6 (CH₂), 14.0 (CH₃). ESI MS: $m/z = 519.5$ [M

+ K]⁺, 503.6 [M + Na]⁺. Anal. Calcd for C₂₇H₄₄O₂: C, 67.47; H, 9.23. Found: C, 67.54; H, 9.30.

Methyl 4,6-O-(4-Methoxybenzylidene)-2,3-di-O-tetradecyl- α -D-glucopyranoside (16).³⁷ To a solution of methyl 4,6-O-(4-methoxybenzylidene)- α -D-glucopyranoside (0.80 g, 2.57 mmol) in DMF (60 mL), NaH (60% suspension in mineral oil, 0.62 g, 15.42 mmol) was carefully added in small portions. Tetradecyl bromide (3.8 mL, 12.85 mmol) was added dropwise and the resulting mixture was stirred at 60 °C overnight. After cooling to rt, the mixture was quenched with methanol (2 mL), then the solution was stirred for 20 min. Solvents were then evaporated and the residue was diluted with EtOAc (50 mL). Citric acid (satd aq soln, 40 mL) was added, the layers were separated, the organic layer was washed with water (3 \times 40 mL), dried (Na₂SO₄) and evaporated. Flash column chromatography on silica gel of the residue (1:9 EtOAc–cyclohexane) afforded 16. Yield 74% (1.33 g, 1.89 mmol); R_f = 0.65 (1:9 EtOAc–cyclohexane); [α]_D = +23.3 (c 1.0 in CHCl₃). ¹H NMR (300 MHz, CDCl₃): δ = 7.40, 6.87 (2 d, 4 H, A₂X₂, aromatics), 5.49 (s, 1 H, PhCH), 4.78 (d, 1 H, J_{1,2} = 3.8 Hz, H-1), 4.25 (dd, 1 H, J_{6,6a} = 9.6, J_{5,6a} = 4.6 Hz, H-6a), 3.80 (s, 3 H, OCH₃), 3.76 (m, 1 H, H-5), 3.75–3.59 (m, 6 H, H-3, H-6b, OCH₂), 3.47 (t, 1 H, J_{3,4} = J_{4,5} = 9.3 Hz, H-4), 3.42 (s, 3 H, OCH₃), 3.34 (dd, 1 H, J_{2,3} = 9.3, H-2), 1.70–1.49 (m, 4 H, CH₂), 1.22 (bs, 44 H, CH₂), 0.87 (t, 6 H, ³J_{H,H} = 5.8 Hz, CH₃). ¹³C NMR (75.5 MHz, CDCl₃): δ = 159.1, 130.0, 127.3, 113.5 (Ph), 101.2 (PhCH), 99.1 (C-1), 81.9 (C-4), 80.4 (C-2), 78.2 (C-3), 73.4, 72.3 (OCH₂), 69.0 (C-6), 62.4 (C-5), 55.2 (OCH₃), 31.9–22.7 (CH₂), 14.1 (CH₃). ESI MS: m/z: 503.6 [M + Na]⁺, 519.5 [M + K]⁺.

Methyl 2,3-Di-O-hexyl-4-O-(p-methoxybenzyl)- α -D-glucopyranoside (17). To a solution of 15 (0.71 g, 1.48 mmol) in a mixture of Et₂O–DCM (2:1, 75 mL), under Ar atmosphere, 1 M LiAlH₄ in THF (7.4 mL, 7.40 mmol) and AlCl₃ (0.81 g, 6.06 mmol) in Et₂O (25 mL) were added dropwise, and the resulting mixture was refluxed for 4 h. After cooling to rt, EtOAc (250 mL) and H₂O (250 mL) were added. The organic layer was washed with brine (2 \times 200 mL), dried (MgSO₄), evaporated, and purified by column chromatography (1:2 EtOAc–cyclohexane). Yield 83% (0.60 g, 1.22 mmol); R_f = 0.26 (1:2 EtOAc–cyclohexane); [α]_D = +76.2 (c 1.0, DCM). IR: ν_{max} = 1076, 1035 cm⁻¹. ¹H NMR (300 MHz, CDCl₃): δ = 7.26, 6.87 (A₂X₂ system, 4 H, aromatics), 4.81 (d, 1 H, ³J_{H,H} = 10.8 Hz, PhCHa), 4.75 (d, 1 H, J_{1,2} = 3.5 Hz, H-1), 4.57 (d, 1 H, PhCHb), 3.86 (m, 1 H, OCH₂), 3.79 (s, 3 H, PhOCH₃), 3.77–3.64 (m, 3 H, H-6a, H-6b, OCH₂), 3.68 (m, 1 H, H-3), 3.67–3.53 (m, 3 H, OCH₂, H-5), 3.42 (t, 1 H, J_{3,4} = J_{4,5} = 9.5 Hz, H-4), 3.37 (s, 3 H, OCH₃), 3.26 (dd, 1 H, J_{2,3} = 9.5 Hz, H-2), 1.75 (bs, 1 H, OH), 1.64–1.57 (m, 4 H, CH₂), 1.37–1.28 (m, 12 H, CH₂), 0.88 (t, 6 H, ³J_{H,H} = 7.0 Hz, CH₃), 0.87 (t, 6 H, ³J_{H,H} = 6.8 Hz, CH₃). ¹³C NMR (75.5 MHz, CDCl₃): δ = 159.3–113.8 (Ph), 98.0 (C-1), 81.6 (C-3), 80.8 (C-2), 77.1 (C-4), 74.5 (PhCH₂), 73.7, 71.7 (OCH₂), 70.6 (C-5), 62.0 (C-6), 55.2, 55.0 (OCH₃), 31.8–22.6 (CH₂), 14.0 (CH₃). ESI MS: m/z: 505.6 [M + Na]⁺, 521.5 [M + K]⁺. Anal. Calcd for C₂₇H₄₄O₂: C, 67.19; H, 9.61. Found: C, 66.92; H, 9.67.

Methyl 6-Deoxy-2,3-di-O-hexyl-6-iodo-4-O-(p-methoxybenzyl)- α -D-glucopyranoside (19). To a solution of 17 (0.60 g, 1.23 mmol) in toluene (25 mL), TPP (0.49 g, 1.85 mmol) and imidazole (0.25 g, 3.70 mmol) were added. Iodine (0.49 g, 1.73 mmol) was added in portions, and the resulting solution was stirred at 70 °C for 5 h. After cooling to rt, NaHCO₃ (satd 25 mL) was added and the mixture was stirred for 5 min. Additional iodine was added, and the mixture was stirred for 10 min. Then Na₂S₂O₃ aq 10% was added to remove the iodine excess. The organic layer was separated, washed with H₂O (3 \times 25 mL), dried (MgSO₄), filtered, concentrated, and purified by column chromatography (1:4 EtOAc–cyclohexane). Yield 94% (0.69 g, 1.16 mmol); R_f = 0.52 (1:4 EtOAc–cyclohexane); [α]_D = +84.3 (c 1.0, DCM). ¹H NMR (300 MHz, CDCl₃): δ = 7.26, 6.88 (A₂X₂ system, 4 H, aromatics), 4.87 (d, 1 H, ³J_{H,H} = 10.6 Hz, PhCHa), 4.77 (d, 1 H, J_{1,2} = 3.4 Hz, H-1), 4.62 (d, 1 H, PhCHb), 3.87 (m, 1 H, CH₂), 3.80 (s, 3 H, PhOCH₃), 3.75–3.64 (m, 2 H, H-3, OCH₂), 3.63–3.50 (m, 2 H, OCH₂), 3.46 (dd, 1 H, J_{6,6b} = 10.4 Hz, J_{5,6a} = 2.4 Hz, H-6a), 3.42 (s, 3 H, OCH₃), 3.37 (m, 1 H, H-5), 3.35–3.26 (m, 2 H, H-2, H-6b), 3.24 (t, 1 H, J_{3,4} = J_{4,5} = 9.0 Hz, H-4), 1.66–1.55 (m, 4 H, CH₂), 1.39–1.25 (m, 12 H, CH₂), 0.88 (t, 6 H, ³J_{H,H} = 6.5 Hz, CH₃), 0.87 (t, 6 H, ³J_{H,H}

= 6.8 Hz, CH₃). ¹³C NMR (75.5 MHz, CDCl₃): δ = 159.4–113.9 (Ph), 98.0 (C-1), 81.2 (C-3), 81.1 (C-2), 80.8 (C-4), 74.9 (PhCH₂), 73.7, 71.7 (OCH₂), 69.2 (C-5), 55.4, 55.2 (OCH₃), 31.7–22.6 (CH₂), 14.0 (CH₃), 8.1 (C-6). ESI MS: m/z: 631.3 [M + K]⁺, 615.4 [M + Na]⁺. Anal. Calcd for C₂₇H₄₃I₂O₆: C, 54.73; H, 7.65. Found: C, 54.88; H, 7.71.

Methyl 6-(2-tert-Butoxycarbonylaminoethylthio)-2,3-di-O-hexyl-4-O-p-methoxybenzyl- α -D-glucopyranoside (21). To a suspension of 19 (0.69 g, 1.16 mmol) and Cs₂CO₃ (0.53 g, 1.62 mmol) in dry DMF (10 mL), tert-butyl (2-mercaptoethyl)carbamate (0.27 mL, 1.62 mmol) was added and the reaction mixture was stirred at 60 °C, under Ar atmosphere, for 24 h. The mixture was concentrated, EtOAc (25 mL) and water (25 mL) were added, and then the organic layer was separated, washed with H₂O (3 \times 25 mL), dried (MgSO₄), filtered, and concentrated and the residue was purified by column chromatography (1:6 \rightarrow 1:4 EtOAc–cyclohexane). Yield 99% (0.74 g, 1.15 mmol); R_f = 0.17 (1:6 EtOAc–cyclohexane); [α]_D = +64.2 (c 1.0, DCM). IR: ν_{max} = 1714 cm⁻¹. ¹H NMR (300 MHz, CDCl₃): δ = 7.24, 6.87 (2 d, 4 H, ³J_{H,H} = 8.7 Hz, aromatics), 4.98 (bs, 1 H, NH), 4.84 (d, 1 H, ³J_{H,H} = 10.8 Hz, PhCHa), 4.74 (d, 1 H, J_{1,2} = 3.4 Hz, H-1), 4.54 (d, 1 H, PhCHb), 3.85 (m, 1 H, OCH₂), 3.79 (s, 3 H, PhOCH₃), 3.74–3.52 (m, 3 H, OCH₂), 3.71 (m, 1 H, H-5), 3.64 (t, 1 H, J_{2,3} = J_{3,4} = 9.3 Hz, H-3), 3.40 (s, 3 H, OCH₃), 3.31–3.25 (m, 4 H, H-2, H-4, CH₂N), 2.84 (dd, 1 H, J_{6,6b} = 13.9 Hz, J_{5,6a} = 2.6 Hz, H-6a), 2.71 (t, 2 H, ³J_{H,H} = 6.4 Hz, CH₂S), 2.57 (dd, 1 H, J_{5,6a} = 7.5 Hz, H-6b), 1.65–1.55 (m, 4 H, CH₂), 1.44 (s, 9 H, CMe₃), 1.36–1.24 (m, 12 H, CH₂), 0.88, 0.87 (2 t, 6 H, ³J_{H,H} = 6.6 Hz, CH₃). ¹³C NMR (75.5 MHz, CDCl₃): δ = 159.3 (CO), 130.5–113.9 (Ph), 97.8 (C-1), 81.6 (C-3), 80.9 (C-2), 80.1 (C-4), 79.3 (CMe₃), 74.7 (CH₂Ph), 73.7, 71.7 (2 CH₂), 70.7 (C-5), 55.3, 55.0 (2 OCH₃), 39.7 (CH₂N), 33.6 (C-6), 33.5 (CH₂S), 31.7–29.6 (CH₂), 28.4 (CMe₃), 26.9–22.6 (CH₂), 14.0 (CH₃). ESI MS: m/z: 664 [M + Na]⁺, 680 [M + K]⁺. Anal. Calcd for C₄₁H₆₀N₂O₈S: C, 63.62; H, 9.26; N, 2.18; S, 5.00. Found: C, 63.73; H, 9.21; N, 1.98; S, 4.86.

Methyl 6-(2-Aminoethylthio)-2,3-di-O-hexyl- α -D-glucopyranoside Hydrochloride (3). Treatment of 21 (0.35 g, 0.55 mmol) with 1:1 TFA–DCM (2 mL) and freeze-drying from 10:1 H₂O/0.1 N HCl solution afforded 3. Yield quant (0.20 g, 0.54 mmol); R_f = 0.45 (45:55 EtOAc–EtOH–H₂O); [α]_D = +74.4 (c 1.0, MeOH). IR: ν_{max} = 3404, 1109 cm⁻¹. ¹H NMR (300 MHz, CD₃OD): δ = 4.80 (d, 1 H, J_{1,2} = 3.9 Hz, H-1), 3.74 (t, 1 H, ³J_{H,H} = 6.8 Hz, OCH₂), 3.67–3.51 (m, 4 H, H-5, OCH₂), 3.42 (s, 3 H, OCH₃), 3.40 (t, 1 H, J_{2,3} = J_{3,4} = 9.3 Hz, H-3), 3.29 (t, 1 H, J_{4,5} = 9.3 Hz, H-4), 3.23 (dd, 1 H, H-2), 3.16 (t, 2 H, ³J_{H,H} = 6.8 Hz, CH₂N), 2.99 (dd, 1 H, J_{6,6b} = 14.4 Hz, J_{5,6a} = 2.3 Hz, H-6a), 2.90 (m, 2 H, CH₂S), 2.72 (dd, 1 H, J_{5,6a} = 8.0 Hz, H-6b), 1.60–1.52 (m, 4 H, CH₂), 1.42–1.31 (bs, 12 H, CH₂), 0.90, 0.89 (2 t, 6 H, ³J_{H,H} = 6.6 Hz, CH₃). ¹³C NMR (75.5 MHz, CD₃OD): δ = 99.1 (C-1), 82.6 (C-3), 81.6 (C-2), 74.6 (OCH₂), 74.0 (C-4), 73.4 (C-5), 72.2 (OCH₂), 55.5 (OCH₃), 40.0 (CH₂N), 34.2 (C-6), 33.0–31.1 (CH₂), 31.1 (CH₂S), 26.9, 26.8, 23.7 (CH₂), 14.4 (CH₃). ESI MS: m/z: 422.5 [M – Cl]⁺. Anal. Calcd for C₂₁H₃₃N₂O₅S·HCl: C, 55.06; H, 9.68; N, 3.06; S, 7.00. Found: C, 54.87; H, 9.45; N, 2.79; S, 6.78.

Methyl 4,6-O-(4-methoxybenzylidene)-2,3-di-O-tetradecyl- α -D-glucopyranoside (18). Methyl 4,6-O-(4-methoxybenzylidene)-2,3-di-O-tetradecyl- α -D-glucopyranoside (0.70 g, 0.98 mmol) was dissolved in a mixture of Et₂O–DCM (2:1, 15 mL) under Ar atmosphere. AlCl₃ (0.81 g, 6.06 mmol) in Et₂O (15 mL) was added dropwise, and the resulting mixture was refluxed for 4 h. After cooling to rt, EtOAc (150 mL) and H₂O (150 mL) were added and the layers separated. The organic layer was washed with brine (3 \times 100 mL), dried (MgSO₄), and evaporated. Column chromatography of the residue (1:1 EtOAc–cyclohexane) afforded 18. Yield 87% (0.50 mg, 0.85 mmol); R_f = 0.47 (1:1 EtOAc–cyclohexane); [α]_D = +24.7 (c 1.0, DCM). IR: ν_{max} 3362, 2953, 1468 cm⁻¹. ¹H NMR (300 MHz, CDCl₃): δ = 4.78 (d, 1 H, J_{1,2} = 3.5 Hz, H-1), 3.94–3.43 (m, 9 H, H-3, H-4 H-5, H-6a, H-6b, 2 OCH₂), 3.41 (s, 3 H, OCH₃), 3.26 (dd, 1 H, J_{2,3} = 9.2 Hz, H-2), 1.69–1.48 (m, 4 H, CH₂), 1.25 (bs, 44 H, CH₂), 0.87 (t, 6 H, ³J_{H,H} = 6.9 Hz, CH₃). ¹³C NMR (75.5 MHz, CDCl₃): δ = 98.1 (C-1), 81.0, 80.6 (C-2, C-3), 73.6 (C-4), 71.3, 70.7 (OCH₂), 70.5 (C-5), 62.5 (C-6), 55.2 (OCH₃), 31.9–22.6 (CH₂), 14.1 (CH₃). ESI MS: m/z: 625.6 [M + K]⁺, 609.8

[M + Na]⁺. Anal. Calcd for C₃₅H₇₀O₆: C, 71.62; H, 12.02. Found: C, 71.38; H, 11.76.

Methyl 2,3-Di-O-tetradecyl-6-deoxy-6-iodo- α -D-glucopyranoside (20). To a solution of 18 (0.49 g, 0.84 mmol) in toluene (17 mL), triphenylphosphine (0.33 g, 1.26 mmol) and imidazole (0.17 g, 2.52 mmol) were added. Iodine (0.33 g, 1.17 mmol) was added in portions, and the resulting solution was stirred at 70 °C for 3 h. After cooling at rt, NaHCO₃ satd (20 mL) was added and the mixture was stirred for 5 min. Additional iodine was added up to turn the organic phase brown, and the mixture was stirred for 10 min. Then aq 10% Na₂S₂O₃ was added to remove the iodine excess. The organic layer was separated, washed with H₂O (3 × 20 mL), dried (MgSO₄), filtered, concentrated, and purified by column chromatography (1:9 EtOAc–cyclohexane). Yield 91% (0.03 g, 0.76 mmol); R_f = 0.30 (1:9 EtOAc–cyclohexane); [α]_D²⁰ = +44.1 (c 1.0, DCM). IR: ν_{max} = 1041, 722 cm⁻¹. ¹H NMR (300 MHz, CDCl₃): δ = 4.81 (d, 1 H, J_{1,2} = 3.6 Hz, H-1), 3.91 (m, 1 H, OCH₂), 3.66–3.49 (m, 5 H, H-6a, OCH₂, H-3), 3.47 (s, 3 H, OCH₃), 3.45 (ddd, 1 H, J_{4,5} = 9.2 Hz, J_{5,6a} = 6.8 Hz, J_{5,6b} = 2.2 Hz, H-5), 3.31 (m, 1 H, H-4), 3.29 (dd, 1 H, J_{2,3} = 10.0 Hz, H-2), 3.26 (dd, 1 H, J_{6a,6b} = 11.2 Hz, H-6b), 2.41 (d, 1 H, J_{6,OH} = 2.3 Hz, OH-4), 1.61–1.54 (m, 4 H, CH₂), 1.25 (bs, 44 H, CH₂), 0.88 (t, 6 H, J_{H,H} = 6.9 Hz, CH₃). ¹³C NMR (75.5 MHz, CDCl₃): δ = 98.2 (C-1), 80.7, 80.5 (C-2, C-3), 73.8 (C-4), 73.6, 71.2 (OCH₂), 69.7 (C-5), 55.5 (OCH₃), 31.9–22.7 (CH₂), 14.1 (CH₃), 7.2 (C-6). ESI MS: m/z: 735.6 [M + K]⁺, 719.7 [M + Na]⁺. Anal. Calcd for C₃₅H₆₉I O₅: C, 60.33; H, 9.98. Found: C, 59.89; H, 9.72.

Methyl 6-(2-tert-Butoxycarbonylaminoethylthio)-2,3-di-O-tetradecyl- α -D-glucopyranoside (22). To a suspension of 20 (0.53 g, 0.77 mmol) and Cs₂CO₃ (0.35 g, 1.07 mmol) in DMF (7 mL), tert-butyl (2-mercaptoethyl)carbamate (0.18 mL, 1.07 mmol) was added and the reaction mixture was stirred at 60 °C, under Ar atmosphere, for 24 h. The mixture was concentrated then EtOAc (20 mL) and H₂O (20 mL) were added, and the organic layer was separated, washed with H₂O (3 × 20 mL), dried (MgSO₄), filtered, and concentrated. The residue was purified by column chromatography (1:3 EtOAc–cyclohexane), affording 22. Yield 95% (0.54 g, 0.73 mmol); R_f = 0.40 (1:3 EtOAc–cyclohexane); [α]_D²⁰ = +50.4 (c 1.0, DCM). IR: ν_{max} = 3631, 1698 cm⁻¹. ¹H NMR (300 MHz, CDCl₃): δ = 4.99 (bs, 1 H, NH), 4.77 (d, 1 H, J_{1,2} = 3.6 Hz, H-1), 3.90 (m, 1 H, OCH₂), 3.72 (ddd, 1 H, J_{4,5} = 9.3 Hz, J_{5,6a} = 7.5 Hz, J_{5,6b} = 2.6 Hz, H-5), 3.64–3.46 (m, 3 H, OCH₂), 3.48 (t, 1 H, J_{2,3} = J_{3,4} = 9.3 Hz, H-3), 3.43 (s, 3 H, OCH₃), 3.36 (t, 1 H, H-4), 3.31 (m, 2 H, CH₂N), 3.27 (dd, 1 H, H-2), 2.98 (dd, 1 H, J_{6a,6b} = 14.1 Hz, H-6a), 2.71 (m, 3 H, H_{6b}, CH₂S), 2.63 (bs, 1 H, OH-4), 1.65–1.50 (m, 4 H, CH₂), 1.43 (s, 9 H, CMe₃), 1.24 (bs, 44 H, CH₂), 0.87 (t, 6 H, J_{H,H} = 7.0 Hz, CH₃). ¹³C NMR (75.5 MHz, CDCl₃): δ = 156 (CO), 97.9 (C-1), 80.9 (C-3), 80.6 (C-2), 79.4 (CMe₃), 73.5 (OCH₂), 72.4 (C-4), 71.2 (OCH₂), 71.0 (C-5), 55.2 (OCH₃), 39.6 (CH₂N), 33.5 (C-6), 33.4 (CH₂S), 31.8–29.3 (CH₂), 28.4 (CMe₃), 26.1–22.6 (CH₂), 14.0 (CH₃). ESI MS: m/z: 784.7 [M + K]⁺, 768.8 [M + Na]⁺. Anal. Calcd for C₄₂H₈₃NO₅S: C, 67.60; H, 11.21; N, 1.88; S, 4.30. Found: C, 67.45; H, 10.90; N, 1.62; S, 4.24.

Methyl 6-(2-Aminoethylthio)-2,3-di-O-tetradecyl- α -D-glucopyranoside Hydrochloride (4). Treatment of 22 (0.25 g, 0.33 mmol) with 1:1 TFA–DCM (2 mL) and freeze-drying from 10:1 H₂O/0.1 N HCl solution afforded 4. Yield quant (0.22 g, 0.33 mmol). Column chromatography of the residue (4:1 EtOAc–cyclohexane → EtOAc → 45:5:3 EtOAc–EtOH–H₂O). R_f = 0.25 (45:5:3 EtOAc–EtOH–H₂O); [α]_D²⁰ = +41.3 (c 0.9, 9:1 DCM–MeOH). IR: ν_{max} = 3406, 722 cm⁻¹. ¹H NMR (300 MHz, CDCl₃): δ = 8.11 (bs, 2 H, NH₂HCl), 4.78 (d, 1 H, J_{1,2} = 3.2 Hz, H-1), 3.87 (m, 1 H, OCH₂), 3.74 (ddd, 1 H, J_{4,5} = 9.4 Hz, J_{5,6a} = 6.7 Hz, J_{5,6b} = 2.7 Hz, H-5), 3.66–3.54 (m, 3 H, OCH₂), 3.49 (t, 1 H, J_{2,3} = J_{3,4} = 8.9 Hz, H-3), 3.42 (s, 3 H, OCH₃), 3.38 (t, 1 H, H-4), 3.27 (dd, 1 H, H-2), 3.18 (t, 2 H, J_{H,H} = 6.2 Hz, CH₂N), 2.97 (dd, 1 H, J_{6a,6b} = 14.2 Hz, H-6a), 2.90 (m, 2 H, CH₂S), 2.74 (dd, 1H, H_{6b}), 1.60–1.54 (m, 4 H, CH₂), 1.25 (bs, 44 H, CH₂), 0.87 (t, 6 H, J_{H,H} = 6.9 Hz, CH₃). ¹³C NMR (75.5 MHz, CDCl₃): δ = 97.9 (C-1), 80.9 (C-3), 80.5 (C-2), 73.7 (OCH₂), 72.1 (C-4), 71.3 (OCH₂), 70.7 (C-5), 55.2 (OCH₃), 38.7 (CH₂N), 33.2 (C-6), 31.9 (CH₂), 30.3 (CH₂S), 30.3–22.7 (CH₂), 14.1 (CH₃). ESI MS: m/z:

646.7 [M – HCl]⁺. Anal. Calcd for C₃₇H₇₂NO₅·HCl·2H₂O: C, 61.85; H, 11.22; N, 1.95; S, 4.46. Found: C, 61.79; H, 11.03; N, 2.01; S, 4.43.

Methyl 6-(2-tert-Butoxycarbonylaminoethylthio)-2,3,4-tri-O-hexanoyl- α -D-glucopyranoside (24). To a solution of 23 (0.49 g, 0.83 mmol) in dry DMF (7.5 mL), Cs₂CO₃ (0.38 g, 0.16 mmol) and tert-butyl N-(2-mercaptoethyl)carbamate (196 μ L, 1.16 mmol) were added, under Ar atmosphere, and the reaction mixture was stirred at 60 °C for 48 h. The reaction mixture was concentrated, and the crude product was dissolved in DCM (10 mL) and washed with H₂O (2 × 15 mL). The organic phase was dried (MgSO₄), filtered, and concentrated, and the residue was purified by flash column chromatography (1:4 EtOAc–cyclohexane). Yield 85% (0.45 mg, 0.70 mmol); R_f = 0.38 (1:3 EtOAc–cyclohexane); [α]_D²⁰ = +62.1 (c 1.0, DCM). IR: ν_{max} = 2958, 1747, 1701 cm⁻¹. ¹H NMR (300 MHz, CDCl₃): δ = 5.46 (t, 1 H, J_{2,3} = J_{3,4} = 10 Hz, H-3), 4.95 (t, 1 H, J_{4,5} = 10.0 Hz, H-4), 3.41 (s, 3 H, OCH₃), 4.90 (d, 1 H, J_{1,2} = 3.7 Hz, H-1), 4.83 (dd, 1 H, H-2), 3.90 (dt, 1 H, J_{5,6a} = 8.0 Hz, H-5), 3.27 (q, 2 H, J_{H,H} = 6.0 Hz, CH₂N), 2.80–2.50 (m, 4 H, CH₂S, H-6a, H-6b), 2.52 (m, 2 H, H-6a, H-6b), 2.31 (m, 6 H, H-2_{H_{ex}}), 1.54 (m, 6 H, H-3_{H_{ex}}), 1.41 (s, 9 H, CMe₃), 1.25 (m, 12 H, H-4_{H_{ex}}, H-5_{H_{ex}}), 0.86 (t, 9 H, H-6_{H_{ex}}). ¹³C NMR (75.5 MHz, CDCl₃): δ = 172.9–172.0 (CO ester), 155.7 (CO carbamate) 96.7 (C-1), 71.5 (C-4), 70.9 (C-2), 69.3 (C-3), 69.9 (C-5), 55.1 (OMe), 39.58 (CH₂N), 33.7 (CH₂S), 33.0 (C-6), 34.0 (C-2_{H_{ex}}), 24.5 (C-3_{H_{ex}}), 28.2 (CMe₃), 22.1 (C-5_{H_{ex}}), 13.6 (C-6_{H_{ex}}). ESI MS: m/z = 670.4 [M + Na]⁺. Anal. Calcd for C₃₂H₅₇NO₁₀S: C, 59.32; H, 8.87; N, 2.16; S, 4.95. Found: C, 59.45; H, 8.93; N, 2.31; S, 4.71.

Methyl 6-(2-Aminoethylthio)-2,3,4-tri-O-hexanoyl- α -D-glucopyranoside Hydrochloride (25). Treatment of 24 (0.29 g, 0.44 mmol) with 1:1 TFA–DCM (6 mL) and freeze-drying from 10:1 H₂O/0.1 N HCl solution afforded 25. Yield quant (0.27 mg, 0.44 mmol); [α]_D²⁰ = +72.0 (c 0.7, EtOAc). IR: ν_{max} = 2962, 1749 cm⁻¹. ¹H NMR (300 MHz, CD₃OD): δ = 8.05 (bs, 3 H, NH₂), 5.28 (t, 1 H, J_{2,3} = 9.7 Hz, J_{3,4} = 9.7 Hz, H-3), 4.94 (t, 1 H, J_{4,5} = 9.7 Hz, H-4), 4.88 (m, 1 H, J_{1,2} = 3.8 Hz, H-1), 4.82 (dd, 1 H, H-2), 3.8 (m, 1 H, H-5), 3.34 (s, 1 H, OCH₃), 2.93 (bs, 2 H, CH₂N), 2.78 (m, 2 H, CH₂S), 2.73 (dd, 1 H, J_{6a,6b} = 14.0 Hz, J_{5,6a} = 2.7, H-6a), 2.62 (dd, 1 H, J_{5,6b} = 7.7 Hz, H-6b), 2.26 (m, 6 H, H-2_{H_{ex}}), 1.44 (m, 6 H, H-3_{H_{ex}}), 1.21 (m, 12 H, H-4_{H_{ex}}, H-5_{H_{ex}}), 0.82 (t, 9 H, H-6_{H_{ex}}). ¹³C NMR (75.5 MHz, CD₃OD): δ = 172–171 (CO), 95.98 (C-1), 71.2 (C-4), 70.6 (C-2), 69.4 (C-3), 69.1 (C-5), 55.1 (OMe), 39.1 (CH₂N), 32.5 (C-6), 30.5 (CH₂S), 33.1 (C-2_{H_{ex}}), 31.1 (C-4_{H_{ex}}), 24 (C-3_{H_{ex}}), 22.1 (C-2_{H_{ex}}), 14.4 (C-5_{H_{ex}}). ESIMS: m/z = 548.3 [M + H]⁺. Anal. Calcd for C₂₇H₅₀ClNO₅·HCl: C, 55.51; H, 8.63; N, 2.40; S, 5.49. Found: C, 55.37; H, 8.62; N, 2.26; S, 5.27.

Methyl 6-(2-(N-(2-(N,N-Di-(2-(N-tert-butoxycarbonylamino)ethyl)amino)ethyl)thio)ureido)-ethylthio)-2,3,4-tri-O-hexanoyl- α -D-glucopyranoside (27). To a solution of 25 (0.12 g, 0.20 mmol) and Et₃N (56 μ L, 0.4 mmol) in DCM (6 mL), 2-[N,N-bis(2-(N-tert-butoxycarbonylamino)ethylamino)ethyl]isothiocyanate (0.09 g, 0.24 mmol) was added and the reaction mixture was stirred, under Ar atmosphere, at rt for 48 h. The reaction mixture was washed with aqueous diluted HCl (2 × 20 mL), dried (MgSO₄), filtered, and concentrated. The residue was purified by column chromatography (1:1 → 3:1 EtOAc–cyclohexane). Yield 50% (0.08 g, 0.10 mmol); R_f = 0.2 (1:1 EtOAc–cyclohexane); [α]_D²⁰ = +71.6 (c 1.0, DCM). IR: ν_{max} = 2959, 1748, 1685 cm⁻¹. ¹H NMR (300 MHz, CDCl₃): δ = 7.46, 6.96 (2 bs, 2 H, NHCS), 5.46 (t, 1 H, J_{2,3} = J_{3,4} = 9.8 Hz, H-3), 4.96 (t, 1 H, J_{4,5} = 9.8 Hz, H-4), 4.90 (d, 1 H, J_{1,2} = 3.5 Hz, H-1), 4.88 (bs, 2 H, NHBoc), 4.84 (dd, 1 H, H-2), 3.93 (bd, 1 H, H-5), 3.77 (q, 2 H, NHCH₂CH₂N), 3.52 (bs, 2 H, SCH₂CH₂N), 3.42 (s, 3 H, OCH₃), 3.11 (q, 4 H, NCH₂CH₂NHoc), 2.82 (t, 2 H, J_{H,H} = 7.0 Hz, NHCH₂CH₂N), 2.77–2.56 (m, 4 H, H-6a, H-6b, SCH₂), 2.50 (bs, 4 H, NCH₂CH₂NHoc), 2.37–2.1 (m, 6 H, H-2_{H_{ex}}), 1.57 (m, 6 H, J_{H,H} = 7 Hz, H-3_{H_{ex}}), 1.43 (s, 9 H, CMe₃), 1.27 (m, 12 H, H-4_{H_{ex}}, H-5_{H_{ex}}), 0.87 (t, 9 H, H-6_{H_{ex}}). ¹³C NMR (75.5 MHz, CDCl₃): δ = 182.1 (CS), 172.0–171.0 (CO ester), 155.2 (CO carbamate), 96.6 (C-1), 70.9 (C-4), 70.1 (C-2), 69.9 (C-5), 69.6 (C-3), 55.8 (NCH₂CH₂NHoc), 55.5 (OMe), 54.0 (SCH₂), 44.1 (NHCH₂CH₂N), 42.4 (SCH₂CH₂N), 39.4 (NCH₂CH₂NHoc), 33.1 (C-6), 32.6 (NHCH₂CH₂N), 34.1 (C-2_{H_{ex}}), 31.2 (C-5_{H_{ex}}), 28.4 (CMe₃), 24.5 (C-3_{H_{ex}}), 22.1 (C-5_{H_{ex}}), 13.9

(C-6_{H_{ex}}). ESI MS: $m/z = 958.6$ [M + Na]⁺. Anal. Calcd for C₄₄H₈₁N₃O₁₂S₂: C, 56.44; H, 8.72; N, 7.48; S, 6.85. Found: C, 56.61; H, 8.89; N, 7.21; S, 6.60.

Methyl 6-(2-(N'-(2-(N,N-Bis(2-aminoethyl)amino)ethyl)thioureido)ethylthio)-2,3,4-tri-O-hexanoyl- α -D-glucopyranoside Trihydrochloride (5). Treatment of 27 (0.15 g, 0.16 mmol) with 1:1 TFA–DCM (2 mL) and freeze-drying from 10:1 H₂O/0.1 N HCl solution afforded 5. Yield quant (0.13 g, 0.16 mmol). $[\alpha]_D = +46.8$ (c 0.85, MeOH). IR: $\nu_{\max} = 2958, 1747, 1675$ cm⁻¹. ¹H NMR (300 MHz, CDCl₃): $\delta = 7.98$ (bs, 4 H, NHCS, NH₂HCl), 7.60 (bs, 1 H, NHCS), 5.47 (t, $J_{3,4} = J_{2,3} = 9.5$ Hz, 1 H, H-3), 4.99 (t, 1 H, $J_{4,5} = 9.5$ Hz, H-4), 4.91 (dd, 1 H, $J_{1,2} = 4$ Hz, H-1), 4.85 (dd, 1 H, H-2), 3.96 (td, 1 H, $J_{5,6} = 7.3$ Hz, $J_{5,6a} = 2.4$ Hz, H-5), 3.73 (bs, 2 H, SCH₂CH₂NHCS), 3.68 (bs, 2 H, NHCSCH₂CH₂N), 3.41 (s, 3 H, OCH₃), 3.11 (bs, 4 H, CH₂NH₂Cl), 2.84 (bs, 6 H, CH₂CH₂NH₂Cl, SCH₂CH₂NHCS), 2.75 (m, 3 H, H-6a, NHCSCH₂CH₂N), 2.66 (dd, 1 H, $J_{6a,6b} = 13.8$ Hz, H-6b), 2.32–2.19 (m, 6 H, H-2_{H_{ex}}), 1.55 (m, 6 H, H-3_{H_{ex}}), 1.27 (m, 12 H, H-4_{H_{ex}}, H-5_{H_{ex}}), 0.87 (m, 9 H, H-6_{H_{ex}}). ¹³C NMR (75 MHz, CDCl₃): 173.1, 173.0, 172.6 (CO), 96.6 (C-1), 71.2 (C-4), 70.8 (C-2), 69.6 (C-3), 69.1 (C-5), 55.4 (OCH₃), 53.4 (NHCSCH₂CH₂N), 52.0 (CH₂CH₂NH₂HCl), 43.1 (SCH₂CH₂NHCS), 41.7 (NHCSCH₂CH₂N), 37.6 (CH₂NH₂Cl), 34.1, 34.0 (C-2_{H_{ex}}), 33.0 (C-6), 32.7 (SCH₂CH₂NHCS), 31.2, 31.1 (C-4_{H_{ex}}), 24.5, 24.4 (C-3_{H_{ex}}), 22.2 (C-5_{H_{ex}}), 13.8 (C-6_{H_{ex}}). ESI MS: $m/z = 736.4$ [M]⁺. Anal. Calcd for C₃₄H₆₂N₆O₈S₂·3HCl: C, 48.30; H, 8.11; N, 8.28; S, 7.58. Found: C, 48.24; H, 8.39; N, 8.15; S, 7.41.

Methyl 6-(4-(2,2-Bis-tert-butoxycarbonylamino)ethylaminomethyl)-1H-1,2,3-triazol-1-yl-6-deoxy-2,3,4-tri-O-hexanoyl- α -D-glucopyranoside (29). To a solution of 28 (0.20 g, 0.39 mmol) and 3-bis[2-tert-butoxycarbonylamino]ethylpropargylamine (0.29 g, 0.85 mmol) in H₂O–BuOH 9:1 (15 mL), the Cu-supported catalyst Si-BPA–Cu⁺ (0.02g) was added and the reaction mixture was refluxed for 36 h at 85 °C. The catalyst was filtered, and the solvent was removed. The residue was purified by column chromatography (1:1 → 2:1 EtOAc–cyclohexane). Yield 78% (0.25 g, 0.30 mmol). $R_f = 0.61$ (9:1 DCM–MeOH); $[\alpha]_D = +50.5$ (c 1.0, DCM). IR: $\nu_{\max} = 2957, 2359, 1748, 1703, 1734$ cm⁻¹. ¹H NMR (300 MHz, CDCl₃): $\delta = 7.59$ (s, 1 H, =CH), 5.49 (t, 1 H, $J_{2,3} = J_{3,4} = 10.3$ Hz, H-3), 4.89 (bs, 2 H, NHBoc), 4.87 (dd, 1 H, $J_{1,2} = 3.5$ Hz, H-1), 4.85 (t, 1 H, $J_{4,5} = 10.3$ Hz, H-4), 4.81 (dd, 1 H, H-2), 4.53 (dd, 1 H, $J_{6a,6b} = 14.0$ Hz, $J_{5,6a} = 2.6$ Hz, H-6a), 4.29 (dd, 1 H, $J_{5,6b} = 9.0$ Hz, H-6b), 4.17 (ddd, 1 H, H-5), 3.80 (m, 2 H, CH₂-triazole), 3.18 (bs, 4 H, CH₂NHBoc), 3.07 (s, 3 H, OCH₃), 2.55 (t, 4 H, CH₂CH₂NHBoc), 2.27 (m, 6 H, H-2_{H_{ex}}), 1.58 (s, 9 H, CMe₃), 1.44 (m, 6 H, H-3_{H_{ex}}), 1.30 (m, 12 H, H-4_{H_{ex}}, H-5_{H_{ex}}), 0.89 (m, 9 H, H-6_{H_{ex}}). ¹³C NMR (75.5 MHz, CDCl₃): $\delta = 173.9, 173.5, 173.1$ (CO ester), 156.2 (CO carbamate), 144.1 (C-4 triazole), 124.3 (C-5 triazole), 91.4 (C-1), 78.1 (CMe₃), 70.6 (C-2), 69.8 (C-4), 69.3 (C-3), 68.0 (C-5), 53.1 (CH₂CH₂NHBoc), 50.6 (C-6), 48.3 (CH₂ triazole), 38.4 (CH₂NHBoc), 34.1 (C-2_{H_{ex}}), 31.7 (C-4_{H_{ex}}), 28.5 (CMe₃), 24.6 (C-3_{H_{ex}}), 22.6 (C-5_{H_{ex}}), 13.8 (C-6_{H_{ex}}). ESI MS: $m/z = 877.5$ [M + Na]⁺. Anal. Calcd for C₄₆H₇₄N₆O₁₂: C, 59.00; H, 8.72; N, 9.83. Found: C, 59.09; H, 8.77; N, 9.64.

Methyl 6-Deoxy-6-(4-(2,2-diaminoethylaminomethyl)-1H-1,2,3-triazol-1-yl)-2,3,4-tri-O-hexanoyl- α -D-glucopyranoside Dihydrochloride (30). Treatment of 29 (0.42 g, 0.49 mmol) with 1:1 TFA–DCM (5 mL) and freeze-drying from 10:1 H₂O/0.1 N HCl solution afforded 30. Yield quant (0.35 g, 0.49 mmol); $[\alpha]_D = +38.1$ (c 1.0, MeOH). IR: $\nu_{\max} = 2957, 1748, 1675$ cm⁻¹. ¹H NMR (300 MHz, CD₃OD): $\delta = 8.07$ (s, 1 H, =CH), 5.42 (t, 1 H, $J_{2,3} = J_{3,4} = 9.5$ Hz, H-3), 4.93 (dd, 1 H, $J_{1,2} = 3.5$ Hz, H-1), 4.82 (dd, 1 H, H-2), 4.76 (t, 1 H, $J_{4,5} = 9.5$ Hz, H-4), 4.64 (m, 2 H, H-6a, H-6b), 4.27 (ddd, 1 H, $J_{5,6a} = 3.7$ Hz, $J_{5,6b} = 6.0$ Hz, H-5), 3.92 (s, 2 H, CH₂ triazole), 3.26 (s, 3 H, OMe), 3.16 (t, 4 H, $J_{H,H} = 6.4$ Hz, CH₂CH₂NH₂), 2.82 (t, 4 H, CH₂CH₂NH₂), 2.48–2.15 (m, 6 H, H-2_{H_{ex}}), 1.58 (m, 6 H, H-3_{H_{ex}}), 1.33 (m, 12 H, H-4_{H_{ex}}, H-5_{H_{ex}}), 0.92 (m, 9 H, H-6_{H_{ex}}). ¹³C NMR (75.5 MHz, CD₃OD): $\delta = 174.2$ – 173.9 (CO), 143.8 (C-4 triazole), 126.9 (C-5 triazole), 98.6 (C-1), 71.8 (C-2), 70.7 (C-3), 70.3 (C-4), 68.9 (C-5), 56.0 (OCH₃), 52.0 (CH₂CH₂NH₂), 51.6 (C-6), 47.4 (CH₂ triazole), 38.2 (CH₂CH₂NH₂), 34.9, 34.8, 34.7 (C-2_{H_{ex}}), 32.4, 32.2 (C-4_{H_{ex}}), 25.6, 25.5 (C-3_{H_{ex}}), 23.4 (C-5_{H_{ex}}), 14.2 (C-6_{H_{ex}}). ESI MS: $m/z =$

831.3 [M + TFA + Cl + Cu]⁺; 717.3 [M + Cu + Cl]⁺. Anal. Calcd for C₃₂H₆₉N₆O₈·2HCl: C, 52.81; H, 8.31; N, 11.55. Found: C, 52.69; H, 8.1; N, 11.72.

Dendritic Boc-Protected Diminoethyl-bis(thiourea) Glucopyranoside Derivative 31. To a solution of 30 (0.20 g, 0.27 mmol) and Et₃N (115 μ L, 0.82 mmol) in DCM (12 mL), *tert*-butyl *N*-(2-isothiocyanatoethyl)carbamate (0.17 mg, 0.82 mmol) was added and the mixture was stirred overnight at rt. The reaction mixture was washed with aqueous diluted HCl (3 \times 10 mL), and the organic phase was dried (MgSO₄), filtered, and concentrated. The residue was purified by column chromatography (3:1 EtOAc–cyclohexane → 20:1 DCM–MeOH). Yield 52% (0.15 g, 0.14 mmol); $R_f = 0.44$ (9:1 DCM–MeOH); $[\alpha]_D = +31.7$ (c 1.0, DCM). IR: $\nu_{\max} = 2959, 1750, 1698, 736$ cm⁻¹. UV (DCM): 248 nm (ϵ_{\max} 47.8). ¹H NMR (300 MHz, CDCl₃): $\delta = 7.62$ (s, 1 H, =CH), 7.18, 6.94 (bs, 4 H, NHCS), 5.49 (t, 1 H, $J_{2,3} = J_{3,4} = 9.5$ Hz, H-3), 5.38 (bs, 2 H, NHBoc), 4.82 (d, 1 H, $J_{1,2} = 3.5$ Hz, H-1), 4.80 (t, 1 H, $J_{4,5} = 9.5$ Hz, H-4), 4.80 (dd, 1 H, H-2), 4.53 (dd, 1 H, $J_{6a,6b} = 14.5$ Hz, $J_{5,6a} = 2.6$ Hz, H-6a), 4.37 (dd, 1 H, $J_{5,6b} = 8.0$ Hz, H-6b), 4.17 (ddd, 1 H, H-5), 3.79 (s, 2 H, CH₂ triazole), 3.62 (bs, 4 H, CH₂CH₂NHBoc), 3.54 (bs, 4 H, NCH₂CH₂NHCS), 3.31 (m, 4 H, CH₂NHBoc), 3.12 (s, 1 H, OCH₃), 2.69 (bs, 4 H, NCH₂CH₂NHCS), 2.42–2.13 (m, 6 H, H-2_{H_{ex}}), 1.55 (m, 6 H, H-3_{H_{ex}}), 1.42 (s, 18 H, CMe₃), 1.26 (m, 12 H, H-4_{H_{ex}}, H-5_{H_{ex}}), 0.87 (t, 9 H, H-6_{H_{ex}}). ¹³C NMR (75.5 MHz, CDCl₃): $\delta = 182.7$ (CS), 173.0–172.5 (CO ester), 155.5 (CO carbamate), 144.5 (C-4 triazole), 124.4 (C-5 triazole), 96.7 (C-1), 79.8 (CMe₃), 70.2 (C-2), 69.6 (C-4), 69.2 (C-3), 67.8 (C-5), 55.4 (OMe), 52.4 (NCH₂CH₂NHCS), 50.7 (C-6), 48.0 (CH₂ triazole), 44.6 (CH₂CH₂NHBoc), 42.1 (NCH₂CH₂NHCS), 40.1 (CH₂NHBoc), 34.3 (C-2_{H_{ex}}), 30.8 (C-4_{H_{ex}}), 28.1 (CMe₃), 24.2 (C-3_{H_{ex}}), 22.6 (C-5_{H_{ex}}), 14.1 (C-6_{H_{ex}}). ESI MS: $m/z = 1081.5$ [M + Na]⁺. Anal. Calcd for C₄₈H₉₂N₁₀O₁₂S₂: C, 54.42; H, 8.18; N, 13.22; S, 6.05. Found: C, 54.37; H, 7.98; N, 13.28; S, 5.85.

Dendritic Diaminoethyl-bis(thiourea) Glucopyranoside Dihydrochloride Derivative (6). Treatment of 31 (0.12 g, 0.12 mmol) with 1:1 TFA–DCM (2 mL) and freeze-drying from 10:1 H₂O/0.1 N HCl solution afforded 6. Yield 91% (0.10 g, 0.11 mmol); $[\alpha]_D = +47.7$ (c 1.0, MeOH). IR: $\nu_{\max} = 2955, 1748, 1676$ cm⁻¹. UV (MeOH): 244 nm (ϵ_{\max} 29.1). ¹H NMR (300 MHz, CD₃OD): $\delta = 8.43$ (s, 1 H, =CH), 5.43 (t, 1 H, $J_{2,3} = J_{3,4} = 9.7$ Hz, H-3), 4.97 (d, 1 H, $J_{1,2} = 3.5$ Hz, H-1), 4.90 (dd, 1 H, H-2), 4.82 (t, 1 H, $J_{4,5} = 9.7$ Hz, H-4), 4.77 (m, 2 H, CH₂ triazole), 4.70 (m, 2 H, H-6a, H-6b), 4.27 (ddd, 1 H, $J_{5,6a} = 3.7$ Hz, $J_{5,6b} = 5.6$ Hz, H-5), 4.06 (bs, 4 H, CH₂CH₂NH₂), 3.87 (t, 4 H, $J_{H,H} = 5.8$ Hz, NCH₂CH₂NHCS), 3.52 (t, 4 H, $J_{H,H} = 5.8$ Hz, CH₂NH₂), 3.25 (s, 3 H, OCH₃), 3.21 (t, 4 H, $J_{H,H} = 6.0$ Hz, NCH₂CH₂NHCS), 2.50–2.15 (m, 6 H, H-2_{H_{ex}}), 1.56 (m, 6 H, H-3_{H_{ex}}), 1.31 (m, 12 H, H-4_{H_{ex}}, H-5_{H_{ex}}), 0.91 (m, 9 H, H-6_{H_{ex}}). ¹³C NMR (75.5 MHz, CD₃OD): $\delta = 184.1$ (CS), 174.3–173.9 (CO), 137.2 (C-4 triazole), 130.1 (C-5 triazole), 98.2 (C-1), 71.8 (C-2), 71.2 (C-3), 70.5 (C-4), 68.7 (C-5), 56.2 (OMe), 54.4 (CH₂NH₂), 51.4 (C-6), 48.4 (CH₂ triazole), 42.2 (CH₂CH₂NH₂), 40.4 (NCH₂CH₂NHCS), 40.0 (CH₂NH₂), 34.4 (C-2_{H_{ex}}), 32.0 (C-4_{H_{ex}}), 25.2 (C-3_{H_{ex}}), 22.8 (C-5_{H_{ex}}), 14.0 (C-6_{H_{ex}}). ESI MS: $m/z = 859.5$ [M + Na]⁺; 921.4 [M + Cu]⁺. Anal. Calcd for C₃₈H₇₂Cl₂N₁₀O₈S₂: C, 48.97; H, 7.79; N, 15.03; S, 6.88. Found: C, 48.71; H, 77.40; N, 15.23; S, 6.65.

2,3,4,2',3',4'-Hexa-O-hexyl-6,6'-di-O-trityl- α , α' -trehalose (33). To a solution of 32 (1.00 g, 1.21 mmol) in dry DMF (11 mL), NaH (871 mg, 21.78 mmol) was added and the mixture was stirred at 0 °C for 10 min. 1-Bromohexane (3.06 mL, 21.78 mmol) was added dropwise under Ar atmosphere, and the mixture was stirred overnight at rt. The reaction was quenched with MeOH (5 mL) and stirred for 10 min. The solvents were removed, and the resulting residue was suspended in DCM (50 mL) and washed with H₂O (3 \times 15 mL), and the organic layer was separated, dried (MgSO₄), filtered, concentrated, and purified by column chromatography (1:8 → 1:6 EtOAc–cyclohexane). Yield 92% (1.50 g, 1.11 mmol); $R_f = 0.74$ (1:5 EtOAc–cyclohexane); $[\alpha]_D = +70.3$ (c 1.0, DCM). IR: $\nu_{\max} = 2923, 2855$ cm⁻¹. ¹H NMR (300 MHz, CDCl₃): $\delta = 7.53$ – 7.23 (m, 30 H, Ph), 5.34 (d, 2 H, $J_{1,2} = 3.7$ Hz, H-1), 4.03 (bd, 2 H, $J_{4,5} = 9.3$ Hz, H-5), 3.80 (m, 2 H, OCH₂),

3.78–3.41 (m, 8 H, OCH₂), 3.57 (t, 2 H, J_{2,3} = J_{3,4} = 9.3 Hz, H-3), 3.51–3.41 (m, 4 H, H-4, H-6a), 3.39 (dd, 2 H, H-2), 3.24 (m, 2 H, OCH₂), 3.13 (dd, 2 H, J_{6a,6b} = 10.0 Hz, J_{5,6b} = 3.3 Hz, H-6b), 1.65–1.56 (m, 12 H, CH₂), 1.38–1.0489 (m, 36 H, CH₂), 0.93–0.82 (m, 18 H, CH₂). ¹³C NMR (75.5 MHz, CDCl₃): δ = 144.0, 128.8, 127.6, 126.8 (Ph), 93.6 (C-1), 86.1 (Ph₃C), 81.5 (C-3), 80.6 (C-2), 78.1 (C-4), 73.7, 73.0, 71.3 (OCH₂), 70.0 (C-5), 62.0 (C-6), 31.8–22.5 (CH₂), 14.1 (CH₃). ESI MS: m/z = 1353.8 [M + Na]⁺. Anal. Calcd for C₈₆H₁₂₂O₁₁: C, 77.55; H, 9.23. Found: C, 77.67; H, 9.31.

2,3,4,2',3',4'-Hexa-O-tetradecyl-6,6'-di-O-trityl-α,α'-trehalose (34). To a solution of **32** (1.00 g, 1.21 mmol) in dry DMF (11 mL), NaH (0.87 g, 21.78 mmol) was added and the mixture was stirred at 0 °C for 10 min. 1-Bromotetradecane (6.68 mL, 21.78 mmol) was added dropwise, under Ar atmosphere, and the mixture was stirred overnight at 60 °C. The reaction was quenched with MeOH (5 mL) and stirred for 10 min. Solvents were removed, and the resulting residue was suspended in DCM (50 mL). The suspension was washed with H₂O (3 × 15 mL), and the organic layer was dried (MgSO₄), filtered, concentrated, and purified by column chromatography (1:50 → 1:30 EtOAc–cyclohexane). Yield 77% (1.50 g, 0.93 mmol); R_f = 0.77 (1:15 EtOAc–cyclohexane); [α]_D = +50.2 (c 1.0, DCM). ¹H NMR (300 MHz, CDCl₃): δ = 7.52–7.22 (m, 30 H, Ph), 5.33 (d, 2 H, J_{1,2} = 3.6 Hz, H-1), 4.03 (bd, 2 H, J_{4,5} = 9.4 Hz, H-5), 3.79 (m, 2 H, OCH₂), 3.71–3.52 (m, 8 H, OCH₂), 3.55 (t, 2 H, J_{2,3} = J_{3,4} = 9.4 Hz, H-3), 3.44 (t, 2 H, H-4), 3.46–3.35 (m, 6 H, OCH₂, H-6a, H-2), 3.22 (m, 2 H, OCH₂), 3.12 (dd, 2 H, J_{6a,6b} = 10.0 Hz, J_{5,6b} = 3.1 Hz, H-6b), 1.76–1.56 (m, 12 H, CH₂), 1.28 (m, 132 H, CH₂), 0.91 (t, 18 H, ³J_{H,H} = 6.3 Hz, CH₃). ¹³C NMR (75.5 MHz, CDCl₃): δ = 144.1, 128.8, 127.6, 126.8 (Ph), 93.7, 73.0, 71.3 (OCH₂), 70.5 (C-5), 62.1 (C-6), 31.9–22.7 (CH₂), 14.1 (CH₃). ESI MS: m/z = 2027.4 [M + Na]⁺. Anal. Calcd for C₁₃₄H₂₁₀O₁₁: C, 80.26; H, 10.96. Found: C, 80.35; H, 11.05.

2,3,4,2',3',4'-Hexa-O-hexyl-α,α'-trehalose (35). To a solution of **33** (0.68 g, 0.52 mmol) in 1:1 DCM–MeOH (25 mL), *p*-toluenesulfonic acid monohydrate (0.08 g, 0.42 mmol) was added and the solution was stirred at rt for 4 h. The mixture was diluted with DCM, washed with saturated aqueous NaHCO₃, dried (MgSO₄), filtered, and concentrated. The resulting residue was purified by column chromatography (1:8 → 1:2 EtOAc–cyclohexane). Yield 48% (0.21 g, 0.24 mmol); R_f = 0.25 (1:2 EtOAc–cyclohexane); [α]_D = +103.0 (c 1.0, DCM). ¹H NMR (300 MHz, CDCl₃): δ = 5.06 (d, 2 H, J_{1,2} = 3.7 Hz, H-1), 3.90 (dt, 2 H, J_{4,5} = 9.2 Hz, J_{5,6a} = J_{5,6b} = 2.9 Hz, H-5), 3.79 (m, 4 H, OCH₂), 3.73–3.63 (m, 8 H, H-6a, H-6b, OCH₂), 3.60–3.43 (m, 4 H, OCH₂), 3.57 (t, 2 H, J_{2,3} = J_{3,4} = 9.2 Hz, H-3), 3.23 (t, 2 H, H-4), 3.18 (dd, 2 H, H-2), 2.03 (bs, 2 H, OH), 1.60–1.47 (m, 12 H, CH₂), 1.37–1.27 (m, 36 H, CH₂), 0.87 (m, 18 H, CH₃). ¹³C NMR (75.5 MHz, CDCl₃): δ = 93.6 (C-1), 81.0 (C-3), 80.4 (C-2), 77.9 (C-4), 73.6, 73.3, 71.5 (OCH₂), 71.4 (C-5), 61.8 (C-6), 31.8–22.6 (CH₂), 14.0 (CH₃). ESI MS: m/z = 869.7 [M + Na]⁺, 885.7 [M + K]⁺. Anal. Calcd for C₄₈H₈₆O₁₁: C, 68.05; H, 11.18. Found: C, 67.89; H, 11.04.

2,3,4,2',3',4'-Hexa-O-tetradecyl-α,α'-trehalose (36). To a solution of **34** (1.49 g, 0.74 mmol) in 1:1 DCM–MeOH (36 mL), *p*-toluenesulfonic acid monohydrate (0.11 g, 0.50 mmol) was added and the solution was stirred at rt for 4 h. The mixture was diluted with DCM, washed with saturated aqueous NaHCO₃, dried (MgSO₄), filtered, and concentrated. Purification by column chromatography (1:9 → 1:5 EtOAc–cyclohexane) of the residue afforded **37**. Yield 47% (0.53 g, 0.34 mmol); R_f = 0.20 (1:5 EtOAc–cyclohexane); [α]_D = +58.4 (c 1.0, DCM). ¹H NMR (300 MHz, CDCl₃): δ = 5.06 (d, 2 H, J_{1,2} = 3.7 Hz, H-1), 3.90 (dt, 2 H, J_{4,5} = 9.2 Hz, J_{5,6a} = J_{5,6b} = 2.6 Hz, H-5), 3.84–3.64 (m, 4 H, OCH₂), 3.73–3.63 (m, 12 H, H-6a, H-6b, OCH₂), 3.58 (t, 2 H, J_{2,3} = J_{3,4} = 9.2 Hz, H-3), 3.24 (t, 2 H, H-4), 3.19 (dd, 2 H, H-2), 1.86 (bs, 2 H, OH), 1.61–1.49 (m, 12 H, CH₂), 1.26 (bs, 132 H, CH₂), 0.88 (t, 18 H, ³J_{H,H} = 6.9 Hz, CH₃). ¹³C NMR (75.5 MHz, CDCl₃): δ = 93.7 (C-1), 81.1 (C-3), 80.5 (C-2), 78.0 (C-4), 73.6, 73.3, 71.6 (OCH₂), 71.1 (C-5), 61.9 (C-6), 31.9–22.7 (CH₂), 14.1 (CH₃). ESI MS: m/z = 1543.2 [M + Na]⁺. Anal. Calcd for C₉₆H₁₉₈O₁₁: C, 75.83; H, 12.59. Found: C, 75.70; H, 12.41.

6,6'-Dideoxy-2,3,4,2',3',4'-hexa-O-hexyl-6,6'-diiodo-α,α'-trehalose (37). To a solution of **35** (0.10 g, 0.12 mmol) in toluene (5 mL),

triphenylphosphine (0.11 g, 0.43 mmol) and imidazole (0.05 g, 0.81 mmol) were added and the mixture was stirred at rt until complete dissolution. Iodine (0.11 g, 0.40 mmol) was added in portions, and the solution was vigorously stirred at 70 °C for 5 h. Satd aq NaHCO₃ solution (10 mL) was added, and the mixture was stirred for 5 min. Additional iodine was then added until the aqueous solution turned to a slightly brown color, then aqueous 10% Na₂S₂O₃ was added until complete decoloration of both organic and aqueous layer. The organic layer was then separated, dried (MgSO₄), filtered, concentrated, and purified by column chromatography (1:15 EtOAc–cyclohexane). Yield 94% (0.12 g, 0.12 mmol); R_f = 0.75 (1:8 EtOAc–cyclohexane); [α]_D = +50.1 (c 1.0, DCM). ¹H NMR (300 MHz, CDCl₃): δ = 5.17 (d, 2 H, J_{1,2} = 3.3 Hz, H-1), 3.83 (m, 4 H, OCH₂), 3.72–3.47 (m, 12 H, H-5, H-3, OCH₂), 3.39 (m, 4 H, H-6a, H-6b), 3.24 (dd, 2 H, H-2, H-4), 3.05 (t, 2 H, J_{3,4} = J_{4,5} = 9.1 Hz, H-4), 1.62–1.49 (m, 12 H, CH₂), 1.30 (m, 36 H, CH₂), 0.89 (m, 18 H, CH₃). ¹³C NMR (75.5 MHz, CDCl₃): δ = 92.9 (C-1), 81.9 (C-4), 80.8 (C-3), 80.2 (C-2), 73.5, 73.4, 71.9 (OCH₂), 69.1 (C-5), 31.8–22.6 (CH₂), 14.0 (CH₃), 8.7 (C-6). ESI MS: m/z = 1089.6 [M + Na]⁺. Anal. Calcd for C₄₆H₈₂I₂O₅: C, 54.03; H, 8.69. Found: C, 53.88; H, 8.77.

6,6'-Dideoxy-2,3,4,2',3',4'-hexa-O-tetradecyl-6,6'-diiodo-α,α'-trehalose (38). To a solution of **36** (0.44 g, 0.29 mmol) in toluene (13 mL), triphenylphosphine (0.27 g, 1.02 mmol) and imidazole (0.07 g, 1.89 mmol) were added and the mixture was stirred at rt until complete dissolution. Iodine (0.26 g, 0.93 mmol) was added in portions, and the solution was vigorously stirred at 70 °C for 5 h. Satd NaHCO₃ solution (20 mL) was added, and the mixture was stirred for 5 min. Additional iodine was then added until the aqueous solution got slightly brown, and then an aqueous 10% Na₂S₂O₃ solution was added until complete decoloration of both the organic and aqueous layers. The organic layer was then separated, dried (MgSO₄), filtered, concentrated, and purified by column chromatography (1:25 EtOAc–cyclohexane). Yield 96% (0.52 g, 0.28 mmol); R_f = 0.69 (1:20 EtOAc–cyclohexane); [α]_D = +47.2 (c 1.0, DCM). ¹H NMR (300 MHz, CDCl₃): δ = 5.17 (d, 2 H, J_{1,2} = 3.5 Hz, H-1), 3.83 (m, 4 H, OCH₂), 3.70–3.48 (m, 12 H, H-5, H-3, OCH₂), 3.42 (dd, 2 H, J_{6a,6b} = 10.7 Hz, J_{5,6a} = 2.9 Hz, H-6a), 3.36 (dd, 2 H, J_{6a,6b} = 5.2 Hz, H-6b), 3.24 (dd, 2 H, H-2, H-4), 3.23 (t, 2 H, J_{3,4} = J_{4,5} = 9.4 Hz, H-4), 1.59–1.51 (m, 12 H, CH₂), 1.26 (bs, 132 H, CH₂), 0.88 (t, 18 H, ³J_{H,H} = 6.9 Hz, CH₃). ¹³C NMR (75.5 MHz, CDCl₃): δ = 92.9 (C-1), 81.9 (C-4), 80.8 (C-3), 80.3 (C-2), 73.6, 73.5, 71.9 (OCH₂), 69.1 (C-5), 31.9–22.7 (CH₂), 14.1 (CH₃), 8.7 (C-6). ESI MS: m/z = 1763.0 [M + Na]⁺. Anal. Calcd for C₉₆H₁₈₈I₂O₅: C, 66.25; H, 10.89. Found: C, 66.09; H, 10.74.

6,6'-Di-(2-tert-butoxycarbonylaminoethylthio)-2,3,4,2',3',4'-hexa-O-hexyl-α,α'-trehalose (39). To a solution of **37** (0.11 g, 0.10 mmol) in dry DMF (12 mL), Cs₂CO₃ (0.09 g, 0.29 mmol) and *tert*-butyl *N*-(2-mercaptoethyl)carbamate (49 μL, 0.29 mmol) were added, under Ar atmosphere, and the reaction mixture was stirred at 60 °C for 24 h. The reaction mixture was concentrated, and the crude product was dissolved in DCM (20 mL) and washed with H₂O (2 × 30 mL). The organic phase was dried (MgSO₄), filtered, concentrated, and purified by column chromatography (1:8 → 1:6 EtOAc–cyclohexane). Yield 85% (0.10 g, 0.08 mmol); R_f = 0.26 (1:5 EtOAc–cyclohexane); [α]_D = +86.4 (c 1.0, DCM). IR: ν_{max} = 3350, 2928, 2855, 1710 cm⁻¹. ¹H NMR (300 MHz, CDCl₃): δ = 5.12 (d, 2 H, J_{1,2} = 3.3 Hz, H-1), 4.99 (bs, 2 H, NH(Boc)), 4.01 (ddd, 2 H, J_{4,5} = 9.2 Hz, J_{5,6a} = 6.3 Hz, J_{5,6b} = 2.7 Hz, H-5), 3.81 (m, 6 H, H-3, OCH₂), 3.70–3.46 (m, 8 H, OCH₂), 3.58 (t, 2 H, J_{2,3} = J_{3,4} = 9.2 Hz, H-3), 3.29 (q, 2 H, ³J_{H,H} = ³J_{H,NH} = 6.0 Hz, CH₂N), 3.23 (dd, 2 H, H-2), 3.16 (t, 2 H, H-4), 2.82 (dd, 1 H, J_{6a,6b} = 13.5 Hz, H-6a), 2.72 (dd, 2 H, H-6b), 2.69 (t, 4 H, CH₂S), 1.60–1.47 (m, 12 H, CH₂), 1.43 (s, 18 H, C(CH₃)₃), 1.34–1.28 (m, 36 H, CH₂), 0.89 (m, 18 H, CH₃). ¹³C NMR (75.5 MHz, CDCl₃): δ = 155.7 (CO), 92.3 (C-1), 81.0 (C-3), 80.5 (C-2), 80.4 (C-4), 79.2 (CMe₃), 73.4, 73.2, 71.7 (OCH₂), 71.2 (C-5), 39.8 (CH₂S), 33.8 (C-6), 33.7 (CH₂N), 31.8–30.2 (CH₂), 28.4 (CMe₃), 25.9, 25.8, 22.6 (CH₂), 14.0 (CH₃). ESI MS: m/z = 1187.9 [M + Na]⁺, 1203.8 [M + K]⁺. Anal. Calcd for C₆₂H₁₂₆N₂O₁₅S₂: C, 63.88; H, 10.38; N, 2.40. Found: C, 63.69; H, 10.21; N, 5.19.

6,6'-Di-(2-tert-butoxycarbonylaminoethylthio)-2,3,4,2',3',4'-hexa-O-tetradecyl- α,α' -trehalose (40). To a solution of **38** (0.28 g, 0.13 mmol) in dry DMF (15 mL), Cs₂CO₃ (0.12 g, 0.36 mmol) and *tert*-butyl *N*-(2-mercaptoethyl)carbamate (61 μ L, 0.36 mmol) were added, under Ar atmosphere, and the reaction mixture was stirred at 60 °C for 24 h. The solvent was evaporated, and the crude product was dissolved in DCM (20 mL) and washed with H₂O (2 \times 30 mL). The organic phase was separated, dried (MgSO₄), filtered, concentrated, and purified by column chromatography (1:8 EtOAc–cyclohexane). Yield 99% (0.24 g, 0.13 mmol); *R*_f = 0.53 (1:5 EtOAc–cyclohexane); $[\alpha]_D^{25}$ = +49.3 (c 1.0, DCM). ¹H NMR (300 MHz, CDCl₃): δ = 5.12 (d, 2 H, *J*_{1,2} = 3.4 Hz, H-1), 4.99 (bs, 2 H, NHBoc), 4.01 (ddd, 2 H, *J*_{4,5} = 9.6 Hz, *J*_{5,6a} = 2.6 Hz, *J*_{5,6b} = 6.1 Hz, H-5), 3.81 (m, 4 H, OCH₂), 3.69–3.46 (m, 8 H, OCH₂), 3.58 (t, 2 H, *J*_{3,4} = *J*_{3',4'} = 9.6 Hz, H-3), 3.30 (bq, 2 H, ³*J*_{H,H} = ³*J*_{H,NH} = 6.0 Hz, CH₂N), 3.23 (dd, 2 H, H-2), 3.17 (t, 2 H, H-4), 2.83 (dd, 2 H, *J*_{6a,6b} = 13.7 Hz, H-6a), 2.72 (dd, 2 H, H-6b), 2.69 (t, 4 H, CH₂S), 1.60–1.51 (m, 12 H, CH₂), 1.44 (s, 18 H, CMe₃), 1.26 (bs, 132 H, CH₂), 0.88 (t, 18 H, ³*J*_{H,H} = 6.9 Hz, CH₃). ¹³C NMR (75.5 MHz, CDCl₃): δ = 155.7 (CO), 92.3 (C-1), 81.0 (C-3), 80.5 (C-2), 80.4 (C-4), 79.3 (CMe₃), 73.5, 73.2, 71.6 (OCH₂), 71.2 (C-5), 39.8 (CH₂S), 33.8 (C-6), 33.7 (CH₂N), 31.9, 30.7, 30.5, 30.3 (CH₂), 29.7 (CMe₃), 29.4–22.7 (CH₂), 14.1 (CH₃). ESI MS: *m/z* = 1861.5 [M + Na]⁺. Anal. Calcd for C₁₁₈H₂₁₆N₂O₁₅S₂: C, 71.84; H, 11.84; N, 1.52; S, 3.49. Found: C, 71.90; H, 11.72; N, 1.44; S, 3.38.

6,6'-Di-(2-aminoethylthio)-2,3,4,2',3',4'-hexa-O-hexyl- α,α' -trehalose Dihydrochloride (7). Treatment of **39** (0.10 g, 0.09 mmol) with 1:1 TFA–DCM (2 mL) and freeze-drying from 10:1 H₂O/0.1 N HCl solution afforded **7**. Yield quant (0.09 g, 0.09 mmol); *R*_f = 0.72 (10:1:1 CH₂Cl–H₂O–NH₄OH); $[\alpha]_D^{25}$ = +90.3 (c 1.0, DCM). IR: ν_{\max} = 3300, 2928, 2859, 1099 cm⁻¹. ¹H NMR (300 MHz, CDCl₃): δ = 8.13 (bs, 6 H, NH₃⁺), 5.20 (d, 2 H, *J*_{1,2} = 3.2 Hz, H-1), 3.98 (dt, 2 H, *J*_{4,5} = 9.5 Hz, *J*_{5,6a} = *J*_{5,6b} = 4.3 Hz, H-5), 3.79 (m, 4 H, OCH₂), 3.69–3.43 (m, 8 H, OCH₂), 3.56 (t, 2 H, *J*_{2,3} = *J*_{3,4} = 9.5 Hz, H-3), 3.25 (dd, 2 H, H-2), 3.18 (bs, 4 H, CH₂N), 3.11 (t, 2 H, H-4), 2.97 (bd, 2 H, *J*_{6a,6b} = 14.0 Hz, H-6a), 2.82 (m, 6 H, CH₂S, H-6b), 1.59–1.50 (m, 12 H, CH₂), 1.28 (m, 36 H, CH₂), 0.88 (m, 18 H, CH₃). ¹³C NMR (75.5 MHz, CDCl₃): δ = 91.9 (C-1), 80.9 (C-3), 80.2 (C-2), 80.0 (C-4), 73.5, 73.4, 71.8 (OCH₂), 71.0 (C-5), 39.4 (CH₂N), 34.4 (C-6), 31.8 (CH₂S), 31.7, 30.6, 30.4, 30.2, 25.9, 25.8, 22.6, 22.5 (CH₂), 14.0 (CH₃). ESI MS: *m/z* = 965.9 [M – 2Cl]⁺. Anal. Calcd for C₆₂H₁₀₆N₂O₈S₂·2HCl: C, 60.14; H, 10.29; N, 2.70; S, 6.17. Found: C, 59.86; H, 10.02; N, 2.41; S, 5.88.

6,6'-Di-(2-aminoethylthio)-2,3,4,2',3',4'-hexa-O-tetradecyl- α,α' -trehalose Dihydrochloride (8). Treatment of **40** (0.09 mg, 0.05 mmol) with 1:1 TFA–DCM (1 mL) and freeze-drying from 10:1 H₂O/0.1 N HCl solution afforded **8**. Yield quant (0.09 g, 0.05 mmol); *R*_f = 0.21 (EtOAc); $[\alpha]_D^{25}$ = +61.2 (c 1.0, DCM). ¹H NMR (300 MHz, CDCl₃): δ = 6.39 (bs, 6 H, NH₃⁺), 5.21 (d, 2 H, *J*_{1,2} = 3.5 Hz, H-1), 3.97 (dt, 2 H, *J*_{4,5} = 9.6 Hz, *J*_{5,6a} = *J*_{5,6b} = 4.7 Hz, H-5), 3.79 (m, 4 H, OCH₂), 3.69–3.43 (m, 8 H, OCH₂), 3.56 (t, 2 H, *J*_{2,3} = *J*_{3,4} = 9.6 Hz, H-3), 3.25 (dd, 2 H, H-2), 3.18 (t, 4 H, ³*J*_{H,H} = 6.3 Hz, CH₂N), 3.11 (t, 2 H, H-4), 3.07–2.94 (m, 4 H, H-6a, H-6b), 2.82 (m, 4 H, CH₂S), 1.58–1.49 (m, 12 H, CH₂), 1.26 (bs, 132 H, CH₂), 0.88 (m, 18 H, ³*J*_{H,H} = 7.0 Hz, CH₃). ¹³C NMR (75.5 MHz, CDCl₃): δ = 91.9 (C-1), 80.9 (C-3), 80.2 (C-2), 80.0 (C-4), 73.5, 73.4, 71.8 (OCH₂), 71.0 (C-5), 39.5 (CH₂N), 34.6 (C-6), 31.9 (CH₂S), 31.9–22.7 (CH₂), 14.1 (CH₃). ESI MS: *m/z* = 1639.4 [M – 2Cl]⁺. Anal. Calcd for C₁₀₀H₂₀₀N₂O₈S₂·2HCl: C, 70.17; H, 11.90; N, 1.64; S, 3.75. Found: C, 69.82; H, 11.77; N, 1.39; S, 3.41.

6,6'-Dideoxy-2,3,4,2',3',4'-hexa-O-hexanoyl-6,6'-diiodo- α,α' -trehalose (42). To a solution of 6,6'-dideoxy-6,6'-diiodo-trehalose **41** (5.78 g, 10.30 mmol) and DMAP (6.37 g, 52.20 mmol) in dry DMF (80 mL), hexanoic anhydride (16 mL, 69.60 mmol) was added dropwise, under Ar atmosphere at 0 °C, and the reaction mixture was stirred at rt for 6 h. Then MeOH (60 mL) was added, and the mixture was stirred at rt for 2 h. The solution was poured into H₂O–ice mixture (100 mL) and extracted with DCM (50 mL). The organic phase was then washed with 2N H₂SO₄ (2 \times 50 mL), H₂O (2 \times 50 mL), and saturated aqueous NaHCO₃ (2 \times 50 mL), dried (MgSO₄,

filtered, concentrated, and purified by column chromatography (1:12 EtOAc–petroleum ether). Yield 76% (1.20 g, 7.82 mmol); *R*_f = 0.35 (1:6 EtOAc–petroleum ether). ¹H NMR (300 MHz, CDCl₃): δ = 5.44 (t, 2 H, *J*_{1,2} = *J*_{3,4} = 9.5 Hz, H-3), 5.35 (d, 2 H, *J*_{1,2} = 3.7 Hz, H-1), 5.1 (dd, 2 H, H-2), 4.84 (t, 2 H, *J*_{4,5} = 9.5 Hz, H-4), 3.82 (ddd, 2 H, *J*_{5,6a} = 2.5 Hz, H-5), 3.11 (dd, 2 H, *J*_{6a,6b} = 11.0 Hz, H-6a), 2.97 (dd, 2 H, H-6b), 2.22 (m, 12 H, H-2_{H_{ex}}), 1.58 (m, 12 H, H-3_{H_{ex}}), 1.17 (m, 24 H, H-4_{H_{ex}}, H-5_{H_{ex}}), 0.84 (m, 18 H, H-6_{H_{ex}}). ¹³C NMR (75.5 MHz, CDCl₃): δ = 172.6, 172.5, 172.4 (CO), 91.5 (C-1), 72.0 (C-4), 70.0 (C-5), 69.3 (C-3), 69.2 (C-2), 34 (C-2_{H_{ex}}), 31.2 (C-4_{H_{ex}}), 24.4 (C-3_{H_{ex}}), 22.2 (C-5_{H_{ex}}), 14.1 (C-6_{H_{ex}}), 2.6 (C-6_{H_{ex}}). ESI MS: *m/z* = 1173.4 [M + Na]⁺. Anal. Calcd for C₄₇H₇₈I₂O₅: C, 49.65; H, 6.92. Found: C, 50.12; H, 7.01.

2,3,4,2',3',4'-Hexa-O-hexanoyl-6,6'-bis(2-tert-butoxycarbonylaminoethylthio)- α,α' -trehalose (43). To a solution of **42** (0.19 g, 0.17 mmol) in dry DMF (1.5 mL), Cs₂CO₃ (0.15 g, 0.47 mmol) and *tert*-butyl *N*-(2-mercaptoethyl)carbamate (80 μ L, 0.47 mmol) were added, under Ar atmosphere, and the reaction mixture was stirred at 60 °C for 24 h. The reaction mixture was concentrated, and the crude product was dissolved in DCM (10 mL) and washed with water (2 \times 20 mL). The organic phase was dried (MgSO₄), filtered, and concentrated. The residue was purified by column chromatography (1:3 EtOAc–cyclohexane). Yield 58% (0.12 mg, 0.10 mmol); *R*_f = 0.52 (1:2 EtOAc–cyclohexane); $[\alpha]_D^{25}$ = +84.5 (c 1.0, DCM). IR: ν_{\max} = 2959, 1749, 1709 cm⁻¹. ¹H NMR (300 MHz, CDCl₃): δ = 5.43 (t, 2 H, *J*_{1,2} = *J*_{3,4} = 9.5 Hz, H-3), 5.25 (d, 1 H, *J*_{1,2} = 4.1 Hz, H-1), 5.00 (dd, 1 H, H-2), 4.94 (t, 2 H, H-4), 3.88 (m, 2 H, H-5), 3.2 (s, 4 H, CH₂N), 2.61 (m, 4 H, CH₂S), 2.52 (m, 4 H, H-6a, H-6b), 2.23 (m, 12 H, H-2_{H_{ex}}), 1.50 (m, 6 H, H-3_{H_{ex}}), 1.41 (s, 18 H, CMe₃), 1.23 (m, 24 H, H-4_{H_{ex}}, H-5_{H_{ex}}), 0.83 (t, 18 H, H-6_{H_{ex}}). ¹³C NMR (75.5 MHz, CDCl₃): δ = 172.6, 172.5, 172.4 (C-1_{H_{ex}}), 155.7 (CO carbamate), 91.4 (C-1), 71.2 (C-4), 71.1 (C-5), 69.6 (C-2, C-3), 39.7 (CH₂N), 34.1, 34.0 (C-2_{H_{ex}}), 33.8 (CH₂S), 24.4 (C-3_{H_{ex}}), 28.4 (CMe₃), 22.3 (C-4_{H_{ex}}, C-5_{H_{ex}}), 13.8 (C-6_{H_{ex}}). ESI MS: *m/z* = 1271.8 [M + Na]⁺. Anal. Calcd for C₆₂H₁₀₆N₂O₁₉S₂: C, 59.59; H, 8.71; N, 2.24; S, 5.13. Found: C, 59.67; H, 8.69; N, 2.32; S, 4.89.

2,3,4,2',3',4'-Hexa-O-hexanoyl-6,6'-bis(2-tert-aminoethylthio)- α,α' -trehalose dihydrochloride (9). Treatment of **43** (0.07 g, 0.04 mmol) with 1:1 TFA–DCM (2 mL) and freeze-drying from 10:1 H₂O/0.1 N HCl solution afforded **9**. Yield quant (0.07 g, 0.04 mmol); $[\alpha]_D^{25}$ = +66.7 (c 0.9, EtOAc). IR: ν_{\max} = 2957, 1740, 1686 cm⁻¹. ¹H NMR (300 MHz, DMSO-*d*₆): δ = 5.35 (t, *J*_{1,2} = 9.7 Hz, 2 H, H-3), 5.29 (d, 2 H, *J*_{1,2} = 4.0 Hz, H-1), 5.08 (m, 2 H, H-2, H-3), 3.95 (m, 2 H, H-5), 2.95 (bs, 4 H, CH₂N), 2.69 (t, 4 H, *J*_{H,H} = 7.0 Hz, CH₂S), 2.67 (bd, 4 H, H-6a, H-6b), 2.27 (m, 12 H, H-2_{H_{ex}}), 1.49 (m, 12 H, H-3_{H_{ex}}), 1.24 (m, 24 H, H-4_{H_{ex}}, H-5_{H_{ex}}), 0.85 (t, 18 H, H-6_{H_{ex}}). ¹³C NMR (75.5 MHz, DMSO-*d*₆): δ = 171.8, 171.7 (CO), 90.9 (C-1), 70.9 (C-5), 70.0, 69.2, (C-2, C-4), 69.4 (C-3), 39.2 (CH₂N), 31.5 (C-6), 33.9 (C-2_{H_{ex}}), 30.3 (CH₂S), 23.9 (C-3_{H_{ex}}), 30.6 (C-4_{H_{ex}}), 21.8 (C-5_{H_{ex}}), 13.3 (C-6_{H_{ex}}). ESI MS: *m/z* = 1049.6 [M]⁺. Anal. Calcd for C₄₅H₈₄Cl₂N₂O₈S₂: C, 55.65; H, 8.44; N, 2.50; S, 5.71. Found: C, 55.29; H, 8.18; N, 2.14; S, 5.33.

6,6'-Diazido-6,6'-dideoxy-2,3,4,2',3',4'-hexa-O-hexanoyl- α,α' -trehalose (45). To a solution of **42** (1.58 g, 1.37 mmol) in dry DMF (8 mL), NaN₃ (0.25 g, 3.60 mmol) was added. The reaction mixture was stirred overnight at 40 °C under Ar atmosphere. The mixture was poured into H₂O–ice mixture (20 mL), and the product was extracted with DCM (4 \times 20 mL). The organic phase was dried (MgSO₄), filtered, and concentrated. The residue was purified by column chromatography (1:12 EtOAc–cyclohexane) to afford **45**. Yield 72% (0.91 g, 0.98 mmol); *R*_f = 0.53 (1:6 EtOAc–cyclohexane); $[\alpha]_D^{25}$ = +108.7 (c 1.0, DCM). IR: ν_{\max} = 2958, 2104, 1750, 735 cm⁻¹. ¹H NMR (300 MHz, CD₃OD): δ = 5.52 (t, 2 H, *J*_{1,2} = *J*_{3,4} = 9.8 Hz, H-3), 5.41 (d, 2 H, *J*_{1,2} = 4.0 Hz, H-1), 5.13 (dd, 2 H, H-2), 5.09 (t, 2 H, *J*_{4,5} = 9.8 Hz, H-4), 4.08 (ddd, 2 H, *J*_{5,6a} = 7.0 Hz, *J*_{5,6b} = 2.6 Hz, H-5), 3.44 (dd, 2 H, *J*_{6a,6b} = 13.0 Hz, H-6a), 2.97 (dd, 2 H, H-6b), 2.33 (m, 12 H, H-2_{H_{ex}}), 1.58 (m, 12 H, H-3_{H_{ex}}), 1.33 (m, 24 H, H-4_{H_{ex}}, H-5_{H_{ex}}), 0.91 (m, 18 H, H-6_{H_{ex}}). ¹³C NMR (75.5 MHz, CD₃OD): δ = 175.2–174.2 (CO), 93.7 (C-1), 71.5 (C-3), 71.3 (C-2), 71.6 (C-5), 71 (C-4), 52.2 (C-6), 34.9 (C-2_{H_{ex}}), 33.2 (C-4_{H_{ex}}), 25.8 (C-3_{H_{ex}}), 23.6 (C-5_{H_{ex}}), 14.8

(C-6_{H₁₀}). ESI MS: *m/z* = 1003.5 [M + Na]⁺. Anal. Calcd for C₂₅H₃₂N₆O₁₅: C, 58.76; H, 8.22; N, 8.57. Found: C, 58.84; H, 8.32; N, 8.60.

6,6'-Di-(4-tert-butoxycarbonylaminoethyl-1H-1,2,3-triazol-1-yl)-6,6'-dideoxy-2,3,4,2',3',4'-hexa-O-hexanoyl- α,α' -trehalose (46). To a solution of 44 (0.25 g, 0.25 mmol) and 45 (0.08 g, 0.56 mmol) in H₂O-BuOH 9:1 (15 mL), the Cu-supported catalyst Si-BPA-Cu⁺ (0.02 g) was added and the reaction mixture was refluxed for 36 h at 85 °C. The catalyst was filtered, and the solvent was concentrated. The residue was purified by column chromatography (1:1 → 2:1 EtOAc-cyclohexane). Yield quant (0.33 g, 0.25 mmol); *R*_f = 0.73 (2:1 EtOAc-cyclohexane); [α]_D = +56.7 (c 1.0, DCM). IR: ν_{max} = 2957, 1752, 1714, 735 cm⁻¹. ¹H NMR (300 MHz, CDCl₃): δ = 7.52 (s, 2 H, =CH), 5.45 (t, 2 H, J_{2,3} = J_{3,4} = 9.8 Hz, H-3), 5.30 (bs, 2 H, NHBoc), 4.97 (dd, 2 H, J_{1,2} = 4.0 Hz, H-2), 4.87 (t, 2 H, J_{4,5} = 9.8 Hz, H-4), 4.83 (d, 2 H, H-1), 4.48 (bd, 2 H, J_{6,6b} = 13.7 Hz, H-6a), 4.37 (d, 4 H, J_{H,H} = 6.0 Hz, CH₂ triazole), 4.12 (dd, 2 H, J_{5,6b} = 8.8 Hz, H-6b), 4.07 (m, 2 H, H-5), 2.25 (m, 12 H, H-2_{H₁₀}), 1.55 (m, 12 H, H-3_{H₁₀}), 1.46 (s, 18 H, CMe₃), 1.29 (m, 24 H, H-4_{H₁₀}, H-5_{H₁₀}), 0.89 (m, 18 H, H-6_{H₁₀}). ¹³C NMR (75.5 MHz, CD₃OD): δ = 173.5–173.2 (CO ester), 155.5 (CO carbamate), 146.0 (C-4 triazole), 122.3 (C-5 triazole), 91.7 (C-1), 79.5 (CMe₃), 69.9 (C-3, C-5), 69.8 (C-4), 69.3 (C-2), 50.7 (C-6), 36.4 (CH₂-triazole), 34.3 (C-2_{H₁₀}), 31.9 (C-4_{H₁₀}), 28.7 (CMe₃), 24.6 (C-3_{H₁₀}), 22.6 (C-5_{H₁₀}), 14.1 (C-6_{H₁₀}). ESI MS: *m/z* = 1313.4 [M + Na]⁺. Anal. Calcd for C₆₄H₁₀₆N₁₂O₁₉: C, 59.52; H, 8.27; N, 8.68. Found: C, 59.61; H, 8.33; N, 8.84.

6,6'-Di-(4-(2-Aminomethyl-1H-1,2,3-triazol-1-yl)-6,6'-dideoxy-2,3,4,2',3',4'-hexa-O-hexanoyl)- α,α' -trehalose Dihydrochloride (47). Treatment of 46 (0.30 g, 0.23 mmol) with 1:1 TFA-DCM (4 mL) and freeze-drying from 10:1 H₂O/0.1 N HCl solution afforded 47. Yield 97% (0.26 g, 0.22 mmol); [α]_D = +48.9 (c 1.0, MeOH). IR: ν_{max} = 2956, 1751, 1464, 1026 cm⁻¹. ¹H NMR (300 MHz, CD₃OD): δ = 8.05 (s, 2 H, CH triazole), 5.49 (t, 2 H, J_{3,4} = J_{2,3} = 9.8 Hz, H-3), 5.06 (dd, 2 H, J_{1,2} = 4.0 Hz, H-2), 4.96 (d, 2 H, J_{1,2} = 3.6 Hz, H-1), 4.95 (t, 2 H, J_{4,5} = 9.8 Hz, H-4), 4.63 (dd, 2 H, J_{5,6a} = 2.6 Hz, J_{5,6b} = 14.6 Hz, H-6), 4.53 (dd, 2 H, J_{5,6b} = 7.9 Hz, H-6b), 4.27 (bs, 4 H, CH₂NH₂), 4.24 (m, 1 H, H-5), 2.32 (m, 12 H, H-2_{H₁₀}), 1.59 (m, 12 H, H-3_{H₁₀}), 1.33 (m, 24 H, H-4_{H₁₀}, H-5_{H₁₀}), 0.93 (m, 18 H, H-6_{H₁₀}). ¹³C NMR (75.5 MHz, CD₃OD): δ = 174.5–173.6 (CO), 141.5 (C-4 triazole), 127.1 (C-5 triazole), 92.7 (C-1), 71.2 (C-2), 70.6 (C-3), 70.4 (C-4), 70.3 (C-5), 51.5 (C-6), 35.2 (CH₂NH₂), 34.8 (C-2_{H₁₀}), 32.1 (C-4_{H₁₀}), 25.8 (C-3_{H₁₀}), 22.6 (C-5_{H₁₀}), 14.2 (C-6_{H₁₀}). ESI MS: *m/z* = 1091.4 [M]⁺. Anal. Calcd for C₆₄H₁₀₆N₁₂O₁₅: C, 55.71; H, 7.96; N, 9.62. Found: C, 55.48; H, 7.77; N, 9.97.

6,6'-Di-(4-(2-N'-(2-(N-tert-butoxycarbonyl)aminoethyl)thioureido)methyl-1H-1,2,3-triazolyl)-2,3,4,2',3',4'-hexa-O-hexanoyl)-6,6'-dideoxy- α,α' -trehalose (48). To a solution of 47 (0.14 g, 0.12 mmol) and Et₃N (37 μ L, 0.36 mmol) in DCM (10 mL), *tert*-butyl N-(2-isothiocyanatoethyl) carbamate (0.07 g, 0.36 mmol) was added and the reaction mixture was stirred overnight at rt. The reaction mixture was washed with aqueous diluted HCl (3 \times 10 mL), and the organic phase was dried (MgSO₄), filtered, and concentrated. The residue was purified by column chromatography (2:1 → 3:1 EtOAc-cyclohexane). Yield 67% (0.12 g, 0.08 mmol); *R*_f = 0.40 (3:1 EtOAc-cyclohexane); [α]_D = +59.8 (c 1.0, DCM). UV (DCM): 249 nm (ϵ_{max} 53.9). IR: ν_{max} = 2959, 1752, 1701, cm⁻¹. ¹H NMR (300 MHz, CDCl₃): δ = 7.80 (s, 2 H, CH triazole), 7.07 (bs, 4 H, NHCS), 5.39 (t, 2 H, J_{3,4} = J_{2,3} = 9.7 Hz, H-3), 5.29 (bs, 2 H, NHBoc), 4.98–4.76 (m, 4 H, H-1, H-4, CH₂ triazole), 4.62 (dd, 2 H, H-2), 4.47 (d, 2 H, J_{6,6b} = 14.0 Hz, H-6a), 4.28 (dd, 2 H, J_{5,6b} = 8.0 Hz, H-6b), 3.97 (bt, 2 H, H-5), 3.60 (bs, 4 H, CH₂CH₂NHoc), 3.31 (m, 4 H, J_{H,H} = 5.4 Hz, CH₂NHoc), 2.22 (m, 12 H, H-2_{H₁₀}), 1.53 (m, 12 H, H-3_{H₁₀}), 1.39 (s, 18 H, CMe₃), 1.27 (m, 24 H, H-4_{H₁₀}, H-5_{H₁₀}), 0.86 (m, 18 H, H-6_{H₁₀}). ¹³C NMR (75.5 MHz, CDCl₃): δ = 173.2–172.5 (CO ester), 156.2 (CO carbamate), 141.5 (C-4 triazole), 124.3 (C-5 triazole), 96.7 (C-1), 79.7 (CMe₃), 69.6–68.7 (C-2, C-3, C-4, C-5), 50.3 (C-6), 40.0 (CH₂CH₂NHoc), 39.5 (CH₂NHoc), 33.9 (C-2_{H₁₀}), 31.2 (C-4_{H₁₀}), 28.3 (CMe₃), 24.3 (C-3_{H₁₀}), 22.2 (C-5_{H₁₀}), 13.1 (C-6_{H₁₀}). ESI MS: *m/z* = 1517.4 [M + Na]⁺. Anal. Calcd for C₇₀H₁₁₈N₁₂O₁₉S₂: C, 56.20; H,

7.95; N, 11.24; O, 20.32; S, 4.29. Found: C, 55.95; H, 7.84; N, 11.04; S, 11.04

[[6,6'-Di-(4-(2-N'-(2-(aminoethyl)thioureido)methyl-1H-1,2,3-triazol-1-yl)-6,6'-dideoxy-2,3,4,2',3',4'-hexa-O-hexanoyl)- α,α' -trehalose Dihydrochloride (10). Treatment of 48 (0.11 g, 0.07 mmol) with TFA-DCM (2 mL) and freeze-drying from 0.1 N HCl solution afforded 10. Yield quant (0.10 g, 0.07 mmol); [α]_D = +38.2 (c 1.0, MeOH). UV (MeOH): 243 nm (ϵ_{max} 16.9). IR: ν_{max} = 2956, 2862, 1752, 1675 721 cm⁻¹. ¹H NMR (300 MHz, CD₃OD): δ = 7.92 (s, 2 H, CH triazole), 5.44 (t, 2 H, J_{2,3} = J_{3,4} = 9.7 Hz, H-3), 5.08 (dd, 2 H, J_{1,2} = 4.2 Hz, H-2), 4.95 (t, 2 H, H-4), 4.82 (m, 4 H, H-4, H-1, CH₂ triazole), 4.62 (dd, 2 H, J_{6,6b} = 14.0 Hz, J_{5,6a} = 2.5 Hz, H-6a), 4.48 (dd, 2 H, J_{5,6b} = 8.2 Hz, H-6b), 4.19 (ddd, 2 H, H-5), 3.91 (m, 4 H, CH₂CH₂NH₂), 3.21 (dt, 4 H, J_{H,H} = 5.8 Hz, CH₂NH₂), 2.31 (m, 12 H, H-2_{H₁₀}), 1.59 (m, 12 H, H-3_{H₁₀}), 1.32 (m, 24 H, H-4_{H₁₀}, H-5_{H₁₀}), 0.93 (m, 18 H, H-6_{H₁₀}). ¹³C NMR (75.5 MHz, CD₃OD): δ = 182.6 (CS), 176.0–174.5 (CO), 146.1 (C-4 triazole), 125.6 (C-5 triazole), 92.4 (C-1), 71.4 (C-4), 70.6 (C-3), 70.4 (C-5), 70.3 (C-2), 51.5 (C-6), 42.6 (CH₂CH₂NH₂), 40.9 (CH₂NH₂), 40.2 (CH₂-triazole), 35.0–34.8 (C-2_{H₁₀}), 32.5–32.4 (C-4_{H₁₀}), 25.7–25.4 (C-3_{H₁₀}), 23.2 (C-5_{H₁₀}), 14.3 (C-6_{H₁₀}). ESI MS: *m/z* = 1357 [M + Cu]⁺; 711 [M + Cu]²⁺. Anal. Calcd for C₆₀H₁₀₄N₁₂O₁₅S₂: C, 52.66; H, 7.66; N, 12.28; S, 4.69. Found: C, 52.71; H, 7.50; N, 12.55, 4.69.

6,6'-[4-(2,2-Bis-tert-butoxycarbonylamino)ethylaminomethyl]-1H-1,2,3-triazol-1-yl]-6-deoxy-2,3-di-O-hexanoyl)- α,α' -trehalose (49). To a solution of 44 (0.31 g, 0.31 mmol) and 29 (0.24 g, 0.73 mmol) in H₂O-BuOH 9:1 (15 mL), the Cu-supported catalyst Si-BPA-Cu⁺ (0.02 g) was added and the reaction mixture was refluxed for 36 h at 85 °C. The catalyst was filtered, and the solvent was removed. The residue was purified by column chromatography (2:1 → 3:1 EtOAc-cyclohexane). Yield 91% (0.54 g, 0.29 mmol); *R*_f = 0.36 (3:1 EtOAc-cyclohexane); [α]_D = +57.0 (c 1.0, DCM). IR: ν_{max} = 2958, 2359, 2341, 1751, 1700 cm⁻¹. ¹H NMR (300 MHz, CDCl₃): δ = 7.57 (s, 2 H, =CH), 5.47 (t, 2 H, J_{2,3} = J_{3,4} = 9.8 Hz, H-3), 5.20 (bs, 4 H, NHoc), 4.93 (dd, 2 H, J_{1,2} = 3.8 Hz, H-2), 4.86 (t, 2 H, J_{4,5} = 10.0 Hz, H-4), 4.77 (d, 2 H, H-1), 4.46 (bd, 2 H, J_{6,6b} = 14.0 Hz, H-6a), 4.25 (dd, 2 H, J_{5,6b} = 8.7 Hz, H-6b), 4.12 (m, 2 H, H-5), 3.83 (bs, 4 H, CH₂ triazole), 3.19 (bd, 8 H, J_{H,H} = 6.0 Hz, CH₂NHoc), 2.55 (t, 8 H, J_{H,H} = 6.0 Hz, CH₂CH₂NHoc), 2.27 (m, 12 H, H-2_{H₁₀}), 1.58 (s, 36 H, CMe₃), 1.44 (m, 12 H, H-3_{H₁₀}), 1.30 (m, 24 H, H-4_{H₁₀}, H-5_{H₁₀}), 0.89 (m, 18 H, H-6_{H₁₀}). ¹³C NMR (75.5 MHz, CDCl₃): δ = 174.2–173.0 (CO ester), 156.2 (CO carbamate), 143.9 (C-4 triazole), 124.3 (C-5 triazole), 91.4 (C-1), 79.1 (CMe₃), 69.5 (C-4), 69.3 (C-3), 69.2 (C-5), 68.8 (C-2), 53.1 (CH₂CH₂NHoc), 50.6 (C-6), 48.0 (CH₂-triazole), 38.4 (CH₂NHoc), 34.1 (C-2_{H₁₀}), 31.7 (C-4_{H₁₀}), 28.5 (CMe₃), 24.6 (C-3_{H₁₀}), 22.6 (C-5_{H₁₀}), 13.8 (C-6_{H₁₀}). ESI MS: *m/z* = 1686.6 [M + Na]⁺. Anal. Calcd for C₈₂H₁₄₂N₁₂O₂₃: C, 59.18; H, 8.60; N, 10.10. Found: C, 59.20; H, 8.51; N, 10.15.

6,6'-[4-(2,2-Diaminoethylaminomethyl)-1H-1,2,3-triazol-1-yl]-6,6'-dideoxy-2,3,4,2',3',4'-tri-O-hexanoyl)- α,α' -trehalose Tetrahydrochloride (11). Treatment of 49 (0.56 g, 0.34 mmol) with TFA-DCM 1:1 (6 mL) and freeze-drying from 0.1 N HCl solution afforded 11. Yield quant (0.48 g, 0.33 mmol); [α]_D = +22.1 (c 1.0, MeOH). IR: ν_{max} = 2956, 2356, 1753, 1676, 721 cm⁻¹. ¹H NMR (300 MHz, CD₃OD): δ = 8.33 (s, 2 H, CH triazole), 5.51 (t, 2 H, J_{3,4} = J_{2,3} = 9.7 Hz, H-3), 5.08 (dd, 2 H, J_{1,2} = 3.9 Hz, H-2), 5.01 (t, 2 H, J_{4,5} = 9.7 Hz, H-4), 4.95 (d, 2 H, H-1), 4.65 (dd, 2 H, J_{5,6a} = 3.0 Hz, J_{5,6b} = 14.5 Hz, H-6a), 4.56 (dd, 2 H, J_{5,6b} = 8.1 Hz, H-6b), 4.28 (bs, 4 H, CH₂ triazole), 4.18 (ddd, 2 H, H-5), 3.41 (bt, 8 H, J_{H,H} = J_{H,NH} = 6.0 Hz, CH₂NH₂), 3.22 (bt, 8 H, CH₂CH₂NH₂), 2.31 (m, 12 H, H-2_{H₁₀}), 1.59 (m, 12 H, H-3_{H₁₀}), 1.33 (m, 24 H, H-4_{H₁₀}, H-5_{H₁₀}), 0.93 (m, 18 H, H-6_{H₁₀}). ¹³C NMR (75.5 MHz, CD₃OD): δ = 174.2–173.2 (CO), 141.1 (C-4 triazole), 128.8 (C-5 triazole), 91.9 (C-1), 71.0 (C-4), 70.6 (C-3), 70.5 (C-5), 70.4 (C-2), 51.8 (C-6), 51.6 (CH₂CH₂NH₂), 47.9 (CH₂-triazole), 37.2 (CH₂NH₂), 35.1–34.8 (C-2_{H₁₀}), 32.5–32.4 (C-4_{H₁₀}), 25.6–25.5 (C-3_{H₁₀}), 23.4 (C-5_{H₁₀}), 14.3 (C-6_{H₁₀}). ESI MS: *m/z* = 1263.5 [M]⁺; 632.0 [M]²⁺. Anal. Calcd for C₆₂H₁₁₄N₁₂O₁₅: C, 52.83; H, 8.15; N, 11.93. Found: C, 52.87; H, 8.04; N, 11.74.

Determination of CMC via Pyrene Fluorescence Measurements. To assess the amphiphilicity, the critical micelle concen-

trations (CMC) of all derivatives have been determined using an established fluorescence technique based on pyrene.⁴⁶ This extremely hydrophobic dye is preferentially incorporated in the interior of micelles. The onset of micelle formation can be observed in a shift of the fluorescence excitation spectra of the samples at an emission wavelength of 372 nm. In the concentration range of aqueous micellar solutions, a shift of the excitation band in the 335 nm region toward higher wavelengths confirms the incorporation of pyrene in the hydrophobic interior of micelles. The ratio of the fluorescence intensities at 339 and 335 nm was used to quantify the shift of the broad excitation band. The critical micelle concentrations were determined from the crossover point in the low concentration range. Fluorescence spectra were recorded with an F-2500 Hitachi spectrofluorophotometer and conventional 1 cm quartz cuvettes at 37 ± 0.1 °C, using 2.5 nm excitation and emission slits.

Synthesis of Dodecanethiol Coated Gold Nanoparticles (DDT-Au NPs). A solution of tetrachloroaurate acid in milli-Q water (25 mL, 0.03 M) was mixed with a solution of tetraoctylammonium bromide in toluene (80 mL, 0.05 M). The two phases mixture was vigorously stirred until all the tetrachloroaurate was transferred into the organic layer, and the aqueous layer was discarded. To the solution was added dropwise a NaBH₄ aqueous solution (25 mL, 0.35 M) for 1 min, then the mixture was stirred for 1 h. The biphasic system was washed with 0.01 M HCl (1 × 25 mL), 0.01 M NaOH (1 × 25 mL), and H₂O milli-Q (3 × 25 mL). Aqueous layers were discarded, and the organic phase was stirred overnight at rt. Dodecanethiol (10 mL, 42 mmol) was added, and the mixture was refluxed for 3 h. The system was cooled to rt and spin-dried at 2000 rpm for 10 min. The supernatant was recovered, and MeOH was added to reach 1:1 mixture to precipitate the NPs and eliminate the excess of dodecanethiol, and the system was spin-dried for 10 min at 2000 rpm. Then supernatant was discarded, and the precipitate was suspended in 1 mL of CHCl₃.

The final concentration of DDT-Au NPs was determined by UV spectrometry. A small aliquot of NPs was 1000-fold diluted and absorbance was measured using a $\epsilon = 8.63 \times 10^4 \text{ M}^{-1} \text{ cm}^{-1}$.⁵⁰

Coating of DDT-Au NPs with Compound 11. To a solution of DDT-Au NP (120 μL) in CHCl₃ (30 mL) was added a solution of compound 11 in MeOH (1 mL, 2 mM). The mixture was concentrated, and milli-Q water (300 μL) was added before 1 min sonication. The dark-red solution was spin-dried in a ultrafiltration device with a poly(ether sulfone) membrane (Corning Spin-X UF) for 5 min at 6000 rpm. The precipitate was recovered by addition of milli-Q water (500 μL). Final concentration was determined measuring the absorbance at 450 nm using a $\epsilon = 3.07 \times 10^4 \text{ M}^{-1} \text{ cm}^{-1}$.

Biological Assays. Reagents and Cell Cultures. Expression plasmid for mouse MD-2 was a gift from Dr. Y. Nagai (University of Tokyo, Japan). Expression plasmid for mouse TLR4 was purchased from InvivoGen (CA, USA). Expression plasmids containing sequences of human TLR4 and MD-2 as well as the pELAM-1 firefly luciferase plasmid were a gift from Dr. C. Kirschning (Technical University of Munich, Germany). The Renilla luciferase pRL-TK plasmid was purchased from Promega (WI, USA).

The human embryonic kidney (HEK) 293 cells were provided by Dr. J. Chow (Eisai Research Institute, Andover, MA, USA). HEK293 cells were grown in DMEM supplemented with 10% FBS. Compounds were dissolved in 100% DMSO to provide 4 mM stock solutions; further working dilutions were prepared immediately before stimulation with cell medium (DMEM supplemented with 10% FBS).

Cell Activation Assay: NF- κ B-Luciferase Reporter Assay. HEK 293 cells were seeded in 96-well Costar plates (Corning, NY, USA) at 1.6×10^4 cells/well and incubated overnight in a humidified atmosphere (5% CO₂) at 37 °C. The next day, when cells were 40–60% confluent, they were cotransfected with MD-2 (10 ng), NF- κ B-dependent luciferase (70 ng), and constitutive Renilla (15 ng) reporter plasmids and TLR4 plasmid (1 ng) using PEI (7.5 molar polyethylenimine pH 7.5, Polysciences) transfection reagent. Cells were stimulated 4 h after transfection with the synthetic compounds, then 1 h later with LPS (5 nM) that was extensively vortexed immediately prior to stimulation. Cells were lysed after 16 h of stimulation in 1× reporter assay lysis

buffer (Promega, USA) and analyzed for reporter gene activities using a dual-luciferase reporter assay system. Relative luciferase activity (RLA) was calculated by normalizing each sample's firefly luciferase activity for constitutive Renilla activity measured within the same sample. When plotting the data, the value of the wild type MD-2-TLR4 sample stimulated with LPS was normalized to 100 and other values were adjusted accordingly.

HEK-Blue Assay. HEK-Blue-TLR4 cells (InvivoGen) were cultured according to manufacturer's instructions. Briefly, cells were cultured in DMEM high glucose medium supplemented with 10% fetal bovine serum (FBS), 2 mM glutamine, 1× Normocin (InvivoGen), 1× HEK-Blue Selection (InvivoGen). Cells were detached by the use of a cell scraper, and the cell concentration was estimated by using Trypan Blue (Sigma-Aldrich). The cells were diluted in DMEM high glucose medium supplemented as described before and seeded in multiwell plate at a density of 2×10^4 cells/well in 200 μL . After overnight incubation (37 °C, 5% CO₂, 95% humidity), supernatant was removed, and cell monolayers were washed with warm PBS without Ca²⁺ and Mg²⁺ and treated with increasing concentrations of compounds dissolved in DMSO–ethanol (1:1). After 30 min, the cells were stimulated with 10 nM LPS from *E. coli* O55:B5 (Sigma-Aldrich) and incubated overnight at 37 °C, 5% CO₂, and 95% humidity. As a control, the cells were treated with or without LPS (10 nM) alone. Then the supernatants were collected, and 50 μL of each sample was added to 100 μL PBS, pH 8, 0.84 mM *para*-nitrophenylphosphate (pNPP) for a final concentration of 0.8 mM pNPP. Plates were incubated for 2–4 h in the dark at rt, and then the plate reading was assessed by using a spectrophotometer at 405 nm (LT 4000, Labtech). The results were normalized with positive control (LPS alone) and expressed as the mean of percentage \pm SD of at least three independent experiments.

MTT Cell Viability Assay. HEK-Blue cells were seeded in 100 μL of DMEM without Phenol Red at a density of 2×10^4 cells per well. After overnight incubation, 10 μL of compounds were added and the plates were incubated overnight at 37 °C, 5% CO₂, 95% humidity. DMSO and PBS were included as control. Then 10 μL of MTT solution (5 mg/mL in PBS) were added to each well. After 3 h incubation (37 °C, 5% CO₂, 95% humidity), HCl 0.1 N in 2-propanol was added (100 μL /well) to dissolve formazan crystals. Formazan concentration in the wells was determined by measuring the absorbance at 570 nm (LT 4000, Labtech). The results were normalized with untreated control (PBS) and expressed as the mean of percentage \pm SD of three independent experiments.

In Vivo Endotoxin Inhibition. C57BL/6j mice (11–13 weeks old) were randomly assigned into groups and injected intraperitoneally with vehicle control (5% DMSO in PBS) (groups none and LPS only) or the inhibitory compound (2×10^{-7} mol compound/mouse for compounds 5–11, all in 5% DMSO solution). One hour later, the mice were injected intraperitoneally with vehicle control (PBS) (group none) or with LPS from *E. coli* O55:B5 (1×10^{-9} mol/mouse \approx 10 μg LPS/mouse). Three hours later, the blood was collected. Serum was tested with the mouse TNF- α ELISA kit ("ReadySetGo", eBioscience) to determine the levels of mouse TNF- α . The experiment was performed according to the manufacturer's instructions.

■ ASSOCIATED CONTENT

● Supporting Information

Activity of compounds 5, 9, and 10 on bone marrow-derived murine macrophages (BMDM); MTT cell toxicity tests for synthetic molecules. This material is available free of charge via the Internet at <http://pubs.acs.org>.

■ AUTHOR INFORMATION

Corresponding Author

*Phone: +39.0264483453. E-mail: francesco.peri@unimib.it

Notes

The authors declare no competing financial interest.

■ ACKNOWLEDGMENTS

This study was financially supported by the Italian Ministry of University and Research (MIUR), PRIN 2010-11, project: "Italian network for the development of multivalent nano-systems," the Spanish Ministerio de Economía y Competitividad (contract nos. SAF2013-44021-R and CTQ2010-15848), the Junta de Andalucía (contract no. FQM 1467), COST actions CM1102 "MultiGlycoNano" and BM 1003 "Microbial cell surface determinants of virulence as targets for new therapeutics for Cystic Fibrosis"; the Slovenian Research Agency grant P4-176 and J1-4170, and the European Regional Development Funds (FEDER and FSE). Technical assistance from the research support services of the University of Seville (CITIUS) is acknowledged.

■ ABBREVIATIONS USED

BMDM, bone marrow derived macrophages; CNS, central nervous system; DC, dendritic cell; DCC, dicyclohexylcarbodiimide; DMEM, Dulbecco's Modified Eagle's Medium; DMAP, 4-dimethylaminopyridine; DMSO, dimethylsulfoxide; HEK, human embryonic kidney; PTSA, *p*-toluenesulfonic acid; MTT, 3-(4,5-dimethylthiazol-2-yl)-2,5-diphenyltetrazolium bromide test; NF- κ B, nuclear factor kappa-light-chain-enhancer of activated B cells; TPP, triphenylphosphine; TRAM, TRIF-related adaptor molecule; TRIF, TIR-domain-containing adapter-inducing interferon- β

■ REFERENCES

- (1) Akira, S.; Takeda, K. Toll-like receptor signalling. *Nature Rev. Immunol.* **2004**, *4*, 499–511.
- (2) Poltorak, A.; He, X.; Smirnova, I.; Liu, M.; Van Huffel, C.; Du, X.; Birdwell, D.; Alejos, E.; Silva, M.; Galanos, C.; Freudenberg, M.; Ricciardi-Castagnoli, P.; Layton, B.; Beutler, B. Defective LPS signaling in C3H/HeJ and C57BL/10ScCr mice: mutations in TLR4 gene. *Science* **1998**, *282*, 2085–2088.
- (3) Beutler, B. TLR4 as the mammalian endotoxin sensor. *Curr. Top. Microbiol. Immunol.* **2002**, *270*, 109–120.
- (4) Lucas, K.; Maes, M. Role of the Toll-like receptor (TLR) radical cycle in chronic inflammation: possible treatments targeting the TLR4 pathway. *Mol. Neurobiol.* **2013**, *48* (1), 190–204.
- (5) Cribbs, S.; Martin, G. Expanding the global epidemiology of sepsis. *Crit. Care Med.* **2007**, *35*, 2646–2648.
- (6) Peri, F.; Calabrese, V. Toll-like receptor 4 (TLR4) modulation by synthetic and natural compounds: an update. *J. Med. Chem.* **2014**, *57*, 3612–3622.
- (7) Peri, F.; Piazza, M. Therapeutic targeting of innate immunity with Toll-like receptor 4 (TLR4) antagonists. *Biotechnol. Adv.* **2012**, *30*, 251–260.
- (8) Jerala, R. Structural biology of the LPS recognition. *Int. J. Med. Microbiol.* **2007**, *297*, 353–363.
- (9) Schumann, R.; Leong, S.; Flagg, G.; Gray, P.; Wright, S.; Mathison, J.; Tobias, P.; Ulevitch, R. Structure and function of lipopolysaccharide binding protein. *Science* **1990**, *249*, 1429–1431.
- (10) Wright, S.; Ramos, R.; Tobias, P.; Ulevitch, R.; Mathison, J. CD14, a receptor for complexes of lipopolysaccharide (LPS) and LPS binding protein. *Science* **1990**, *249*, 1431–1433.
- (11) Shimazu, R.; Akashi, S.; Ogata, H.; Nagai, Y.; Fukudome, K.; Miyake, K.; Kimoto, M. MD-2, a molecule that confers lipopolysaccharide responsiveness on Toll-like receptor 4. *J. Exp. Med.* **1999**, *189*, 1777–1782.
- (12) Gioannini, T.; Teghanemt, A.; Zhang, D.; Coussens, N.; Dockstader, W.; Ramaswamy, S.; Weiss, J. Isolation of an endotoxin-MD-2 complex that produces Toll-like receptor 4-dependent cell activation at picomolar concentrations. *Proc. Natl. Acad. Sci. U. S. A.* **2004**, *101*, 4186–4191.
- (13) Park, B.; Song, D.; Kim, H.; Choi, B.; Lee, H.; Lee, J. The structural basis of lipopolysaccharide recognition by the TLR4-MD-2 complex. *Nature* **2009**, *458*, 1191–1195.
- (14) Baldrige, J.; McGowan, P.; Evans, J.; Cluff, C.; Mossman, S.; Johnson, D.; Persing, D. Taking a Toll on human disease: Toll-like receptor 4 agonists as vaccine adjuvants and monotherapeutic agents. *Expert Opin. Biol. Ther.* **2004**, *4*, 1129–1138.
- (15) Golenbock, D. T.; Hampton, R. Y.; Qureshi, N.; Takayama, K.; Raetz, C. R. Lipid A-like molecules that antagonize the effects of endotoxins on human monocytes. *J. Biol. Chem.* **1991**, *266*, 19490–19498.
- (16) Kim, H.; Park, B.; Kim, J.; Kim, S.; Lee, J.; Oh, S.; Enkhbayar, P.; Matsushima, N.; Lee, H.; Yoo, O.; Lee, J. Crystal structure of the TLR4-MD-2 complex with bound endotoxin antagonist Eritoran. *Cell* **2007**, *130*, 906–917.
- (17) Loney, C.; Vandenbranden, M.; Ruyschaert, J. M. Cationic lipids activate intracellular signaling pathways. *Adv. Drug Delivery Rev.* **2012**, *64*, 1749–1758.
- (18) Tanaka, T.; Legat, A.; Adam, E.; Steuve, J.; Gatot, J. S.; Vandenbranden, M.; Ulianov, L.; Loney, C.; Ruyschaert, J. M.; Muraile, E.; Tuynder, M.; Goldman, M.; Jacquet, A. DiC14-amidine cationic liposomes stimulate myeloid dendritic cells through Toll-like receptor 4. *Eur. J. Immunol.* **2008**, *38*, 1351–1357.
- (19) Yan, W.; Chen, W.; Huang, L. Mechanism of adjuvant activity of cationic liposome: phosphorylation of a MAP kinase, ERK and induction of chemokines. *Mol. Immunol.* **2007**, *44*, 3672–3681.
- (20) Vangasser, D. P.; Cui, Z.; Chen, W.; Hokey, D. A.; Faló, L. D.; Huang, L. Immunostimulation of dendritic cells by cationic liposomes. *Mol. Membr. Biol.* **2006**, *23*, 385–395.
- (21) Leon-Ponte, M.; Kirchoff, M. G.; Sun, T.; Stephens, T.; Singh, B.; Sandhu, S.; Madrenas, J. Polycationic lipids inhibit the pro-inflammatory response to LPS. *Immunol. Lett.* **2005**, *96*, 73–83.
- (22) Piazza, M.; Yu, L.; Teghanemt, A.; Gioannini, T.; Weiss, J.; Peri, F. Evidence of a specific interaction between new synthetic antiseptics agents and CD14. *Biochemistry* **2009**, *48*, 12337–12344.
- (23) Piazza, M.; Calabrese, V.; Baruffa, C.; Gioannini, T.; Weiss, J.; Peri, F. The cationic amphiphile 3,4-bis(tetradecyloxy)benzylamine inhibits LPS signaling by competing with endotoxin for CD14 binding. *Biochem. Pharmacol.* **2010**, *80*, 2050–2056.
- (24) Piazza, M.; Rossini, C.; Della Fiorentina, S.; Pozzi, C.; Comelli, F.; Bettioni, L.; Fusi, P.; Costa, B.; Peri, F. Glycolipids and benzylammonium lipids as novel antiseptics agents: synthesis and biological characterization. *J. Med. Chem.* **2009**, *52*, 1209–1213.
- (25) Kim, J.; Lee, C.; Jin, M.; Lee, C.; Paik, S.; Lee, H.; Lee, J. Crystal structure of CD14 and its implications for lipopolysaccharide signaling. *J. Biol. Chem.* **2005**, *280*, 11347–11351.
- (26) Ortiz Mellet, C.; Benito, J. M.; García Fernández, J. M. Preorganized, macromolecular, gene-delivery systems. *Chem.—Eur. J.* **2010**, *16*, 6728–6742.
- (27) Tvaroska, I.; Bleha, T. Anomeric and Exo-Anomeric Effects in Carbohydrate Chemistry. *Adv. Carbohydr. Chem. Biochem.* **1989**, *47*, 45–123.
- (28) Rodríguez-Lucena, D.; Benito, J. M.; Alvarez, E.; Jaime, C.; Perez-Miron, J.; Ortiz Mellet, C.; García Fernández, J. M. Synthesis, structure, and inclusion capabilities of trehalose-based cyclodextrin analogues (cyclotrehalans). *J. Org. Chem.* **2008**, *73*, 2967–2979.
- (29) Cighetti, R.; Ciaramelli, C.; Sestito, S. E.; Zanooni, I.; Kubik, L.; Ardá-Freire, A.; Calabrese, V.; Granucci, F.; Jerala, R.; Martín-Santamaría, S.; Jiménez-Barbero, J.; Peri, F. Modulation of CD14 and TLR4-MD-2 activities by a synthetic lipid A mimetic. *ChemBioChem* **2014**, *15*, 250–258.
- (30) Artner, D.; Oblak, A.; Ittig, S.; Garate, J. A.; Horvat, S.; Arriueurolou, C.; Hofinger, A.; Oostenbrink, C.; Jerala, R.; Kosma, P.; Zamyatina, A. Conformationally constrained lipid A mimetics for exploration of structural basis of TLR4/MD-2 activation by lipopolysaccharide. *ACS Chem. Biol.* **2013**, *8*, 2423–2432.
- (31) Barath, M.; Petrusova, M.; Bystricky, S.; Křen, V.; Petruš, L. Synthesis of a precursor of a lipid A mimic. *Chem. Pap.* **2003**, *57*, 125–130.

- (32) Gobolobov, Y. G.; Zhmurova, I. N.; Kasukhin, L. F. Sixty years of Staudinger reaction. *Tetrahedron* **1981**, *37*, 437–472.
- (33) Peri, F.; Marini, C.; Barath, M.; Granucci, F.; Urbano, M.; Nicotra, F. Synthesis and biological evaluation of novel lipid A antagonists. *Bioorg. Med. Chem.* **2006**, *14*, 190–199.
- (34) Chen, J.; Dormán, G.; Prestwich, G.; Glenn, D. Asymmetric total synthesis of D-myoinositol 1,2,4,5-tetrakisphosphate and its P-2-(O-aminopropyl) derivative. *J. Org. Chem.* **1996**, *61*, 393–397.
- (35) Garegg, P. J.; Samuelsson, B. Novel reagent system for converting a hydroxy-group into an iodo-group in carbohydrates with inversion of configuration. Part 2. *J. Chem. Soc., Perkin Trans. 1* **1980**, 2866–2868.
- (36) Méndez-Ardoy, A.; Guilloteau, N.; Di Giorgio, C.; Vierling, P.; Santoyo-González, F.; Ortiz Mellet, C.; García Fernández, J. M. β -Cyclodextrin-based polycationic amphiphilic “click” clusters: effect of structural modifications in their DNA complexing and delivery properties. *J. Org. Chem.* **2011**, *76*, 5882–5894.
- (37) Díaz-Moscoso, A.; Le Gourriérec, L.; Gómez-García, M.; Benito, J. M.; Balbuena, P.; Ortega-Caballero, F.; Guilloteau, N.; Di Giorgio, C.; Vierling, P.; Defaye, J.; Ortiz Mellet, C.; García Fernández, J. M. Polycationic amphiphilic cyclodextrins for gene delivery: synthesis and effect of structural modifications on plasmid DNA complex stability, cytotoxicity, and gene expression. *Chem.—Eur. J.* **2009**, *15*, 12871–12888.
- (38) Méndez-Ardoy, A.; Gómez-García, M.; Ortiz Mellet, C.; Sevillano, N.; Girón, M. D.; Salto, R.; Santoyo-González, F.; García Fernández, J. M. Preorganized macromolecular gene delivery systems: amphiphilic beta-cyclodextrin “click clusters”. *Org. Biomol. Chem.* **2009**, *7*, 2681–2684.
- (39) Megia-Fernandez, A.; Ortega-Muñoz, M.; Lopez-Jaramillo, J.; Hernandez-Mateo, F.; Santoyo-Gonzalez, F. Non-magnetic and magnetic supported copper(I) chelating adsorbents as efficient heterogeneous catalysts and copper scavengers for click chemistry. *Adv. Synth. Catal.* **2010**, *352*, 3306–3320.
- (40) Gallego-Yerga, L.; González-Álvarez, M. J.; Mayordomo, N.; Santoyo-González, F.; Benito, J. M.; Ortiz Mellet, C.; Mendicuti, F.; García Fernández, J. M. Dynamic self-assembly of polycationic clusters based on cyclodextrins for pH-sensitive DNA nanocondensation and delivery by component design. *Chem.—Eur. J.* **2014**, *20*, 6622–6627.
- (41) Kneeland, D. M.; Ariga, K.; Lynch, V. M.; Huang, C. Y.; Anslyn, E. V. Bis(alkylguanidinium) receptors for phosphodiesterates: effect of counterions, solvent mixtures, and cavity flexibility on complexation. *J. Am. Chem. Soc.* **1993**, *115*, 10042–10055.
- (42) Liav, A.; Goren, M. B. An improved synthesis of (2,3,4-tri-O-acetyl- α -D-glucopyranosyl)uronic acid (2,3,4-tri-O-acetyl- α -D-glucopyranosid)uronic acid. *Carbohydr. Res.* **1980**, *84*, 171–174.
- (43) García Fernández, J. M.; Ortiz Mellet, C.; Jiménez Blanco, J. L.; Fuentes Mota, J.; Gadelle, A.; Coste-Sarguet, A.; Defaye, J. Isothiocyanates and cyclic thiocarbamates of α,α' -trehalose, sucrose, and cyclomaltooligosaccharides. *Carbohydr. Res.* **1995**, *268*, 57–61.
- (44) Shirey, K. A.; Lai, W.; Scott, A. J.; Lipsky, M.; Mistry, P.; Pletneva, L. M.; Karp, C. L.; McAlees, J.; Gioannini, T. L.; Weiss, J.; Chen, W. H.; Ernst, R. K.; Rossignol, D. P.; Gusovsky, F.; Blanco, J. C.; Vogel, S. N. The TLR4 antagonist Eritoran protects mice from lethal influenza infection. *Nature* **2013**, *497*, 498–502.
- (45) Ohto, U.; Fukase, K.; Miyake, K.; Shimizu, T. Structural basis of species-specific endotoxin sensing by innate immune receptor TLR4/MD-2. *Proc. Natl. Acad. Sci. U. S. A.* **2012**, *109*, 7421–7426.
- (46) Hofmann, A. M.; Wurm, F.; Frey, H. Rapid access to polyfunctional lipids with complex architecture via oxyanionic ring-opening polymerization. *Macromolecules* **2011**, *44*, 4648–4657.
- (47) Piazza, M.; Colombo, M.; Zaroni, I.; Granucci, F.; Tortora, P.; Weiss, J.; Gioannini, T.; Prosperi, D.; Peri, F. Uniform lipopolysaccharide (LPS)-loaded magnetic nanoparticles for the investigation of LPS-TLR4 Signaling. *Angew. Chem., Int. Ed.* **2011**, *50*, 622–626.
- (48) Barr, T. A.; Krembuszewski, M.; Gupta, M.; Gray, D.; Mareque-Rivas, J. C. Quantum dots decorated with pathogen associated molecular patterns as fluorescent synthetic pathogen models. *Mol. Biosyst.* **2010**, *6*, 1572–1575.
- (49) Pellegrino, T.; Manna, L.; Kudera, S.; Liedl, T.; Koktysh, D.; Rogach, A. L.; Keller, S.; Rädler, J.; Natile, G.; Parak, W. Hydrophobic nanocrystals coated with an amphiphilic polymer shell: a general route to water soluble nanocrystals. *Nano Lett.* **2004**, *4*, 703–707.
- (50) Klar, T. A.; Dulkeith, E.; Feldmann, J. *Time-Resolved Fluorescence Measurements of Fluorophores Close to Metal Nanoparticles*. Springer: Berlin, 2004; Vol. 8, pp 249–273.

Modulation of CD14 and TLR4-MD-2 Activities by a Synthetic Lipid A Mimetic

Roberto Cighetti,^[a] Carlotta Ciaramelli,^[a] Stefania Enza Sestito,^[a] Ivan Zanoni,^[a] Łukasz Kubik,^[b, c] Ana Ardá-Freire,^[d] Valentina Calabrese,^[a] Francesca Granucci,^[a] Roman Jerala,^[e] Sonsoles Martín-Santamaría,^[b] Jesus Jiménez-Barbero,^[d] and Francesco Peri^{j*^[a]}

Monosaccharide lipid A mimetics based on a glucosamine core linked to two fatty acid chains and bearing one or two phosphate groups have been synthesized. Compounds **1** and **2**, each with one phosphate group, were practically inactive in inhibiting LPS-induced TLR4 signaling and cytokine production in HEK-blue cells and murine macrophages, but compound **3**, with two phosphate groups, was found to be active in efficiently inhibiting TLR4 signal in both cell types. The direct interaction between compound **3** and the MD-2 coreceptor was investigated by NMR spectroscopy and molecular modeling/

docking analysis. This compound also interacts directly with the CD14 receptor, stimulating its internalization by endocytosis. Experiments on macrophages show that the effect on CD14 reinforces the activity on MD-2-TLR4 because compound **3**'s activity is higher when CD14 is important for TLR4 signaling (i.e., at low LPS concentration). The dual targeting of MD-2 and CD14, accompanied by good solubility in water and lack of toxicity, suggests the use of monosaccharide **3** as a lead compound for the development of drugs directed against TLR4-related syndromes.

Introduction

Activation of Toll-like receptor 4 (TLR4) and subsequent intracellular signaling in response to minute amounts of circulating endotoxins (Gram-negative bacterial lipopolysaccharides, LPSs), results in the rapid triggering of proinflammatory processes necessary for optimal host immune responses to invading Gram-negative bacteria in mammals.^[1] TLR4 does not bind directly to LPSs, and TLR4 activation by endotoxin is a complex event, involving the participation of other LPS-binding proteins—namely LBP, CD14, and MD-2—and ending with the for-

mation of the activated (TLR4-MD-2-LPS)₂ complex.^[2] In particular, CD14 was the first identified Pattern Recognition Receptor (PRR) that binds directly to LPSs,^[3] and chaperones the formation of the (TLR4-MD-2-LPS)₂ complex.^[4] At low endotoxin concentrations CD14 has a fundamental role in assisting the formation of the signaling complex and the consequent initiation of the MyD88-dependent pathway leading to NF-κB activation. In contrast, CD14 is not indispensable for the activation of this pathway when LPS is more concentrated.^[5]

CD14 is also required for endotoxin-induced TLR4 endocytosis^[6] and relocalization of the entire LPS receptor complex into the endosome, where a second signaling pathway, namely the TRIF-dependent pathway, leading to a second wave of NF-κB and IRF3 activation and inflammatory cytokine production initiates. It has recently been observed that TLR4 antagonists, such as Eritoran,^[7] lipid IVa, and cationic glycolipids,^[8] strongly interact with CD14 and inhibit the formation of CD14-endotoxin complex. Excessively potent and deregulated TLR4 activation and signaling causes serious systemic syndromes such as fatal septic shock, associated with a high mortality (20–30%),^[9] and organ-specific syndromes. CD14-dependent TLR4 activation in the central nervous system (CNS) by endogenous factors has been recently related to a wide array of inflammatory neurological diseases such as amyotrophic lateral sclerosis (ALS),^[10] neuropathic pain,^[11] and Alzheimer's disease (AD).^[12] Efficient and selective TLR4 antagonists with chemical structures simpler than that of lipid A are therefore required for the development of potential new drugs with a wide array of medical and pharmacological applications (from sepsis to CNS pathologies).^[13]


[a] R. Cighetti, C. Ciaramelli, S. E. Sestito, Dr. I. Zanoni, Dr. V. Calabrese, F. Granucci, Prof. F. Peri
Department of Biotechnology and Biosciences
University of Milano-Bicocca
Piazza della Scienza 2, 20126 Milano (Italy)
E-mail: francesco.peri@unimib.it

[b] Ł. Kubik, Prof. S. Martín-Santamaría
Department of Chemistry and Biochemistry, Faculty of Pharmacy
Universidad CEU San Pablo
Urb. Montepríncipe, 28668 Boadilla del Monte, Madrid (Spain)

[c] Ł. Kubik
Department of Biopharmaceutics and Pharmacodynamics
Medical University of Gdańsk
Gen. Józefa Hallera 107 Street, 80-416 Gdańsk (Poland)

[d] Dr. A. Ardá-Freire, Prof. J. Jiménez-Barbero
Department of Chemical and Physical Biology
Centro de Investigaciones Biológicas, CSIC-CSIC C/
Ramiro de Maeztu 9, 28040 Madrid (Spain)

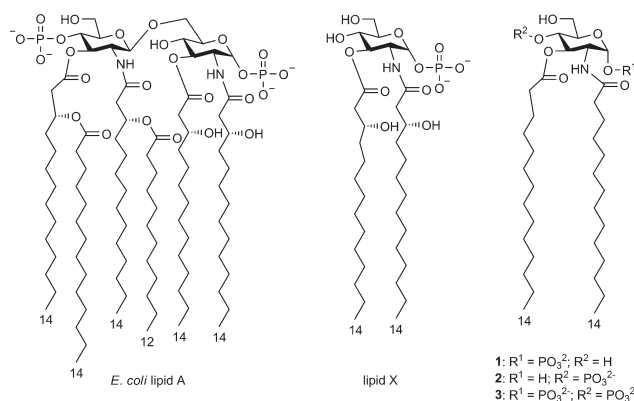
[e] Prof. R. Jerala
Department of Biotechnology, National Institute of Chemistry
Hajdrihova 19, 1000 Ljubljana (Slovenia)

 Supporting information for this article is available on the WWW under <http://dx.doi.org/10.1002/cbic.201300588>.

The LPS lipid A moiety (cf. Scheme 1), which anchors LPSs to the outer membranes of Gram-negative bacteria, is responsible for the immunostimulatory activity of LPSs.^[14,15] Lipid A consists of a 1,4- β -diphosphorylated diglucosamine backbone to which variable numbers of fatty acid (FA) acyl chains of different length are covalently linked.^[15] The numbers and structures of the acyl chains, as well as the two phosphate groups, determine the agonistic activity of lipid A.

Lipid X (Scheme 1), a biosynthetic precursor of lipid A with a structure that corresponds to the reducing GlcNAc monosac-

charide with different acylation patterns (including compound 1, named GLA-26, with two linear acyl chains) acted as agonists in murine macrophages and antagonists in human monocytes.^[18,20] Compound 2, with a phosphate group at C-4, has been described (compound 880.244)^[21] as a very weak TLR4 modulator.^[21,22] Of all lipid X synthetic analogues, the diphosphoryl lipid X (Scheme 1) showed the most potent antagonist activity on both murine macrophages and human monocytes.^[23] Compound 3 closely resembles diphosphoryl lipid X, but its structure is further simplified by the removal of the C-3 hydroxy groups on the FA chains.



Scheme 1. *E. coli* lipid A and its biosynthetic precursor lipid X, together with mono- (1 and 2) and diphosphorylated (3) lipid X mimetics.

charide of *Escherichia coli* lipid A, blocks LPS-induced septic shock and priming of TLR4-dependent human neutrophils.^[16] Because of its anti-endotoxic activity^[17] lipid X has been considered a simplified monosaccharide scaffold for the development of TLR4 agonists and antagonists.

Here we present the synthesis and biological characterization of monosaccharides 1–3 (Scheme 1): compound 1 corresponds to a lipid X mimetic with an α -anomeric phosphate, whereas 2 has a phosphate ester at the C-4 position, and 3 is phosphorylated at both C-1 and C-4 positions. Natural lipid A and lipid X have the (C-1) anomeric phosphate exclusively in the α -configuration, and the stereochemistry at the anomeric bond is very important for biological activity.^[15] Accordingly, we introduced anomeric (C-1) phosphate esters into compounds 1 and 3 through stereoselective reactions that exclusively afforded the α -configuration.

Extensive structure–activity studies are available for lipid X mimetics based on a GlcNAc monosaccharide with a C-4 phosphate group and acylated in the C-2 and C-3 positions with different linear and branched FA chains.^[18,19] Whereas compounds with two C₁₄ FA acyl chains—at C-3 and one at C-2—have TLR4 agonist activity in human and mouse macrophages,

position with tetrabutylammonium fluoride (TBAF) and AcOH to afford 7, which was phosphorylated with tetrabenzyl diphosphate in the presence of lithium bis(trimethylsilyl)amide to afford the α -anomer 8 exclusively. Catalytic hydrogenolysis in the presence of Pd/C allowed simultaneous removal of the *p*-methoxybenzylidene group and the benzyl groups on the phosphate, affording compound 1.

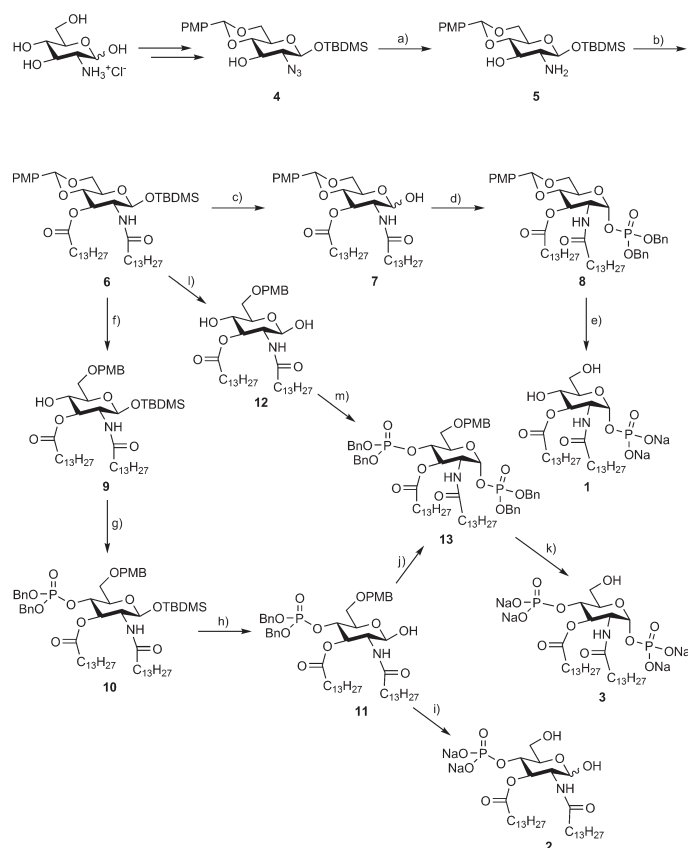
Alternatively, the benzylidene protecting group of compound 6 was reductively opened by treatment with NaCNBH₃ in dry THF to provide compound 9, protected as a *p*-methoxybenzyl (PMB) ether at C-4. Compound 9 was phosphitylated with dibenzyl *N,N*-diisopropylphosphoramidite and imidazolium triflate and was then oxidized to a phosphate with *m*-chloroperbenzoic acid to obtain 10. Compound 10 was deprotected at C-1 with TBAF and AcOH to afford 11, and subsequent catalytic hydrogenolysis in the presence of Pd/C allowed compound 2 to be obtained.

To give access to compound 3, compound 6 was treated with NaCNBH₃; this resulted in regioselective opening of the benzylidene ring and formation of the C-6 PMB ether. This reaction was quenched by addition of an acidic solution (HCl, 1 M in dioxane at pH 1.5 for 1 h); this promoted the removal of

Results and Discussion

Synthesis of lipid X mimetics 1–3

Compounds 1–3 were synthesized by using a divergent strategy starting from the common intermediate 4 (Scheme 2),^[24] obtained from commercial *D*-glucosamine hydrochloride. Compound 4 was treated with PPh₃ in THF/H₂O to transform the azido group into an amine (compound 5) and was then acylated in the C-2 and C-3 positions with myristic acid in the presence of the condensing agent 1-ethyl-3-(3-dimethylaminopropyl)carbodiimide (EDC), thus affording 6. Monosaccharide 6 was deprotected at the anomeric (C-1) position



Scheme 2. Reagents and conditions: a) PPh_3 , THF/ H_2O , 60 °C, 87%; b) myristic acid, EDC, DMAP, CH_2Cl_2 , 97%; c) TBAF, AcOH, THF, -15 °C to RT, 76%; d) tetrabenzyl diphosphate, $\text{LiN}(\text{TMS})_2$, dry THF, -78 to -20 °C, 43%; e) H_2 , Pd/C, AcOH, dry $\text{MeOH}/\text{CH}_2\text{Cl}_2$, quant.; f) NaCNBH_3 , 4 Å MS, dry THF, 84%; g) $(\text{BnO})_2\text{PNiPr}_2$, imidazolium triflate, dry CH_2Cl_2 , then *m*-CPBA, 0 °C, 42%; h) TBAF, AcOH, THF, -15 °C to RT, 57%; i) H_2 , Pd/C, AcOH, dry $\text{MeOH}/\text{CH}_2\text{Cl}_2$, quant.; j) tetrabenzyl diphosphate, $\text{LiN}(\text{TMS})_2$, dry THF, -78 to -20 °C, 71%; k) H_2 , Pd/C, AcOH, dry $\text{MeOH}/\text{CH}_2\text{Cl}_2$, quant.; l) NaCNBH_3 , 4 Å MS, dry THF, then HCl in dioxane until pH 1.5, 61%; m) $(\text{BnO})_2\text{PNiPr}_2$, imidazolium tosylate, dry CH_2Cl_2 , then *m*-CPBA, 0 °C, 38%.

the anomeric *tert*-butyldimethylsilyl (TBDMS) protective group, thus providing compound **12** in one reaction step. Double phosphorylation at C-1 (stereoselective) and C-4 positions the phosphoramidite plus oxidation method and subsequent catalytic hydrogenolysis afforded monosaccharide **3**.

Compounds **1**, **2** and **3** were recovered as triethylammonium salts after hydrogenolysis and then treated with Amberlite IR 120 Na^+ exchange resin to change the counterion. The final compounds used for biological characterization contained sodium as counterion for the phosphate groups.

Inhibition of LPS-induced, TLR4-dependent NF- κ B activation in HEK-blue cells

The abilities of molecules **1**, **2**, and **3** to interfere with LPS-triggered TLR4 activation were first investigated in HEK-blue cells. HEK-blue cells are HEK293 cells stably transfected with human TLR4, MD-2, and CD14 genes. In addition, HEK-blue cells stably express a secreted alkaline phosphatase (sAP) produced upon activation of NF- κ B. LPS binding activates TLR4 and NF- κ B, leading to sAP secretion, which is detected in cell culture media by an alkaline phosphatase substrate.

When supplied alone, compounds **1–3** were unable to stimulate TLR4-dependent sAP production at a range of concentrations between 0 and 50 μM , thus confirming the lack of any agonist activity for the three monosaccharides on human TLR4. Cells were then pretreated with increasing concentrations of the synthetic monosaccharides (from 0 to 50 μM) and then stimulated with *E. coli* O55:B5 LPS (100 ng mL^{-1}). In this concentration range compounds **1** and **2** were weakly active in inhibiting LPS-stimulated TLR4 signaling, whereas **3** was active. The experiment was also run for compound **3** at two LPS concentrations (10 ng mL^{-1} and 1 $\mu\text{g mL}^{-1}$) by administering LPS 30 min after the pretreatment with compound **3**. At both these LPS concentrations the percentage activation of HEK cells reached similar values, thus indicating

that the lower concentration (10 ng mL^{-1}) also saturated the signal corresponding to TLR4-dependent NF- κ B stimulation (100% on the vertical scale, Figure 1). Compound **3** turned out to be more active as an antagonist at the low LPS concentration (10 ng mL^{-1}), with a calculated IC_{50} of 0.46 μM , whereas when LPS was more concentrated the IC_{50} was increased to 3.42 μM (Figure 2). As a negative control a HEK-293 cell line (InvivoGen) transfected with the same plasmids as HEK-blue but without TLR4, MD-2, and CD14 genes was used, and no effect was observed (data not shown). The toxicities of all com-

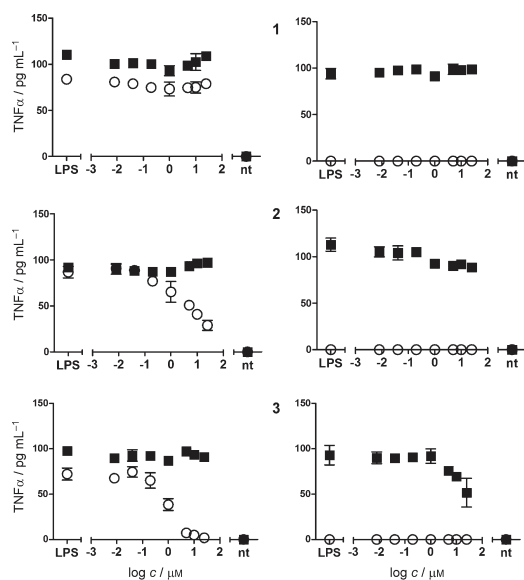


Figure 1. Effects of compounds 1–3 on LPS-induced TNF- α production by BM-derived macrophages. WT or CD14^{-/-} BM macrophages were preincubated with synthetic compounds for 30 min and then treated either with a high LPS concentration (1 $\mu\text{g mL}^{-1}$, ■) or a low one (10 ng mL^{-1} , ○). Readout was the TNF- α production after one night's incubation.

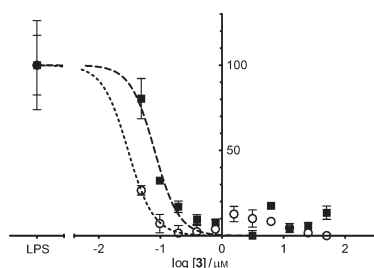


Figure 2. HEK-blue cells assay. Compound 3 inhibits LPS-triggered TLR4 activation in a dose-dependent way (monitored as sAP colorimetric reaction, normalized data, $n=3$ experiments). Low concentrations of LPS (10 ng mL^{-1} ; ○) gave an IC_{50} value of 0.46 μM for compound 3; high LPS doses (1 $\mu\text{g mL}^{-1}$; ■) shifted the IC_{50} to 3.42 μM .

compounds were assessed by MTT tests, and all compounds showed no or very limited toxicity up to the highest concentration tested (50 μM ; see the Supporting Information).

Inhibition of LPS-induced TLR4 activation in murine macrophages

The abilities of compounds 1–3 to modulate the LPS-stimulated TLR4 pathway were further investigated in bone-marrow-derived murine macrophages (BMM Φ s). TNF- α production was determined from TLR4–MyD88 pathway activation. BMM Φ s from wild-type and CD14^{-/-} mice were treated with increasing concentrations (0–50 μM) of compounds 1–3 in DMEM + BSA (0.03%) in the presence or in the absence of LPS. Two LPS concentrations (10 and 1000 ng mL^{-1}) were tested, and LPS was administered 30 min after pretreatment with the synthetic compounds.

The LPS-induced TNF- α production after one night's incubation was assessed by ELISA test (Figure 1). As expected, the high concentration of smooth LPS also activated TLR4 signaling in the absence of CD14,^[5] whereas at the low LPS concentration the signal was absent in CD14-defective cells. Compound 1 was inactive in both cell types, whereas molecule 2 showed a weak antagonist effect on wt macrophages at low LPS concentration. Compound 3 showed a dose-dependent LPS antagonistic activity in wt cells at the low LPS concentration and in CD14^{-/-} at the high LPS concentration (Figure 1). The antagonist activity on both wt and CD14-defective cells suggests that molecule 3 competes with LPS in interaction both with CD14 and with the MD-2-TLR4 complex.

Compound 3 selectively stimulates endocytosis of CD14 (and not of the MD-2-TLR4 complex)

Because CD14 favors the activation of the TLR4–MyD88 pathway at low LPS doses, and because compounds 2 and 3 are more active as inhibitors at low LPS concentrations, we evaluated whether CD14 could be directly targeted by the synthetic compounds. We analyzed the capacities of compounds 1–3 to induce CD14 and MD-2-TLR4 complex internalization in BMM Φ s. CD14 is in fact efficiently internalized together with the entire LPS receptor complex after LPS or lipid A binding, and this process has been demonstrated to be directed by CD14 in a TLR4-independent manner.^[6] BMM Φ s were incubated with compounds 1–3 at a concentration of 10 μM , and the amounts of CD14 remaining at the cell surface over time were analyzed by flow cytometry. Compound 3, showing the best antagonistic activity, was also capable of efficiently inducing CD14 internalization, whereas compounds 1 and 2 did not show any effect on CD14 surface expression (Figure 3). Interestingly, MD-2-TLR4 complex was not internalized after exposure to compounds 1–3 (Figure 3). These results suggest that compound 3, an antagonist of the TLR4 signal pathway, can interact directly with CD14, causing its internalization.

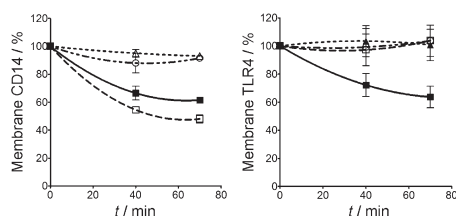


Figure 3. Internalization of CD14 (left) and TLR4 (right) induced by compounds **1** (\blacktriangle), **2** (\circ), and **3** (\square). BMMΦs were treated with LPS ($1 \mu\text{g mL}^{-1}$; \blacksquare) or with the synthetic compounds, and the systems were incubated at 37°C for the times indicated. Flow cytometry was then used to examine receptor endocytosis by determining the surface levels of the proteins indicated. Panels represent the mean fluorescence intensity (MFI) of specific receptor staining at each time point.

NMR binding experiments—interaction between synthetic compound **3** and MD-2

The binding of monosaccharide **3** to the MD-2 receptor in solution was then investigated by means of NMR techniques. Because of the tendency of compound **3** to form stable aggregates at the concentrations required for NMR measurements ($150\text{--}300 \mu\text{M}$), it turned out to be impossible to detect ligand-protein interaction by saturation transfer difference (STD) experiments. However, it was possible to record good-quality ^1H NMR spectra of **3**, of MD-2, and of a **3**/MD-2 mixture (ratio 5:1, at a $150 \mu\text{M}$ ligand concentration, Figure 4). Selective attenuation of the signals corresponding to the fatty acid C_{14} chain protons of **3** was observed upon addition of MD-2 to the monosaccharide sample solution (Figure 4). Although broadening of all the resonance signals was detected, the decrease in signal intensities was significantly higher for those hydrogen atoms belonging to the FA aliphatic chains, in particular for

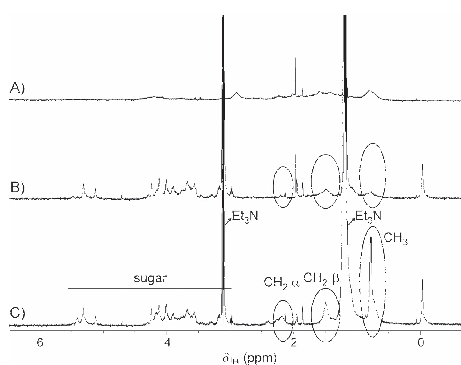


Figure 4. A) ^1H NMR of $30 \mu\text{M}$ MD-2 protein in deuterated acetate buffer at pH 5, 298 K, 120 scans. B) ^1H NMR of $30 \mu\text{M}$ MD-2 protein and $150 \mu\text{M}$ compound **3** in deuterated acetate buffer at pH 5, 298 K, 120 scans. C) ^1H NMR of $150 \mu\text{M}$ compound **3** in deuterated acetate buffer at pH 5, 298 K, 120 scans.

the signals of the ω -methyl groups and for those of the contiguous CH_2 moieties, followed by the rest of the chain hydrogen atoms. In contrast, the intensities of the signals corresponding to the hydrogen atoms on the sugar ring proved to be practically unaltered.

The experimentally observed reductions in intensity, due to specific line broadening of these signals, arise from the changes in the transverse relaxation times of these signals. This dramatic change likely arises from the existence of interaction between **3** and MD-2, precisely focused at the aliphatic side chain region. In fact, the FA chains–MD-2 interactions outlined here are reminiscent of those previously observed for positively charged amphiphiles.^[6] These data suggest the existence of a major interaction of both FA chains of the sugar ligand with the hydrophobic binding cavity of MD-2, as also confirmed by docking calculations (see below). The exchange process between the free and the bound states provides the basis for the increased relaxation rate and the corresponding observed increases in line width.

Additional features of the interaction were also investigated by DOSY (diffusion ordered spectroscopy) NMR. Firstly, the aggregation properties of **3** were evaluated by use of DOSY. The DOSY of the free ligand showed a strikingly small diffusion coefficient, corresponding to a high-molecular-weight species in solution. This evidence can be correlated with the observation that compound **3** forms relatively large aggregates (Figure S2 in the Supporting Information) in water solution. The DOSY spectrum of the **3**/MD-2 mixture (at 5:1 molar ratio) was then also recorded. As stated above, the signals of the ligand aliphatic chains were no longer visible in the NMR spectrum, thus strongly suggesting the interaction of this part of the molecule with MD-2. In addition, the observation of a higher diffusion coefficient for the ligand molecule indicated that the existing aggregate for isolated **3** is indeed disrupted (see the Supporting Information).

Molecular modeling studies and docking of monosaccharide **3** with CD14 and MD-2

Docking studies were performed with the AutoDock^[25] and AutoDock Vina^[26] programs, by the protocol described in the Experimental Section. Firstly, the use of these computational programs was validated by docking the natural antagonist lipid IVa, with employment of the X-ray crystallographic structure of the human MD-2 protein in complexation with lipid IVa (PDB ID: 2E59) as the starting geometry.^[27] Both the AutoDock and the Vina programs satisfactorily reproduced the crystallographic binding mode, showing the four FA acyl chains inside the lipophilic pocket, and the phosphorylated glucosamine moieties located at the entrance to the cavity (data not shown).

Once the docking procedures were validated, the same docking protocol was applied to compound **3**. Reasonable binding poses were predicted in both proteins (CD14 and MD-2), thus pointing to this compound being a suitable binder. The docked theoretical MD-2 binding energies for compounds **1** and **2** were significantly higher than that for compound **3**, by at least 8 kJ mol^{-1} (data not shown), thus pointing to

a more favorable binding process for **3**. Analysis of the AutoDock and AutoDock Vina docked binding poses in MD-2 showed the ability of compound **3** to bind in two different fashions, with close predicted binding energies. Most of the best docked solutions corresponded to binding poses with the two FA chains deeply confined inside the MD2 pocket, similarly to what had been seen with lipid IVa. One of the FA chains establishes hydrophobic contacts and CH- π interactions with Leu74, Phe76, Phe104, and Ile117, in a similar way to the equivalent FA chain present in lipid IVa (Figure 5A). The second FA chain is directed into the region delimited by Ile52, Leu54,

FA chains with MD-2 protein, as well as for putative polar interactions involving the phosphate groups.

Docking calculations for compound **3** into CD14 were also carried out. In this case, the CD14 protein, like the MD-2 protein, also possesses a highly lipophilic wide pocket, but with fewer charged residues in the opening portion. Compound **3** showed binding poses presenting both FA chains inside the pocket, with the polar phosphate groups and sugar placed at the entrance of the cavity (Figure S3), thus supporting the experimental evidence of CD14 binding properties for this compound.

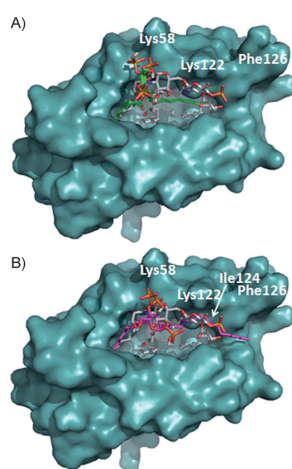


Figure 5. AutoDock binding poses of compound **3** characterized with either two (green) or one (magenta) FA chains oriented inside the lipophilic MD-2 pocket. Lipid IVa is shown as reference in CPK colors.

Phe121, Ile124, Tyr131, and Ile153, a subpocket also occupied by a FA chain in the complex with lipid IVa. In few cases, results from docking showed a second binding mode, with one FA chain extending towards Val82 and placed over Ile124 (Figure 5B). Interestingly, this Ile124 moves “up” in the agonist conformation, and its position is occupied by Phe126, thus acting as an agonist/antagonist switch.

Polar interactions were also identified in some of the docked binding poses. One phosphate group participates in hydrogen bonds—with Ser118, for instance—and is always located in the vicinity of Lys58 and/or Lys122, similarly to one of the lipid IVa phosphates. The second phosphate group is found in the vicinity of positively charged side chains, such as that from Arg96 or, in other docked solutions, exposed to the outside. In addition, in some of the docking results either the amide CO group or an ester CO group from compound **3** was found to establish a hydrogen bond with the Ser120 CO group. These predicted binding poses are in agreement with the NMR experiments and provide a 3D model for the interaction of the

Conclusions

With the aim of obtaining TLR4 antagonists with chemical structures simpler than that of lipid A, mono- and diphosphate lipid X analogues (compounds **1–3**) were synthesized. Monosaccharides **1** and **2**, with one phosphate group linked to the anomeric (C-1) and the C-4 positions, respectively, showed weak antagonism in HEK-blue cells and macrophages. Monosaccharide **3**, a diphosphorylated lipid X analogue lacking the C-3 hydroxy groups on its FA acyl chains, proved to be active in inhibiting, in a dose-dependent way, the LPS-stimulated NF- κ B activation in HEK-blue cells (Figure 2) and LPS-induced TNF- α production in macrophages (Figure 1). Monosaccharide **3** was much more active in inhibiting cytokine production at low LPS concentrations (10 ng mL^{-1}) than it was at higher ones ($1 \mu\text{g mL}^{-1}$, Figure 1). When the LPS concentration is low, the CD14-catalyzed extraction of LPS monomers from aggregates in solution and LPS presentation to the MD-2-TLR4 complex is essential for TLR4 activation and signaling.^[5] On the other hand, it has been reported that highly concentrated LPS can bind directly to the MD-2-TLR4 complex and activate the TLR4 cascade without the need for the CD14 chaperone.

The higher activity of compound **3** under the experimental conditions under which CD14 contributes to TLR4 activation is a first indication that compound **3** probably interferes both in LPS/MD-2-TLR4 and in LPS/CD14 interactions. This behavior is reminiscent of that of a first generation of positively charged monosaccharides we developed that blocked *in vitro* and *in vivo* TLR4 activation^[28] mainly by displacing endotoxin from CD14 interaction.^[8]

The capacity of compound **3** to stimulate CD14 internalization (Figure 3) provides further evidence of a direct interaction between the synthetic molecule and CD14. The interaction with MD-2 has been characterized by NMR studies, allowing the identification of the FA acyl chain moieties as the part of compound **3** that directly interacts with MD-2 (Figure 4). Once again, analogously with what has been observed with synthetic cationic amphiphiles,^[8] the FA acyl chains of the molecule proved to interact with MD-2 more strongly than the sugar part. Computational models for this complex have shown that the most stable docked complexes always correspond to binding poses in which the FA chains of compound **3** are deep inside the MD-2 pocket; this is consistent with the NMR observation of FA chain-protein interactions. Additionally, polar interactions of the phosphate groups with the outer polar resi-

dues can be identified in some of the binding poses. Overall, our calculations thus provide a theoretical 3D view of the interaction of this compound with MD-2. A docked model for CD14 in complexation with compound **3**, in accordance with the experimental results, has also been proposed.

Monosaccharide **3** is a promising lead for the development of drugs targeting TLR4 activation in a variety of medical settings.^{19–131} This nontoxic TLR4 antagonist shows a high water solubility (completely soluble up to 1 mM concentration), in contrast with lipid A and lipid A mimetics, previously developed by us and by other groups, that suffer from poor solubility in aqueous media.¹³¹ This is an important prerequisite for good bioavailability and favorable pharmacokinetic (distribution) properties. The critical micelle concentrations (CMCs) for compounds **1–3** were determined through pyrene fluorescence measurements.²⁹¹ The CMC values for compounds **1**, **2**, and **3** are 13, 28, and 9 μM , respectively. The TLR4 antagonist activity of compound **3** is observed in cells at concentration values below the CMC (IC_{50} from 0.46 to 3.2 μM). In this concentration range compound **3** is mainly in the monomeric form in solution. In contrast, at the higher concentrations required for NMR experiments (from 150 to 330 μM) compound **3** prevalently exists in the form of aggregates in solution. According to the data presented in this study, compound **3** interacts efficiently with both MD-2-(TLR4) and CD14 receptors. Multiple targeting could explain and contribute to the compound's efficacy in blocking TLR4 signaling.

Experimental Section

Chemistry

General procedures: All reagents were commercially available and used without further purification unless indicated otherwise. All solvents were anhydrous grade unless indicated otherwise. When dry conditions were required, the reactions were carried out in oven-dried glassware under a slight pressure of argon. Reactions were magnetically stirred and monitored by thin-layer chromatography (TLC) on silica gel. TLC was performed with Silica Gel 60 F254 plates (Merck) and UV detection or use of a molybdate developing solution [aqueous H_2SO_4 (5%) with $(\text{NH}_4)_6\text{Mo}_7\text{O}_{24}\cdot 4\text{H}_2\text{O}$ (4%) and 0.2% $\text{Ce}(\text{SO}_4)_2$] followed by heating at 120 °C. Flash column chromatography was performed on silica gel 230–400 mesh (Merck). The petroleum ether used as eluent in chromatography has a boiling range of 40–60 °C. ^1H and ^{13}C NMR spectra were recorded with a Varian 400 MHz Mercury instrument at 298 K. Chemical shifts are reported in ppm downfield from TMS as internal standard. Mass spectra were recorded with an ESI-MS triple quadrupole instrument (model API2000 QTrap, Applied Biosystems).

Phosphoryl 2-deoxy-3-O-tetradecanoyl-2-tetradecanoylamino- α -D-glucopyranoside (1): Compound **8** (0.05 g, 0.05 mmol) was dissolved in dry $\text{CH}_2\text{Cl}_2/\text{MeOH}$ (1:2, 6 mL), and Pd on activated charcoal (catalytic amount) and AcOH were then added. The reaction mixture was stirred overnight at RT under H_2 , with monitoring of the disappearance of starting material by TLC (toluene/AcOEt 7:3). Triethylamine (100 μL) was then added to the reaction mixture, and the suspension was filtered with a syringe filter in order to remove Pd/C catalyst and washed with CH_2Cl_2 . The product was then passed over an Amberlite IR 120 Na^+ exchange resin in order to remove triethylamine to give compound **1** as its sodium salt (0.04 g, quantitative).

^1H NMR (400 MHz, $\text{CD}_3\text{OD}+3\%$ D_2O , 25 °C, TMS): δ = 5.44 (dd, $^3J_{\text{HP}}=6.8$ Hz, $^3J_{\text{HH}}=3.4$ Hz, 1H; H-1), 5.20 (dd, $^3J_{\text{HH}}=10.6$, 9.4 Hz, 1H; H-3), 4.15 (dt, $^3J_{\text{HH}}=5.7$, 3.2 Hz, 1H; H-2), 3.95 (m, 1H; H-5), 3.85 (dd, $^3J_{\text{HH}}=11.8$, 2.0 Hz, 1H; H-6a), 3.72 (dd, $^3J_{\text{HH}}=11.8$, 5.2 Hz, 1H; H-6b), 3.63–3.54 (m, 1H; H-4), 2.42–2.27 (m, 2H; $\text{CH}_2\alpha$ chains), 2.27–2.14 (m, 2H; $\text{CH}_2\beta$ chains), 1.56 (m, 4H; $\text{CH}_2\beta$ chains), 1.37–1.20 (m, 40H; CH_2 bulk), 0.89 ppm (t, $^3J_{\text{HH}}=6.8$ Hz, 6H; CH_3); ^{13}C NMR (101 MHz, $\text{CD}_3\text{OD}+3\%$ D_2O , 25 °C, TMS): δ = 175.23, 174.18, 93.77, 73.33, 72.91, 68.06, 60.60, 51.83, 35.80, 33.81, 33.31, 31.67, 29.47, 29.42, 29.38, 29.29, 29.19, 29.14, 29.08, 28.95, 25.69, 25.31, 24.60, 24.56, 22.35, 13.16, 7.88 ppm; MS (ESI): m/z calcd: 679.44; found: 678.6, 339.4.

2-Deoxy-4-O-phosphoryl-3-O-tetradecanoyl-2-tetradecanoylamino- α,β -D-glucopyranose (2): Compound **11** (0.14 g, 0.15 mmol) was dissolved in dry $\text{CH}_2\text{Cl}_2/\text{MeOH}$ (1:2, 6 mL), and Pd on activated charcoal was then added in catalytic amounts. The reaction mixture was stirred at RT under H_2 overnight, with monitoring of the disappearance of starting material by TLC (ETP/AcOEt 7:3). Triethylamine (100 μL) was added to the reaction mixture, and the suspension was filtered with a syringe filter in order to remove Pd/C catalyst. The pure triethylammonium salt was then passed over an Amberlite IR 120 Na^+ exchange resin in order to remove triethylamine, giving compound **2** as its sodium salt (mixture of α - and β -anomers, 5:1) in quantitative yield. ^1H NMR (400 MHz, $\text{CD}_3\text{OD}+2.5\%$ CDCl_3 , 25 °C, TMS): δ = 7.66 (d, $^3J_{\text{HH}}=9.6$ Hz, 1H; NH), 5.34 (t, $^3J_{\text{HH}}=9.8$ Hz, 1H; H-3 α), 5.14 (t, $^3J_{\text{HH}}=9.7$ Hz, 1H; H-3 β), 5.05 (d, $^3J_{\text{HH}}=3.6$ Hz, 1H; H-1 α), 4.68 (d, $^3J_{\text{HH}}=8.4$ Hz, 1H; H-1 β), 4.26–4.10 (m, 3H; H-2 α , H-4 α , H-4 β), 3.98–3.90 (m, 3H; H-5 α , H-6 $\alpha\alpha$, H-6 $\alpha\beta$), 3.85–3.75 (m, 2H; H-2 β ; H-6 $\beta\beta$), 3.68 (m, 1H; H-6 $\beta\alpha$), 3.40 (m, 1H; H-5 β), 2.44–2.11 (m, 8H; $\text{CH}_2\alpha$ chains), 1.56 (m, 8H; $\text{CH}_2\beta$ chains), 1.45–1.17 (m, 80H; CH_2 bulk), 0.89 ppm (t, $^3J_{\text{HH}}=6.7$ Hz, 12H; CH_3); ^{13}C NMR (101 MHz, $\text{CD}_3\text{OD}+2.5\%$ CDCl_3 , 25 °C, TMS): δ = 78.97, 178.15, 99.68, 95.74, 75.93, 75.44, 75.16, 64.65, 59.48, 56.55, 50.39, 46.21, 40.31, 39.87, 37.99, 35.90, 33.69, 33.63, 33.59, 33.55, 33.52, 33.33, 33.25, 29.98, 28.69, 26.55, 17.27, 11.93 ppm; MS (ESI): m/z calcd: 679.44; found: 678.52.

Phosphoryl 2-deoxy-4-O-phosphoryl-3-O-tetradecanoyl-2-tetradecanoylamino- α -D-glucopyranoside (3): Compound **13** (0.08 g, 0.06 mmol) was dissolved in dry $\text{CH}_2\text{Cl}_2/\text{MeOH}$ 1:2 (5 mL), and Pd on activated charcoal was then added in catalytic amounts. The reaction mixture was stirred at RT under H_2 overnight (TLC AcOEt). Triethylamine (150 μL) was then added to the reaction mixture, and the suspension was filtered with a syringe filter. The triethylammonium salt was then passed over an Amberlite IR 120 Na^+ exchange resin to remove triethylamine, giving compound **3** as its sodium salt in quantitative yield (61 mg). ^1H NMR (400 MHz, CD_3OD , 25 °C, TMS): δ = 5.45 (dd, $^3J_{\text{HP}}=6.4$ Hz, $^3J_{\text{HH}}=3.5$ Hz, 1H; H-1), 5.37 (t, $^3J_{\text{HH}}=9.9$ Hz, 1H; H-3), 4.31–4.18 (m, 2H; H-2, H-4), 4.02–3.95 (m, 2H; H-5, H-6a), 3.72 (d, $^3J_{\text{HH}}=12.6$ Hz, 1H; H-6b), 2.46–2.14 (m, 4H; $\text{CH}_2\alpha$ chains), 1.56 (m, 4H; $\text{CH}_2\beta$ chains), 1.39–1.20 (m, 40H; CH_2 chains), 0.89 ppm (t, $^3J_{\text{HH}}=6.6$ Hz, 6H; CH_3 chains); ^{13}C NMR (101 MHz, CD_3OD , 25 °C, TMS): δ = 174.60, 173.29, 94.11, 72.22, 71.89, 70.86, 60.22, 53.41, 52.16, 46.14, 35.87, 33.77, 31.72, 29.51, 29.45, 29.42, 29.37, 29.35, 29.32, 29.28, 29.15, 29.09, 25.71, 24.87, 24.49, 22.37, 13.09, 7.74 ppm; MS (ESI): m/z calcd: 759.41; found: 758.5, 378.7.

Biology

HEK-Blue assay: HEK-Blue hTLR4 cells (HEK-Blue LPS Detection Kit, InvivoGen) were cultured according to the manufacturer's instructions. Cells were cultured in Dulbecco's modified Eagle's medium (DMEM) high-glucose medium supplemented with fetal bovine

serum (FBS, 10%), glutamine (2 mM), 1× Normocin (InvivoGen), and 1× HEK-Blue Selection (InvivoGen). Cells were detached by use of a cell scraper, and the cell concentration was estimated by use of a cell counter. Cells were then diluted in DMEM high-glucose medium supplemented with FBS (10%), glutamine (2 mM), 1× Normocin (InvivoGen), and cell suspension (200 µL, 20000 cells) was added to each well. After overnight incubation (37 °C, 5% CO₂, 95% humidity), cells had reached 80% confluency. Supernatant was removed, and cell monolayers were washed with warm PBS without Ca²⁺ and Mg²⁺, preincubated for 30 min in 190 µL DMEM + 0.03% BSA, supplemented with compounds **1**, **2**, or **3** (different concentrations in different wells, from 0 to 50 µM). LPS (*E. coli* O55:B5 strain, Sigma-Aldrich) at a final concentration of 10, 100, or 1000 ng mL⁻¹ was then added as stimulus (10 µL per well), and cells were incubated overnight under the same conditions as above. After the incubation, supernatants were collected. Each sample (50 µL) was added to a pNPP solution in PBS (0.8 mM, 100 µL). Plates were incubated in the dark at room temperature and then analyzed spectrophotometrically (absorbance at 405 nm).

Murine-bone-marrow-derived macrophages (BMMΦs) assay: Murine BMMΦs were obtained from wild-type and CD14^{-/-} mice and cultured by the published procedure.^[30] Cells were washed with PBS and detached by treatment with EDTA in PBS (2 mM). The cellular suspension was then centrifuged at 188g for 5 min, and the cellular pellet was resuspended in DMEM high-glucose + FBS 10% and plated in a 96-well plate (20000 cells per well). After overnight incubation (37 °C, 5% CO₂, 95% humidity), supernatant was removed, and cell monolayers were washed with warm PBS without Ca²⁺ and Mg²⁺, preincubated for 30 min in 190 µL DMEM + 0.03% BSA, and supplemented with compounds **1**, **2**, or **3** (different concentrations in different wells, from 0 to 50 µM). LPS (*E. coli* O55:B5 strain, Sigma-Aldrich) at a final concentration of 10, 100, or 1000 ng mL⁻¹ was then added as stimulus (10 µL per well), and cells were incubated overnight under the same conditions as above. After the incubation, supernatants were collected, and TNF concentration was detected through an ELISA.

Flow cytometry analysis: BMMΦs were washed twice with PBS and detached by treatment with EDTA in PBS (2 mM). The cellular suspension was then centrifuged at 188g for 5 min, and the cellular pellet was resuspended in DMEM high glucose + FBS 10% (100 µL) and incubated at 37 °C, 5% CO₂, and 95% humidity for 40 or 70 min with compound **1**, **2**, or **3** (10 µM) or LPS (1 µg mL⁻¹). Cellular suspensions were then centrifuged at 188g, 4 °C, for 5 min, and the cellular pellet was resuspended with ice-cold PBS. The receptor-specific fluorescent antibodies were then added (αCD14: FITC rat anti-mouse CD14, clone SA2-8, eBioscience; αTLR4: PE rat anti-mouse TLR4, clone SA15-21, Biolegend), at 1 µg mL⁻¹, for 20 min in ice in the dark. The cells were then washed twice with ice-cold PBS, and fluorescence was analyzed with a FaCSCalibur flow cytometer (BD Biosciences).

Production and isolation of MD-2: Recombinant MD-2 was produced in *E. coli* as described previously^[31] with use of solubilization of inclusion bodies in Gdn-HCl (6 M) followed by purification and refolding on a C8 reversed-phase column. Eluted fractions were lyophilized and dialyzed against Milli-Q water. Biological activity of each batch of MD-2 has been assessed for the ability to support LPS induced TLR4 activation in HEK293 cells transfected with TLR4.

Determination of CMCs through pyrene fluorescence measurements:^[29] For every sample, independently of the synthetic compound's concentration, a final pyrene concentration of 0.6 µM is desired. A mother solution of pyrene in THF (1 mM) was prepared

in a 25 mL volumetric flask, and diluted into a solution (237 mM, 6 mL of the concentrated solution, followed by addition of 19 mL of THF, to a final volume of 25 mL). An aliquot of this solution (252 µL) is then diluted with Milli-Q water to a final volume of 100 mL. Aqueous solutions of each compound (0.6 µM in pyrene) were prepared at concentrations from 1 mM to 0.05 µM, by two-fold serial dilutions. The 1 mM solutions were prepared by adding pyrene solution (0.6 µM) to each compound and sonicating for 1 h. The serial dilutions were incubated for 1 h at 37.0 °C. For fluorescence measurements, the solution (1.5 mL) was placed in a conventional 1 cm quartz cuvette; fluorescence spectra were recorded with a Varian Cary Eclipse spectrofluorometer at (37 ± 0.1) °C, with use of 5 mm excitation and emission slits. The onset of micelle formation can be observed in a shift of the fluorescence excitation spectra of the samples at an emission wavelength of 372 nm. In the concentration range of aqueous micellar solutions, a shift of the excitation band in the 335 nm region toward higher wavelengths confirms the incorporation of pyrene in the hydrophobic interiors of micelles. The ratio of the fluorescence intensities at 339 and 335 nm was used to quantify the shift of the broad excitation band. The critical micelle concentrations were determined from the crossover point in the low concentration range.

NMR binding experiments: NMR experiments were performed with a 600 MHz DRX spectrometer (Bruker) equipped with a cryoprobe. ¹H NMR spectra were recorded at 298 K, by acquisition of 120 scans. DOSY spectra were recorded at 311 K with the stebpgls19 Bruker pulse sequence by acquisition of 160 scans, with a diffusion time of 300 ms, a gradient length of 1.9 ms, and a gradient ramp from 2% to 95% in 32 linear steps. Protein samples were prepared by diluting the stock solution of MD-2 (0.11 mM in deuterated acetate buffer at pH 5) with the same buffer. Ligand samples were prepared by dissolving solid compound **3** in deuterated acetate buffer at pH 5. For ¹H NMR experiments the final concentrations reached for the analyzed samples were 30 µM MD-2 and 150 µM compound **3**, whereas for DOSY experiments final concentrations of 60 µM MD-2 and 300 µM compound **3** were needed.

Molecular modeling: 3D coordinates of compound **3** were built with the aid of Maestro (version 9.3, Schrödinger, LLC, New York, NY, 2012). Phosphate groups were considered to be monoprotonated. Molecular mechanics optimization (UFF force field), semiempirical calculations (AM1), and DFT (B3LYP/6-31G*) were subsequently applied by use of Gaussian03.^[32] Final geometry was submitted to MD simulations with implicit water and MM3* as force field, by use of Schrödinger Maestro 9.3 Impact 5.8, [Maestro, v. 9.3, Schrödinger, LLC, New York, NY, 2012. Suite 2012: Impact v. 5.8, Schrödinger, LLC, New York, NY, 2012] and the MM3* force field, dielectric constant 80.0, number of MD steps 100, and time step of 0.001 ps. 3D coordinates of human MD-2 protein (from PDB ID: 2E59), and CD14 protein (from PDB ID: 1WWL) were refined and minimized by use of the Protein Preparation Wizard module of Maestro and the Amber force field.^[33] In the case of CD14, only the sequence from Ala3 to Leu130 was considered for docking purposes. Compound **3** was docked into both MD-2 and CD14 proteins with the aid of AutoDock 4.2,^[25] and separately with the aid of AutoDock Vina 1.1.2.^[26] Predicted binding energies ranged from -2 to -6 kcal mol⁻¹ in the AutoDock results and from -6 to -9 kcal mol⁻¹ in the AutoDock Vina results. For MD-2 the Autogrid grid point spacing was set at 0.375 Å, center coordinates of the grid box were -0.379, 17.201, 16.216 (x, y, z), and number of grid points in xyz was 58, 92, 82. For CD14 the Autogrid grid point spacing was set at 0.375 Å, center coordinates of the grid box were 13.500, 51.000, 56.500 (x, y, z), leading to 66, 72, 88 (x, y, z)

grid points. All allowed torsional bonds were considered rotatable. Docking calculations with AutoDock were performed by use of Genetic Algorithm (number of runs 250, number of individuals in population 150). Docking calculations with AutoDock Vina were also performed. Coordinates and dimensions of grid boxes, starting geometries, and general methodology were the same as for AutoDock. 3D structures of the docked complexes were optimized by performing MD simulations with Impact (implicit water, and AMBER* force field).

Acknowledgements

We thank Julio Rodriguez Lavado for experimental CMC determination. We thank the COST action BM 1003 "Microbial cell surface determinants of virulence as targets for new therapeutics for Cystic Fibrosis"; F.P. thanks the US National Institutes of Health (NIH)/National Institute of Allergy and Infectious Diseases (NIAID), project: "Regulation of MD2 function and expression" (1R01AI059372), the COST action CM1102 "Multivalent Glycosystems for Nanoscience–MultiGlycoNano", and the Italian Ministry of Universities and Research (MIUR), PRIN 2010-11, project: "Italian network for the development of multivalent nanosystems". The Spanish MINECO (grants CTQ2012-32025, and CTQ2011-22724), the Universidad CEU San Pablo (PC14/2011 and PC13/2012), and the European Commission granted GLYOPHARM ITN-project are also gratefully acknowledged. L.K. thanks Airbus-Military for a research contract. The Associazione Italiana per la Ricerca sul Cancro (AIRC), the Fondazione Cariplo (grant 2010-0678), and Regione Lombardia are also gratefully acknowledged.

Keywords: bioorganic chemistry · carbohydrates · drug design · molecular modeling · NMR

- [1] a) A. Poltorak, X. He, I. Smirnova, M. Liu, C. Van Huffel, X. Du, D. Birdwell, E. Alejos, M. Silva, C. Galanos, M. Freudenberg, P. Ricciardi-Castagnoli, B. Layton, B. Beutler, *Science* **1998**, *282*, 2085–2088; b) B. Beutler, X. Du, A. Poltorak, *J. Endotoxin Res.* **2001**, *7*, 277–280; c) B. Beutler, *Curr. Top. Microbiol. Immunol.* **2002**, *270*, 109–120.
- [2] a) B. Park, D. Song, H. Kim, B. Choi, H. Lee, J. Lee, *Nature* **2009**, *458*, 1191–1195; b) U. Ohto, K. Fukase, K. Miyake, T. Shimizu, *Proc. Natl. Acad. Sci. USA* **2012**, *109*, 7421–7426.
- [3] S. Wright, R. Ramos, P. Tobias, R. Ulevitch, J. Mathison, *Science* **1990**, *249*, 1431–1433.
- [4] a) J. da Silva Correia, K. Soldau, U. Christen, P. Tobias, R. Ulevitch, *J. Biol. Chem.* **2001**, *276*, 21129–21135; b) T. Gioannini, A. Teghanemt, D. Zhang, N. Coussens, W. Dockstader, S. Ramaswamy, J. Weiss, *Proc. Natl. Acad. Sci. USA* **2004**, *101*, 4186–4191; c) K. Moore, L. Andersson, R. Ingalls, B. Monks, R. Li, M. Arnaout, D. Golenbock, M. Freeman, *J. Immunol.* **2000**, *165*, 4272–4280.
- [5] M. Triantafyllou, K. Triantafyllou, N. Fernandez, *Eur. J. Biochem.* **2000**, *267*, 2218–2226.
- [6] I. Zanoni, R. Ostuni, L. R. Marek, S. Barresi, R. Barbalat, G. M. Barton, F. Granucci, J. C. Kagan, *Cell* **2011**, *147*, 868–880.
- [7] K. A. Shirey, W. Lai, A. J. Scott, M. Lipsky, P. Mistry, L. M. Pletneva, C. L. Karp, J. McAlees, T. L. Gioannini, J. Weiss, W. H. Chen, R. K. Ernst, D. P. Rossignol, F. Gusovsky, J. C. Blanco, S. N. Vogel, *Nature* **2013**, *497*, 498–502.
- [8] M. Piazza, L. Yu, A. Teghanemt, T. Gioannini, J. Weiss, F. Peri, *Biochemistry* **2009**, *48*, 12337–12344.
- [9] M. S. Rangel-Frausto, *Arch. Med. Res.* **2005**, *36*, 672–681.
- [10] M. Casula, A. M. Iyer, W. G. Spliet, J. J. Anink, K. Steentjes, M. Sta, D. Troost, E. Aronica, *Neuroscience* **2011**, *179*, 233–243.
- [11] L. Cao, F. Tanga, J. Deleo, *Neuroscience* **2009**, *158*, 896–903.
- [12] S. Rivest, *Nat. Rev. Immunol.* **2009**, *9*, 429–439.
- [13] F. Peri, M. Piazza, *Biotechnol. Adv.* **2012**, *30*, 251–260.
- [14] J. Schletter, H. Heine, A. J. Ulmer, E. T. Rietschel, *Arch. Microbiol.* **1995**, *164*, 383–389.
- [15] C. Raetz, C. Whitfield, *Annu. Rev. Biochem.* **2002**, *71*, 635–700.
- [16] R. L. Danner, K. A. Joiner, J. E. Parrillo, *J. Clin. Invest.* **1987**, *80*, 605–612.
- [17] C. Lam, J. Hildebrandt, E. Schütze, B. Rosenwirth, R. A. Proctor, E. Liehl, P. Stütz, *Infect. Immun.* **1991**, *59*, 2351–2358.
- [18] K. Funatogawa, M. Matsuura, M. Nakano, M. Kiso, A. Hasegawa, *Infect. Immun.* **1998**, *66*, 5792–5798.
- [19] A. L. Van Dervort, M. E. Doerfler, P. Stuetz, R. L. Danner, *J. Immunol.* **1992**, *149*, 359–366.
- [20] M. Matsuura, M. Kiso, A. Hasegawa, *Infect. Immun.* **1999**, *67*, 6286–6292.
- [21] L. Brade, K. Brandenburg, H. M. Kuhn, S. Kusumoto, I. Macher, E. T. Rietschel, H. Brade, *Infect. Immun.* **1987**, *55*, 2636–2644.
- [22] a) R. Tamai, Y. Asai, M. Hashimoto, K. Fukase, S. Kusumoto, H. Ishida, M. Kiso, T. Ogawa, *Immunology* **2003**, *110*, 66–72; b) H. M. Kuhn, L. Brade, B. J. Appelmek, S. Kusumoto, E. T. Rietschel, H. Brade, *Infect. Immun.* **1992**, *60*, 2201–2210.
- [23] R. L. Danner, A. L. Van Dervort, M. E. Doerfler, P. Stuetz, J. E. Parrillo, *Pharm. Res.* **1990**, *7*, 260–263.
- [24] J. Chen, Y. Zhou, C. Chen, W. Xu, B. Yu, *Carbohydr. Res.* **2008**, *343*, 2853–2862.
- [25] D. S. Goodsell, G. M. Morris, A. J. Olson, *J. Mol. Recognit.* **1996**, *9*, 1–5.
- [26] O. Trott, A. J. Olson, *J. Comput. Chem.* **2010**, *31*, 455–461.
- [27] U. Ohto, K. Fukase, K. Miyake, Y. Satow, *Science* **2007**, *316*, 1632–1634.
- [28] M. Piazza, C. Rossini, S. Della Fiorentina, C. Pozzi, F. Comelli, I. Bettoni, P. Fusi, B. Costa, F. Peri, *J. Med. Chem.* **2009**, *52*, 1209–1213.
- [29] A. M. Hofmann, F. Wurm, H. Frey, *Macromolecules* **2011**, *44*, 4648–4657.
- [30] F. Granucci, C. Vizzardelli, N. Pavelka, S. Feau, M. Persico, E. Virzi, M. Rescigno, G. Moro, P. Ricciardi-Castagnoli, *Nat. Immunol.* **2001**, *2*, 882–888.
- [31] M. Mancek-Keber, R. Jerala, *FASEB J.* **2006**, *20*, 1836–1842.
- [32] Gaussian 03, Gaussian Inc., Wallingford, CT, USA, **2003**.
- [33] a) Suite 2012: Schrödinger Suite **2012** Protein Preparation Wizard; b) Epik version 2.3, Schrödinger, LLC, New York, NY, **2012**; c) Impact version 5.8, Schrödinger, LLC, New York, NY, **2012**; d) Prime version 3.1, Schrödinger, LLC, New York, NY, **2012**.

Received: September 13, 2013
Published online on December 12, 2013



Clicked and long spaced galactosyl- and lactosylcalix[4]arenes: new multivalent galectin-3 ligands

Silvia Bernardi¹, Paola Fezzardi¹, Gabriele Rispoli¹, Stefania E. Sestito²,
Francesco Peri^{*2}, Francesco Sansone¹ and Alessandro Casnati^{*1}

Full Research Paper

Open Access

Abstract

Four novel calix[4]arene-based glycoclusters were synthesized by conjugating the saccharide units to the macrocyclic scaffold using the CuAAC reaction and using long and hydrophilic ethylene glycol spacers. Initially, two galactosylcalix[4]arenes were prepared starting from saccharide units and calixarene cores which differ in the relative dispositions of the alkyne and azido groups. Once the most convenient synthetic pathway was selected, two further lactosylcalix[4]arenes were obtained, one in the cone, the other one in the 1,3-alternate structure. Preliminary studies of the interactions of these novel glyco-calixarenes with galectin-3 were carried out by using a lectin-functionalized chip and surface plasmon resonance. These studies indicate a higher affinity of lactosyl-over galactosylcalixarenes. Furthermore, we confirmed that in case of this specific lectin binding the presentation of lactose units on a cone calixarene is highly preferred with respect to its isomeric form in the 1,3-alternate structure.

Introduction

Lectins are carbohydrate-binding proteins (CBP) [1-3] without any catalytic or immunogenic activity. In the latest decades, they attracted an increasing interest due to their involvement in a series of fundamental biological processes such as cell adhesion, cell activation, cell growth, differentiation and apoptosis. Among different families of lectins, the ones showing a selectivity for β -D-galactoside and β -D-galactose-terminating oligo-

saccharides are called galectins and play important roles in a series of pathological events such as inflammation, fibrosis, heart diseases and cancer [4,5]. The role of one member of this family in particular, namely galectin-3 (Gal-3), has been intensively investigated lately and it was shown that it is deeply involved in cancer metastasis and migration. Based on these findings and with the aim to inhibit its activity and to target it

for therapeutic or diagnostic purposes, Gal-3 became a rather important target in medicine. Remarkably interesting is the intra-family selectivity and, especially, the ability to block Gal-3 but not Gal-1. Gal-1, in fact, can act as anti-inflammatory agent, while Gal-3 has a pro-inflammatory activity [6]. Furthermore, Gal-3 can act as a competitive inhibitor against Gal-1 which, on the other side, induces anoikis of tumor cells [7,8]. Glycocalixarenes [9–12], calixarenes [13–15] adorned with carbohydrates at the upper and/or at the lower rims, have been demonstrated to be efficient multivalent ligands for a series of pathological lectins. For instance, cholera toxin is bound rather efficiently by calix[4]arene [16] and calix[5]arene [17] derivatives, while examples of *Pseudomonas aeruginosa* LecB binding were reported with galactosylcalixarenes blocked in different conformations [18,19]. A few years ago we [20,21] reported about the synthesis and inhibitory properties of a small library of lactosylthioureidocalixarenes and found that the cone derivatives **I** and **III** (Figure 1) were able to efficiently inhibit the adhesion of Gal-3 to tumor cells in vitro, but not that of galectin-1 [22].

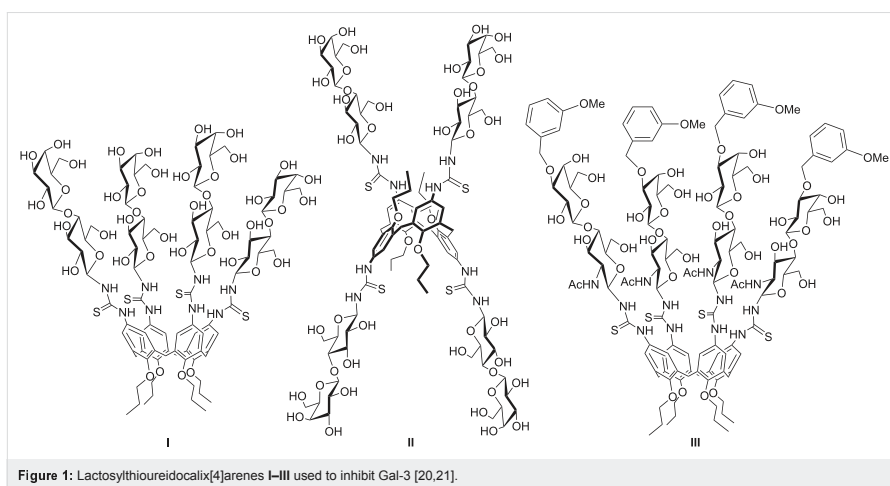
The opposite behavior was observed for the 1,3-alternate derivative **II**, able to inhibit Gal-1 but not Gal-3. On the basis of these findings, we herein report the synthesis of a new subfamily of galactosyl- and lactosylcalix[4]arenes **1–4** (Figure 2) which are characterized by long hydrophilic spacers between the glycosyl units and the multivalent calixarene scaffold. We also report on preliminary studies of the interaction of the novel subfamily of galactosyl- and lactosylcalix[4]arenes with Gal-3 by surface plasmon resonance (SPR).

Results and Discussion

Synthesis of the glycocalixarenes

“Click Chemistry” [23] reactions are extensively used to conjugate (oligo)saccharides to macrocyclic structures due to the mild conditions and the high yields [24]. For the synthesis of glycocalixarenes the amino–isothiocyanate condensation [25–30] or the 1,3-dipolar cycloaddition have been widely studied in their scope and limitations [10,31]. In particular, the Huisgen cycloaddition reaction was first applied to a calixarene in 2000 by Santoyo-González [32]. Later on, Marra et al. [33] demonstrated that the copper-catalyzed azide–alkyne cycloaddition (CuAAC) [34,35] at room temperature could afford divalent and tetravalent glycocalixarenes in very high yields and regioselectivity. Following these studies, a wide series of other examples appeared in the literature [18,36–39] also exploiting the use of microwaves, ionic liquids and protected or even deprotected [17] saccharides. Usually, either the strategy of reacting an alkynylated-saccharide with a polyazide calixarene (dipolarophile-on-the-sugar) or an azido-sugar and a polyalkynocalixarene (dipolarophile-on-the-calix) work smoothly [33]. However, a sort of autocatalytic effect was evidenced in the case of the reaction between a 1-ethynyl-C-glycoside with a tetraazidocalix[4]arene (dipolarophile-on-the sugar strategy). It was suggested by the authors that the first intermolecular reaction, leading to a Cu-triazolide adduct, allows the copper ion to coordinate an ethynyl glycoside, thus entailing an intramolecular CuAAC reaction with an adjacent azido-arm [37].

Firstly, we decided to evaluate the effectiveness of the two approaches dipolarophile-on-the-calix and dipolarophile-on-the-



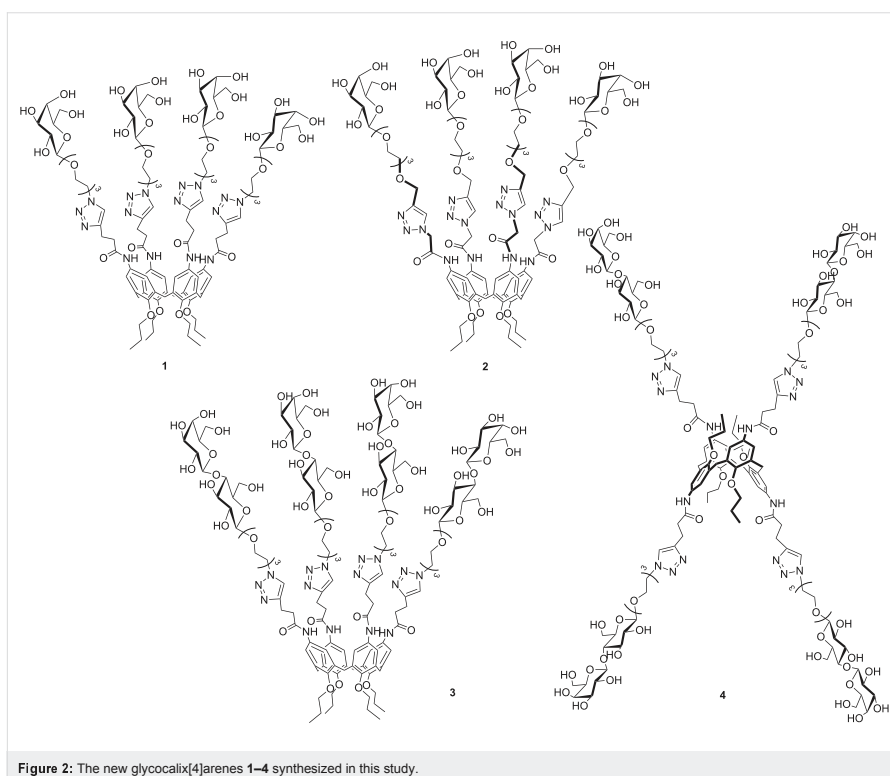
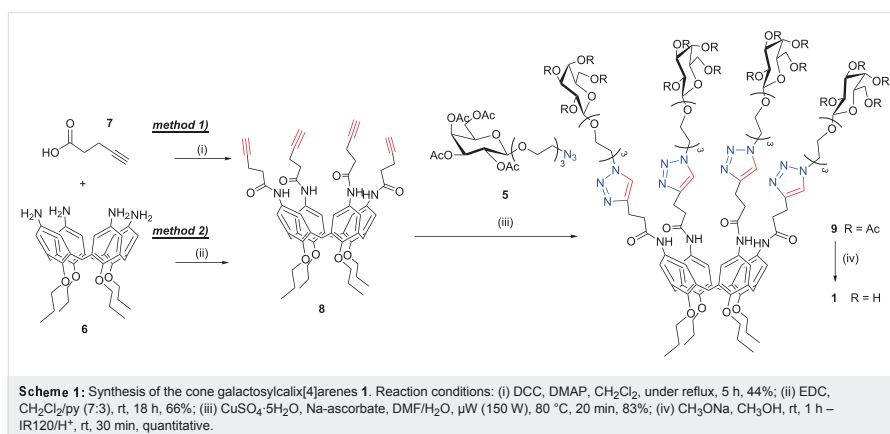


Figure 2: The new glyco-calix[4]arenes 1–4 synthesized in this study.

sugar by using a galactose and cone calixarene scaffolds. This investigation was carried out with the idea to extend the study to stronger ligating units for galectins such as lactose and different calixarene structures, also including the 1,3-alternate isomer. The first route explored (dipolarophile-on-the-calix) was applied to the preparation of the multivalent compound **1**, which could be synthesized by exploiting a convergent synthetic approach. This approach was based on the connection, by CuAAC reaction, of the azido-terminating tetraacetylgalactose **5** [40,41] to calix[4]arene **8** decorated at the upper rim with alkyne terminating chains (Scheme 1).

In order to introduce the alkyne units at the upper rim of the macrocycle, we decided to exploit the easily available and highly versatile *p*-aminocalixarene **6** prepared according to literature procedures [25]. The coupling reaction between amino-calix[4]arene **6** and 4-pentynoic acid (**7**) in the presence of dicyclohexylcarbodiimide (DCC) led to compound **8** in 44%

yield. Due to the concurrent formation of dicyclohexylurea (DCU), several purification steps were necessary to obtain pure calix[4]arene **8**. The use of 1-ethyl-3-(3-dimethylaminopropyl)-carbodiimide (EDC) as an alternative coupling agent allowed us to isolate pure compound **8** in a more straightforward way and higher yield (66%). Any attempts to connect the alkyne functionality in closer proximity to the calixarene core by decreasing the number of carbon atoms between the carboxylic group and the triple bond did not give fruitful results. Reactions between amino-calix[4]arene **6** and propionic acid were carried out with a variety of coupling agents. In the presence of DCC the tetra-condensation product was only obtained in very low yields. Furthermore, it was not possible to purely isolate it from the crude reaction mixture due to the high amount of byproducts formed during the reaction. The CuAAC reaction between the tetraalkyne calix[4]arene **8** and azido-galactoside **5** to give glycocluster **9** (83% yield) was carried out in DMF and H₂O with CuSO₄ and sodium ascorbate following a microwave-

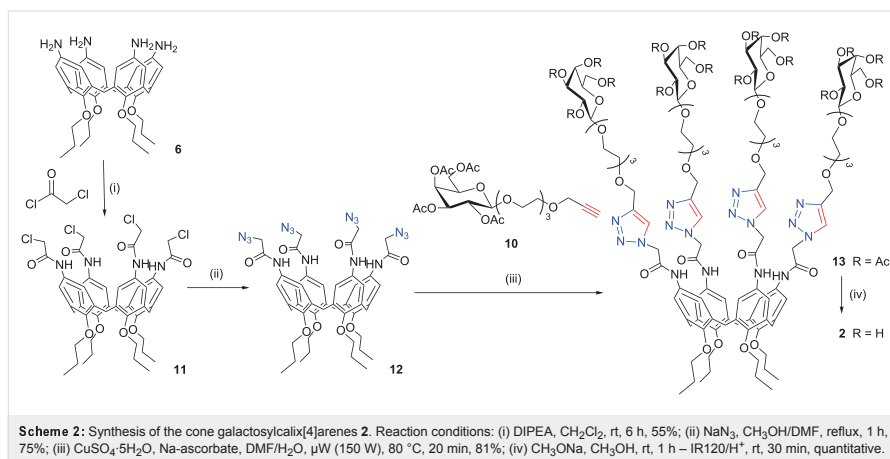


assisted procedure (20 min, 150 W, 80 °C). No partially functionalized compounds or other byproducts were detected in the crude mixtures.

The second strategy studied (dipolarophile-on-the-sugar) also exploits a convergent approach, but in this case an alkyne-functionalized galactose **10** was prepared according to literature [42], so that it reacts with calixarene **12**, which was previously functionalized with azido terminating arms (Scheme 2). This latter compound was synthesized in two steps starting again from tetraamino derivative **6**. In the first step compound **6** was treated with chloroacetyl chloride to give the α -chloroac-

etamido compound **11** [43]. Subsequent substitution of the chlorine ions with azide groups led to the formation of the tetra-azidocalixarene derivative **12** (1 h, 75% yield).

The CuAAC conjugation reaction was carried out following exactly the same procedure as for compound **9** and allowed the isolation of **13** in very high yields (81%). Glycoconjugates **9** and **13** were fully characterized by ^1H and ^{13}C NMR spectroscopy, which displayed the disappearance of the alkyne protons and the appearance of the typical broad signal of 1,4-disubstituted triazole protons at 7.75–7.85 ppm ($\text{CD}_3\text{OD}/\text{CDCl}_3$). ESIMS (+) analyses showed peaks for the $[\text{M} + 2\text{Na}]^{2+}$



and $[M + 3Na]^{3+}$ adducts, which indicates the conjugation of all four macrocycle arms to the saccharide units. On the basis of the comparison between the efficiency of the conjugation steps bringing to glycoconjugates **9** and **13** (yields >80% in both cases) and contrary to the observation by Marra et al. [37], we could not collect any evidence for an autocatalytic effect in the dipolarophile-on-the-sugar approach [44]. The deprotection of compounds **9** and **13** from the acetyl groups was carried out by a transesterification reaction in the presence of CH_3ONa in CH_3OH at room temperature according to the standard Zemplén procedure. Complete deacetylation was achieved in 1 hour, as confirmed by NMR and ESIMS(+) spectra of compounds **1** and **2**. It is noteworthy that while compound **1** exhibited a high stability under Zemplén conditions even if the reaction was continued overnight, compound **2** started to decompose after 18 hours. ESIMS profiles showed the presence of products originating from a cleavage at the amide bond with a loss of the entire glycosylated chain and the formation of an amine group at the upper rim of the calixarene. For this reason and on the basis of the synthetic availability of intermediates, we decided to privilege the dipolarophile-on-the-calix route to synthesize the triazole-containing lactosylcalixarenes **3** and **4**.

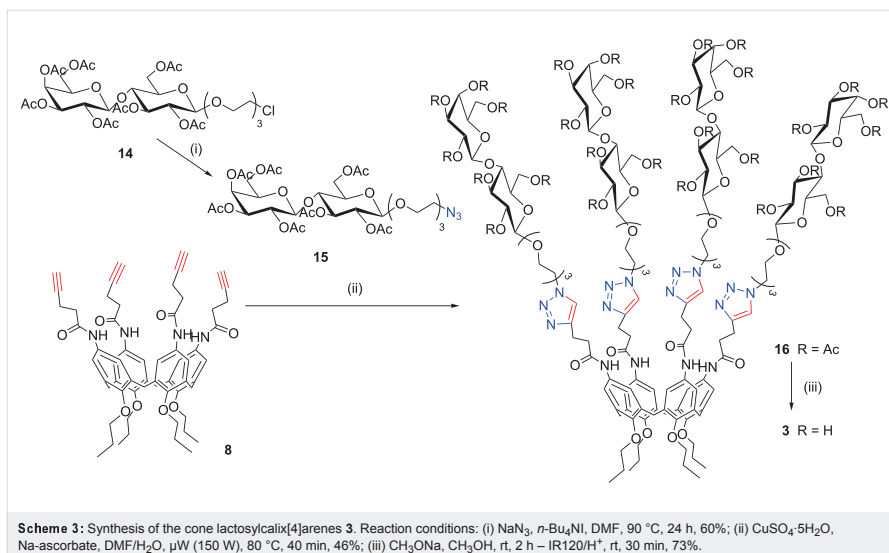
We first attempted to prepare the lactoside derivative **14** by reacting peracetylated-lactose with 2-(2-(2-chloroethoxy)ethoxy)ethanol in the presence of $BF_3 \cdot Et_2O$ [45]. However, we could only obtain a mixture of α and β -anomers (α/β ratio 2:3),

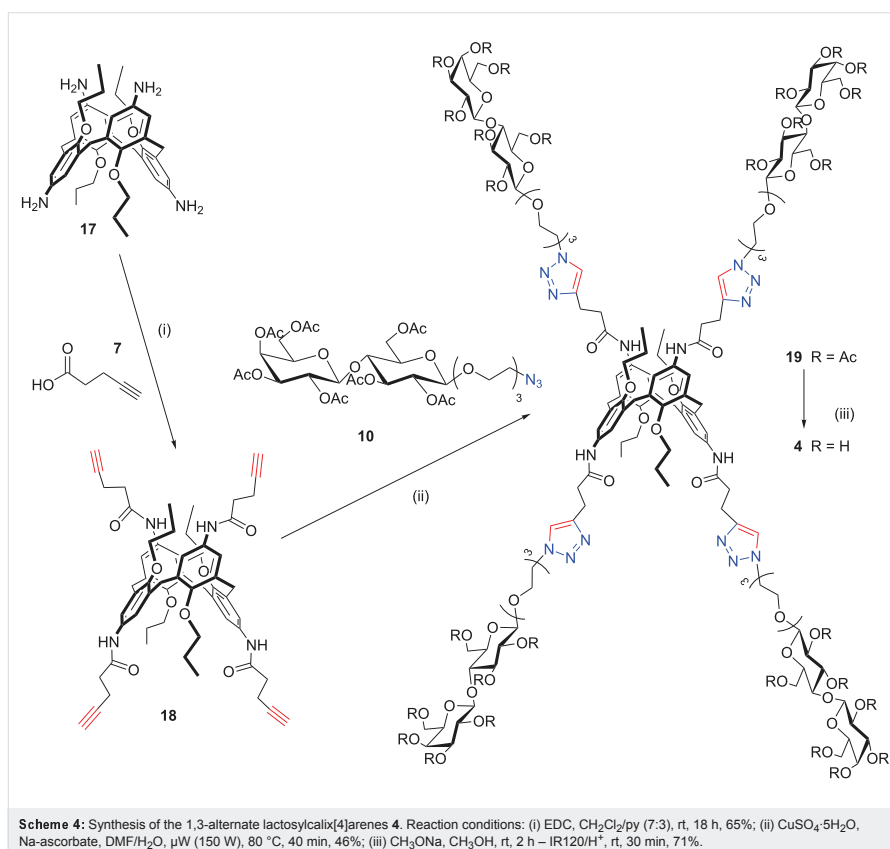
which is very difficult to separate by flash chromatographic methods. On the other hand, the recently reported glycosylation reactions of lactose peracetate exploiting $SnCl_4$ and CF_3CO_2Ag as promoters [46] gave compound **14** mainly as a β -anomer (α/β ratio 1:4) in 74% isolated yield.

The subsequent substitution reaction of chloride with NaN_3 (Scheme 3) led to the corresponding azido derivative **15**, which was used to “click” both the cone (**8**) and 1,3-alternate (**18**) pentyno amides. Compound **18** was obtained from the corresponding 1,3-alternate *p*-aminocalix[4]arene **17** [47] by a reaction with EDC in CH_2Cl_2 and pyridine 7:3 as previously described for compound **8**. The CuAAC “click” reaction was carried out as previously described for the galacto-clusters **9** and **13** and afforded the cone calix[4]arene **16** (Scheme 3) and 1,3-alternate calix[4]arene **19** (Scheme 4) in 46% isolated yield. Microwave irradiation (150 W, 80 °C) facilitated the complete tetra-functionalization in only 40 minutes. Subsequent deacetylation with the Zemplén method led to target compounds **3** and **4**, both of which were characterized by 1D and 2D NMR techniques and ESIMS analyses.

Gal-3/glycolcalixarenes interaction studies by SPR

His₆-tagged full-length Gal-3 was expressed in *E. coli* BL21 and purified on IMAC (immobilized metal ion affinity chromatography) columns. Purified protein was characterized by SDS-





PAGE electrophoresis, circular dichroism (CD), and MS/MS analysis upon digestion on trypsin gel (see Figure S15, Supporting Information File 1). A preliminary evaluation of the interaction between the glyco-calixarenes **1**, **3**, **4** and Gal-3 was obtained by SPR analysis by using a His-tagged Gal-3 immobilized on a Ni-NTA chip and the glyco-calixarenes in solution. This approach differs from other SPR studies of the calixarene–galactin interaction with the protein in solution [38] and is tailored to have the immobilized protein properly oriented for the interaction with ligands. The sensorgrams shown in Figure 3 were obtained by fluxing an 1 mM solution of calixarenes over the protein-coated chip.

The small increases of resonance units in the sensorgrams (Figure 3) showed a weak affinity of all calixarenes for Gal-3.

However, the three synthetic molecules showed a very similar trend of Gal-3 binding affinity in three independent measurements (experiments A, B and C in Figure 4a). In particular, glyco-calixarene **3** (cone structure, four lactosides) exhibited the highest affinity for Gal-3 in all experiments, while **4**, (1,3-alternate structure, four lactosides) displayed a lower affinity and **1** (cone structure, four galactosides) showed no interaction at all. The more efficient ligand, compound **3**, showed a dose-dependent affinity for the protein.

The higher affinities of lactose-containing compounds **3** and **4** for Gal-3 compared to galactose-containing compound **1** reflect the higher affinity of lactose over galactose for Gal-3. The lactosylcalixarene with the cone structure appears to bind better to Gal-3 than the corresponding isomer in the 1,3-alternate

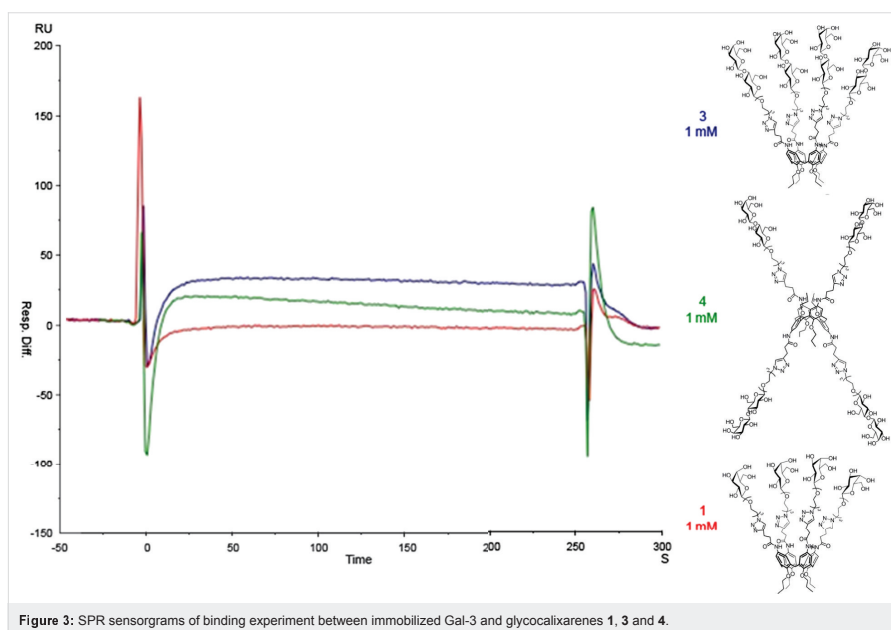


Figure 3: SPR sensorgrams of binding experiment between immobilized Gal-3 and glycolalixarenes 1, 3 and 4.

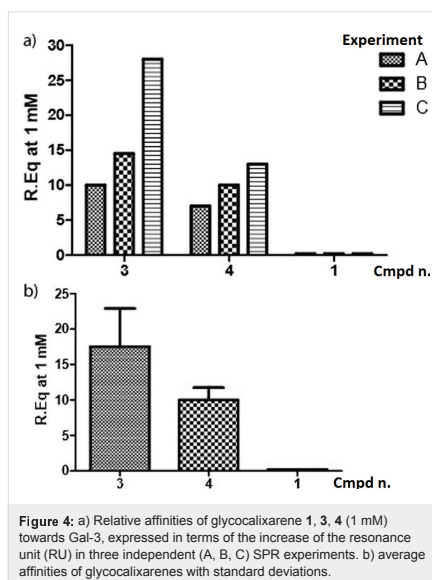


Figure 4: a) Relative affinities of glycolalixarene 1, 3, 4 (1 mM) towards Gal-3, expressed in terms of the increase of the resonance unit (RU) in three independent (A, B, C) SPR experiments. b) average affinities of glycolalixarenes with standard deviations.

structure. This confirms the data previously obtained in a series of inhibition experiments of the same lectin in surface-immobilized asialofetuin and on cells with the lactosylthioureidoalixarenes (I–III) [20,21]. A direct comparison with ligands (I–III) was, however, not feasible since the lactosylthioureido derivatives tend to aggregate and precipitate under the conditions used for SPR experiments.

Conclusion

Four glycolalixarenes 1–4 characterized by long hydrophilic spacers between the glycosyl units and the macrocyclic scaffold were synthesized by the copper(I)-catalyzed azido–alkyne cycloaddition (CuAAC). The homogeneous series of ligands 1, 3 and 4 were subsequently studied in the binding to surface-immobilized His-tagged Gal-3 by SPR experiments. In spite of the weak intensity of the signals, an affinity order for the interaction of ligands 1, 3 and 4 with the immobilized Gal-3 was obtained. A preference for the lactosyl clusters over the galactose functionalized ones ($3 > 4 \gg 1$) and a higher efficiency in the binding of Gal-3 shown by the cone derivative compared to its isomeric 1,3-alternate counterpart ($3 > 4$) were observed. Work is in progress to study by SPR experiments the interaction between lactosylalixarenes covalently immobilized on the chip and Gal-3 samples in solution.

Supporting Information

Detailed experimental procedures (general information, synthetic procedures, expression and purification of Gal-3, Gal-3/glycocalixarene binding experiments), ¹H NMR spectra of selected intermediates, and final glycocalixarenes 1–4 together with electrophoresis gel, circular dichroism spectrum and thermal unfolding of purified Gal-3.

Supporting Information File 1

Experimental part.

[<http://www.beilstein-journals.org/bjoc/content/supplementary/1860-5397-10-175-S1.pdf>]

Acknowledgements

The authors gratefully acknowledge financial support from the Italian Ministry of Instruction, University and Research (MIUR, PRIN2010JMAZML MultiNanoIta) and EU-COST Action CM1102 'MultiGlycoNano'. The Centro Interdipartimentale di Misura (CIM) of the Parma University 'G. Casnati' is acknowledged for the use of the NMR and Mass facilities.

References

- Lis, H.; Sharon, N. *Chem. Rev.* **1998**, *98*, 637–674. doi:10.1021/cr940413g
- Gabius, H.-J. *Eur. J. Biochem.* **1997**, *243*, 543–576. doi:10.1111/j.1432-1033.1997.t01-1-00543.x
- Gabius, H.-J.; Siebert, H.-C.; André, S.; Jiménez-Barbero, J.; Rüdiger, H. *ChemBioChem* **2004**, *5*, 740–764. doi:10.1002/cbic.200300753
- Gabius, H.-J.; André, S.; Jiménez-Barbero, J.; Romero, A.; Solis, D. *Trends Biochem. Sci.* **2011**, *36*, 298–313. doi:10.1016/j.tibs.2011.01.005
- Ingrassia, L.; Camby, I.; Lefranc, F.; Mathieu, V.; Nshimyumukiza, P.; Darro, F.; Kiss, R. *Curr. Med. Chem.* **2006**, *13*, 3513–3527. doi:10.2174/092986706779026219
- Rubinstein, N.; Ilarregui, J. M.; Toscano, M. A.; Rabinovich, G. A. *Tissue Antigens* **2004**, *64*, 1–12. doi:10.1111/j.0001-2815.2004.00278.x
- Sanchez-Ruderisch, H.; Fischer, C.; Deijnen, K. M.; Wetzel, M.; Wimmel, A.; Manning, J. C.; André, S.; Gabius, H.-J. *FEBS J.* **2010**, *277*, 3552–3563. doi:10.1111/j.1742-4658.2010.07764.x
- André, S.; Sanchez-Ruderisch, H.; Nakagawa, H.; Buchholz, M.; Kopitz, J.; Forberich, P.; Kemmner, W.; Böck, C.; Deguchi, K.; Deijnen, K. M.; Wiedenmann, B.; von Knebel Doeberitz, M.; Gress, T. M.; Nishimura, S.-I.; Rosewicz, S.; Gabius, H.-J. *FEBS J.* **2007**, *274*, 3233–3256. doi:10.1111/j.1742-4658.2007.05851.x
- Baldini, L.; Casnati, A.; Sansone, F.; Ungaro, R. *Chem. Soc. Rev.* **2007**, *36*, 254–266. doi:10.1039/b603082n
- Dondoni, A.; Marra, A. *Chem. Rev.* **2010**, *110*, 4949–4977. doi:10.1021/cr100027b
- Sansone, F.; Rispoli, G.; Casnati, A.; Ungaro, R. Multivalent Glycocalixarenes. In *Synthesis and Biological Applications of Multivalent Glycoconjugates*; Renaudet, O.; Spinelli, N., Eds.; Bentham Science Publishers: Dordrecht, 2011; pp 36–63. doi:10.2174/978160805277611101010036
- Sansone, F.; Casnati, A. *Chem. Soc. Rev.* **2013**, *42*, 4623–4639. doi:10.1039/c2cs35437c
- Gutsche, C. D. *Calixarenes: An Introduction*, 2nd ed.; Royal Society of Chemistry: Cambridge, 2008. doi:10.1039/9781847558190
- Baldini, L.; Sansone, F.; Casnati, A.; Ungaro, R. Calixarenes in molecular recognition. In *Supramolecular Chemistry: from Molecules to Nanomaterials*; Steed, J. W.; Gale, P. A., Eds.; John Wiley & Sons: Chichester, 2012; pp 863–894. doi:10.1002/9780470661345.smc052
- Casnati, A. *Gazz. Chim. Ital.* **1997**, *127*, 637–649.
- Arosio, D.; Fontanella, M.; Baldini, L.; Mauri, L.; Bernardi, A.; Casnati, A.; Sansone, F.; Ungaro, R. *J. Am. Chem. Soc.* **2005**, *127*, 3660–3661. doi:10.1021/ja0444029
- Garcia-Hartjes, J.; Bernardi, S.; Weijers, C. A. G. M.; Wennekes, T.; Gilbert, M.; Sansone, F.; Casnati, A.; Zuilhof, H. *Org. Biomol. Chem.* **2013**, *11*, 4340–4349. doi:10.1039/c3ob40515j
- Cecioni, S.; Lalor, R.; Blanchard, B.; Praly, J.-P.; Imbert, A.; Matthews, S. E.; Vidal, S. *Chem.–Eur. J.* **2009**, *15*, 13232–13240. doi:10.1002/chem.200901799
- Moni, L.; Pourceau, G.; Zhang, J.; Meyer, A.; Vidal, S.; Souteyrand, E.; Dondoni, A.; Morvan, F.; Chevotot, Y.; Vasseur, J.-J.; Marra, A. *ChemBioChem* **2009**, *10*, 1369–1378. doi:10.1002/cbic.200900024
- André, S.; Grandjean, C.; Gautier, F.-M.; Bernardi, S.; Sansone, F.; Gabius, H.-J.; Ungaro, R. *Chem. Commun.* **2011**, *47*, 6126–6128. doi:10.1039/c1cc11163a
- André, S.; Sansone, F.; Kaltner, H.; Casnati, A.; Kopitz, J.; Gabius, H.-J.; Ungaro, R. *ChemBioChem* **2008**, *9*, 1649–1661. doi:10.1002/cbic.200800035
- Dings, R. P. M.; Miller, M. C.; Nesmelova, I.; Astorgues-Xerri, L.; Kumar, N.; Serova, M.; Chen, X.; Raymond, E.; Hoye, T. R.; Mayo, K. H. *J. Med. Chem.* **2012**, *55*, 5121–5129. doi:10.1021/jm300014q
- An aglyconocalixarene was also shown to be able to inhibit galectin binding to the cell surface, but it was demonstrated that its action is caused by an allosteric inhibition of the glycan/carbohydrate recognition at a site away from the CRD.
- Kolb, H. C.; Finn, M. G.; Sharpless, K. B. *Angew. Chem., Int. Ed.* **2001**, *40*, 2004–2021. doi:10.1002/1521-3773(20010601)40:11<2004::AID-ANIE2004>3.0.CO;2-5
- Renaudet, O.; Roy, R., Eds. Thematic issue: Multivalent scaffolds in glycosciences. *Chem. Soc. Rev.* **2014**, *42*, 4515.
- Sansone, F.; Chierici, E.; Casnati, A.; Ungaro, R. *Org. Biomol. Chem.* **2003**, *1*, 1802–1809. doi:10.1039/b301595e
- Sansone, F.; Baldini, L.; Casnati, A.; Ungaro, R. *Supramol. Chem.* **2008**, *20*, 161–168. doi:10.1080/10610270701777344
- Torvinen, M.; Neitola, R.; Sansone, F.; Baldini, L.; Ungaro, R.; Casnati, A.; Vainiotalo, P.; Kalenius, E. *Org. Biomol. Chem.* **2010**, *8*, 906–915. doi:10.1039/b916268b
- Consoli, G. M. L.; Cunsolo, F.; Geraci, C.; Mecca, T.; Neri, P. *Tetrahedron Lett.* **2003**, *44*, 7467–7470. doi:10.1016/j.tetlet.2003.08.039
- Viola, S.; Consoli, G. M. L.; Merlo, S.; Drago, F.; Sortino, M. A.; Geraci, C. *J. Neurochem.* **2008**, *107*, 1047–1055. doi:10.1111/j.1471-4159.2008.05656.x

30. Consoli, G. M. L.; Cunsolo, F.; Geraci, C.; Sgarlata, V. *Org. Lett.* **2004**, *6*, 4163–4166. doi:10.1021/ol0485767
31. Cardona, F.; Isoldi, G.; Sansone, F.; Casnati, A.; Goti, A. *J. Org. Chem.* **2012**, *77*, 6980–6988. doi:10.1021/jo301155p
32. Calvo-Flores, F. G.; Isac-Garcia, J.; Hernandez-Mateo, F.; Pérez-Balderas, F.; Calvo-Asin, J. A.; Sánchez-Vaquero, E.; Santoyo-González, F. *Org. Lett.* **2000**, *2*, 2499–2502. doi:10.1021/ol006175v
33. Dondoni, A.; Marra, A. *J. Org. Chem.* **2006**, *71*, 7546–7557. doi:10.1021/jo0607156
34. Rostovtsev, V. V.; Green, L. G.; Fokin, V. V.; Sharpless, K. B. *Angew. Chem., Int. Ed.* **2002**, *41*, 2596–2599. doi:10.1002/1521-3773(20020715)41:14<2596::AID-ANIE2596>3.0.CO;2-4
35. Tornøe, C. W.; Christensen, C.; Meldal, M. *J. Org. Chem.* **2002**, *67*, 3057–3064. doi:10.1021/jo011148j
36. Bew, S. P.; Brimage, R. A.; L'Hermite, N.; Sharma, S. V. *Org. Lett.* **2007**, *9*, 3713–3716. doi:10.1021/ol071047t
37. Vecchi, A.; Melai, B.; Marra, A.; Chiappe, C.; Dondoni, A. *J. Org. Chem.* **2008**, *73*, 6437–6440. doi:10.1021/jo800954z
38. Cecioni, S.; Matthews, S. E.; Blanchard, H.; Praly, J.-P.; Imberty, A.; Vidal, S. *Carbohydr. Res.* **2012**, *356*, 132–141. doi:10.1016/j.carres.2012.02.006
39. Aleandri, S.; Casnati, A.; Fantuzzi, L.; Mancini, G.; Rispoli, G.; Sansone, F. *Org. Biomol. Chem.* **2013**, *11*, 4811–4817. doi:10.1039/c3ob40732b
40. Bouillon, C.; Meyer, A.; Vidal, S.; Jochum, A.; Chevlot, Y.; Cloarec, J.-P.; Praly, J.-P.; Vasseur, J.-J.; Morvan, F. *J. Org. Chem.* **2006**, *71*, 4700–4702. doi:10.1021/jo060572n
41. Sasaki, A.; Murahashi, N.; Yamada, H.; Morikawa, A. *Biol. Pharm. Bull.* **1994**, *17*, 680–685. doi:10.1248/bpb.17.680
42. Michel, O.; Ravoo, B. *J. Langmuir* **2008**, *24*, 12116–12118. doi:10.1021/la802304w
43. Alypyshev, M. Yu.; Babain, V. A.; Boyko, V. I.; Eliseev, I. I.; Kirsanov, D. O.; Klimchuk, O. V.; Legin, A. V.; Mikhailina, E. S.; Rodik, R. V.; Smirnov, I. V. *J. Inclusion Phenom. Macrocyclic Chem.* **2010**, *67*, 117–126. doi:10.1007/s10847-009-9685-8
44. No autocatalytic effect was observed even if the distance between the triazole unit and the macrocycle (3 atoms) is exactly the same.
45. Kato, H.; Uzawa, H.; Nagatsuka, T.; Kondo, S.; Sato, K.; Ohsawa, I.; Kanamori-Kataoka, M.; Takei, Y.; Ota, S.; Furuno, M.; Dohi, H.; Nishida, Y.; Seto, Y. *Carbohydr. Res.* **2011**, *346*, 1820–1826. doi:10.1016/j.carres.2011.06.025
46. Xue, J. L.; Cecioni, S.; He, L.; Vidal, S.; Praly, J.-P. *Carbohydr. Res.* **2009**, *344*, 1646–1653. doi:10.1016/j.carres.2009.06.004
47. Sansone, F.; Dudić, M.; Donofrio, G.; Rivetti, C.; Baldini, L.; Casnati, A.; Cellai, S.; Ungaro, R. *J. Am. Chem. Soc.* **2006**, *128*, 14528–14536. doi:10.1021/ja0634425

License and Terms

This is an Open Access article under the terms of the Creative Commons Attribution License (<http://creativecommons.org/licenses/by/2.0>), which permits unrestricted use, distribution, and reproduction in any medium, provided the original work is properly cited.

The license is subject to the *Beilstein Journal of Organic Chemistry* terms and conditions: (<http://www.beilstein-journals.org/bjoc>)

The definitive version of this article is the electronic one which can be found at: [doi:10.3762/bjoc.10.175](https://doi.org/10.3762/bjoc.10.175)